Technische Universität München

Max-Planck-Institut für Quantenoptik

Quantum many-body states defined through conformal field theory

Benedikt Thomas Herwerth

Vollständiger Abdruck der von der Fakultät für Physik
der Technischen Universität München
zur Erlangung des akademischen Grades eines

Doktors der Naturwissenschaften (Dr. rer. nat.)

genehmigten Dissertation.

Vorsitzender:	Prof. Dr. Alexander Holleitner
Prüfer der Dissertation:	1. Hon.-Prof. J. Ignacio Cirac, Ph.D.
	2. Prof. Dr. Frank Pollmann

Die Dissertation wurde am 01.08.2018
bei der Technischen Universität München eingereicht
und durch die Fakultät für Physik am 05.10.2018 angenommen.

Abstract

In this thesis, we study quantum many-body systems in one (1D) and in two spatial dimensions (2D). We adopt the approach established by Moore and Read, where model states are constructed using conformal field theory (CFT), a scale-invariant quantum field theory. The central themes of this thesis are the definition of states through CFT, their characterization, and the understanding of their properties in terms of the underlying CFT.

The first part of this thesis considers a CFT with an additional SU(2) symmetry. We define a map from CFT states to those of spin-$\frac{1}{2}$ systems on lattices. In 1D, the CFT vacuum is mapped to the ground state of a Heisenberg-like spin chain with long-range inverse-square interactions. We show that the excited states of this spin chain can be constructed from excitations of the CFT. Thus, we establish a correspondence between the spectrum of the CFT and that of the spin chain. In a next step, we study these states in 2D, where the CFT ground state corresponds to a fractional quantum Hall (FQH) lattice state. Excited states of the CFT are mapped to wave functions describing edge excitations of the FQH system. Through Monte Carlo simulations, we provide numerical evidence for a central property of these edge modes, namely that their local bulk correlations coincide with those of the corresponding FQH state as the system size becomes large enough. These results confirm the bulk-edge correspondence stating that the CFT associated with the gapless edge can be used to describe wave functions of the bulk.

We then consider a larger class of states constructed from CFT. In 1D, these are good descriptions of the ground state of the XXZ spin-$\frac{1}{2}$ chain, and they correspond to FQH lattice states in 2D. Through a path integral representation, we propose an approximation for their spin-spin correlations. The effective action determining this approximation differs from that of the underlying CFT through an additional mass-like term at the lattice positions. This explains the behavior of the correlations: While they decay polynomially in 1D and at the edge of 2D systems, bulk correlations in 2D decrease exponentially as a function of the distance. We test the accuracy of the approximation by comparing it to actual spin-spin correlations obtained through Monte Carlo simulations. Our approximation provides an analytical argument for the screening hypothesis, which states that FQH wave functions have exponentially decaying bulk correlations.

The last part of this thesis uses CFT to define nonchiral states with continuous spins on lattices. Opposed to the case of discrete spins, these are Gaussian and thus their properties can be computed efficiently. Through an analysis of entanglement entropies and spectra, we identify signatures of the underlying CFT in 1D. In 2D, we find indications of edge states. Although the topological entanglement entropy vanishes, the entanglement spectrum contains modes that decay exponentially with the distance to the entanglement cut.

Zusammenfassung

Diese Dissertation untersucht Quanten-Vielteilchensysteme in einer (1D) und in zwei räumlichen Dimensionen (2D). Wir arbeiten im Rahmen der von Moore und Read etablierten Herangehensweise, wonach Modellzustände durch konforme Feldtheorie (CFT), einer skaleninvarianten Quantenfeldtheorie, konstruiert werden. Die Schwerpunktthemen dieser Arbeit sind: die Definition von Quantenzuständen vieler Teilchen mittels CFT, deren Charakterisierung und das Verständnis ihrer Eigenschaften in Bezug auf die zugrundeliegende CFT.

Der erste Teil dieser Dissertation betrachtet eine CFT, welche eine zusätzliche SU(2)-Symmetrie aufweist. Wir definieren eine Abbildung von Zuständen der CFT zu solchen eines Spin-$\frac{1}{2}$-Systems auf einem Gitter. In 1D wird das Vakuum der CFT auf den Grundzustand einer Spinkette abgebildet, welche ähnlich einem Heisenberg-Modell ist und langreichweitige Wechselwirkungen hat, die mit dem Quadrat der Distanz abfallen. Wir konstruieren Anregungszustände der Spinkette ausgehend von Anregungen der CFT. In einem weiteren Schritt untersuchen wir diese Zustände in 2D, wo der Grundzustand der CFT dem Zustand eines fraktionalen Quanten-Hall-Effekts (FQH) auf einem Gitter entspricht. Anregungen der CFT werden auf Wellenfunktionen abgebildet, welche Randzustände des FQH-Systems beschreiben. Mittels Monte-Carlo-Simulationen finden wir numerische Belege für eine zentrale Eigenschaft solcher Randzustände: Deren lokale Korrelationen im Inneren des Systems stimmen mit denen des zugrundeliegenden FQH-Zustands überein, sobald die Systemgröße groß genug wird. Dieses Ergebnis bestätigt das Konzept der Korrespondenz zwischen dem Inneren und dem Rand. Dieses besagt, dass die CFT des Randes Zustände des Inneren beschreiben kann.

Danach betrachten wir eine größere Klasse von Zuständen, welche durch CFT definiert sind. Diese sind gute Näherungen für den Grundzustand der XXZ-Spin-$\frac{1}{2}$-Kette in 1D und entsprechen FQH-Zuständen in 2D. Durch eine Pfandintegraldarstellung leiten wir eine Näherung für Spin-Spin-Korrelationen her. Die effektive Wirkung dieser Näherung unterscheidet sich von derjenigen der zugrundeliegenden CFT dadurch, dass sie einen zusätzlichen Term enthält, der einem Masseterm ähnlich ist. Dieser ist an den Gitterplätzen des Systems lokalisiert und erklärt somit das Verhalten der Korrelationen: Diese zerfallen polynomiell in 1D und am Rand eines 2D Systems und exponentiell im Inneren eines 2D Systems. Wir überprüfen die Genauigkeit der Näherung, indem wir sie mit den tatsächlichen Spin-Spin-Korrelationen vergleichen, welche wir mittels Monte-Carlo-Simulationen berechnen. Unsere Näherung stellt einen analytischen Beleg für die Abschirmhypothese dar. Diese besagt, dass Korrelationen von FQH-Zuständen im Inneren des Systems exponentiell zerfallen.

Der letzte Teil dieser Dissertation definiert nicht-chirale Zustände mit kontinuierlichem Spin auf Gittern mittels CFT. Im Unterschied zum Fall diskreter Spins sind dies Gaußsche Zustände. Daher können deren Eigenschaften effizient berechnet werden. Mittels einer Analyse von Verschränkungsentropien und -spektren identifizieren wir Charakteristika der zugrundeliegenden CFT in 1D. In 2D finden wir Hinweise auf Randzustände. Obwohl die topologische Verschränkungsentropie verschwindet, enthält das Verschränkungsspektrum Moden, welche exponentiell am Rand lokalisiert sind.

Publications

Publications related to this thesis

1. B. Herwerth, G. Sierra, H.-H. Tu, and A. E. B. Nielsen, "Excited states in spin chains from conformal blocks", Phys. Rev. B **91**, 235121 (2015), cf. Chapter 3.

2. B. Herwerth, G. Sierra, H.-H. Tu, J. I. Cirac, and A. E. B. Nielsen, "Edge states for the Kalmeyer-Laughlin wave function", Phys. Rev. B **92**, 245111 (2015), cf. Chapter 3.

3. B. Herwerth, G. Sierra, J. I. Cirac, and A. E. B. Nielsen, "Effective description of correlations for states obtained from conformal field theory", Phys. Rev. B **96**, 115139 (2017), cf. Chapter 4.

4. B. Herwerth, G. Sierra, J. I. Cirac, and A. E. B. Nielsen, "Bosonic Gaussian states from conformal field theory", arXiv:1807.01943 (2018), submitted to Phys. Rev. B, cf. Chapter 5.

Further publications

5. J. Erdmenger, B. Herwerth, S. Klug, R. Meyer, and K. Schalm, "S-wave superconductivity in anisotropic holographic insulators", J. High Energ. Phys. **2015**, 94 (2015).

6. B. Herwerth, M. DeKieviet, J. Madroñero, and S. Wimberger, "Quantum reflection from an oscillating surface", J. Phys. B: At. Mol. Opt. Phys. **46**, 141002 (2013)

Contents

1 Introduction

1.1 Motivation

Much of the progress in modern physics like the discovery of general relativity or the formulation of the standard model of particle physics is related to a gradual, more refined understanding of the fundamental laws of nature. On the other hand, even if fundamental interactions between particles are known, the understanding of their implications can be highly challenging. Moreover, it has been argued that the knowledge of fundamental laws is not enough to arrive at an understanding of the behavior of complex systems consisting of many participants [1–3]. In condensed matter physics, the difficulty to derive the behavior of many-body systems from fundamental, microscopic laws lies in the complexity of the problem, which grows rapidly with the number of participants. More precisely, the dimension of a many-body system's Hilbert space depends exponentially on the system size. Thus, even with modern computational resources, only small systems can be solved through numerical methods without further approximations. Effective descriptions and phenomenological models are therefore common in condensed matter physics. Many of them are not derived rigorously from the underlying fundamental interactions but evolve in an interplay between experiment and theory. Within this process, new concepts, ideas, and techniques have emerged to treat complex systems consisting of multiple participants.

This thesis examines model states of quantum many-body systems using a framework that has been established in the past decades: We investigate many-body wave functions that are defined as correlators of a conformal field theory (CFT) [4–6], which is a quantum field theory with a scale invariance. This approach was pioneered by Moore and Read [7], who constructed wave functions of quantum Hall [8–10] systems from CFT.

The following subsections introduce the quantum Hall effect, explain its importance as an example of a topological phase of matter, and describe how CFT can be used to build models for these systems.

1.1.1 The quantum Hall effect

The discovery of the integer quantum Hall (IQH) [8] and of the fractional quantum Hall (FQH) [9] effects in the early 1980s initiated one of the most important developments in physics of the past decades. Quantum Hall phases occur in two-dimensional (2D) electronic systems at low temperatures that are subject to a high perpendicular magnetic field. The effective confinement of the electrons to a 2D plane can be achieved experimentally at the interface of two semiconductors of different type [11, 12]. The key experimental signature of the quantum Hall effect is the behavior of the transverse Hall resistivity ρ_{xy} and the longitudinal one, ρ_{xx}, as a function of the magnetic field B, where ρ_{xx} and ρ_{xy} are determined in a transport measurement as shown in Fig. 1.1. While classical physics predicts a linear dependence of ρ_{xy} on B, the quantum Hall effect is characterized by the formation of plateaus where ρ_{xy} is constant as a function of B to a very high precision. At these plateaus, the longitudinal resistivity ρ_{xx} vanishes, while ρ_{xy} assumes values $\rho_{xy} = \frac{1}{\nu}\frac{h}{e^2}$. Here, h is Planck's constant, e the elementary charge, and ν a rational number known as the filling fraction since it corresponds to the number of Landau levels filled by the quantum Hall state. In the IQH

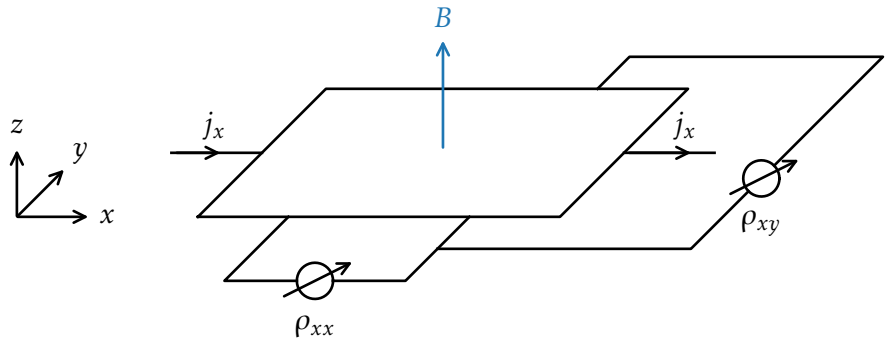

Figure 1.1: Transport measurement in a Hall experiment. Charge carriers are confined to a plane at the interface of two semiconductors. A large perpendicular magnetic field B is applied in the z direction, and a current j_x driven through the system in the x direction. The longitudinal resistivity ρ_{xx} is measured in the x and the Hall resistivity ρ_{xy} in the y direction.

effect, Landau levels are fully filled meaning that ν is an integer. Other values of ν correspond to FQH phases, which have partially filled Landau levels.

For fully filled Landau levels, it is possible to derive the observed values of the Hall resistivity at the plateaus by considering the single-electron problem [13]. The fact that the resistivity develops plateaus, where it is constant for a range of values of the magnetic field, can be explained by taking into account the effect of impurities [13, 14]. If the Fermi energy lies in the gap between two Landau levels leading to a fully filled level as in the IQH effect, there are no states close to the Fermi energy and the system is gapped. This explains the vanishing longitudinal resistivity, since $\rho_{xx} = 0$ is equivalent to having no conductance in the direction of the applied electric field [$\sigma_{xx} = \rho_{xx}/(\rho_{xx}^2 + \rho_{xy}^2)$].

This single-particle picture fails for the FQH effect, where the state is gapped even though the Landau levels are only partially filled. Interactions between the electrons are thus key and are responsible for the incompressibility of the state. Besides being inherently strongly coupled, FQH phases exhibit exotic properties like excitations with fractional charge and anyonic statistics [15–18]. These new quasiparticles are fundamentally different from those of Landau's Bose and Fermi liquid theories [19–22].

A perturbative treatment [23] of electron-electron interactions in the FQH effect is not possible due to a macroscopically large degeneracy of the Landau levels [24]. Rather, a breakthrough in the theoretical description of the FQH effect was achieved by Laughlin's trial states [10]. Laughlin showed that these are consistent with the experimental observations, have excitations with fractional charge, and provide a good variational description of the problem. His wave function represents a paradigmatic model state providing an effective description of a complex physical phenomenon that evades a direct microscopic solution due to the complexity of the many-body problem. Laughlin's state describes quantum Hall phases with filling fractions $\nu = \frac{1}{q}$, where $q \in \{1, 3, 5, \dots\}$. It was later generalized to states of other filling fractions with odd denominators through the hierarchy construction [18, 25]. This paved the way for the composite fermion theory of the FQH effect [26, 27], which interprets FQH states in terms of an IQH effect of composite fermions, new quasiparticles consisting of electrons and magnetic fluxes. Further generalizations of Laughlin's wave function [7, 28, 29] exhibit excitations with nonabelian anyonic statistics. This case is of particular interest due to its potential applications for quantum computing [30, 31].

1.1.2 The quantum Hall effect in lattices and chiral spin liquids

The experimentally observed quantum Hall effect leads to a theoretical description in terms of continuous spatial degrees of freedom. Already in the 1980s, theoretical models on lattices exhibiting quantum Hall phases were constructed. Haldane [32] showed that an IQH effect can occur in a lattice model, where time reversal symmetry is not broken through an external magnetic field. This approach was recently generalized to interacting models [33–36]. Kalmeyer and Laughlin [37, 38] studied a lattice state that is analogous to Laughlin's continuum wave function and thus corresponds to a FQH phase. We will refer to it as the Kalmeyer-Laughlin state in the following. Later, a generalization with nonabelian excitations was constructed [39]. The Kalmeyer-Laughlin state and its nonabelian version can also be characterized as chiral spin liquids, where *chiral* refers to the breaking of time-reversal symmetry. The concept of a spin liquid was introduced by Anderson [40] and later proposed to play a key role [41] in explaining high-temperature superconductivity [42]. A spin liquid is characterized by the absence of a low-temperature phase with long-range magnetic order.

Recently, there has been a great interest in lattice models due to the possibility to implement them in systems of ultracold atoms [43, 44], where interactions can be engineered experimentally. Proposals for realizing FQH states with ultracold atoms were, for example, made in Refs. [45–48]. The realization of the Hofstadter model [49] with ultracold atoms [50, 51] is an example of a recent experimental achievement in this direction.

1.1.3 Landau's theory of phases

The discovery of the quantum Hall effect led to a new paradigm in characterizing quantum matter since it cannot be understood in terms of Landau's theory of phases. The latter represents a key concept in condensed matter physics and describes second-order phase transitions in terms of symmetry-breaking [22, 52]. More precisely, it characterizes a phase transition between a disordered phase at high and an ordered phase at low temperatures by a local order parameter. In the high-temperature phase, the order parameter vanishes, while it acquires a nonzero value and thus breaks the symmetry at low temperatures. This concept is known as spontaneous symmetry breaking and also plays a central role in the standard model of particle physics in the form of the Higgs mechanism [53–55]. The transition to a superfluid phase in liquid Helium [56, 57], for example, but also ordered phases in magnets can be understood in terms of Landau's theory.

1.1.4 Topological phases of matter

Unlike in Landau's theory, there is no local, symmetry-breaking order parameter associated with quantum Hall phases [58]. Rather, they are characterized by global, topological properties. The existence of current-carrying edge states [59–65], for example, shows that topology plays an important role in these systems. Furthermore, the Hall conductance in the case of an IQH effect with a periodic potential was shown to be determined by the topology of the band structure [14]. For FQH phases, the number of ground states was shown to depend on the genus of the surface they are put on [58, 66]. This led to the new concept of topological order [58, 67].

The use of topological properties in describing phases of matter extends beyond quantum Hall physics. Already in the 1970s, Berezinskii, Kosterlitz, and Thouless [68–73] studied a phase transition in the classical 2D XY model, which is characterized by the formation of topological vortices. Haldane studied analogous quantum systems in 1D [74–76], and the corresponding topological phase is now known as the Haldane phase. It occurs in Heisenberg-type spin chains with an odd integer spin like in the exactly solvable spin-1 model studied

by Affleck, Kennedy, Lieb, and Tasaki (AKLT model) [77]. Further examples of systems with topological properties include spin liquids [78], quantum spin Hall systems [79–81], and topological insulators [82].

In the modern characterization of topological phases of matter, entanglement plays a central role [83–86]. States exhibiting long-range entanglement are said to be topologically ordered [66, 67, 87–89]. Paradigmatic models of such systems are given by Laughlin's FQH wave functions and by the Kalmeyer-Laughlin state. In contrast to topologically ordered systems, symmetry protected topological (SPT) phases exhibit topological properties but are not long-range entangled. They were recently classified in terms of group cohomology theory [88, 89]. The Haldane phase mentioned above and also topological insulators are examples of SPT systems [86, 90].

1.1.5 Conformal field theory for building model systems

A complete classification of topological phases of matter is still an open problem, but CFT in 1(+1) dimension (one spatial dimension and time) is one key ingredient for characterizing them [91, 92]. CFT is a quantum field theory with a conformal symmetry, where conformal transformations are those that leave angles invariant. In particular, this implies scale invariance, and therefore the central characteristic of a CFT is the absence of intrinsic length or energy scales. For 1(+1)-dimensional CFT, it was proven that scale invariance and conformal symmetry are equivalent [93]. Due to its inherent scale invariance, CFT is used in statistical physics to describe systems close to a phase transition [94], where the correlation length diverges. Similarly, it emerges as the low-energy effective description of 1D critical quantum systems [6]. An important CFT, which is used throughout this thesis, is given by the relativistic, massless, free boson in 1(+1) dimension. Its dispersion relation is given by $\omega_k = |k|$ and, therefore, it is gapless. We will also refer to this model as the free-boson CFT in the following.

In the context of topological systems, CFT is associated with gapless excitations at the edge. In the single-particle picture appropriate for the integer quantum Hall effect, the existence of such gapless edge modes can be understood as a consequence of the confining potential [24, 61, 95]: In the bulk, the single-particle energies are determined by the external magnetic field and are thus given by the Landau levels. Close to the edge, however, the confining potential causes the energy levels to rise, and thus there are unoccupied states close to the Fermi energy. The gapless edge excitations of a FQH system form a chiral Luttinger liquid [62], where *chiral* means that the edge modes move only in one direction and thus break time-reversal symmetry. A Luttinger liquid [96] is a model of a gapless system in 1D, and it occurs, for example, as the low-energy description of the spin-$\frac{1}{2}$ XXZ model in its critical phase [6, 97]. It can be represented through the free-boson CFT.

In addition to being associated with the gapless *edge*, CFT can also be used to describe the *bulk* of a quantum Hall system. This approach was developed by Moore and Read [7]. It is an example of a bulk-edge correspondence [7, 98, 99] and of the holographic principle [100, 101], the idea that the lower-dimensional boundary of a system contains information about the bulk. In the quantum Hall effect, this bulk-edge correspondence is also important from an experimental point of view: By measuring transport at the edge, it is possible to characterize the state and infer bulk properties like the type of quasiparticle excitations [65].

In Moore and Read's construction [7], a quantum Hall wave function is obtained as the chiral correlator of CFT primary fields. The latter are central objects in CFT and are defined as those fields that transform covariantly under conformal coordinate changes. Moore and Read showed that Laughlin's wave function, originally constructed as a variational ansatz for the ground state of a quantum Hall system in the first Landau level, is of this form. Furthermore, they defined new FQH states as CFT correlators, which have nonabelian quasiparticle excitations.

This is different from Laughlin's original wave function and the hierarchy of states derived from it. Moore and Read's construction thus provides a systematic framework for defining model states.

1.1.6 Lattice models from conformal field theory

In Moore and Read's approach, the wave function describes a system with continuous positional degrees of freedom. A similar construction was later also established for lattice systems [102], where the positions are discrete. In this approach, the wave function's degrees of freedom are spins or occupation numbers. In 1D, states of this form [102–108] were shown to describe critical systems like the ground state of the spin-$\frac{1}{2}$ XXZ model [102]. For lattices in 2D, wave functions corresponding to FQH lattice systems were obtained [109–112]. These are closely related to the Kalmeyer-Laughlin state. Similarly, lattice states corresponding to the nonabelian chiral spin liquid [39] were constructed from CFT [113].

For some lattice states defined through CFT correlators, parent Hamiltonians were constructed [109, 111–117], i.e., Hamiltonians for which the corresponding wave functions are exact ground states. In some cases, these were shown to have good overlaps with ground states of local models [39, 113, 118], which are truncations of the exact parent Hamiltonians. This led to proposals for implementations of these states in systems of ultracold atoms [118, 119].

1.2 Purpose and findings of this thesis

In this thesis, we study model states on lattices that are constructed from CFT. The purpose of this work is to characterize these states, in particular their topological properties, and to relate them to the CFT they are constructed from.

According to their definition as CFT correlators, these states have analytically given wave functions of Laughlin type. Yet, many properties like correlations and entanglement entropies are hard to evaluate for large systems due to the exponential scaling of the Hilbert space.

Therefore, it is desirable to gain conceptual insight provided by exactly solvable toy models and approximate techniques. Here, we study an exactly solvable 1D spin chain and show that its excited states directly correspond to those of the underlying CFT (Chapter 3). Furthermore, we develop an approximation of correlations for a class of FQH lattice states (Chapter 4). This results in an exactly solvable effective theory, which is a modification of the underlying CFT. Finally, we define a class of Gaussian model states from CFT, which allows us to efficiently compute and analyze correlations and entanglement entropies and relate them to those of the CFT (Chapter 5).

In such cases where an efficient, exact solution is not possible, Monte Carlo simulations can be used to compute properties of states obtained from CFT [109, 120]. Thus, much larger system sizes can be achieved than through exact numerical methods. In this thesis, we define candidates for edge states of a FQH system using the bulk-edge correspondence (Chapter 3). Through Monte Carlo simulations, we provide evidence that these indeed exhibit characteristics of edge states.

1.2.1 Excited and edge states from conformal field theory

In the first part of this thesis (Chapter 3), we study lattice states obtained from the $SU(2)_1$ Wess-Zumino-Witten (WZW) CFT. This model has an $SU(2)$ symmetry in addition to being conformally invariant, and its field content can be represented in terms of the free-boson CFT. [The subscript in $SU(2)_1$ indicates the level of the model, which is an integer characterizing a WZW theory. Throughout this thesis, we only consider the case of a WZW theory at level

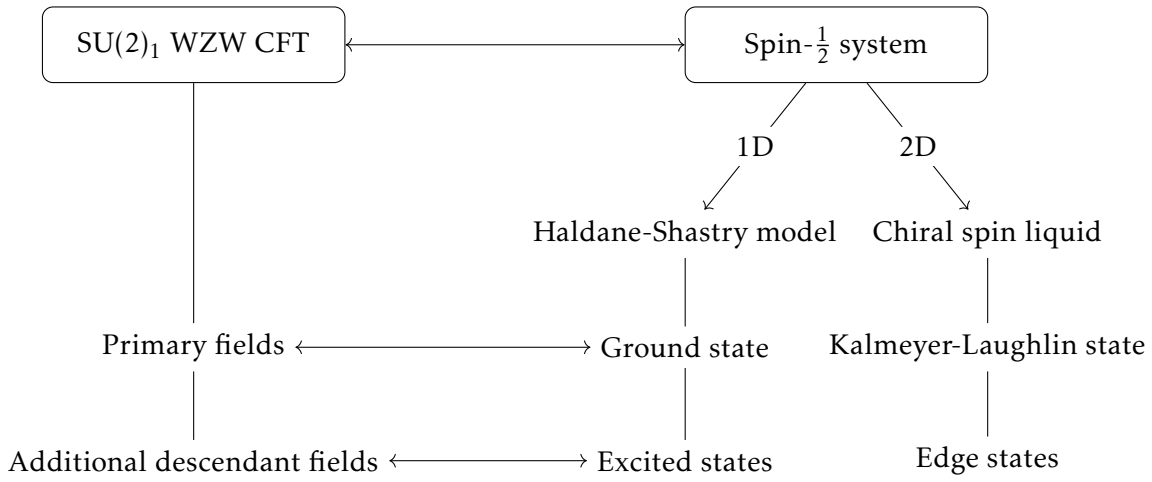

Figure 1.2: SU(2)$_1$ WZW model and its relation to the spin-$\frac{1}{2}$ states of Chapter 3. In 1D, the correlation function of primary fields yields the ground state of the Haldane-Shastry model, which is a Heisenberg-type spin chain with inverse-square interactions. In 2D, the wave function obtained from CFT primaries is equivalent to the Kalmeyer-Laughlin state of a chiral spin liquid. By adding CFT descendant fields, we construct excitations of the Haldane-Shastry model in 1D and edge states in 2D.

one.] It was shown previously [102, 103] that the wave function built from chiral primary WZW fields corresponds to the ground state of the Haldane-Shastry spin-$\frac{1}{2}$ model [121, 122] in 1D. The latter is a Heisenberg-type spin system with an interaction strength that decays with the square of the distance. It is the lattice version of the continuum Calogero-Sutherland model [123–126]. For systems in 2D, the state obtained from WZW primary fields is equivalent [109] to the Kalmeyer-Laughlin state. In this thesis, we consider states defined as the CFT correlator of primary and descendant fields. The latter generate CFT excitations, and thus we obtain a series of spin wave functions that correspond to excited states of the CFT. We show that they can be used to construct excited states of the Haldane-Shastry model in 1D. For a system in 2D, we provide evidence that they describe edge excitations with respect to the Kalmeyer-Laughlin state. This relation between the SU(2)$_1$ WZW model and the states studied in this thesis is illustrated in Fig. 1.2.

The Haldane-Shastry model is exactly solvable: Using the hidden Yangian symmetry, the complete spectrum can be obtained [127, 128]. Here, we provide an alternative way of solving the Haldane-Shastry model by exploiting its SU(2) rather than the Yangian symmetry. Our construction emphasizes the close relationship between the CFT and the Haldane-Shastry lattice model. More precisely, we map excited states of the underlying CFT to states of the spin system. We find that this map from CFT to spin states is surjective, i.e., any state of the spin-$\frac{1}{2}$ system can be obtained in this way. We show that the Haldane-Shastry model is block-diagonal in the states obtained through this map. This permits us to do a block-wise diagonalization of the smaller blocks and thus obtain analytical eigenstates for arbitrary systems sizes, which are not accessible through exact diagonalization.

We then consider the states obtained from primary fields of the SU(2)$_1$ WZW model in 2D. According to the bulk-edge correspondence, the CFT associated with the gapless edge can be used to obtain wave functions for the whole system, including the bulk. Using this idea, we define wave functions by mapping excited states of the CFT to those of the spin-$\frac{1}{2}$ system. While this map allows us to relate excitations of the CFT to those of the Haldane-Shastry

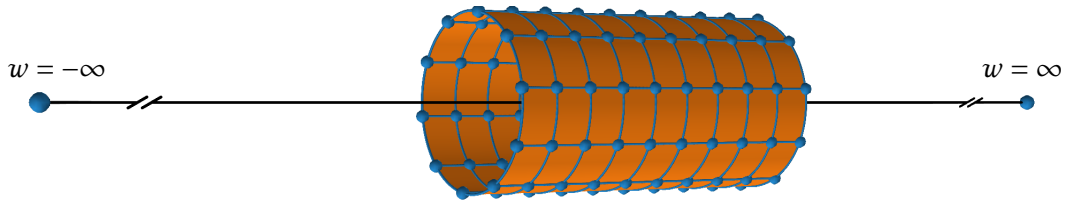

Figure 1.3: Cylinder and the points $w = -\infty$ and $w = \infty$ corresponding to the infinite left and right sides, respectively. The Kalmeyer-Laughlin state is obtained as the correlator of primary WZW fields located at the positions of a lattice on the cylinder (blue points on the orange surface). By inserting additional descendant fields at $w = -\infty$ or $w = \infty$, edge states are constructed.

chain in 1D, we investigate these states in 2D as candidates for edge modes with respect to the Kalmeyer-Laughlin wave function. The geometric interpretation of this construction on a cylinder is illustrated in Fig. 1.3. The Kalmeyer-Laughlin state is obtained as the correlator of primary fields with positions defining a lattice on the cylinder. We then insert descendant fields at positions that lie outside of the cylinder to create additional states. These positions are closest to the boundaries of the system. Therefore, the descendant fields are expected to influence the state primarily at the edges.

For states in the continuum, this map from the CFT's Hilbert space to edge states was discussed in Refs. [99, 129]. Here, we study the case of states on lattices and provide explicit evidence that these indeed describe edge modes by testing a central characteristic: that their local bulk properties are indistinguishable from those of the Kalmeyer-Laughlin state. More precisely, we perform Monte Carlo computations and compare nearest-neighbor spin-spin correlations in the bulk. We find that the relative difference between correlations of the Kalmeyer-Laughlin state and those of the tentative edge states vanishes as the system size is increased. Thus, we provide explicit evidence that they indeed describe edge modes.

It was previously shown that the Kalmeyer-Laughlin state has a large overlap with the ground state of a local spin Hamiltonian consisting of nearest-neighbor two- and three-body interactions [118]. Here, we consider the low-lying excited states of this model. Through an exact diagonalization for a small system size, we show that they have a good overlap with some edge states constructed from CFT.

1.2.2 Effective description of correlations

In a next step (Chapter 4), we investigate a more general class of states obtained from the CFT of a massless, free boson. These correspond to Laughlin wave functions on a half-filled lattice in 2D [109] and have a good overlap with the ground state of the XXZ spin-$\frac{1}{2}$ chain in 1D [102]. They are parameterized by a real, positive number, which is related to the filling of the Landau level in 2D, and corresponds to the anisotropy of the XXZ model in 1D.

Here, we link a central property of these states, namely their spin-spin correlations, to the CFT they are constructed from. We derive an exact field theory representation of the correlations, which is a path-integral average with respect to the free-boson CFT. Through a truncation of this exact expression, we arrive at an approximation of spin-spin correlations, which is efficiently computable for large lattices. The approximation corresponds to a two-point correlator in an effective model that differs from the underlying CFT through a mass-like term inserted at the positions of the lattice. We thus relate a central property of states obtained from CFT to a field theory description and interpret the correlations as a property of a model that is a modification of the underlying CFT. The structure of the effective theory for spin-spin

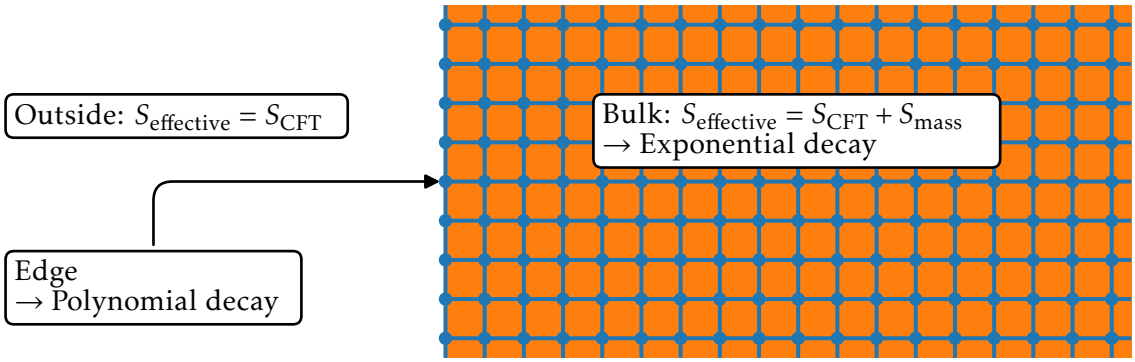

Figure 1.4: Effective action $S_{\text{effective}}$ for spin-spin correlations in states defined through correlators of the free-boson CFT. The effective action differs from the CFT action S_{CFT} by an additional mass-like term S_{mass} located at the lattice positions (blue points on the orange area). Outside of the spin-system, the effective action agrees with that of the CFT. The mass-like term leads to exponentially decaying bulk correlations, while edge correlators decay polynomially.

correlations is illustrated in Fig. 1.4.

Through an extensive comparison of actual spin-spin correlations and those of the approximation, we study the validity of our effective model. We find that it is quantitatively accurate in 1D and in 2D for a certain parameter range and that it is qualitatively correct in 2D for a larger range of parameters. In particular, we find that the approximation retains a central qualitative property of the correlations in 2D: It decays polynomially at the edge and exponentially in the bulk of a 2D system. Through our approximation, we thus provide evidence and an analytical argument for the screening hypothesis, which states that the correlations of a FQH state decay exponentially in the bulk. Within our approximation, this exponential decay is caused by the mass-like term in the effective model.

1.2.3 States with continuous spins

In a next step (Chapter 5), we investigate states with a continuous spin built as correlators of the free-boson CFT. These states have the property that their spin-spin correlations coincide with those of the approximation in our effective model. Compared to the case of discrete spins, their wave functions are Gaussian and their properties can thus be computed efficiently [130].

We use entanglement properties to characterize these continuous-spin states. In 1D, we find signatures of the underlying CFT: The entanglement entropies, spectra, and the energies of a parent Hamiltonian agree with the CFT expectation. For a system in 2D, we compute the topological entanglement entropy [84] and find that the states do not exhibit long-range entanglement and are thus not topologically ordered. However, we provide evidence for the existence of edge states through a determination and analysis of the entanglement spectrum.

1.3 Structure of this thesis

This thesis is structured as follows.

- Chapter 2 provides an introduction to CFT, explains how it can be used to describe quantum Hall states, and defines the spin-$\frac{1}{2}$ model systems studied in this thesis.

- Chapter 3 uses the $SU(2)_1$ WZW model to study excitations of 1D Haldane-Shastry chains and edge states in 2D,
- Chapter 4 studies approximation of correlations for states obtained from CFT,
- Chapter 5 investigates bosonic Gaussian states with continuous spins defined through CFT,
- and Chapter 6 concludes this thesis.

2 Conformal field theory and model systems

CFT describes systems that do not have an intrinsic energy or length scale. The microscopic interactions of nature are not of this kind since the masses of particles define energy scales. However, some physical system can be effectively described as being scale-free in certain regimes. In the context of statistical physics, for example, scale invariance occurs at a phase transition where the correlation length becomes infinite. Similarly, a quantum system at a critical point has a vanishing energy gap, which signals the absence of an energy scale. In the context of the quantum Hall effect, CFT occurs as the low-energy theory of the gapless edge [6, 62]. Moore and Read [7] showed that it can also be used to describe wave functions for the bulk of a quantum Hall system. This chapter introduces CFT, and explains how it can be used to define model states through conformal correlation functions.

This chapter is organized as follows.

- Some elements of CFT are reviewed in Sec. 2.1.
- The relation between CFT and the FQH effect is explained in Sec. 2.2.
- Sec. 2.3 defines the spin-$\frac{1}{2}$ states and lattice geometries studied in this thesis.

2.1 Conformal field theory

2.1.1 The free, massless boson and scale invariance

One of the most important systems with a conformal symmetry is that of a massless, free boson. In one spatial dimension, a free bosonic field $\varphi(x,t)$ with mass m is described by the action

$$S_m[\varphi] = \frac{1}{8\pi}\int dxdt\Big[(\partial_t\varphi(x,t))^2 - (\partial_x\varphi(x,t))^2 - m^2\varphi(x,t)^2\Big], \tag{2.1}$$

where x is the spatial, t the temporal coordinate, and we used units in which the speed of light is set to one ($c = 1$). The prefactor $\frac{1}{8\pi}$ is a convention, which is used throughout this thesis. For $m = 0$, the action is invariant under rescalings of the form $(x,t) \to (\lambda x, \lambda t)$, where $\lambda > 0$. Thus, the action does not have an intrinsic length scale for $m = 0$.

In the Hamiltonian picture, we can understand this scale invariance of the massless case as the absence of an energy gap above the ground state. Up to an additive constant, the Hamiltonian corresponding to the action $S_m[\varphi]$ assumes the form [5]

$$H_m = \int \frac{dp}{2\pi}\omega_p a_p^\dagger a_p, \tag{2.2}$$

where

$$\omega_p = \sqrt{p^2 + m^2}, \tag{2.3}$$

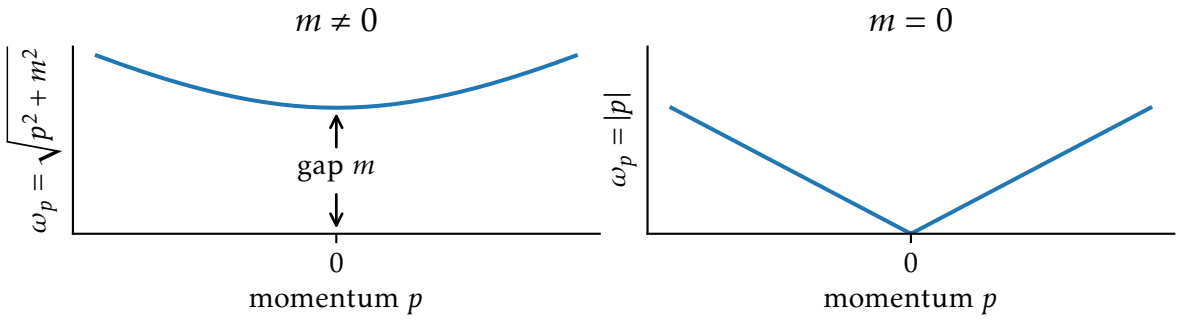

Figure 2.1: Momentum dependence of the relativistic, free boson's single-particle energies ω_p in one spatial dimension. For $m \neq 0$ (left panel), the system has a gap of size m, whereas it is gapless for $m = 0$ (right panel).

and a_p and $a_p^\dagger$ are modes of the field $\varphi(x,t)$ in momentum space satisfying the canonical commutation relations

$$\left[a_p, a_k^\dagger\right] = 2\pi\delta(p-k), \qquad \text{and } \left[a_p, a_k\right] = \left[a_p^\dagger, a_k^\dagger\right] = 0. \tag{2.4}$$

Thus, the excited state of one boson with momentum p above the particle vacuum $|0\rangle$ is given by $a_p^\dagger|0\rangle$ and has an energy of ω_p. If $m \neq 0$, the system is thus gapped since the first excited state has an energy of m corresponding to one boson with a vanishing momentum ($p = 0$). If $m = 0$, on the other hand, there is a continuum of excited states with energies directly above the ground state, and thus the system is gapless. The cases $m \neq 0$ and $m = 0$ are illustrated and contrasted in Fig. 2.1. This absence of an energy scale for $m = 0$ corresponds to the lack of a length scale observed at the level of the action.

2.1.2 Conformal invariance and primary fields

The scale invariance is part of a larger set of symmetries described by the conformal group. For a system in 1(+1) dimension, it is particularly powerful since it gives rise to an infinite number of conserved charges [131]. In this case, it was proven that scale invariance implies conformal symmetry [93], i.e., scale and conformal invariance are equivalent.

To describe the conformal group, it is useful to adopt a formulation in terms of complex numbers z corresponding to the real coordinates x and t [5]. More precisely, given an action of the form of Eq. (2.1), one first imposes periodic boundary conditions in the spatial direction, identifying x with $x + L$ for some length L. After a Wick rotation to imaginary time τ with $t = -i\tau$, the complex coordinate $z = e^{\frac{2\pi}{L}(\tau - ix)}$ and its conjugate $\bar{z} = e^{\frac{2\pi}{L}(\tau + ix)}$ are introduced.

Conformal transformations are then holomorphic maps $z \to w(z)$ and corresponding anti-holomorphic ones $\bar{z} \to \bar{w}(\bar{z})$. We illustrate the map $z \to w(z) = z^2/10$ as an example in Fig. 2.2. In general, such maps distort distances, but they leave angles invariant. A subgroup of conformal maps that is nonsingular in the complete complex plane is given by the Möbius transformations [5]

$$w(z) = \frac{az + b}{cz + d} \tag{2.5}$$

with $a, b, c, d \in \mathbb{C}$ and $ad - bc = 1$. Such maps are also called global conformal transformations.

In terms of z and $\bar{z}$, the action of the free boson for $m = 0$ assumes the form [5]

$$S_0[\varphi] = \frac{1}{4\pi} \int dz d\bar{z} \partial_z \varphi(z,\bar{z}) \partial_{\bar{z}} \varphi(z,\bar{z}). \tag{2.6}$$

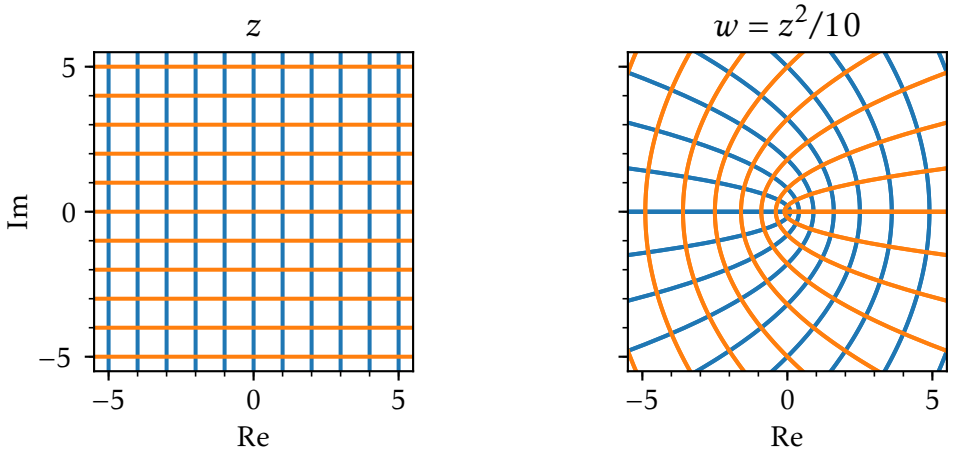

Figure 2.2: A square grid in the z plane (left panel) and its transformation to $w = z^2/10$ (right panel). The conformal map $w = z^2/10$ does not preserve distances, but it preserves angles.

Indeed, $S_0[\varphi]$ is invariant under $z \to w(z)$ and $\bar{z} \to \bar{w}(\bar{z})$ since the transformation of the differential $dzd\bar{z}$ is canceled by that of the derivatives.

The notion of a primary field expresses conformal invariance at a more general level than that of an action. Namely, a primary field with conformal scaling dimensions $h \in \mathbb{R}$ and $\bar{h} \in \mathbb{R}$ is a field $\phi_{h,\bar{h}}(z,\bar{z})$ that transforms according to [5]

$$\phi_{h,\bar{h}}(z,\bar{z}) \to \phi'_{h,\bar{h}}(w,\bar{w}) = \left(\frac{dw}{dz}\right)^{-h} \left(\frac{d\bar{w}}{d\bar{w}}\right)^{-\bar{h}} \phi(z,\bar{z}) \tag{2.7}$$

for $z \to w(z)$ and $\bar{z} \to \bar{w}(\bar{z})$. In analogy to a primary field, one defines a chiral primary field $\phi_h(z)$ with conformal scaling dimension $h \in \mathbb{R}$. It only depends on the chiral coordinate z and transforms according to

$$\phi_h(z) \to \phi'_h(w) = \left(\frac{dw}{dz}\right)^{-h} \phi(z). \tag{2.8}$$

A quasiprimary field is defined analogously to a primary field with the difference that the transformation of Eq. (2.7) is only required to be satisfied for global conformal transformations [Eq. (2.5)].

The Laurent modes $\phi^{(n,\bar{n})}_{h,\bar{h}}$ of a (quasi)primary field are defined through the expansion [5]

$$\phi_{h,\bar{h}}(z,\bar{z}) = \sum_{n,\bar{n}\in\mathbb{Z}} \phi^{(n,\bar{n})}_{h,\bar{h}} z^{-n-h} \bar{z}^{-\bar{n}-\bar{h}}. \tag{2.9}$$

2.1.3 Generators of the conformal group and the central charge

Infinitesimal generators of conformal transformations of primary fields are given by operators L_n and $\bar{L}_n$ for $n \in \mathbb{Z}$. They satisfy the Virasoro algebra [5]

$$[L_m, L_n] = (m-n)L_{m+n} + \frac{c}{12} m(m^2-1)\delta_{n+m,0}, \tag{2.10}$$

$$\left[\bar{L}_m, \bar{L}_n\right] = (m-n)\bar{L}_{m+n} + \frac{c}{12} m(m^2-1)\delta_{n+m,0}, \tag{2.11}$$

and

$$\left[L_m, \bar{L}_n\right] = 0, \tag{2.12}$$

where δ_{mn} is the Kronecker delta. The number c occurring in these equations is known as the central charge. It is a key characteristic of a given CFT. The CFT of a massless, free boson, which is used throughout this thesis, has $c = 1$.

We note that the operators L_n and $\bar{L}_n$ are the Laurent modes of the holomorphic and antiholomorphic parts of the energy momentum tensor of a CFT [5]:

$$T(z) = \sum_{n\in\mathbb{Z}} z^{-n-2} T_n, \qquad \text{and } \bar{T}(\bar{z}) = \sum_{n\in\mathbb{Z}} \bar{z}^{-n-2} \bar{T}_n. \tag{2.13}$$

The fields $T(z)$ and $\bar{T}(\bar{z})$ are quasiprimaries of dimension 2.

2.1.4 Primary fields for the CFT of a free boson

The free boson field $\varphi(z,\bar{z})$ of Eq. (2.6) is not a primary field. However, an infinite number of primary fields with scaling dimensions $h = \bar{h} = \frac{\beta^2}{2}$ for $\beta \in \mathbb{R}$ can be constructed from it, namely the vertex operators $:e^{i\beta\varphi(z,\bar{z})}:$, where the colons stand for normal ordering.

The correlation function of N vertex operators at positions $z_1,\dots,z_N$ in the complex plane and parameters $\beta_1,\dots,\beta_N \in \mathbb{R}$ assumes the form [5]

$$\langle :e^{i\beta_1\varphi(z_1,\bar{z}_1)}: \cdots :e^{i\beta_N\varphi(z_N,\bar{z}_N)}:\rangle = \delta_\beta \prod_{i<j}^{N} \left|z_i - z_j\right|^{2\beta_i\beta_j}, \tag{2.14}$$

where $\delta_\beta = 1$ if $\beta_1 + \cdots + \beta_N = 0$ and $\delta_\beta = 0$ otherwise, and $\langle \dots \rangle$ denotes the radial-ordered expectation value in the CFT ground state. (A time-ordered operator product becomes a radial-ordered one in terms of complex coordinates.) The right-hand side of Eq. (2.14) can be interpreted as the exponential of the potential energy of N charged particles in 2D with charges being proportional to β_i [5]. For this reason, the requirement $\beta_1 + \cdots + \beta_N = 0$ is also known as the *charge neutrality condition*.

Likewise, one can construct a set of chiral primary fields with scaling dimensions $h = \frac{\beta^2}{2}$ as the exponential $:e^{i\beta\varphi(z)}:$. Here, $\varphi(z)$ is the chiral part of the free boson field defined through the decomposition $\varphi(z,\bar{z}) = \varphi(z) + \bar{\varphi}(\bar{z})$ into a chiral field $\varphi(z)$ and an antichiral field $\bar{\varphi}(\bar{z})$. The correlation function of N chiral vertex operators in the complex plane is given by [5]

$$\langle :e^{i\beta_1\varphi(z_1)}: \cdots :e^{i\beta_N\varphi(z_N)}:\rangle = \delta_\beta \prod_{i<j}^{N} \left(z_i - z_j\right)^{\beta_i\beta_j}. \tag{2.15}$$

This equation is central for the construction of wave functions from CFT in Secs. 2.2 and 2.3 below.

Additional primary fields of the free-boson CFT are given by $-i\partial\varphi(z)$ and $-i\bar{\partial}\bar{\varphi}(\bar{z})$, which are the Noether currents corresponding to the symmetry of the action $S_0[\varphi]$ of Eq. (2.6) under a shift of the bosonic field by a constant [$\varphi(z,\bar{z}) \to \varphi(z,\bar{z}) + \text{const.}$].

2.1.5 The free-boson CFT as a low-energy effective theory

In condensed matter physics, a description in terms of CFT occurs as the low-energy effective theory of 1D gapless systems. An example is given by the XXZ spin chain, which has the

Hamiltonian

$$H_{XXZ} = \sum_{j=1}^{N} \left(t_j^x t_{j+1}^x + t_j^y t_{j+1}^y + \Delta t_j^z t_{j+1}^z \right), \tag{2.16}$$

where t_j^a for $a \in \{x, y, z\}$ are N spin-$\frac{1}{2}$ operators, and we define $t_{N+1}^a = t_1^a$ for periodic boundary conditions. For values $-1 < \Delta \leq 1$, this model is in a critical phase [6].

Through the method of bosonization [6, 97, 132, 133], the low-energy physics of the XXZ model can be formulated in terms of the CFT of a free, massless boson. To this end, one first transforms the spin model H_{XXZ} into a fermionic one through a Jordan-Wigner transformation [6]:

$$H_{\text{fermionic}} = \sum_{j=1}^{N} \left[\frac{1}{2} \left(a_j^\dagger a_{j+1} + a_{j+1}^\dagger a_j \right) + \Delta \left(a_j^\dagger a_j - \frac{1}{2} \right) \left(a_{j+1}^\dagger a_{j+1} - \frac{1}{2} \right) \right], \tag{2.17}$$

where a_j and $a_j^\dagger$ are fermionic annihilation and creation operators satisfying the anticommutation relations

$$\left\{ a_i, a_j^\dagger \right\} = \delta_{ij}, \qquad \text{and} \quad \left\{ a_i, a_j \right\} = 0. \tag{2.18}$$

(The Hamiltonian $H_{\text{fermionic}}$ is equal to H_{XXZ} up to a term that modifies the boundary condition between the sites N and 1 so that $H_{\text{fermionic}}$ is periodic with respect to the fermionic operators, cf. Ref. [134].) The case $\Delta = 0$ thus corresponds to free fermions with a dispersion relation of $\omega_k = \cos(2\pi k/N)$ for $k \in \{0, \ldots, N-1\}$ obtained from a Fourier transform of the Hamiltonian.

At half filling, the ground state for $\Delta = 0$ is thus the Fermi sea filled with particles up to the energy 0. A representation in terms of continuous fields for left- and right-moving fermions corresponding to excitations near the two Fermi points leads to a model of continuous, interacting fermions [97]. Remarkably, this fermionic model can be represented in terms of a model of non-interacting bosons [135]. The resulting model is that of a free, massless boson [6, 97]. As a result, the spin-spin correlation functions of the XXZ model can be expressed in terms of correlators of corresponding CFT [97, 136].

Further 1D systems that have a CFT description at low energies include the Luttinger model [96, 137] of 1D electrons, and impurity problems [138, 139], cf. Ref. [6] for a review.

2.2 Quantum Hall model states from conformal field theory

In Sec. 2.1, we introduced CFT and explained how it arises as the low-energy effective theory for critical systems in 1D. Moreover, CFT can also be used to obtain variational states, most importantly for FQH systems, which will be discussed below. The use of CFT in describing a quantum Hall state was introduced by Moore and Read [7, 140], who realized that Laughlin's wave function [10] and generalizations thereof can be obtained as the correlator of primary fields in a CFT.

Laughlin's wave function is a variational ansatz for a quantum Hall fluid with a filling fraction ν of the lowest Landau level [10]:

$$\psi_{\text{Laughlin}}(Z_1, \ldots, Z_M) = \prod_{i<j}^{M} \left(Z_i - Z_j \right)^{\frac{1}{\nu}} e^{-\frac{1}{4} \sum_{j=1}^{M} |Z_j|^2}, \tag{2.19}$$

where $Z_1, \ldots, Z_M$ are positions of electrons in the complex plane, and $\frac{1}{\nu}$ is a positive, odd integer. The magnetic length was set to one in Eq. (2.19), which can be achieved through an

appropriate choice of coordinates $Z_1,\dots,Z_M$. The fact that $\psi_{\text{Laughlin}}(Z_1,\dots,Z_M)$ is a product of an analytic function and a Gaussian factor follows from solving the single-particle problem in the lowest Landau level. The precise form of the wave function, however, was proposed by Laughlin on the basis of the variational principle.

Moore and Read found that Laughlin's wave function can be constructed as the correlator of vertex operators in the CFT of a free boson [7, 99, 141]:

$$\psi_{\text{Laughlin}}(Z_1,\dots,Z_M) = e^{-\frac{1}{4}\sum_{j=1}^{M}|Z_j|^2}\langle M| : e^{\frac{i}{\sqrt{\nu}}\varphi(Z_1)} : \cdots : e^{\frac{i}{\sqrt{\nu}}\varphi(Z_M)} : |0\rangle, \tag{2.20}$$

where $\varphi(z)$ is the chiral part of a free, massless boson field (cf. Sec. 2.1.4), $|0\rangle$ is the CFT ground state and $\langle M|$ is a charged CFT state that compensates for the excess charge of the M vertex operators so that the charge neutrality condition is satisfied [99]. The wave function for a quasihole at position w can be described within this construction [7] by adding a vertex operator $: e^{i\sqrt{\nu}\phi(w)} :$ into the correlator of Eq. (2.20).

More generally, Moore and Read constructed FQH states as CFT correlators of fields that belong to a charge and a statistics sector [7, 99]. In this way, Halperin's states [142] and also wave functions with nonabelian statistics [7] were obtained.

In the context of lattice systems, a similar construction to that of Moore and Read can be made [102, 103]. In this case, one considers fixed complex positions $z_1,\dots,z_N$ that define a lattice. A state of discrete degrees of freedom is then obtained by defining its wave function as a CFT correlator of primary fields. In particular, wave functions that are lattice versions of the continuous Laughlin states introduced above were studied in Refs. [109–111]:

$$\begin{aligned} |\psi_{\mu,\nu}\rangle &= \sum_{n_1,\dots,n_N} \psi_{\mu,\nu}(n_1,\dots,n_N)|n_1,\dots,n_N\rangle, \\ \psi_{\mu,\nu}(n_1,\dots,n_N) &= \chi_{\boldsymbol{n}}\langle : e^{i\frac{1}{\sqrt{\nu}}(n_1-\mu)\varphi(z_1)} : \cdots : e^{i\frac{1}{\sqrt{\nu}}(n_N-\mu)\varphi(z_N)} :\rangle \end{aligned} \tag{2.21}$$

where $|n_1,\dots,n_N\rangle$ is the occupation number basis, $n_j \in \{0,1\}$ corresponding to hard-core particles for which double occupancies are forbidden, $\delta_{\boldsymbol{n}} = 1$ if $n_1+\cdots+n_N = \mu N$ and $\delta_{\boldsymbol{n}} = 0$ otherwise, and $\chi_{\boldsymbol{n}} = \prod_{p=1}^{N}\chi_{p,n_p}$ with $|\chi_{p,n_p}| = 1$ is a product of single-particle phase factors. The rational parameter μ corresponds to the number of particles per lattice site and should be chosen so that μN is an integer. The filling fraction of the first Landau level is given by ν. This becomes apparent by relating $|\psi_{\mu,\nu}\rangle$ to the Laughlin state introduced above. Using Eq. (2.15), the wave function becomes

$$\psi_{\mu,\nu}(n_1,\dots,n_N) \propto \tilde{\chi}_{\boldsymbol{n}}\delta_{\boldsymbol{n}}\prod_{i<j}\left(z_i-z_j\right)^{\frac{1}{\nu}n_in_j}\prod_{i\neq j}\left(z_i-z_j\right)^{-\frac{\mu}{\nu}n_i}, \tag{2.22}$$

where

$$\tilde{\chi}_{\boldsymbol{n}} = \prod_{p=1}^{N}\chi_{p,n_p}e^{-i\frac{\mu}{n}n_p\sum_{q=1}^{p-1}\left[\arg(z_p-z_q)-\arg(z_q-z_p)\right]} \tag{2.23}$$

is another product of single-particle phase factors. It was shown [109, 110] that $\psi_{\mu,\nu}(n_1,\dots,n_N)$ coincides with the Laughlin wave function $\psi_{\text{Laughlin}}(Z_1,\dots,Z_M)$ of Eq. (2.19) in the thermodynamic limit and up to single-particle phase factors, where $Z_1,\dots,Z_M$ with $Z_i \in \{z_1,\dots,z_N\}$ are the occupied positions, i.e., those having $n_i = 1$. Thus, $\psi_{\mu,\nu}(n_1,\dots,n_N)$ describes bosons if ν^{-1} is even, fermions if ν^{-1} is odd, and anyons otherwise, cf. Ref. [143], which studies the anyonic case.

2.3 Model systems studied in this thesis

In Chapters 3 and 4 of this thesis, we study the lattice Laughlin states $|\psi_{\mu,\nu}\rangle$ of Eq. (2.21) on a half-filled lattice, which corresponds to $\mu = \frac{1}{2}$. Furthermore, we map the hard-core particles with occupation numbers $n_j \in \{0,1\}$ to spin-$\frac{1}{2}$ degrees of freedom $s_j = 2n_j - 1 \in \{-1,1\}$. ($s_j$ is two times the spin-z eigenvalue at lattice position j.)

Defining the positive number $\alpha = \frac{1}{4\nu}$ and setting $\mu = \frac{1}{2}$, this leads to the states

$$|\psi_\alpha\rangle = \sum_{s_1,\ldots,s_N} \psi_\alpha(s_1,\ldots,s_N)|s_1,\ldots,s_N\rangle, \tag{2.24}$$

$$\begin{aligned}\psi_\alpha(s_1,\ldots,s_N) &= \chi_{\boldsymbol{s}}\langle : e^{i\sqrt{\alpha}s_1\varphi(z_1)} : \cdots : e^{i\sqrt{\alpha}s_N\varphi(z_N)} :\rangle \\ &= \delta_{\boldsymbol{s}}\chi_{\boldsymbol{s}} \prod_{m<n}(z_m - z_n)^{\alpha s_m s_n},\end{aligned} \tag{2.25}$$

where $s_j \in \{-1,1\}$, $\delta_{\boldsymbol{s}} = 1$ if $s_1 + \cdots + s_N = 0$ and $\delta_{\boldsymbol{s}} = 0$ otherwise, and $\chi_{\boldsymbol{s}} = \prod_{p=1}^N \chi_{p,s_p}$ is a product of single particle phase factors. The basis states $|s_1,\ldots,s_N\rangle$ in Eq. (2.24) are products of eigenstates of the spin-z operator t_j^z at lattice position j:

$$|s_1,\ldots,s_N\rangle = |s_1\rangle \otimes \cdots \otimes |s_N\rangle \tag{2.26}$$

with

$$t_j^z|s_j\rangle = \frac{s_j}{2}|s_j\rangle. \tag{2.27}$$

2.3.1 Definition of geometries and lattices

The positions z_j for $j \in \{1,\ldots,N\}$ in Eq. (2.25) define a lattice in the complex plane and are parameters of the wave function $\psi_\alpha(s_1,\ldots,s_N)$. [For simplicity of notation, we suppress the parametric dependence of $\psi_\alpha(s_1,\ldots,s_N)$ on $z_1,\ldots,z_N$.]

In this thesis, we mostly consider the following geometries: (1) a uniform 1D lattice with periodic boundary conditions, (2) a square lattice on the cylinder, and (3) an approximately uniform distribution of points on the sphere. In the following, we explain how these geometries can be described in terms of coordinates z_j in the complex plane.

Uniform 1D lattice with periodic boundary conditions (circle)

The uniform 1D lattice with periodic boundary conditions is illustrated in the left panel of Fig. 2.3. It is described by N complex numbers z_j on the unit circle:

$$z_j = e^{\frac{2\pi i}{N}j} \tag{2.28}$$

for $j \in \{1,\ldots,N\}$.

Square lattice on the cylinder

Positions on a cylinder of length 2π in the periodic direction can be described through complex numbers w, where w is identified with $w + 2\pi i n$ for any integer n.

The positions w can be mapped onto the complex plane through the exponential $z = e^w$ as illustrated in Fig. 2.4. According to the transformation rules for primary fields under a

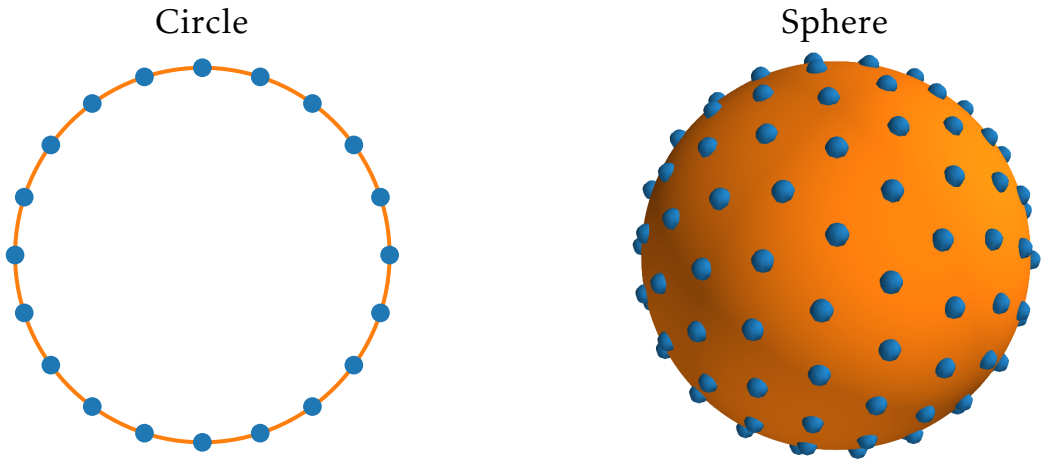

Figure 2.3: Left panel: Uniform 1D lattice with periodic boundary conditions. Right panel: Approximately uniform distribution of points on the sphere. The positions on the sphere were computed numerically by minimizing $f_{\min}(\Omega_1,\ldots,\Omega_N)$ of Eq. (2.33).

conformal map (cf. Sec. 2.1.2), the correlation function of vertex operators on the cylinder becomes

$$\langle : e^{i\sqrt{\alpha}s_1\varphi(w_1)} : \cdots : e^{i\sqrt{\alpha}s_N\varphi(w_N)} : \rangle = \left(\prod_{j=1}^{N} z_j^{\frac{\alpha}{2}}\right) \langle : e^{i\sqrt{\alpha}s_1\varphi(z_1)} : \cdots : e^{i\sqrt{\alpha}s_N\varphi(z_N)} : \rangle, \tag{2.29}$$

where $z_j = e^{w_j}$, and it was used that all vertex operators $: e^{i\sqrt{\alpha}s_j\varphi(z_j)} :$ have a scaling dimension of $\frac{\alpha}{2}$. The correlator of primary fields on the cylinder thus agrees with that on the plane up to a prefactor that depends on the positions z_j but not on the spins $s_j \in \{-1,1\}$.

Therefore, the wave function $\psi_\alpha(s_1,\ldots,s_N)$ on the cylinder can be defined by projecting the positions w_j onto the complex plane through $z_j = e^{w_j}$ and evaluating the CFT correlator on the plane as in Eq. (2.25).

The square lattice on the cylinder with N_x sites in the open and N_y sites in the periodic direction is then given by

$$z_j \equiv z_{j_x j_y} = e^{\frac{2\pi}{N_y}(j_x + i j_y)}, \tag{2.30}$$

where $j_x \in \{1,\ldots,N_x\}$ is the x and $j_y \in \{1,\ldots,N_y\}$ the y component of the index $j \in \{1,\ldots,N_xN_y\}$ [$j = (j_x-1)N_y + j_y$]. Throughout this thesis, we use a double-index notation as in Eq. (2.30) for the x and y components of the index j, whenever this is convenient.

Approximately uniform distribution of points on the sphere

Let us consider N positions on the sphere described by pairs of angular variables $\Omega_j = (\theta_j, \phi_j)$, where θ_j the polar and ϕ_j the azimuthal angle. A unit vector

$$\mathbf{n}_{\Omega_j} = \begin{pmatrix} \sin(\theta_j)\cos(\phi_j) \\ \sin(\theta_j)\sin(\phi_j) \\ \cos(\theta_j) \end{pmatrix} \in S^2 \tag{2.31}$$

can be mapped onto the complex plane through the stereographic projection

$$z_j = \tan\left(\frac{\theta_j}{2}\right) e^{-i\phi_j}. \tag{2.32}$$

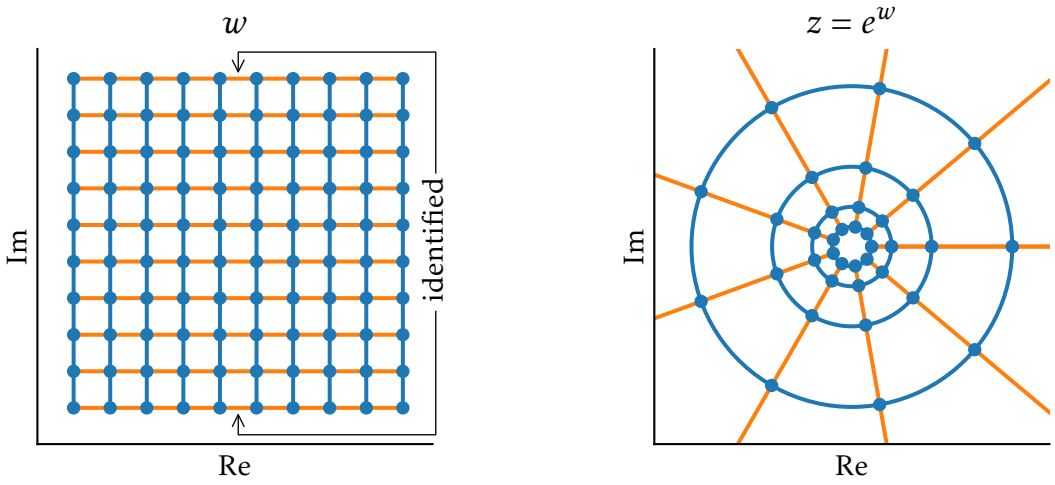

Figure 2.4: Mapping from a square lattice on the cylinder (left panel) to the complex plane (right panel) through the exponential. The lines with a constant position in the open direction of the cylinder become concentric circles in the complex plane (blue curves). The position along the open direction of the cylinder corresponds to the radial distance in the complex plane (orange lines).

We thus define the wave function $\psi_\alpha(s_1,\ldots,s_N)$ on the sphere through the projected coordinates z_j on the plane.

It is not possible to put a square lattice onto the sphere due to the sphere's curvature. Instead, we follow Ref. [109] and determine the angular variables $\Omega_j = (\theta_j, \phi_j)$ of an approximately uniform distribution of points by numerically minimizing the function

$$f_{\min}(\Omega_1,\ldots,\Omega_N) = \sum_{m<n}^{N} \frac{1}{\left|\mathbf{n}_{\Omega_m} - \mathbf{n}_{\Omega_n}\right|^2}. \tag{2.33}$$

A resulting distribution of points on the sphere is plotted in the right panel of Fig. 2.3.

3 Excited and edge states obtained from the $SU(2)_1$ Wess-Zumino-Witten model

This chapter considers spin states built from correlation functions of the $SU(2)_1$ WZW CFT. In 1D, the wave function obtained from primary fields of the CFT is the ground state of the Haldane-Shastry model [121, 122], whereas it is equivalent to the Kalmeyer-Laughlin [37, 38] state in 2D. We construct a tower of spin states that is derived from the excited states of the CFT by adding WZW currents, i.e., descendant fields.

In the first part of this chapter, we use these states to construct eigenstates of the Haldane-Shastry model. Previous solutions of the Haldane-Shastry spin chain were based on polynomial functions in the particle basis [121, 144] or exploited the hidden Yangian symmetry [127, 128]. The main motivation for our construction is to show that there is a close relationship between the $SU(2)_1$ WZW model and the Haldane-Shastry chain: As anticipated in Ref. [127], we show that the excited states of the CFT generated by the current algebra are in correspondence with the eigenstates of the Haldane-Shastry model. For the case of an even number of spins, we establish this relationship by demonstrating that the Haldane-Shastry Hamiltonian is block-diagonal in terms of the states containing WZW currents. This allows us to construct eigenstates block-wise, and we derive analytical solutions for states up to order eight in current operators. Through numerical computations, we provide evidence that a similar construction is possible for the case of an odd number of sites and for the Haldane-Shastry chain with open boundary conditions [145, 146], which was recently obtained from CFT in Ref. [108].

The second part of this chapter is devoted to an analysis in 2D. We use the states obtained by inserting additional descendant fields as candidates for edge states with respect to the Kalmeyer-Laughlin wave function. A similar correspondence between CFT states and edge modes of a FQH system was studied in Refs. [99, 129] for wave functions with continuous spatial degrees of freedom. The goal of this work is to provide explicit numerical evidence for the lattice case that these states indeed describe edge modes. We use the criterion that local bulk properties should be indistinguishable for large enough system sizes. Through Monte Carlo simulations, we determine nearest-neighbor bulk correlation functions and find that those of the tentative edge states approach the correlations of the Kalmeyer-Laughlin state as the system size increases. This confirms the bulk-edge correspondence: The CFT associated with the gapless edge can be used to construct wave functions of the bulk.

It was found previously that the state obtained from primary fields of the WZW model has a good overlap with the ground state of a local Hamiltonian [118]. Here, we use exact diagonalization to show that the low-lying excitations of that Hamiltonian are well-approximated by some edge states constructed from CFT.

This chapter is structured as follows.

- Sec. 3.1 defines spin states as correlators of primary fields and introduces the map from CFT excited states to spin wave functions.
- In Sec. 3.2, we discuss global transformation properties of these states on the cylinder and on the circle.
- Sec. 3.3 constructs excited states of the Haldane-Shastry model,

- Sec. 3.4 studies edge states for the Kalmeyer-Laughlin wave function,
- and Sec. 3.5 concludes this chapter.

Most of the rest of this chapter and the corresponding appendices are adaptations of the following previously published work:

- B. Herwerth, G. Sierra, H.-H. Tu, and A. E. B. Nielsen, "Excited states in spin chains from conformal blocks", Phys. Rev. B **91**, 235121 (2015), ©2015 American Physical Society (Ref. [147]),
- B. Herwerth, G. Sierra, H.-H. Tu, J. I. Cirac, and A. E. B. Nielsen, "Edge states for the Kalmeyer-Laughlin wave function", Phys. Rev. B **92**, 245111 (2015), ©2015 American Physical Society (Ref. [148]).

3.1 Spin states from the $SU(2)_1$ Wess-Zumino-Witten model

This section defines the states studied in this chapter through correlation functions of the $SU(2)_1$ WZW CFT. In particular, we describe a map from states of the CFT to those of a spin-$\frac{1}{2}$ system. The basic idea of constructing spin states from CFT is illustrated in Table 3.1.

Table 3.1: Map from states of the $SU(2)_1$ WZW model to wave functions of a spin-$\frac{1}{2}$ system. We map the CFT ground state $|0\rangle$ to a wave function constructed from primary fields $\phi_{s_j}(z_j)$. CFT excited states are generated by modes of the descendant field $J^a(z)$. By mapping these to states of the spin-$\frac{1}{2}$ system, we obtain excited states of the Haldane-Shastry model in 1D (see Sec. 3.3) and edge states in 2D (see Sec. 3.4).

	CFT		Spin system
Ground state	$\|0\rangle$	$\leftrightarrow$	$\langle 0\|\phi_{s_1}(z_1)\dots\phi_{s_N}(z_N)\|0\rangle$
	$\downarrow$		$\downarrow$
Excited/edge states	$\left(J^{a_l}_{-n_l}\dots J^{a_1}_{-n_1}\right)(0)\|0\rangle$	$\leftrightarrow$	$\langle 0\|\phi_{s_1}(z_1)\dots\phi_{s_N}(z_N)\left(J^{a_l}_{-n_l}\dots J^{a_1}_{-n_1}\right)(0)\|0\rangle$

3.1.1 States from $SU(2)_1$ Wess-Zumino-Witten primary fields

In this chapter, we study the case $\alpha = \frac{1}{2}$ of the spin-$\frac{1}{2}$ model states $|\psi_\alpha\rangle$ introduced in Sec. 2.3. The primary fields that define $|\psi_\alpha\rangle$ for $\alpha = \frac{1}{2}$ are not only conformally invariant, but they also have an SU(2) symmetry. More precisely, they are primary fields of the $SU(2)_1$ WZW model. Let us briefly review some properties of this model and then explain how $|\psi_\alpha\rangle$ for $\alpha = \frac{1}{2}$ can be constructed from it.

WZW models [149, 150] are conformal field theories with an additional structure of a Lie algebra. In the case of the $SU(2)_1$ model, the Lie algebra is spanned by the spin operators t^a for $a \in \{x, y, z\}$, which are related to the Pauli matrices σ^a through $t^a = \frac{\sigma^a}{2}$. Their algebra is given by

$$\left[t^a, t^b\right] = i\varepsilon_{abc}t^c, \tag{3.1}$$

where ε_{abc} is the Levi-Civita symbol. (For indices $c \in \{x, y, z\}$, we adopt the Einstein summation convention unless explicitly stated otherwise.)

At the level of the field theory, the Lie algebra is represented by modes J^a_n of the current $J^a(z)$ defined through the Laurent expansion

$$J^a(z) = \sum_{n=-\infty}^{\infty} z^{-n-1} J^a_n. \tag{3.2}$$

The field $J^a(z)$ is a conformal, chiral primary of dimension $h = 1$. The algebra formed by its modes J^a_n is known as a Kac-Moody algebra [151], and it given by:

$$\left[J^a_m, J^b_n\right] = i\varepsilon_{abc} J^c_{m+n} + \frac{m}{2}\delta_{ab}\delta_{m+n,0}. \tag{3.3}$$

The zero modes J^a_0 have the same commutation relations as t^a.

Chiral WZW primary fields are conformal primaries that additionally transform covariantly with respect to the symmetry of the Kac-Moody algebra. In addition to the identity, the SU(2)$_1$ WZW model has one chiral primary field $\phi_s(z)$ with scaling dimension $h = \frac{1}{4}$, where z is a complex number, and $s \in \{-1, 1\}$ denotes the two components of the field $\phi_s(z)$. The SU(2) symmetry of $\phi_s(z)$ is expressed by the operator product expansion (OPE) [151]

$$J^a(z)\phi_s(w) = -\frac{1}{z-w}\sum_{s'} t^a_{ss'}\phi_{s'}(w) + \ldots, \tag{3.4}$$

where the dots stand for terms that are finite for $z \to w$.

The WZW primary field $\phi_s(z)$ and the current $J^a(z)$ can be represented in term of the chiral part $\varphi(z)$ of a free, massless boson as

$$\phi_s(z) = e^{\frac{i\pi}{2}(q-1)(s+1)} : e^{\frac{i}{\sqrt{2}}s\varphi(z)} :, \tag{3.5}$$

$$J^z(z) = -\frac{i}{\sqrt{2}}\partial_z\varphi(z), \tag{3.6}$$

and

$$J^{\pm}(z) = J^x(z) \pm iJ^y(z) = e^{i\pi(q-1)} : e^{\mp i\sqrt{2}\varphi(z)} :, \tag{3.7}$$

where the colons denote normal ordering, and $q \in \{0, 1\}$ corresponds to the two sectors of the WZW CFT. ($q = 0$ if $\phi_s(z)$ acts on a state with an even number of modes of the $h = \frac{1}{4}$ primary field and $q = 1$ otherwise.)

The Hilbert space of the SU(2)$_1$ WZW model is generated by modes of the current $J^a(z)$ and contains two sectors corresponding to the two primary fields. The identity sector is spanned by vectors [152]

$$\left(J^{a_l}_{-n_l} \ldots J^{a_1}_{-n_1}\right)(0)|0\rangle, \tag{3.8}$$

where $|0\rangle$ is the CFT vacuum, n_j are positive mode numbers, and $a_j \in \{x, y, z\}$. A state in the sector corresponding to the primary field $\phi_s(z)$ is a linear combination of vectors

$$\left(J^{a_l}_{-n_l} \ldots J^{a_1}_{-n_1}\phi_s\right)(0)|0\rangle, \tag{3.9}$$

where $s \in \{-1, 1\}$. Using the Kac-Moody algebra of Eq. (3.3), one can choose a basis for which the mode numbers in Eqs. (3.8) and (3.9) are ordered, $n_l \geq n_{l-1} \geq \cdots \geq n_1 > 0$.

According to the free-boson representation [Eq. (3.5)], the correlator of N WZW primary fields agrees with the wave function of $|\psi_\alpha\rangle$ for $\alpha = \frac{1}{2}$ [Eq. (2.25)]. In this chapter, we use the notation $|\psi_0\rangle$,

$$|\psi_0\rangle \equiv |\psi_{\alpha=\frac{1}{2}}\rangle, \tag{3.10}$$

for this state. The motivation for this notation is that $|\psi_0\rangle$ is the state with respect to which we will consider excitations in 1D and edge modes in 2D. In terms of WZW primary fields, $|\psi_0\rangle$ is given by

$$|\psi_0\rangle = \sum_{s_1,\ldots,s_N} \psi_0(s_1,\ldots,s_N)|s_1,\ldots,s_N\rangle, \tag{3.11}$$

$$\psi_0(s_1,\ldots,s_N) = \langle \phi_{s_1}(z_1)\ldots\phi_{s_N}(z_N)\rangle = \delta_{\boldsymbol{s}}\chi_{\boldsymbol{s}}\prod_{i<j}^{N}(z_i-z_j)^{\frac{1}{2}s_is_j}, \tag{3.12}$$

where

$$\chi_{\boldsymbol{s}} = \prod_{p=1}^{N} e^{\frac{i\pi}{2}(p-1)(s_p+1)} \tag{3.13}$$

is the Marshall sign factor.

While we left $\chi_{\boldsymbol{s}}$ unspecified in the definition of $|\psi_\alpha\rangle$ (Sec. 2.3), the representation in terms of WZW primary fields leads to the Marshall sign of Eq. (3.13). As a consequence, $|\psi_0\rangle$ is a singlet of the total spin [103]:

$$T^a|\psi_0\rangle = 0, \tag{3.14}$$

where

$$T^a = t_1^a + \cdots + t_N^a. \tag{3.15}$$

Table 3.2: Summary of the different towers of states obtained by insertion of current operator modes. Using the OPE between $\phi_s(z)$ and $J^a(z)$, the wave functions for these states can be written as the application of l spin operators $u^{a_j}_{-n_j}$ [cf. Eq. (3.25)] to the state without current operators.

	Tower of states	See Eq.
N even	$\langle \phi_{s_1}(z_1)\ldots\phi_{s_N}(z_N)\left(J^{a_l}_{-n_l}\ldots J^{a_1}_{-n_1}\right)(0)\rangle$	(3.17)
N even	$\langle \phi_{s_\infty}(\infty)\phi_{s_1}(z_1)\ldots\phi_{s_N}(z_N)\left(J^{a_l}_{-n_l}\ldots J^{a_1}_{-n_1}\phi_{s_0}\right)(0)\rangle$	(3.40)
N odd	$\langle \phi_{s_\infty}(\infty)\phi_{s_1}(z_1)\ldots\phi_{s_N}(z_N)\left(J^{a_l}_{-n_l}\ldots J^{a_1}_{-n_1}\right)(0)\rangle$	(3.46)
N odd	$\langle \phi_{s_1}(z_1)\ldots\phi_{s_N}(z_N)\left(J^{a_l}_{-n_l}\ldots J^{a_1}_{-n_1}\phi_{s_0}\right)(0)\rangle$	(3.48)

In the following, we define further states by adding descendant and/or additional primary fields into the CFT correlator. Table 3.2 summarizes these classes of states and contains references to their definitions.

3.1.2 Tower of states from descendant fields

The state $|\psi_0\rangle$ defined in the previous subsection can be viewed as corresponding to the CFT vacuum $|0\rangle$ (cf. Table 3.1). We now describe a map from CFT states $(J^{a_l}_{-n_l}\dots J^{a_1}_{-n_1})(0)|0\rangle$ to states of the spin-$\frac{1}{2}$ system.

To each CFT state $(J^{a_l}_{-n_l}\dots J^{a_1}_{-n_1})(0)|0\rangle$, we associate a state

$$|\psi^{a_l\dots a_1}_{n_l\dots n_1}\rangle = \sum_{s_1,\dots,s_N} \psi^{a_l\dots a_1}_{n_l\dots n_1}(s_1,\dots,s_N)|s_1,\dots,s_N\rangle, \tag{3.16}$$

where

$$\psi^{a_l\dots a_1}_{n_l\dots n_1}(s_1,\dots,s_N) = \langle \phi_{s_1}(z_1)\dots\phi_{s_N}(z_N)\left(J^{a_l}_{-n_l}\dots J^{a_1}_{-n_1}\right)(0)\rangle. \tag{3.17}$$

Compared to $|\psi_0\rangle$ of Eq. (3.11), $|\psi^{a_l\dots a_1}_{n_l\dots n_1}\rangle$ has additional modes of the descendant field $J^a(z)$ inserted at the origin $z_0 = 0$. The point $z_0 = 0$ on the plane corresponds to $w = -\infty$ on the cylinder through the map $z = e^w$. The descendant fields are thus inserted at a position left of the cylinder as illustrated in Fig. 1.3. Later, we will study $|\psi^{a_l\dots a_1}_{n_l\dots n_1}\rangle$ as candidates for edge states on the cylinder. Fig. 1.3 provides an intuitive picture for why the addition of modes at $z_0 = 0$ corresponds to modifying the state $|\psi_0\rangle$ at the edge.

It is possible to obtain the states $|\psi^{a_l\dots a_1}_{n_l\dots n_1}\rangle$ by applying spin operators to $|\psi_0\rangle$. To see this, we first note that

$$\langle \phi_{s_1}(z_1)\dots\phi_{s_N}(z_N)(J^a_{-n}B)(0)\rangle = \frac{1}{2\pi i}\oint_0 \frac{dw}{w^n}\langle \phi_{s_1}(z_1)\dots\phi_{s_N}(z_N)J^a(w)B(0)\rangle, \tag{3.18}$$

where n is a positive integer, B an arbitrary operator, and the integral encircles the origin in the counter-clockwise direction. Applying this relation to the definition of $\psi^{a_l\dots a_1}_{n_l\dots n_1}(s_1,\dots,s_N)$, we obtain

$$\begin{aligned}\psi^{a_l\dots a_1}_{n_l\dots n_1}(s_1,\dots,s_N) &= \langle \phi_{s_1}(z_1)\dots\phi_{s_N}(z_N)\left(J^{a_l}_{-n_l}\dots J^{a_1}_{-n_1}\right)(0)\rangle \\ &= \frac{1}{2\pi i}\oint_0 \frac{dw}{w^{n_l}}\langle \phi_{s_1}(z_1)\dots\phi_{s_N}(z_N)J^{a_l}(w)\left(J^{a_{l-1}}_{-n_{l-1}}\dots J^{a_1}_{-n_1}\right)(0)\rangle.\end{aligned} \tag{3.19}$$

Since the integrand is meromorphic and has no pole at $w = \infty$,

$$0 = \frac{1}{2\pi i}\sum_{w_j\in\{0\}\cup\{z_1,\dots,z_N\}}\oint_{w_j}\frac{dw}{w^{n_l}}\langle \phi_{s_1}(z_1)\dots\phi_{s_N}(z_N)J^{a_l}(w)\left(J^{a_{l-1}}_{-n_{l-1}}\dots J^{a_1}_{-n_1}\right)(0)\rangle. \tag{3.20}$$

Therefore,

$$\psi^{a_l\dots a_1}_{n_l\dots n_1}(s_1,\dots,s_N) = -\frac{1}{2\pi i}\sum_{j=1}^{N}\oint_{z_j}\frac{dw}{w^{n_l}}\langle \phi_{s_1}(z_1)\dots\phi_{s_N}(z_N)J^{a_l}(w)\left(J^{a_{l-1}}_{-n_{l-1}}\dots J^{a_1}_{-n_1}\right)(0)\rangle. \tag{3.21}$$

Using the OPE between a current operator and a primary field [Eq. (3.4)], we get

$$\begin{aligned}\psi^{a_l\dots a_1}_{n_l\dots n_1}(s_1,\dots,s_N) = \frac{1}{2\pi i}\sum_{j=1}^{N}\sum_{s\in\{-1,1\}}\oint_{z_j}\frac{dw}{w^{n_l}}\frac{t^{a_l}_{s_j s}}{w-z_j}&\langle \phi_{s_1}(z_1)\dots\phi_{s_{j-1}}(z_{j-1})\phi_s(z_j) \\ &\times\phi_{s_{j+1}}(z_{j+1})\dots\phi_{s_N}(z_N)\left(J^{a_{l-1}}_{-n_{l-1}}\dots J^{a_1}_{-n_1}\right)(0)\rangle\end{aligned} \tag{3.22}$$

and therefore

$$|\psi^{a_l\dots a_1}_{n_l\dots n_1}\rangle = \sum_{j=1}^{N} \frac{t_j^{a_l}}{\left(z_j\right)^{n_j}} |\psi^{a_{l-1}\dots a_1}_{n_{l-1}\dots n_1}\rangle. \tag{3.23}$$

Successively applying the same argument, we thus obtain

$$|\psi^{a_l\dots a_1}_{n_l\dots n_1}\rangle = u^{a_l}_{-n_l}\dots u^{a_1}_{-n_1}|\psi_0\rangle, \tag{3.24}$$

where we defined

$$u^a_k \equiv \sum_{i=1}^{N} (z_i)^k\, t^a_i. \tag{3.25}$$

The commutation relations of the operators u^a_k are given by

$$\left[u^a_m, u^b_n\right] = i\varepsilon_{abc} u^c_{m+n}, \tag{3.26}$$

which is a direct consequence of $[t^a_m, t^b_n] = i\varepsilon_{abc}\delta_{mn}t^c_m$. Eq. (3.26) is a Kac-Moody algebra with vanishing central extension, cf. Eq. (3.3). Thus, the operators u^a_k are spin-system analogs of the CFT modes J^a_k.

Completeness of states built from current operators

The definition of $|\psi^{a_l\dots a_1}_{n_l\dots n_1}\rangle$ defines a map from the identity sector of the CFT's Hilbert space to states of a spin-$\frac{1}{2}$ system. We now show that this map is surjective, i.e., any state in the Hilbert space $\mathcal{H}_N$ of N spin-$\frac{1}{2}$ degrees of freedom can be written as a linear combination of states $|\psi^{a_l\dots a_1}_{n_l\dots n_1}\rangle$.

The definition of the operators u^a_k [Eq. (3.25)] can be expressed as

$$\begin{pmatrix} u^a_0 \\ u^a_{-1} \\ \vdots \\ u^a_{-(N-1)} \end{pmatrix} = Z \begin{pmatrix} t^a_1 \\ t^a_2 \\ \vdots \\ t^a_N \end{pmatrix}, \tag{3.27}$$

where

$$Z = \begin{pmatrix} 1 & \dots & 1 \\ (z_1)^{-1} & \dots & (z_N)^{-1} \\ (z_1)^{-2} & \dots & (z_N)^{-2} \\ \vdots & \vdots & \vdots \\ (z_1)^{-(N-1)} & \dots & (z_N)^{-(N-1)} \end{pmatrix}. \tag{3.28}$$

The $N \times N$ matrix Z is a Vandermonde matrix with the well-known determinant

$$\det(Z) = \prod_{i<j}^{N} \left(z_j^{-1} - z_i^{-1}\right). \tag{3.29}$$

We assume that all positions z_j are distinct, since otherwise $|\psi_0\rangle = 0$. Therefore, $\det(Z) \neq 0$ and Z is invertible. According to Eq. (3.27), we then have

$$\begin{pmatrix} t_1^a \\ t_2^a \\ \vdots \\ t_N^a \end{pmatrix} = Z^{-1} \begin{pmatrix} u_0^a \\ u_{-1}^a \\ \vdots \\ u_{-(N-1)}^a \end{pmatrix}. \tag{3.30}$$

The Hilbert space $\mathcal{H}_N$ is spanned by the states obtained from any nonzero state $|\psi\rangle \in \mathcal{H}_N$ by successive application of spin operators t_j^a. The reason for this is as follows. Since $|\psi\rangle \neq 0$, there is at least one spin configuration $(\tilde{s}_1, \ldots, \tilde{s}_N)$ with $\tilde{s}_j \in \{-1, 1\}$ so that $\psi(\tilde{s}_1, \ldots, \tilde{s}_N) \neq 0$. Therefore,

$$|-\tilde{s}_1, \ldots, -\tilde{s}_N\rangle = \frac{1}{\psi(\tilde{s}_1, \ldots, \tilde{s}_N)} \prod_{j=1}^{N} t_j^{\sigma(\tilde{s}_j)} |\psi\rangle, \tag{3.31}$$

where

$$\sigma(s) = \begin{cases} + & \text{if } s = -1, \\ - & \text{if } s = +1, \end{cases} \tag{3.32}$$

and $t_j^{\pm} = t_j^x \pm i t_j^y$. By applying ladder operators $t_j^{\pm}$ to $|-\tilde{s}_1, \ldots, -\tilde{s}_N\rangle$, any product state $|s_1, \ldots, s_N\rangle$ can be obtained. Thus, $\mathcal{H}_N$ is spanned by the states obtained from $|\psi\rangle$ by applying spin operators $t_j^{\pm}$ with $j \in \{1, \ldots, N\}$. Since $t_j^{\pm}$ can be written in terms of t_j^x and t_j^y, $\mathcal{H}_N$ can then also be obtained by applying operators t_j^a with $a \in \{x, y, z\}$ and $j \in \{1, \ldots, N\}$ to $|\psi\rangle$.

According to Eq. (3.30), the operators t_j^a are linear combinations of $u_{-n_j}^a$ with $n_j \in \{0, \ldots, N-1\}$. Therefore, it follows that $|\psi_{n_l \ldots n_1}^{a_l \ldots a_1}\rangle = u_{-n_l}^{a_l} \ldots u_{-n_1}^{a_1} |\psi_0\rangle$ with $n_j \in \{0, \ldots, N-1\}$ span $\mathcal{H}_N$. Since $|\psi_0\rangle$ is a singlet and $u_0^a = \sum_{j=1}^N t_j^a$ is the total spin, a state

$$u_0^a u_{-n_l}^{a_l} \ldots u_{-n_1}^{a_1} |\psi_0\rangle \tag{3.33}$$

can be written in terms of states for which all mode numbers are greater than zero by commuting u_0^a to the right until it annihilates $|\psi_0\rangle$ [cf. the commutator of Eq. (3.26)]. Therefore, $\mathcal{H}_N$ is spanned by the states $|\psi_{n_l \ldots n_1}^{a_l \ldots a_1}\rangle$ with $n_j > 0$.

The fact that the states $|\psi_{n_l \ldots n_1}^{a_l \ldots a_1}\rangle$ span $\mathcal{H}_N$ raises the question about the minimal level $k = n_1 + \cdots + n_l$ needed to obtain the complete Hilbert space. We note that an upper bound is given by $k = N(N-1)$, since any product of spin operators t_i^a can be reduced to a product of at most N spin operators. Each of these spin operators can then be expanded in terms of the operators u_{-n}^a with $n \in \{0, \ldots, N-1\}$. We carried out numerical calculations for the states $|\psi_{n_l \ldots n_1}^{a_l \ldots a_1}\rangle$ which indicate that the states up to level $k = (N/2)^2$ are enough to obtain the complete Hilbert space from $|\psi_0\rangle$.

Relation to spinon basis

The map from CFT states $(J_{-n_l}^{a_l} \ldots J_{-n_1}^{a_1})(0)|0\rangle$ to states $|\psi_{n_l \ldots n_1}^{a_l \ldots a_1}\rangle$ assumes a basis of the Hilbert space where excited states are obtained from the CFT vacuum $|0\rangle$ by applying modes of the current $J^a(z)$, which is a *descendant* field. It is also possible to construct the CFT Hilbert space in terms of modes $\phi_{s,-m}$ of the *primary* field $\phi_s(z)$ [153]. These are defined through the Laurent expansion [153]

$$\phi_s(z) = \sum_m z^{m + \frac{q}{2}} \phi_{s, -m - \frac{1}{4} - \frac{q}{2}}, \tag{3.34}$$

where $q = 0$ if $\phi_s(z)$ acts on a state with an even number of modes of the primary field $\phi_s(z)$ and $q = 1$ otherwise. The basis obtained from modes $\phi_{s,-m}$ is known as the spinon basis [153] and assumes the form

$$\left(\phi_{s_r,-m_r}\dots\phi_{s_1,-m_1}\right)(0)|0\rangle. \tag{3.35}$$

The generalized commutation relations of Ref. [153] allow expressing modes of the primary field in terms of current operator modes. Thus, they relate basis states in the spinon construction to CFT states obtained from modes of the current $J^a(z)$. This relation induces a transformation from spin states $|\psi^{a_l\dots a_1}_{n_l\dots n_1}\rangle$ constructed from $J^a(z)$ to spin states constructed from modes of the primary field. The spin wave function

$$\psi^a_1(s_1,\dots,s_N) = \langle\phi_{s_1}(z_1)\dots\phi_{s_N}(z_N)J^a_{-1}(0)\rangle, \tag{3.36}$$

for example, corresponds a state with wave function

$$\sum_{s,s'} t^a_{ss'}\langle\phi_{s_1}(z_1)\dots\phi_{s_N}(z_N)\left(\phi_{-s,-\frac{3}{4}}\phi_{s',-\frac{1}{4}}\right)(0)\rangle. \tag{3.37}$$

Similarly, a general state $|\psi^{a_l\dots a_1}_{n_l\dots n_1}\rangle$ with $k = n_1 + \dots + n_l$ will be a linear combination of states with spinon modes $\phi_{s_r,-m_r}\dots\phi_{s_1,-m_1}$ at the same level $k = m_1 + \dots + m_r$.

3.1.3 States with additional spins at zero and at infinity

We define an additional class of states by inserting two extra vertex operators into the correlator $\langle\phi_{s_1}(z_1)\dots\phi_{s_N}(z_N)\rangle$, one at $z_0 = 0$ and one at $z_\infty = \infty$,

$$\begin{aligned}|\psi^{s_0,s_\infty}_0\rangle &= \sum_{s_1,\dots,s_N}\psi^{s_0,s_\infty}_0(s_1,\dots,s_N)|s_1,\dots,s_N\rangle,\\ \psi^{s_0,s_\infty}_0(s_1,\dots,s_N) &= \langle\phi_{s_\infty}(z_\infty)\phi_{s_1}(z_1)\dots\phi_{s_N}(z_N)\phi_{s_0}(0)\rangle,\end{aligned} \tag{3.38}$$

where we take $z_\infty \to \infty$. The two additional spins s_0 and s_∞ are parameters of the state $|\psi^{s_0,s_\infty}_0\rangle$, i.e., we are still working in the Hilbert space of N spin-$\frac{1}{2}$ particles.

In the picture of the cylinder, the additional primary fields are inserted at $w = -\infty$ (corresponding to $z_0 = 0$) and at $w = \infty$ (corresponding to $z_\infty = \infty$), cf. Fig. 1.3.

The wave function is

$$\psi^{s_0,s_\infty}_0(s_1,\dots,s_N) \propto \delta_{\bar{\mathbf{s}}}(-1)^{\frac{1}{2}s_0(1-s_\infty)}\chi_{\mathbf{s}}\prod_{n=1}^{N} z_n^{\frac{1}{2}s_0 s_n}\prod_{n<m}^{N}(z_n - z_m)^{\frac{1}{2}s_n s_m}, \tag{3.39}$$

where $\delta_{\bar{\mathbf{s}}} = 1$ for $s_0 + s_\infty + \sum_{i=1}^N s_i = 0$ and $\delta_{\bar{\mathbf{s}}} = 0$ otherwise.

The extra fields at $z_0 = 0$ and $z_\infty = \infty$ are *primary* fields. By inserting additional current operators, we generate *descendant* states. We thus define a tower of states on top of $|\psi^{s_0 s_\infty}_0\rangle$,

$$\psi^{a_l\dots a_1,s_0,s_\infty}_{n_l\dots n_1}(s_1,\dots,s_N) = \langle\phi_{s_\infty}(z_\infty)\phi_{s_1}(z_1)\dots\phi_{s_N}(z_N)\left(J^{a_l}_{-n_l}\dots J^{a_1}_{-n_1}\phi_{s_0}\right)(0)\rangle \tag{3.40}$$

where, again, we take $z_\infty \to \infty$. This ansatz corresponds to the tower of CFT descendant states $(J^{a_l}_{-n_l}\dots J^{a_1}_{-n_1}\phi_s)(0)|0\rangle$.

To derive the form of the wave function $\psi^{a_l\dots a_1,s_0,s_\infty}_{n_l\dots n_1}(s_1,\dots,s_N)$, we consider the system consisting of the N spins and the two additional ones. A calculation analogous to the case of

$|\psi^{a_l\dots a_1}_{n_l\dots n_1}\rangle$ (cf. Sec. 3.1.2) shows that

$$\sum_{s_0,s_\infty} |s_0\rangle\otimes|\psi^{a_l\dots a_1,s_0,s_\infty}_{n_l\dots n_1}\rangle\otimes|s_\infty\rangle$$
$$= \left(\frac{t^{a_l}_\infty}{(z_\infty)^{n_l}} + \sum_{j_k=1}^{N}\frac{t^{a_l}_{j_k}}{\left(z_{j_k}\right)^{n_l}}\right)\dots\left(\frac{t^{a_1}_\infty}{(z_\infty)^{n_1}} + \sum_{j_1=1}^{N}\frac{t^{a_1}_{j_1}}{\left(z_{j_1}\right)^{n_1}}\right)\sum_{s_0,s_\infty}|s_0\rangle\otimes|\psi_0^{s_0,s_\infty}\rangle\otimes|s_\infty\rangle. \tag{3.41}$$

In the limit $z_\infty\to\infty$, the terms $t^{a_j}_\infty/(z_\infty)^{n_j}$ do not contribute. Therefore,

$$|\psi^{a_l\dots a_1,s_0,s_\infty}_{n_l\dots n_1}\rangle = u^{a_l}_{-n_l}\dots u^{a_1}_{-n_1}|\psi_0^{s_0,s_\infty}\rangle \tag{3.42}$$

in terms of the operators u^a_n of Eq. (3.25).

3.1.4 Odd number of spins

According to the charge neutrality condition (cf. Sec. 2.1.4), a correlation function of WZW primary fields $\langle\phi_{s_1}(z_1)\dots\phi_{s_N}(z_N)\rangle$ is only nonzero if the sum $s_1+\dots+s_N$ vanishes. As a consequence, the number of vertex operators, and therefore the number of spins, needs to be even. We can, however, still consider a model with N odd by adding an extra vertex operator that compensates the excess charge of the odd number of particles.

Inserting an additional vertex operator at $z_\infty=\infty$, we obtain the state

$$\psi_0^{s_\infty}(s_1,\dots,s_N) = \langle\phi_{s_\infty}(z_\infty)\phi_{s_1}(z_1)\dots\phi_{s_N}(z_N)\rangle \propto \delta_{\bar{\mathbf{s}}}(-1)^{\frac{1}{2}(s_\infty+1)}\chi_{\mathbf{s}}\prod_{i<j}^{N}(z_i-z_j)^{\frac{1}{2}s_is_j}, \tag{3.43}$$

where $\delta_{\bar{\mathbf{s}}}=1$ if $s_\infty+\sum_{i=1}^N s_i=0$ and $\delta_{\bar{\mathbf{s}}}=0$ otherwise, and the limit $z_\infty\to\infty$ was taken. The state $|\psi_0^{s_\infty}\rangle$ has spin $\frac{1}{2}$,

$$T^aT^a|\psi_0^{s_\infty}\rangle = \frac{3}{4}|\psi_0^{s_\infty}\rangle, \tag{3.44}$$

where T^a is the total spin. This follows from the singlet property of the state that includes the spin at infinity:

$$(t^a_\infty+T^a)\sum_{s_\infty,s_1,\dots,s_N}\langle\phi_{s_\infty}(z_\infty)\phi_{s_1}(z_1)\dots\phi_{s_N}(z_N)\rangle|s_1,\dots,s_N,s_\infty\rangle = 0. \tag{3.45}$$

As in the case of an even number of spins, we define a tower of states by insertion of current operators,

$$\psi^{a_l\dots a_1,s_\infty}_{n_l\dots n_1}(s_1,\dots,s_N) = \langle\phi_{s_\infty}(\infty)\phi_{s_1}(z_1)\dots\phi_{s_N}(z_N)\left(J^{a_l}_{-n_l}\dots J^{a_1}_{-n_1}\right)(0)\rangle. \tag{3.46}$$

We obtain a second class of states by inserting the additional vertex operator at $z_0=0$ instead of at infinity,

$$\psi_0^{s_0}(s_1,\dots,s_N) = \langle\phi_{s_1}(z_1)\dots\phi_{s_N}(z_N)\phi_{s_0}(0)\rangle \propto \delta_{\bar{\mathbf{s}}}\chi_{\mathbf{s}}\prod_{i=1}^{N}z_i^{\frac{1}{2}s_0s_i}\prod_{i<j}^{N}(z_i-z_j)^{\frac{1}{2}s_is_j}. \tag{3.47}$$

The corresponding tower of states is given by

$$\psi^{a_l\dots a_1,s_0}_{n_l\dots n_1}(s_1,\dots,s_N) = \langle\phi_{s_1}(z_1)\dots\phi_{s_N}(z_N)\left(J^{a_l}_{-n_l}\dots J^{a_1}_{-n_1}\phi_{s_0}\right)(0)\rangle. \tag{3.48}$$

By applying the operators u^a_n of Eq. (3.25), these can be obtained from $|\psi_0^{s_\infty}\rangle$ as

$$|\psi^{a_l\dots a_1,s_\infty}_{n_l\dots n_1}\rangle = u^{a_l}_{-n_l}\dots u^{a_1}_{-n_1}|\psi_0^{s_\infty}\rangle \tag{3.49}$$

and from $|\psi_0^{s_0}\rangle$ as

$$|\psi^{a_l\dots a_1,s_0}_{n_l\dots n_1}\rangle = u^{a_l}_{-n_l}\dots u^{a_1}_{-n_1}|\psi_0^{s_0}\rangle, \tag{3.50}$$

respectively.

Comparing the wave functions of Eq. (3.43) and Eq. (3.47) with the case of an even number of spins [Eqs. (3.12) and (3.39)], we conclude that $|\psi_0^{s_\infty}\rangle$ is the analog of $|\psi_0\rangle$ and $|\psi_0^{s_0}\rangle$ of $|\psi_0^{s_0 s_\infty}\rangle$, respectively.

3.2 Global properties of states on the cylinder

In this section, we study global transformation properties of the states $|\psi_0\rangle$, $|\psi^{a_l\dots a_1}_{n_l\dots n_1}\rangle$, and $|\psi_0^{s_0,s_\infty}\rangle$ on the cylinder. This serves two purposes: First, it allows us to conclude that states with a different momentum are orthogonal, i.e., they have different global properties. Later, we will study their local behavior numerically and compare spin correlation functions in the bulk. Furthermore, the symmetries derived in this section will be exploited in our numerical calculations to obtain efficient Monte Carlo estimates.

We consider a square lattice on the cylinder with N_x sites in the open and N_y sites in the periodic direction. After mapping the cylinder to the complex plane as explained in Sec. 2.3.1, the coordinates assume the form

$$z_j \equiv z_{j_x j_y} = e^{\frac{2\pi}{N_y}(j_x + i j_y)} e^{-\frac{2\pi}{N_y}\frac{N_x+1}{2}}. \tag{3.51}$$

Here, $j_x \in \{1,\dots,N_x\}$ is the x component of the index and $j_y \in \{1,\dots,N_y\}$ is the y component of the index j. One has the freedom to rescale the coordinates z_j since this changes the wave functions only by a total factor. In this chapter, we include a constant factor in Eq. (3.51) so that the center of the cylinder with respect to the x direction coincides with the unit circle ($|z| = 1$). The advantage of this choice is that the transformations derived below assume a simpler form.

The coordinates of Eq. (3.51) include the case of a 1D uniform lattice on the circle as the special case $N_x = 1$. Thus, the results of this section are also valid on the circle.

We consider the translation operator in the periodic direction $\mathcal{T}_y$ and the inversion operator $\mathcal{I}$. Their precise definition and the derivation of their action on the states $|\psi_0\rangle$, $|\psi^{a_l\dots a_1}_{n_l\dots n_1}\rangle$, and $|\psi_0^{s_0,s_\infty}\rangle$ are given in Appendix B.3. Geometrically, the translation operator rotates the system in the periodic direction and the inversion operator corresponds to a reflection of the cylinder along its two central cross sections. We call it an inversion because it acts on the coordinates defined in Eq. (3.51) as $z_j \to z_j^{-1}$.

Eigenstates of $\mathcal{T}_y$ and $\mathcal{I}$ are given in Table 3.3. As we show in Appendix B.3.3, applying the inversion $\mathcal{I}$ to $|\psi^{a_l\dots a_1}_{n_l\dots n_1}\rangle$ corresponds to inserting the current operators at $z_\infty = \infty$ instead of $z_0 = 0$. We use the notation $|\psi^{a_l\dots a_1}_{-n_l\dots -n_1}\rangle$ for these states:

$$\begin{aligned}\psi^{a_l\dots a_1}_{-n_l\dots -n_1}(s_1,\dots,s_N) &= \langle J^{a_1}_{n_1}\dots J^{a_l}_{n_l}\phi_{s_1}(z_1)\dots\phi_{s_N}(z_1)\rangle,\\ |\psi^{a_l\dots a_1}_{-n_l\dots -n_1}\rangle &= u^{a_l}_{n_l}\dots u^{a_1}_{n_1}|\psi_0\rangle.\end{aligned} \tag{3.52}$$

Since the momentum in the periodic direction P_y is related to $\mathcal{T}_y$ through the relation $\mathcal{T}_y = e^{iP_y}$, we conclude from Table 3.3 that an additional insertion of a current operator J^a_{-n} into the correlation function of primary fields adds a momentum $-\frac{2\pi n}{N_y}$ to the state. In particular, the states $|\psi_0\rangle$ and $|\psi^{a_l\dots a_1}_{n_l\dots n_1}\rangle$ have a different momentum if $k = n_1 + \dots + n_l$ is different from 0 modulo N_y.

Table 3.3: Eigenstates of the translation operator $\mathcal{T}_y$ and the inversion $\mathcal{I}$. The sum of mode numbers $n_1 + \cdots + n_l$ is denoted by k. For the states $|\psi^{a_l \ldots a_1}_{-n_l \cdots -n_1}\rangle$, the current operators are inserted at $z_\infty = \infty$ [cf. Eq. (3.52)].

Eigenstate	$\mathcal{T}_y$	$\mathcal{I}$
$\|\psi_0\rangle$	$(-1)^{N_x \frac{N}{2}}$	$(-1)^{N_y \frac{N}{2}}$
$\|\psi^{a_l \ldots a_1}_{n_l \ldots n_1}\rangle$	$(-1)^{N_x \frac{N}{2}} e^{-\frac{2\pi i}{N_y} k}$	—
$\|\psi^{a_l \ldots a_1}_{n_l \ldots n_1}\rangle \pm \|\psi^{a_l \ldots a_1}_{-n_l \cdots -n_1}\rangle$	—	$(\pm 1)(-1)^{N_y \frac{N}{2}}$
$\|\psi_0^{s_0, s_\infty}\rangle$:	$(-1)^{N_x \frac{N}{2} + N_x}$	—
$\quad \|\psi_0^{\uparrow,\downarrow}\rangle - \|\psi_0^{\downarrow,\uparrow}\rangle$	$(-1)^{N_x \frac{N}{2} + N_x}$	$(-1)^{N_y \frac{N}{2} + N_x}$
$\quad \|\psi_0^{\uparrow,\uparrow}\rangle$, $\|\psi_0^{\uparrow,\downarrow}\rangle + \|\psi_0^{\downarrow,\uparrow}\rangle$, and $\|\psi_0^{\downarrow,\downarrow}\rangle$	$(-1)^{N_x \frac{N}{2} + N_x}$	$(-1)^{N_y \frac{N}{2} + N_x + 1}$

3.3 Excited states for the Haldane-Shastry model

We now choose a lattice of positions uniformly distributed on the circle (cf. Sec. 2.3.1):

$$z_j = e^{\frac{2\pi i}{N} j}, \tag{3.53}$$

where $j \in \{1, \ldots, N\}$. For this choice of coordinates, $|\psi_0\rangle$ is the ground state of the Haldane-Shastry spin chain [102]. In this section, we show that excited states of the Haldane-Shastry model can be constructed from those of the CFT using the map of Table 3.1.

3.3.1 The Haldane-Shastry model

Let us for now assume that the number of spins N is even. The Haldane-Shastry model [121, 122] is given by an SU(2) symmetric, Heisenberg-like spin Hamiltonian defined as

$$H_{\mathrm{HS}} = \frac{1}{2} \sum_{i \neq j}^{N} \frac{t_i^a t_j^a}{\sin^2\left[\frac{(i-j)\pi}{N}\right]}. \tag{3.54}$$

It has long-range interactions decaying with the square of the distance $|z_i - z_j| = 2|\sin\left(\frac{(i-j)\pi}{N}\right)|$ between positions z_i and z_j on the unit circle. The Haldane-Shastry model is the lattice analog of the continuous Calogero-Sutherland model [123–126]. As shown in Ref. [102], the wave function $\psi_0(s_1, \ldots, s_N)$ for positions on the unit circle as in Eq. (3.53) coincides with the ground state wave function [121, 122] of H_{HS}. Given the construction of $\psi_0(s_1, \ldots, s_N)$ from CFT, this confirms the close relationship [144] between the Haldane-Shastry model and the $\mathrm{SU}(2)_1$ WZW CFT.

In fact, the Haldane-Shastry model can be systematically obtained from CFT using the technique of null vectors [103]. These allow constructing operators $\mathcal{C}_i^a$ that annihilate $|\psi_0\rangle$, $\mathcal{C}_i^a |\psi_0\rangle = 0$, cf. also Ref. [154], where $\mathcal{C}_i^a$ were first obtained without the use of CFT. In terms of spin operators,

$$\mathcal{C}_i^a = \frac{2}{3} \sum_{j=1, j \neq i}^{N} w_{ij} \left(t_j^a + i \varepsilon_{abc} t_i^b t_j^c \right), \tag{3.55}$$

where

$$w_{ij} \equiv \frac{z_i + z_j}{z_i - z_j}. \tag{3.56}$$

A parent Hamiltonian of $|\psi_0\rangle$ is then given by [103]

$$H = \frac{1}{4}\sum_{i=1}^{N}\left(\mathcal{C}_i^a\right)^\dagger \mathcal{C}_i^a \tag{3.57}$$

since H is positive semidefinite and $H|\psi_0\rangle = 0$. For a uniform lattice on the circle as in Eq. (3.53), H is equivalent to the Haldane-Shastry model up to a term proportional to the spin Casimir T^aT^a:

$$H_{\mathrm{HS}} = H + \frac{N+1}{6}T^aT^a + E_0, \tag{3.58}$$

where $E_0 = -(N^3+5N)/24$ [$E_0 = -(N^3-N)/24$ for N odd] is the ground state energy of the Haldane-Shastry Hamiltonian. Since $|\psi_0\rangle$ is a spin singlet ($T^a|\psi_0\rangle = 0$), Eq. (3.58) implies that $H_{\mathrm{HS}}|\psi_0\rangle = E_0|\psi_0\rangle$, i.e., $|\psi_0\rangle$ is indeed the ground state of the Haldane-Shastry model.

From now on, we will work with the positive semidefinite Hamiltonian

$$\mathcal{H} = H + \frac{N+1}{6}T^aT^a, \tag{3.59}$$

which differs from H_{HS} by the subtraction of the ground state energy.

3.3.2 Block-diagonal form of the Hamiltonian

We now systematically construct the excited states of $\mathcal{H}$ for N even from conformal correlation functions. Specifically, we build the excited states as linear combinations of the states $|\psi^{a_l\ldots a_1}_{n_l\ldots n_1}\rangle$, which are defined through the insertion of current operators $J^{a_k}_{-n_k}$ into the correlator of primary fields [cf. Eq. (3.12) and (3.17)].

The key to this construction is that the Hamiltonian does not couple states with a fixed mode number sum $k = n_1 + \cdots + n_l$ to those with a different mode number sum, i.e., it is block-diagonal in this basis. In the following, we will also refer to k as the level of a state.

We can thus diagonalize the Hamiltonian in the subspaces of states at a certain level k. It is not necessary to construct the Hamiltonian in the full Hilbert space of dimension 2^N in order to find eigenstates beyond the ground state. Rather, we obtain eigenstates by successively adding current operators and diagonalizing the blocks.

Let us now show that $\mathcal{H}|\psi^{a_l\ldots a_1}_{n_l\ldots n_1}\rangle$ is a linear combination of states with the same mode number sum k. First, we note that is suffices to prove this for states $|\psi^{a_k\ldots a_1}_{1\ \ldots 1}\rangle$ with all mode numbers n_j being equal to 1. The reason is that any operator J^a_{-n} with $n>0$ can be rewritten as

$$J^a_{-n} = \frac{i}{2}\varepsilon_{abc}\left[J^c_{-1}, J^b_{-n+1}\right] \quad (n\neq 0), \tag{3.60}$$

where the Kac-Moody algebra of Eq. (3.3) was used. Successively applying Eq. (3.60), any state $|\psi^{a_l\ldots a_1}_{n_l\ldots n_1}\rangle$ with $k = n_1+\cdots+n_l$ can be expressed as a linear combination of states $|\psi^{a_k\ldots a_1}_{1\ \ldots 1}\rangle$.

According to Eq. (3.24), the insertion of k current operator modes $J^{a_j}_{-1}$ ($j=1,\ldots,k$) into the correlation function of vertex operators is equivalent to the successive application of operators $u^{a_j}_{-1}$ to the ground state $|\psi_0\rangle$. Therefore, we computed the commutator between $\mathcal{H}$ and u^a_{-1} by an explicit expansion of the Hamiltonian in terms of u^a_l for $l\in\{0,\ldots,N-1\}$. This calculation can be found in Appendix B.2, and the result is

$$[\mathcal{H}, u^a_{-1}] = (N-1)u^a_{-1} + \sum_{i=1}^{N}\frac{3}{2}\frac{\mathcal{C}^a_i}{z_i} + i\varepsilon_{abc}u^b_{-1}T^c. \tag{3.61}$$

From this commutator, we can already conclude that the energy of a state with one current operator J^a_{-1} is $N-1$:

$$\mathcal{H}u^a_{-1}|\psi_0\rangle = [\mathcal{H}, u^a_{-1}]|\psi_0\rangle = (N-1)u^a_{-1}|\psi_0\rangle \tag{3.62}$$

since $\mathcal{H}$, $\mathcal{C}^a_i$, and T^c annihilate the ground state $|\psi_0\rangle$.

We need to know how $\mathcal{C}^a_i$ acts on $|\psi^{a_k\dots a_1}_{1\ \dots 1}\rangle$ to determine the energy of states with more than one current operator. As we show in Appendix B.1,

$$\begin{aligned}
&\mathcal{C}^a_i|\psi^{a_k\dots a_1}_{1\ \dots 1}\rangle \\
&= \sum_{q=1}^{k} \frac{\left(K^a_{a_q}\right)_i}{z_i}|\psi^{a_k\dots a_{q+1}a_{q-1}\dots a_1}_{1\ \dots 1\quad 1\quad \dots 1}\rangle + \left(K^a_b\right)_i T^b|\psi^{a_k\dots a_1}_{1\ \dots 1}\rangle \\
&\quad + 2\left(K^a_b\right)_i \sum_{q=2}^{k}\sum_{n=0}^{q-1}\sum_{s_1,\dots,s_N} \frac{i\varepsilon_{ba_qc}}{z_i^{n+1}}\langle\phi_{s_1}(z_1)\dots\phi_{s_N}(z_N)\left(J^{a_k}_{-1}\dots J^{a_{q+1}}_{-1}J^c_n J^{a_{q-1}}_{-1}\dots J^{a_1}_{-1}\right)(0)\rangle|s_1,\dots,s_N\rangle,
\end{aligned} \tag{3.63}$$

where

$$\left(K^a_b\right)_j = \frac{2}{3}\left(\delta_{ab} - i\varepsilon_{abc}t^c_j\right). \tag{3.64}$$

Combining Eqs. (3.61) and (3.63), we obtain

$$\begin{aligned}
\mathcal{H}|\psi^{a_k\dots a_1}_{1\ \dots 1}\rangle &= \sum_{r=1}^{k} u^{a_k}_{-1}\dots u^{a_{r+1}}_{-1}\left[\mathcal{H}, u^{a_r}_{-1}\right]u^{a_{r-1}}_{-1}\dots u^{a_1}_{-1}|\psi_0\rangle \\
&= k(N-1)|\psi^{a_k\dots a_1}_{1\ \dots 1}\rangle + \sum_{2\le q<r\le k}\sum_{n=0}^{q-1}\sum_{s_1,\dots,s_N} F^{qr,n}_{a_k\dots a_1}(s_1,\dots,s_N)|s_1,\dots,s_N\rangle \\
&\quad + \sum_{1\le q<r\le k}\Big(2|\psi^{a_k\dots a_{r+1}a_qa_{r-1}\dots a_{q+1}a_ra_{q-1}\dots a_1}_{1\ \dots 1\quad 1\ 1\quad \dots 1\quad 1\ 1\quad \dots 1}\rangle - 2\delta_{a_ra_q}|\psi^{a_k\dots a_{r+1}ca_{r-1}\dots a_{q+1}ca_{q-1}\dots a_1}_{1\ \dots 1\quad 11\quad \dots 1\quad 11\quad \dots 1}\rangle \\
&\qquad + |\psi^{a_k\dots a_{r+1}a_qa_ra_{r-1}\dots a_{q+1}a_{q-1}\dots a_1}_{1\ \dots 1\quad 1\ 1\ 1\quad \dots 1\quad 1\quad \dots 1}\rangle - |\psi^{a_k\dots a_{r+1}a_ra_qa_{r-1}\dots a_{q+1}a_{q-1}\dots a_1}_{1\ \dots 1\quad 1\ 1\ 1\quad \dots 1\quad 1\quad \dots 1}\rangle \\
&\qquad + 2\delta_{N,2}\delta_{a_ra_q}|\psi^{a_k\dots a_{r+1}a_{r-1}\dots a_{q+1}a_{q-1}\dots a_1}_{1\ \dots 1\quad 1\quad \dots 1\quad 1\quad \dots 1}\rangle\Big),
\end{aligned} \tag{3.65}$$

where

$$\begin{aligned}
&F^{qr,n}_{a_k\dots a_1}(s_1,\dots,s_N) \\
&= 2\langle\phi_{s_1}(z_1)\dots\phi_{s_N}(z_N)\left(J^{a_k}_{-1}\dots J^{a_{r+1}}_{-1}J^{a_q}_{-n-2}J^{a_{r-1}}_{-1}\dots J^{a_{q+1}}_{-1}J^{a_r}_n J^{a_{q-1}}_{-1}\dots J^{a_1}_{-1}\right)(0)\rangle \\
&\quad - 2\delta_{a_ra_q}\langle\phi_{s_1}(z_1)\dots\phi_{s_N}(z_N)\left(J^{a_k}_{-1}\dots J^{a_{r+1}}_{-1}J^c_{-n-2}J^{a_{r-1}}_{-1}\dots J^{a_{q+1}}_{-1}J^c_n J^{a_{q-1}}_{-1}\dots J^{a_1}_{-1}\right)(0)\rangle \\
&\quad + 2N\tilde{\delta}_{n+2}i\varepsilon_{a_ra_qc}\langle\phi_{s_1}(z_1)\dots\phi_{s_N}(z_N)\left(J^{a_k}_{-1}\dots J^{a_{r+1}}_{-1}J^{a_{r-1}}_{-1}\dots J^{a_{q+1}}_{-1}J^c_n J^{a_{q-1}}_{-1}\dots J^{a_1}_{-1}\right)(0)\rangle,
\end{aligned} \tag{3.66}$$

and

$$\tilde{\delta}_m = \begin{cases} 1 & \text{if } m \bmod N = 0, \\ 0 & \text{otherwise.} \end{cases} \tag{3.67}$$

On the right-hand side of Eq. (3.65), the term with the prefactor $\delta_{N,2}$ and the term containing the function $F^{qr,n}_{a_k\dots a_1}(s_1,\dots,s_N)$ are not yet explicitly written in terms of states at level k. Let us now show that they can also be brought into this form. First, we note that current operators with non-negative mode numbers can be successively commuted to the right until they annihilate the CFT vacuum using the commutator [cf. Eq. (3.3)]

$$\left[J^a_n, J^b_{-1}\right] = i\varepsilon_{abc}J^c_{n-1} + \frac{1}{2}\delta_{ab}\delta_{n-1,0}. \tag{3.68}$$

In this way, a CFT state

$$\left(J^a_n J^{a_{q-1}}_{-1}\dots J^{a_1}_{-1}\right)(0)|0\rangle \tag{3.69}$$

with $n \in \{0,\dots,q-1\}$ can be written as a linear combination of terms with $q-1-n$ current operators of order -1. Thus, the first two terms in $F^{qr,n}_{a_k\dots a_1}(s_1,\dots,s_N)$ are linear combinations of terms with mode number sums

$$k-2+\underbrace{n+2}_{J^{a_q}_{-n-2}}\underbrace{-n}_{J^{a_r}_n} = k. \tag{3.70}$$

Similarly, the third term in $F^{qr,n}_{a_k\dots a_1}(s_1,\dots,s_N)$ can be written in terms of states with mode number sums $k-n-2$. It is, however, only nonzero if $n+2 = mN$ for an integer $m \in \{1,2,\dots\}$. Since $u^a_{-1-mN} = u^a_{-1}$ for the uniform and periodic 1D lattice, these states are contained in those having a mode number sum of k. The same argument applies to the term with the prefactor $\delta_{N,2}$.

Thus, the Hamiltonian is block diagonal in the states $|\psi^{a_l\dots a_1}_{n_l\dots n_1}\rangle$ with a fixed mode number sum $k = n_1+\dots+n_l$. We note that this observation does not follow from translational invariance, which implies that the Hamiltonian does not mix states with different lattice momenta. As shown in Sec. 3.2, the states $|\psi^{a_l\dots a_1}_{n_l\dots n_1}\rangle$ are eigenstates of the translation operator with eigenvalue $(-1)^{\frac{N}{2}}e^{-\frac{2\pi i}{N}k}$. Therefore, it follows from translational invariance that $\mathcal{H}|\psi^{a_l\dots a_1}_{n_l\dots n_1}\rangle$ is a linear combination of states with k mod N current operators. The above considerations moreover show that it is possible to write $\mathcal{H}|\psi^{a_l\dots a_1}_{n_l\dots n_1}\rangle$ as a linear combination of states with the same mode number sum. This allows us to block-diagonalize the Hamiltonian starting with the smaller blocks, i.e., those with a small number of current operators. As shown in Sec. 3.1.2, the complete Hilbert space is covered by linear combinations of the states $|\psi^{a_l\dots a_1}_{n_l\dots n_1}\rangle$. Therefore, it follows that one can construct all eigenstates of $\mathcal{H}$ in this way.

The number of CFT states at level k is determined by the characters of the SU(2)$_1$ algebra [103]. For the levels $k = 0,1,2,3$, and 4, there are 1, 3, 4, 7, and 13 states, respectively. These numbers determine the sizes of the blocks in Eq. (3.65). In particular, the block-size it not determined by N, which means that the diagonalization can be done for arbitrary system sizes.

3.3.3 Analytical construction of eigenstates from current operators

Eigenstates and energies

We solved the eigenvalue problem of Eq. (3.65) for up to eight current operator modes analytically. Since the Hamiltonian is SU(2) invariant, we decomposed the eigenstates into different spin sectors. We summarize our results for up to $k = 4$ current operators in Table 3.4. At level $k = 1$ we find a triplet (spin one), at level $k = 2$ a singlet and a triplet, at level $k = 3$ we find a singlet and two triplets with different energies. The first quintet (spin two) occurs at level $k = 4$.

Table 3.4: Eigenstates of the Haldane-Shastry model in terms of states obtained by insertion current operators with mode number sums $k = n_1 + \cdots + n_l \leq 4$. The momentum of each state is given by $p_0 - \frac{2\pi}{N}k$, where $p_0 = 0$ if $\frac{N}{2}$ is even and $p_0 = \pi$ otherwise.

k	State	Null for	Energy	Spin
0	$\|\varphi^{(0)}\rangle = \|\psi_0\rangle$		0	0
1	$\|\varphi^{(1)}_a\rangle = \|\psi^a_1\rangle$		$N-1$	1
2	$\|\varphi^{(2)}\rangle = \|\psi^{c\,c}_{1,1}\rangle - 3\delta_{N2}\|\psi_0\rangle$	$N \leq 2$	$2(N-3)$	0
2	$\|\varphi^{(3)}_a\rangle = \|\psi^a_2\rangle$	$N \leq 2$	$2(N-3)$	1
3	$\|\varphi^{(4)}\rangle = \|\psi^{c\,c}_{2,1}\rangle$	$N \leq 4$	$3(N-5)$	0
3	$\|\varphi^{(5)}_a\rangle = 2\|\psi^a_3\rangle - i\varepsilon_{acd}\|\psi^{c\,d}_{2,1}\rangle - 4\delta_{N2}\|\psi^a_1\rangle$	$N \leq 4$	$3(N-5)$	1
3	$\|\varphi^{(6)}_a\rangle = \|\psi^a_3\rangle + i\varepsilon_{acd}\|\psi^{c\,d}_{2,1}\rangle + \delta_{N2}\|\psi^a_1\rangle$	$N \leq 2$	$3(N-3)$	1
4	$\|\varphi^{(7)}\rangle = \|\psi^{c\,c}_{2,2}\rangle + 4\|\psi^{c\,c}_{3,1}\rangle - 12\delta_{N2}\|\psi_0\rangle - 16\delta_{N4}\|\psi_0\rangle$	$N \leq 6$	$4(N-7)$	0
4	$\|\varphi^{(8)}_a\rangle = 3\|\psi^a_4\rangle - 2i\varepsilon_{acd}\|\psi^{c\,d}_{3,1}\rangle$	$N \leq 6$	$4(N-7)$	1
4	$\|\varphi^{(9)}\rangle = \|\psi^{c\,c}_{2,2}\rangle - \|\psi^{c\,c}_{3,1}\rangle + 3\delta_{N2}\|\psi_0\rangle - 6\delta_{N4}\|\psi_0\rangle$	$N \leq 4$	$4N-18$	0
4	$\|\varphi^{(10)}_a\rangle = \|\psi^a_4\rangle + i\varepsilon_{acd}\|\psi^{c\,d}_{3,1}\rangle$	$N \leq 4$	$4N-18$	1
4	$\|\varphi^{(11)}_{ab}\rangle = 3\left(\|\psi^{a\,b}_{3,1}\rangle + \|\psi^{b\,a}_{3,1}\rangle\right) - 2\delta_{ab}\|\psi^{c\,c}_{3,1}\rangle$	$N \leq 2$	$4N-10$	2

The dependence of the energies E on the number of spins N is solely determined by the diagonal term $k(N-1)|\psi^{a_k\ldots a_1}_{1\ \ldots 1}\rangle$ in Eq. (3.65). The reason for this is as follows. All other N-dependent terms in Eq. (3.65) are only nonzero if $k \geq N$. Since these can be written in terms of $N - mk$ current operators with $m \in \{1, 2, \ldots\}$, they represent strictly upper triangular terms in the space of states with current operators up to level k. This upper triangular structure is preserved by a diagonalization of all other terms. Therefore, only the diagonal term $k(N-1)|\psi^{a_l\ldots a_1}_{n_l\ldots n_1}\rangle$ contributes to the N-dependence of the energies. An N-independent representation of the eigenvalues is, therefore, given by subtracting the diagonal contribution:

$$\tilde{E} = \begin{cases} \frac{E-(N-1)k}{k}, & k > 0, \\ 0, & k = 0, \end{cases} \tag{3.71}$$

where we also rescaled the energies for $k \neq 0$ for convenience. This structure of the energies will now be used to detect null states of the spin system.

Null states

The number of eigenstates in Table 3.4 is smaller than the number of possible combinations of up to four current operators of order −1. The reason is that certain linear combinations of states $|\psi^{a_l\ldots a_1}_{n_l\ldots n_1}\rangle$ are null, i.e., they have a vanishing norm. For some of these, the corresponding CFT state is also null. This is, for example, the case for the state

$$\sum_b \left(3|\psi^{b\,a\,b}_{1,1,1}\rangle + 3|\psi^{b\,b\,a}_{1,1,1}\rangle - 2|\psi^{a\,b\,b}_{1,1,1}\rangle\right) \tag{3.72}$$

occurring at level 3. The spin system, however, has also null states for which the corresponding CFT state has a nonzero norm. This reflects the fact that the spin system has a finite, while the CFT has an infinite Hilbert space.

In principle, one can determine those null states numerically by computing inner products between states $|\psi^{a_l\ldots a_1}_{n_l\ldots n_1}\rangle$. This is also possible for large systems since the spin correlations in

$|\psi_0\rangle$ are known to satisfy algebraic equations [103]. Here, we use the following criterion to detect some of these null states analytically. According to Eq. (3.71), the energies for $k \neq 0$ are given by $E = k(\tilde{E} + N - 1)$, where $\tilde{E}$ is independent of N. For states having $\tilde{E} < 0$, this leads to $E < 0$ if N is small enough. Since $\mathcal{H}$ is positive semidefinite, these states must be null.

For $k \neq 0$, the condition $E < 0$ is equivalent to $N < 1 - \tilde{E}$. For each value of $\tilde{E}$, we can thus determine an integer N' so that the corresponding state is null for all number of spins N with $N \leq N'$, cf. the third column in Table 3.4. By applying current operators to these states, further null states at higher levels can be obtained. These do not necessarily satisfy $E < 0$ for a given N. In these cases, the value of N' is larger than the one inferred from the energy condition $E < 0$.

Spectrum for up to eight current operators

In Fig. 3.1, we plot the analytically determined energies for current operator levels up to $k = 8$. The boxes associated with the energy levels in Fig. 3.1 also show the spin content and the values of N' so that the corresponding state is null for all $N \leq N'$.

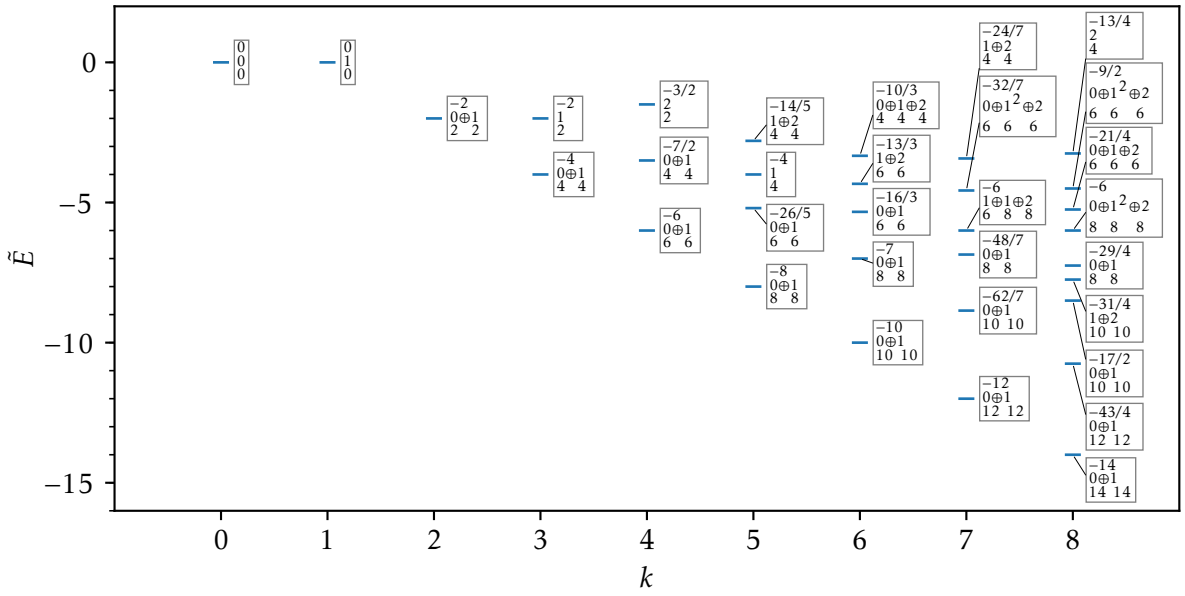

Figure 3.1: Analytically computed spectrum of the Haldane-Shastry model determined in terms of linear combinations of $|\psi^{a_l \ldots a_1}_{n_l \ldots n_1}\rangle$ with mode number sums $k = n_1 + \cdots + n_l$ (horizontal axis). The vertical axis shows the N-independent shifted and rescaled energies $\tilde{E}$, cf. Eq. (3.71). The rows in the boxes associated with the energy levels show (1) the value of $\tilde{E}$, (2) the spin content, (3) an integer N' so that the corresponding state is null for all systems with $N \leq N'$ spins.

At $k = 8$ and $\tilde{E} = -6$, for example, we find a multiplet consisting of a singlet, two triplets, and a quintet (spin-2 state). These states are null for numbers of spins $N \leq 8$. In Fig. 3.1, this multiplet is shown as

$$\begin{array}{|ccccc|} \hline -6 & & & & \\ 0 & \oplus & 1^2 & \oplus & 2 \\ 8 & & 8 & & 8 \\ \hline \end{array}, \tag{3.73}$$

where the first row shows the value of $\tilde{E}$, the second row the spin content with the superscript denoting the degeneracy, and the third row the values of N' so that the corresponding state is

null for all $N \leq N'$ spins.

3.3.4 Yangian highest-weight states in terms of current operators

The Haldane-Shastry model of Eq. (3.54) is manifestly SU(2) invariant, $[H_{\mathrm{HS}}, T^a] = 0$. Furthermore, it commutes with the rapidity operator [127],

$$\Lambda^a = \frac{i}{2} \sum_{i \neq j}^{N} w_{ij} \varepsilon_{abc} t_i^b t_j^c = \frac{i}{2} \sum_{i \neq j}^{N} w_{ij} (\vec{t}_i \times \vec{t}_j)^a, \tag{3.74}$$

where $a \in \{x, y, z\}$, and w_{ij} was defined in Eq. (3.56). The total spin T^a and the rapidity Λ^a generate the Yangian algebra. Opposed to the SU(2) invariance, the symmetry under the rapidity Λ^a is not directly visible at the level of the Hamiltonian of Eq. (3.54). For this reason, the Yangian symmetry of the Haldane-Shastry model is also called a *hidden* symmetry. It expresses the close relationship between the Haldane-Shastry model and the $\mathrm{SU}(2)_1$ WZW model since the latter also exhibits a Yangian symmetry. According to the Kac-Moody algebra of Eq. (3.3), the CFT operator corresponding to the total spin T^a is given by J_0^a. The operators J_0^a and

$$Q^a = \frac{i}{2} \sum_{m=1}^{\infty} \varepsilon_{abc} J_{-m}^b J_m^c \tag{3.75}$$

span the Yangian algebra at the level of the CFT [127].

Previous solutions to the Haldane-Shastry model [127, 128] made use of the Yangian symmetry by first constructing an eigenstate $|h\rangle$ that is the same time a highest-weight state of the Yangian algebra, i.e., it satisfies $T^+|h\rangle = \Lambda^+|h\rangle = 0$, where $T^\pm = T^x \pm iT^y$ and $\Lambda^\pm = \Lambda^x \pm i\Lambda^y$. Additional eigenstates of the Haldane-Shastry model with the same energy are then obtained from $|h\rangle$ by applying powers of Λ^- to $|h\rangle$. Since Λ^a does not commute with the spin Casimir $T^a T^a$, the application of Λ^- changes the spin of a state. This explains the occurrence of degenerate energy levels with different values of the total spin.

To relate our SU(2)-invariant approach to the construction in terms of Yangian multiplets, we now determine the highest-weight states $|h\rangle$ in terms of the eigenstates given in Table 3.4. This require to determine the action of T^a and Λ^a on states $|\psi_{1\ \ldots 1}^{a_k \ldots a_1}\rangle$. (As explained in Sec. 3.3.2, states $|\psi_{n_l \ldots n_1}^{a_l \ldots a_1}\rangle$ with general mode numbers can be expressed in terms of $|\psi_{1\ \ldots 1}^{a_k \ldots a_1}\rangle$ with $k = n_1 + \cdots + n_l$.)

The rapidity Λ^a is related to $\mathcal{C}_i^a$ of Eq. (3.55) through

$$\Lambda^a = \frac{3}{4} \sum_{i=1}^{N} \mathcal{C}_i^a, \tag{3.76}$$

where we used

$$\sum_{j=1, j \neq i}^{N} w_{ij} = 0 \tag{3.77}$$

for positions z_j on the unit circle as in Eq. (3.53). Using Eq. (3.76) and the decoupling equation

derived in Appendix B.1, we obtain

$$2\Lambda^a|\psi_{1\ \ldots 1}^{a_k\ldots a_1}\rangle = \sum_{q=1}^{k}(N-1)i\varepsilon_{aa_qc}|\psi_{1\ \ldots 1\ \ 11\ \ \ldots 1}^{a_k\ldots a_{q+1}ca_{q-1}\ldots a_1}\rangle + \sum_{q=1}^{k} i\varepsilon_{a_qac}|\psi_{11\ \ldots 1\ \ 1\ \ \ldots 1}^{ca_k\ldots a_{q+1}a_{q-1}\ldots a_1}\rangle$$
$$+ \sum_{q=2}^{k}\sum_{n=0}^{q-1}\sum_{s_1,\ldots,s_N} G_{a_k\ldots a_1}^{q,n}(s_1,\ldots,s_N)|s_1,\ldots,s_N\rangle, \tag{3.78}$$

where

$$\begin{aligned} G_{a_k\ldots a_1}^{q,n}(s_1,\ldots,s_N) &= 2\langle\phi_{s_1}(z_1)\ldots\phi_{s_N}(z_N)\left(J_{-n-1}^{a_q}J_{-1}^{a_k}\ldots J_{-1}^{a_{q+1}}J_n^aJ_{-1}^{a_{q-1}}\ldots J_{-1}^{a_1}\right)(0)\rangle \\ &\quad - 2\delta_{a_qa}\langle\phi_{s_1}(z_1)\ldots\phi_{s_N}(z_N)\left(J_{-n-1}^{c}J_{-1}^{a_k}\ldots J_{-1}^{a_{q+1}}J_n^cJ_{-1}^{a_{q-1}}\ldots J_{-1}^{a_1}\right)(0)\rangle \\ &\quad + 2N\tilde{\delta}_{n+1}i\varepsilon_{aa_qc}\langle\phi_{s_1}(z_1)\ldots\phi_{s_N}(z_N)\left(J_{-1}^{a_k}\ldots J_{-1}^{a_{q+1}}J_n^cJ_{-1}^{a_{q-1}}\ldots J_{-1}^{a_1}\right)(0)\rangle. \end{aligned} \tag{3.79}$$

Furthermore,

$$T^a|\psi_{1\ \ldots 1}^{a_k\ldots a_1}\rangle = i\sum_{q=1}^{N}\varepsilon_{aa_qc}|\psi_{1\ \ldots 1\ \ 11\ \ \ldots 1}^{a_k\ldots a_{q+1}ca_{q-1}\ldots a_1}\rangle \tag{3.80}$$

since $T^a|\psi_0\rangle = 0$ and $\left[T^a, u_{-1}^b\right] = i\varepsilon_{abc}u_{-1}^c$ according to Eq. (3.26) with $u_0^a = T^a$.

Table 3.5: Eigenstates $|h\rangle$ of the Haldane-Shastry model that are at the same time highest-weight states of the Yangian algebra ($T^+|h\rangle = \Lambda^+|h\rangle = 0$). The highest-weight states are expressed in terms of the eigenstates of Table 3.4. By applying Λ^- to a state $|h\rangle$, further eigenstates with the same energy can be obtained.

k	State $\|h\rangle$	Energy	Spin
0	$\|\varphi^0\rangle$	0	0
1	$\|\varphi_x^{(1)}\rangle + i\|\varphi_y^{(1)}\rangle$	$N-1$	1
2	$\|\varphi_x^{(3)}\rangle + i\|\varphi_y^{(3)}\rangle$	$2(N-3)$	1
3	$\|\varphi_x^{(5)}\rangle + i\|\varphi_y^{(5)}\rangle$	$3(N-5)$	1
3	$\|\varphi_x^{(6)}\rangle + i\|\varphi_y^{(6)}\rangle$	$3(N-3)$	1
4	$\|\varphi_x^{(8)}\rangle + i\|\varphi_y^{(8)}\rangle$	$4(N-7)$	1
4	$\|\varphi_x^{(10)}\rangle + i\|\varphi_y^{(10)}\rangle$	$4N-18$	1
4	$\|\varphi_{zz}^{(11)}\rangle + 2\|\varphi_{xx}^{(11)}\rangle + 2i\|\varphi_{xy}^{(11)}\rangle$	$4N-10$	2

Through Eqs. (3.78) and (3.80), we can express the solutions of $T^+|h\rangle = \Lambda^+|h\rangle = 0$ in terms of the eigenstates of Table 3.4. The result is shown in Table 3.5 and provides an explicit relation between the construction of eigenstates using the Yangian symmetry and our SU(2)-invariant approach.

We also considered the action of the CFT Yangian operators J_0^a and Q^a of Eq. (3.75) on the CFT states that correspond to the Yangian highest-weight states shown in Table 3.5. We found that these are precisely the highest-weight states with respect to J_0^a and Q^a. This is an indication that there is a direct correspondence between the Yangian highest-weight states of the spin system and those of the CFT.

3.3.5 Numerical spectra for the second tower and an odd number of spins

In the previous subsections, we constructed analytical eigenstates of the Haldane-Shastry model for N even in terms of states $|\psi^{a_l\dots a_1}_{n_l\dots n_1}\rangle$, which correspond to CFT states $(J^{a_l}_{-n_l}\dots J^{a_1}_{-n_1})(0)|0\rangle$. As shown in Sec. 3.1.2, the complete Hilbert space and therefore all eigenstates can be constructed by increasing the mode number sum $k = n_1 + \dots + n_l$. We now provide numerical evidence that a similar construction can be made for states obtained from the second sector of the CFT's Hilbert space and also in the case of N being odd.

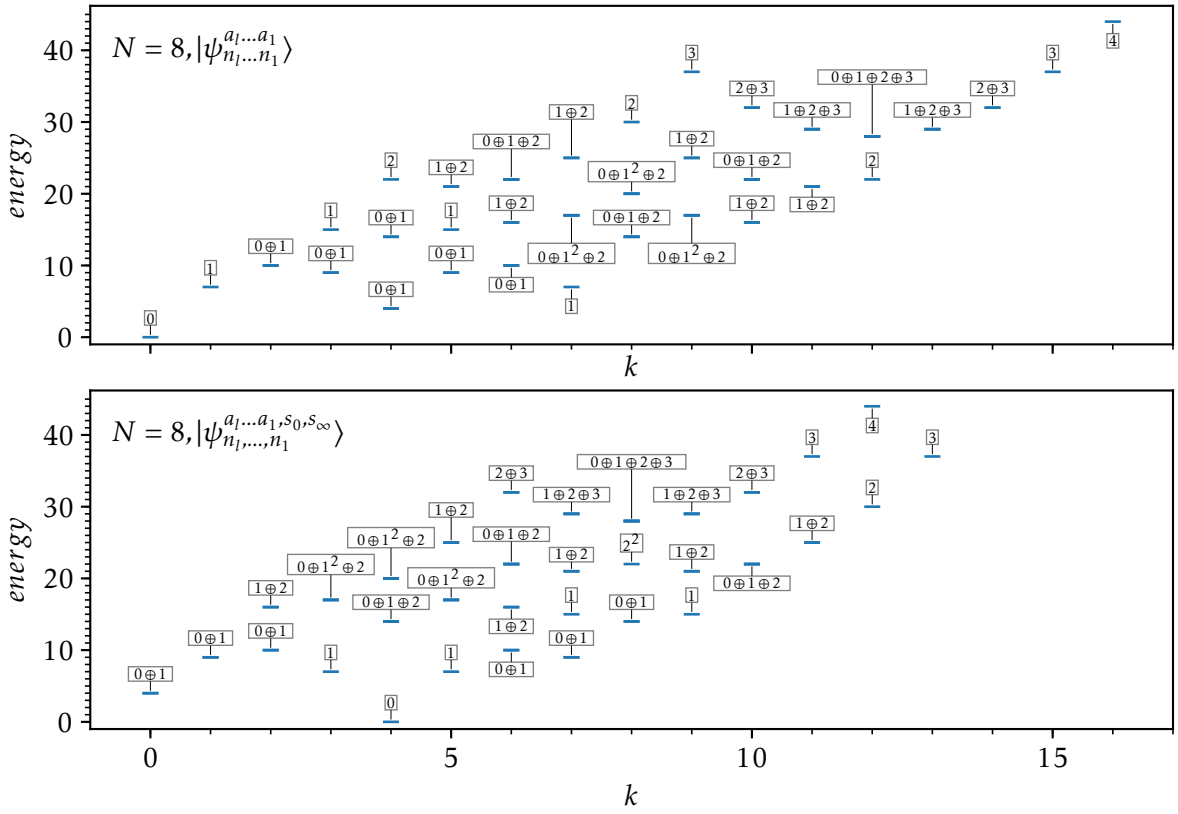

Figure 3.2: Numerically constructed spectrum of the Haldane-Shastry model for $N = 8$ built from states $|\psi^{a_l\dots a_1}_{n_l\dots n_1}\rangle$ (upper panel) and $|\psi^{a_l\dots a_1,s_0,s_\infty}_{n_l\dots n_1}\rangle$ (lower panel). The horizontal axes show the mode number sum $k = n_1 + \dots + n_l$ of the corresponding eigenstates. The labels associated with the energy levels indicate the spin content with the superscript denoting possible degeneracies.

In addition to the span of $(J^{a_l}_{-n_l}\dots J^{a_1}_{-n_1})(0)|0\rangle$, the CFT Hilbert space has another sector spanned by vectors $(J^{a_l}_{-n_l}\dots J^{a_1}_{-n_1}\phi_s)(0)|0\rangle$. A mapping to corresponding spin states $|\psi^{a_l\dots a_1,s_0,s_\infty}_{n_l\dots n_1}\rangle$ was defined in Sec. 3.1.3 by inserting additional primary fields at $z_0 = 0$ and $z_\infty = \infty$. We constructed the states $|\psi^{a_l\dots a_1,s_0,s_\infty}_{n_l\dots n_1}\rangle$ for small system sizes numerically and used them to build eigenstates of the Haldane-Shastry model. (The numerical method of exact diagonalization is explained in Appendix A.1.) For $N = 8$, the numerically computed spectrum is shown in Fig. 3.2. We find the same block-diagonal structure of the Hamiltonian as for the states $|\psi^{a_l\dots a_1}_{n_l\dots n_1}\rangle$ and that all eigenstates can be built in this way (the upper and lower panels in Fig. 3.2 show the same spectrum).

Let us now turn to the case of an odd number of spins. In this case, there are two towers of states ($|\psi^{a_l,\dots,a_1,s_\infty}_{n_l,\dots,n_1}\rangle$ and $|\psi^{a_l,\dots,a_1,s_0}_{n_l,\dots,n_1}\rangle$) introduced in Sec. 3.1.4. Our numerical results for $N = 7$ spins are shown in Fig. 3.3. As for the case of N even, we find that the Hamiltonian is block

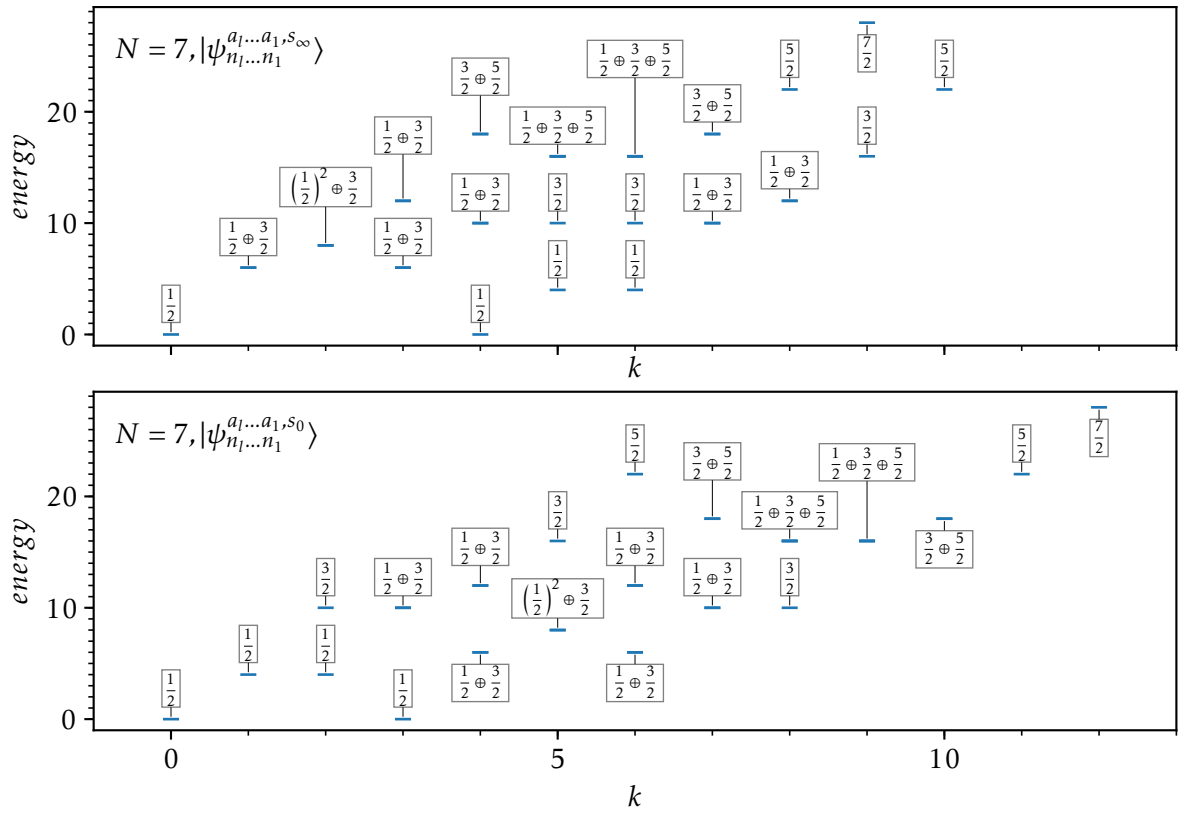

Figure 3.3: Numerically constructed spectrum of the Haldane-Shastry model for $N = 7$ in terms of states obtained by the insertion of current operators. Eigenstates were built as linear combinations of states $|\psi^{a_l \ldots a_1, s_\infty}_{n_l \ldots n_1}\rangle$ (upper panel) and $|\psi^{a_l \ldots a_1, s_0}_{n_l \ldots n_1}\rangle$ (lower panel). The horizontal axes show the mode number sum $k = n_1 + \cdots + n_l$ and the labels associated with the energies indicate the spin content with the superscripts corresponding to possible degeneracies.

diagonal and that the complete spectrum can be built from states $|\psi^{a_l, \ldots, a_1, s_\infty}_{n_l, \ldots, n_1}\rangle$ and $|\psi^{a_l, \ldots, a_1, s_0}_{n_l, \ldots, n_1}\rangle$, respectively.

The upper panel of Fig. 3.2 corresponds to our analytical results shown in Fig. 3.1. Not all energy levels of Fig. 3.1 appear in the numerically calculated spectrum because certain states of Fig. 3.1 are null for $N = 8$. This is the case for the all states with $E < 0$, which are those having $\tilde{E} < -7$ for $N = 8$. The remaining null states have the values

k	$\tilde{E}$	E	Spin
6	-7	0	$0 \oplus 1$
7	$-\frac{48}{7}$	1	$0 \oplus 1$
7	-6	7	$1 \oplus 2$
8	-6	8	$0 \oplus 1^2 \oplus 2$

and can be obtained from null states violating the energy condition by the insertion of additional current operators.

3.3.6 First excited states

Finally, let us comment on how the first excited states of the Haldane-Shastry model for N even are related to the states $|\psi^{a_l \ldots a_1}_{n_l \ldots n_1}\rangle$. While the states with one current operator $|\psi^a_1\rangle$ have an

energy of $E = N - 1$, the states $|\psi_0^{s_0,s_\infty}\rangle$ are eigenstates with $E = \frac{N}{2}$. This follows from

$$\mathcal{C}_i^a \sum_{s_0,s_\infty} |s_0\rangle \otimes |\psi_0^{s_0,s_\infty}\rangle \otimes |s_\infty\rangle = \left(K_b^a\right)_i \left(t_\infty^b - t_0^b\right) \sum_{s_0,s_\infty} |s_0\rangle \otimes |\psi_0^{s_0,s_\infty}\rangle \otimes |s_\infty\rangle \tag{3.81}$$

and

$$\left(\mathcal{C}_i^a\right)^\dagger = \mathcal{C}_i^a - \frac{4}{3} \sum_{j=1, j\neq i}^{N} w_{ij} t_j^a, \tag{3.82}$$

where the latter equation is a consequence of the uniform 1D lattice of Eq. (3.53). Except for $N = 2$, the states $|\psi_1^a\rangle$ are therefore not the first excited states of the Haldane-Shastry model since $|\psi_0^{s_0,s_\infty}\rangle$ have a lower energy. We did numerical calculations and found the first excited states are spanned by $|\psi_0^{s_0,s_\infty}\rangle$ with $s_0, s_\infty \in \{-1, 1\}$.

In the numerical spectrum of Fig. 3.2, we observe a singlet and a triplet at $k = \frac{N}{2} = 4$ with an energy of $E = \frac{N}{2} = 4$. Similarly, the analytically computed spectrum of Fig. 3.1 shows levels $\tilde{E} = -2k + 2$ with spin content $0 \oplus 1$. For $k = \frac{N}{2}$, these have an energy of $E = \frac{N}{2}$, cf. Eq. (3.71). Since $|\psi_0^{s_0,s_\infty}\rangle$ can be decomposed into a singlet and a triplet, this suggests that the first excited states have $k = \frac{N}{2}$ current operator modes.

3.3.7 Outlook: The Haldane-Shastry model with open boundary conditions

Recently [108], the Haldane-Shastry model with open boundary conditions [145, 146] was obtained from CFT similarly to the case of periodic boundary conditions. Given that the excited states of the Haldane-Shastry model with periodic boundary conditions can be obtained using CFT currents as shown above, we now investigate whether a similar construction is possible for the models with open boundary conditions.

Ref. [108] defines three types of lattices (type I, II, and III) that can be described in terms of uniformly distributed points on the unit circle. In these cases, the Hamiltonian of the open Haldane-Shastry model is given by [108]

$$\mathcal{H}_{\text{open}} = \sum_{i\neq j}^{N} \left(\frac{1}{|\zeta_i - \zeta_j|^2} + \frac{1}{|\zeta_i - \bar{\zeta}_j|^2} \right) t_i^a t_j^a - E_0. \tag{3.83}$$

The complex numbers ζ_j for $j \in \{1, \ldots, N\}$ with N even and the energy E_0 are given by [108, 155]

$$\zeta_j = e^{i\frac{\pi}{N}(j-\frac{1}{2})}, \qquad E_0 = -\frac{1}{48} N(4N^2 + 3N + 5) \qquad \text{for the type I lattice,} \tag{3.84}$$

$$\zeta_j = e^{i\frac{\pi}{N+1} j}, \qquad E_0 = -\frac{1}{48} N(4N^2 + 9N + 11) \qquad \text{for the type II lattice,} \tag{3.85}$$

and

$$\zeta_j = e^{i\frac{2\pi}{2N+1} j}, \qquad E_0 = -\frac{1}{24} N(2N^2 + 3N + 4) \qquad \text{for the type III lattice.} \tag{3.86}$$

The subtraction of E_0 in Eq. (3.83) results in $\mathcal{H}_{\text{open}}$ having a vanishing ground state energy.

The ground state of $\mathcal{H}_{\text{open}}$ is given by $|\psi_0\rangle$ defined in Eq. (3.11) with coordinates z_j chosen as projections of ζ_j onto the real line, $z_j = \text{Re}(\zeta_j)$ [108].

We did numerical calculations indicating that the open Haldane-Shastry Hamiltonian of Eq. (3.83) is block-diagonal in the states $|\psi_{-n_l \cdots -n_1}^{a_l \cdots a_1}\rangle$ [cf. Eq. (3.52)], where the current modes are inserted at infinity. For $N = 6$, the numerically computed spectra are shown in Fig. 3.4.

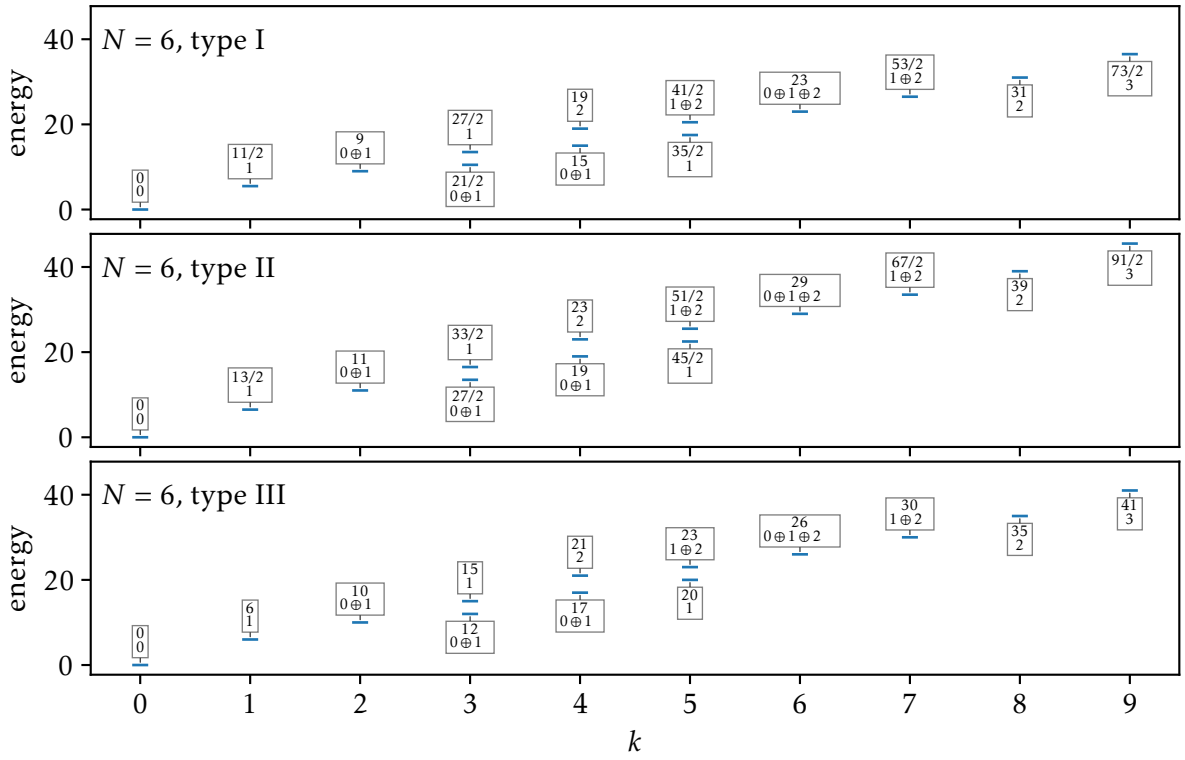

Figure 3.4: Numerically computed spectrum of the open Haldane-Shastry model [Eq. (3.83)] for $N = 6$ spins. The excited states were obtained in terms of $|\psi^{a_l \cdots a_1}_{-n_l \cdots -n_1}\rangle$, which are defined by inserting current operators at infinity [Eq. (3.52)]. The horizontal axes show the level $k = n_1 + \cdots + n_l$. The rows in the boxes associated with the energy levels show (1) the energy and (2) the spin content.

As a step towards an analytical solution analogous to the case of the periodic Haldane-Shastry model, we found the following commutator between $\mathcal{H}_{\text{open}}$ and u_1^a:

$$\left[\mathcal{H}_{\text{open}}, u_1^a\right] = i\varepsilon_{abc} u_1^b T^c - i\frac{3}{4}\sum_{j=1}^{N} \text{Im}(\zeta_j)\mathcal{D}_j^a + \frac{4N + C - 2}{4} u_1^a, \tag{3.87}$$

where

$$\mathcal{D}_i^a = \frac{2}{3}\sum_{j=1, j\neq i}^{N}\left(\frac{\zeta_i + \zeta_j}{\zeta_i - \zeta_j} + \frac{\zeta_i + \bar{\zeta}_j}{\zeta_i - \bar{\zeta}_j}\right)\left(t_i^a + i\varepsilon_{abc} t_i^b t_j^c\right) \quad \text{and} \quad C = \begin{cases} 0 & \text{for the type I chain,} \\ 4 & \text{for the type II chain,} \\ 2 & \text{for the type III chain.} \end{cases} \tag{3.88}$$

The operators $\mathcal{D}_i^a$ annihilate $|\psi_0\rangle$ for coordinates $z_j = \text{Re}(\zeta_j)$ and can be used to construct $\mathcal{H}_{\text{open}}$ as [108]

$$\mathcal{H}_{\text{open}} = \frac{1}{8}\sum_{i=1}^{N}\left(\mathcal{D}_i^a\right)^\dagger \mathcal{D}_i^a + \left(\frac{N}{3} + \frac{C}{12}\right) T^a T^a, \tag{3.89}$$

which is analogous to Eqs. (3.57) and (3.58) in the case of the periodic chain. We do not have a complete analytical derivation of the commutator of Eq. (3.87), but we confirmed it numerically for small systems.

An analytical solution of the open boundary case would also require the derivation of the action of $\mathcal{D}_i^a$ on states $|\psi^{a_k\dots a_1}_{-1\dots-1}\rangle$ analogous to Eq. (3.63) in the case of periodic boundary conditions. Together with Eq. (3.87), one could then derive an analytical expression for $\mathcal{H}_{\text{open}}|\psi^{a_k\dots a_1}_{-1\dots-1}\rangle$. As your numerical calculations suggest, we expect $\mathcal{H}_{\text{open}}|\psi^{a_k\dots a_1}_{-1\dots-1}\rangle$ to be a linear combination of states of the same level k.

3.4 Edge states for the Kalmeyer-Laughlin wave function

In this section, we study the state $|\psi_0\rangle$ and modifications of $|\psi_0\rangle$ obtained by inserting additional fields at $z_0 = 0$ and/or $z_\infty = \infty$. In Sec. 3.3 above, we considered the 1D case and showed that eigenstates of the Haldane-Shastry model can be constructed in terms of these states. We now consider square lattices on the cylinder with coordinates z_j as defined in Eq. (3.51). In the 2D case, $|\psi_0\rangle$ is equivalent to the Kalmeyer-Laughlin state [109], and we study the states corresponding to excitations of the CFT as candidates for edge modes with respect to $|\psi_0\rangle$. By comparing spin-spin correlation functions, we provide numerical evidence that these indeed describe edge states.

In this section, we assume that the number of sites N is even. It is also possible to study the case of N being odd which will show the existence of two topological sectors. However, we can already identify the two anyonic sectors for N even. As will be shown below in Sec. 3.4.1, the state $|\psi_0\rangle$ and the singlet component $|\psi_0^{\text{sgl}}\rangle \equiv |\psi_0^{\uparrow,\downarrow}\rangle - |\psi_0^{\downarrow,\uparrow}\rangle$ of the state with two additional spins $|\psi_0^{s_0,s_\infty}\rangle$ (one at $z_0 = 0$ and one at $z_\infty = \infty$) can be obtained from the wave function of N primary fields on the torus in the limit where the torus becomes a cylinder. This argumentation shows that the two states $|\psi_0\rangle$ and $|\psi_0^{\text{sgl}}\rangle$ represent the two anyonic sectors in the case of an even number of spins. As in the 1D case, it is possible to consider an odd number of sites on the cylinder by putting an additional spin either at $z_0 = 0$ or at $z_\infty = \infty$ so that the charge neutrality condition is satisfied (cf. Sec. 3.1.4). On the torus, however, such a construction is not possible and the argumentation that we used to identify the two sectors for even N does not directly apply.

3.4.1 Relation to the Kalmeyer-Laughlin states on the torus

We now show that $|\psi_0\rangle$ and the singlet component $|\psi_0^{\text{sgl}}\rangle$ of $|\psi_0^{s_0,s_\infty}\rangle$ on the cylinder can be obtained from the wave function constructed from N CFT primaries on the torus. To this end, we consider a torus and take a limit in which the torus becomes a cylinder.

We define the torus for $\omega_1 > 0$ and $\omega_2 = iL$ with $L > 0$ by identifying a complex number z with $z + n\omega_1 + m\omega_2$ for $m, n \in \mathbb{Z}$. The two circumferences of the torus are therefore given by ω_1 and $|\omega_2|$. Let us denote the positions on the torus by v_i, i.e. we assume that v_i lie in the rectangle spanned by ω_1 and ω_2. Keeping the positions v_i fixed and taking the circumference $L = |\omega_2| \to \infty$ transforms the torus into a cylinder, as illustrated in Fig. 3.5.

On the torus, there are two states $|\psi_k^{\text{torus}}\rangle$ with $k \in \{0, \frac{1}{2}\}$. These are given by [156]

$$\begin{aligned}\psi_k^{\text{torus}}(s_1,\dots,s_N) &= \langle \phi_{s_1}(v_1)\dots\phi_{s_N}(v_N)\rangle_k \\ &\propto \delta_{\mathbf{s}}\chi_{\mathbf{s}}\theta\begin{bmatrix}k\\0\end{bmatrix}\left(\sum_{i=1}^N \zeta_i s_i, 2\tau\right)\prod_{i<j}^N\left(\theta\begin{bmatrix}\frac{1}{2}\\\frac{1}{2}\end{bmatrix}(\zeta_i-\zeta_j,\tau)\right)^{\frac{1}{2}s_is_j}.\end{aligned} \tag{3.90}$$

Here, $\zeta_i = v_i/\omega_1$ are the rescaled positions, $\tau = \omega_2/\omega_1$ is the modular parameter of the torus, and θ the Riemann theta function defined as

$$\theta\begin{bmatrix}a\\b\end{bmatrix}(\zeta,\tau) = \sum_{n\in\mathbb{Z}} e^{i\pi\tau(n+a)^2+2\pi i(n+a)(\zeta+b)}. \tag{3.91}$$

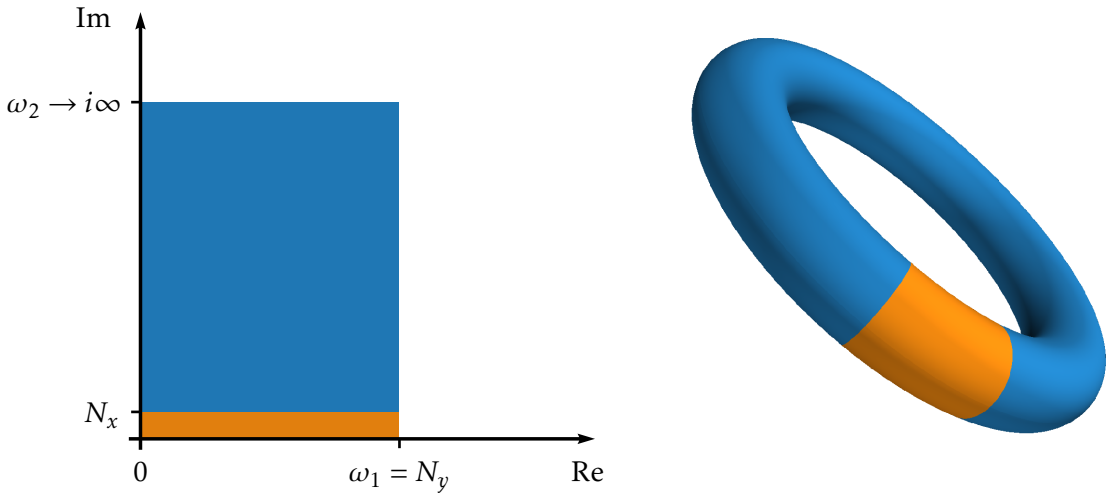

Figure 3.5: Limit in which the torus becomes a cylinder: The circumference $|\omega_2|$ is taken to infinity while the positions lie in the finite region of size $N_x \times N_y$ shown as the orange patch.

The limit $\omega_2 \to i\infty$, which transforms the torus into a cylinder, implies $\tau \to i\infty$. In this case, only the terms with the smallest value of $(n+a)^2$ contribute to the sum of Eq. (3.91). These terms have $n = 0$ for $a = 0$ and $n \in \{-1, 0\}$ for $a = \frac{1}{2}$. Therefore,

$$\begin{aligned}
\theta\begin{bmatrix}0\\0\end{bmatrix}(\zeta, 2\tau) \quad &\to 1, \\
\theta\begin{bmatrix}\frac{1}{2}\\0\end{bmatrix}(\zeta, 2\tau) \quad &\to e^{\frac{\pi i \tau}{2}}(e^{i\pi\zeta} + e^{-i\pi\zeta}), \quad \text{and} \\
\theta\begin{bmatrix}\frac{1}{2}\\\frac{1}{2}\end{bmatrix}\left(\zeta_i - \zeta_j, \tau\right) &\to i e^{-i\pi(\zeta_i+\zeta_j)} e^{\frac{i\pi\tau}{4}}(e^{2\pi i\zeta_i} - e^{2\pi i\zeta_j}),
\end{aligned} \tag{3.92}$$

for $\tau \to i\infty$. With $s_1 + \cdots + s_N = 0$, it follows that

$$\prod_{m<n}^{N} e^{-i\frac{\pi}{2}(\zeta_m+\zeta_n)s_m s_n} = e^{i\frac{\pi}{2}\sum_{n=1}^{N}\zeta_n}. \tag{3.93}$$

In the limit $\omega_2 \to i\infty$, we therefore obtain

$$\psi_0^{\text{torus}}(s_1, \ldots, s_N) \propto \delta_{\mathbf{s}}\chi_{\mathbf{s}} \prod_{m<n}^{N}\left(e^{2\pi i\frac{v_m}{\omega_1}} - e^{2\pi i\frac{v_n}{\omega_1}}\right)^{\frac{1}{2}s_m s_n} \tag{3.94}$$

and

$$\psi_{\frac{1}{2}}^{\text{torus}}(s_1, \ldots, s_N) \propto \delta_{\mathbf{s}}\chi_{\mathbf{s}}\left(\prod_{n=1}^{N} e^{\pi i\frac{v_n}{\omega_1}s_n} + \prod_{n=1}^{N} e^{-\pi i\frac{v_n}{\omega_1}s_n}\right)\prod_{m<n}^{N}\left(e^{2\pi i\frac{v_m}{\omega_1}} - e^{2\pi i\frac{v_n}{\omega_1}}\right)^{\frac{1}{2}s_m s_n}. \tag{3.95}$$

The exponentials $e^{2\pi i v_n/\omega_1}$ lie on a cylinder of circumference ω_1. We therefore identify $z_n = e^{2\pi i v_n/\omega_1}$ and $N_y = \omega_1$. Comparing the expressions for $|\psi_k^{\text{torus}}\rangle$ in the limit $\omega_2 \to \infty$ to Eqs. (3.12) and (3.39), we conclude that $|\psi_0^{\text{torus}}\rangle \propto |\psi_0\rangle$ and $|\psi_{\frac{1}{2}}^{\text{torus}}\rangle \propto |\psi_0^{\uparrow,\downarrow}\rangle - |\psi_0^{\downarrow,\uparrow}\rangle \equiv |\psi_0^{\text{sgl}}\rangle$.

3.4.2 Spin correlation functions and edge states

We calculated two-point spin correlation functions in the states $|\psi_0\rangle$, $|\psi_1^a\rangle$ and in the singlet state

$$|\psi_0^{\mathrm{sgl}}\rangle \equiv |\psi_0^{\uparrow,\downarrow}\rangle - |\psi_0^{\downarrow,\uparrow}\rangle \tag{3.96}$$

using a Metropolis Monte Carlo algorithm as explained in Appendix A.2. This allowed us to compare properties of the states numerically for large system sizes by sampling the relevant probability distributions. We furthermore exploited the translation and inversion symmetries of Table 3.3 to average over equivalent correlation functions, thus obtaining a faster converging Monte Carlo estimate.

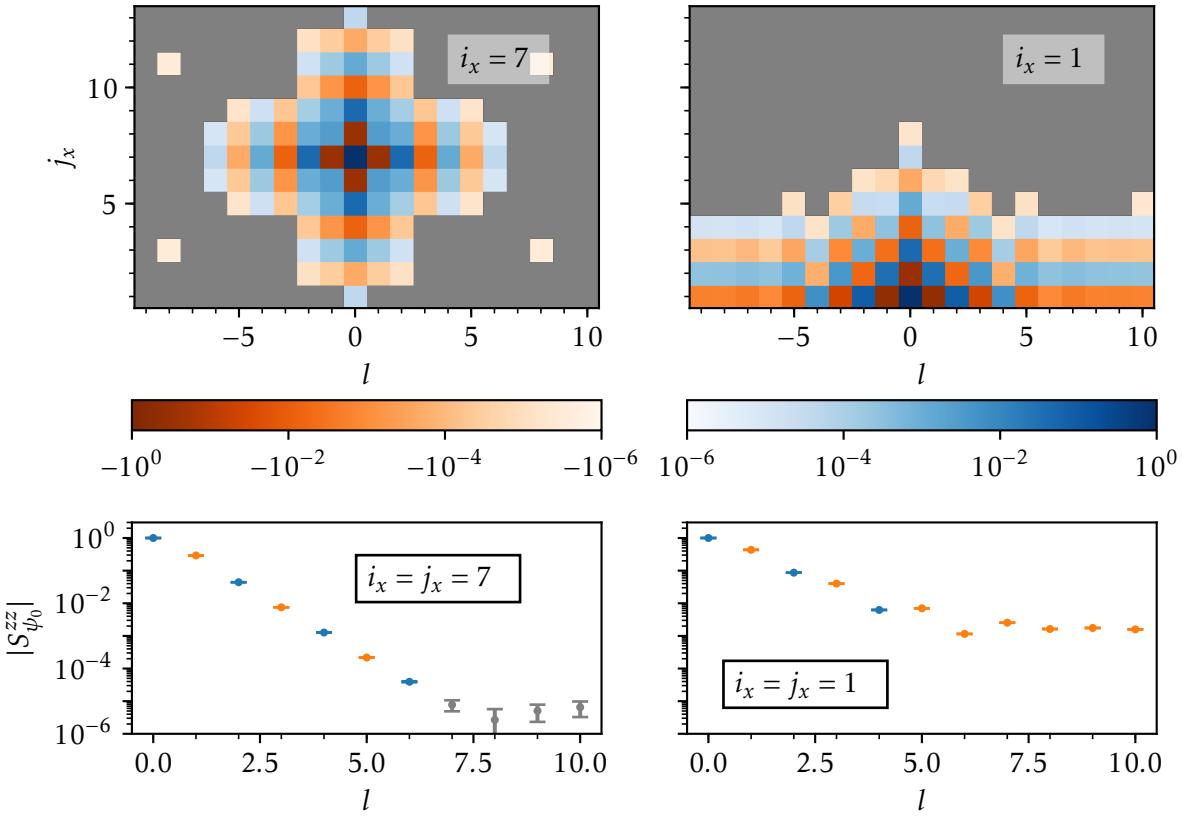

Figure 3.6: Two-point spin correlation function $S^{zz}_{\psi_0}(i_x, j_x, l)$ in the bulk (left panels) and at the edge (right panels) for $N_x = 13$ and $N_y = 20$. The upper panels show the two-dimensional dependency in a color plot. Whenever the value of the correlation function does not differ from zero by more than three times the estimated error, we excluded the data point from the plot (gray fields). In the lower panels, the absolute value $|S^{zz}_{\psi_0}(i_x, i_x, l)|$ of the correlation function along the y direction is plotted. Points for which the sign of the correlation function is positive (negative) are shown in blue (orange). For the data shown in gray, the mean value does not differ from zero by more than three times the estimated error. In the bulk, the correlations decay exponentially, while a nonzero, negative correlation remains at the edge for $l \geq 5$.

In this subsection, we shall use the notation

$$S^{ab}_{\psi}(i_x, j_x, l) = 4\frac{\langle\psi|t^a_{i_x,l+1}t^b_{j_x,1}|\psi\rangle}{\langle\psi|\psi\rangle} \tag{3.97}$$

for the two-point correlation function in a state $|\psi\rangle$. Since all wave functions that we consider have a translational symmetry in the periodic direction, their value only depends on the difference l of the positions in the y direction.

Before comparing the wave functions with each other, we discuss the spin ordering pattern in $|\psi_0\rangle$, which is encoded in the correlation function $S^{zz}_{\psi_0}(i_x, j_x, l)$. (Since $|\psi_0\rangle$ is a singlet, xx, yy and zz correlations are the same, and only correlation functions with $a = b$ are nonzero.) Our numerical results are shown in Fig. 3.6. In the bulk of the system, we observe a ring-like structure with an alternating magnetization. At the edge, the correlations are antiferromagnetic at short distances. At larger distances along the y direction, however, the sign becomes stationary and a negative correlation remains. In the two-dimensional picture, the ordering is still characterized by an alternating magnetization with the sign of the correlation function changing along the x direction.

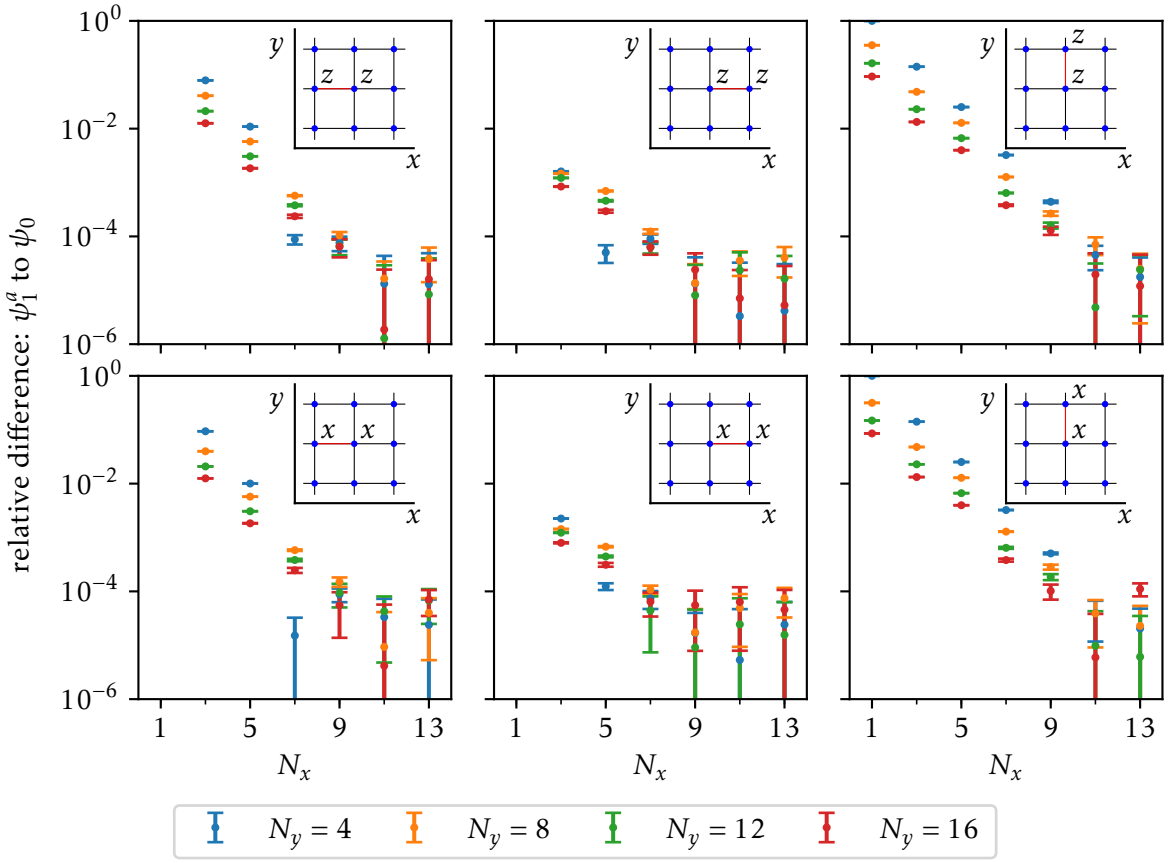

Figure 3.7: Comparison of nearest-neighbor bulk correlations in $|\psi_1^z\rangle$ and $|\psi_0\rangle$. The vertical axes show the relative differences $|S^{bc}_{\psi_1^z} - S^{bc}_{\psi_0}|/|S^{bc}_{\psi_0}|$ with $b = c = z$ (upper panels) and $b = c = x$ (lower panels). Along the horizontal axis, the number of spins in the open direction (N_x) is varied. The different colors correspond to configurations with different N_y. The insets show for which sites the correlation functions were computed. The sites in the central column of the insets correspond to the middle of the cylinder in the x direction. The relative difference decreases exponentially in N_x.

We now discuss whether the states $|\psi_1^a\rangle$ can be considered as edge states. If so, then the local properties of $|\psi_1^a\rangle$ and $|\psi_0\rangle$ in the bulk should be the same. Since these are encoded in the spin correlation functions, we compared the nearest-neighbor two-point correlators in the bulk for

different system sizes. The relative differences

$$\left| \frac{S^{bc}_{\psi_1^a}(i_x, j_x, l) - S^{bc}_{\psi_0}(i_x, j_x, l)}{S^{bc}_{\psi_0}(i_x, j_x, l)} \right| \tag{3.98}$$

are shown in Fig. 3.7 for $a = b = c = z$ (upper panels) and $a = z, b = c = x$ (lower panels). Correlation functions for other choices of a, b, and c either vanish or can be reduced to these due to the SU(2) invariance of $|\psi_0\rangle$. In the left and middle panels, the correlations along the x direction are shown and in the right panels those along the y direction. We find that the relative differences approach zero exponentially as a function of N_x. Even though the differences tend to be larger for smaller N_y, they are still exponentially suppressed as N_x is increased. This is an indication that $|\psi_1^a\rangle$ for $a \in \{x, y, z\}$ indeed describe edge states compared to $|\psi_0\rangle$ as the thermodynamic limit in the open direction is taken.

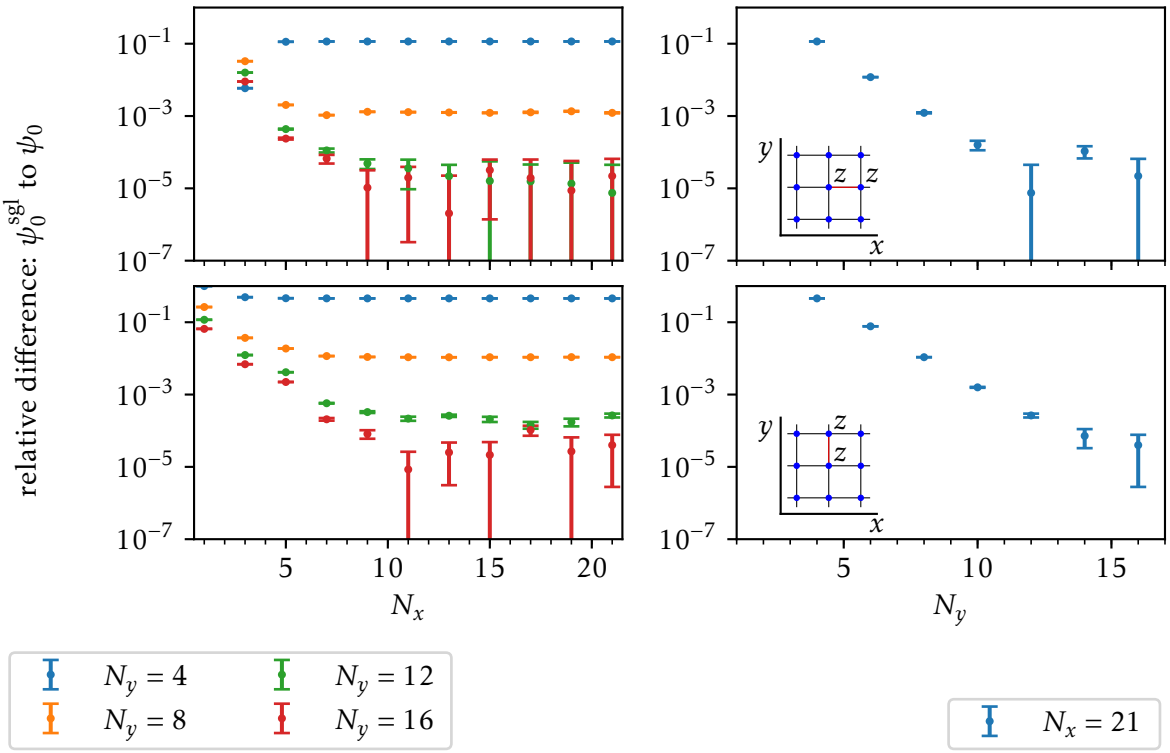

Figure 3.8: Comparison of nearest-neighbor bulk correlations in $|\psi_0^{\mathrm{sgl}}\rangle$ and $|\psi_0\rangle$. The vertical axes show the relative differences $|S^{zz}_{\psi_0^{\mathrm{sgl}}} - S^{zz}_{\psi_0}|/|S^{zz}_{\psi_0}|$. In the left panels, N_x is varied along the horizontal axes and the different colors correspond to different choices of N_y. On the right panels, N_y varies along the horizontal axes and N_x is fixed. For N_x large enough, the differences tend to zero exponentially as a function of N_y.

Our results for the comparison between $|\psi_0^{\mathrm{sgl}}\rangle$ and $|\psi_0\rangle$ are shown in Fig. 3.8. Since both $|\psi_0\rangle$ and $|\psi_0^{\mathrm{sgl}}\rangle$ are singlets, it is enough to compare the zz correlations. Furthermore, the correlations in the positive and the negative x direction are the same in the middle of the cylinder since $|\psi_0\rangle$ and $|\psi_0^{\mathrm{sgl}}\rangle$ are symmetric under the inversion, cf. Sec. 3.2. In contrast to $|\psi_1^a\rangle$, we find that the thermodynamic limit in the x direction is not enough for the differences to vanish. Rather, we observe that the differences become stationary if N_y is held fixed and N_x

increased. As shown in the right panels of Fig. 3.8, the differences do, however, tend to zero exponentially as a function of N_y if N_x is chosen large enough.

3.4.3 States at a higher level

In the previous subsection, the states at level one in current operators were considered. We also compared spin correlations in $|\psi_n^a\rangle$ to those in $|\psi_0\rangle$ for higher values of n. For very large mode numbers n, only the terms at the edge contribute to the sum in u_{-n}^a. To see this, let us consider

$$u^a_{-n-mN_y} = \sum_{j=1}^{N} \frac{1}{z_j^{n+mN_y}} t_j^a \propto \sum_{j_x=1}^{N_x} e^{-\frac{2\pi}{N_y}(n+mN_y)j_x} \sum_{j_y=1}^{N_y} e^{-\frac{2\pi i}{N_y} n j_y} t^a_{j_x,j_y}. \tag{3.99}$$

For large values of m, the terms with $j_x > 1$ are exponentially suppressed with respect to those that have $j_x = 1$. We denote the corresponding states with one current operator by $|\chi_n^a\rangle$:

$$|\chi_n^a\rangle = \lim_{m\to\infty} |\psi^a_{n+mN_y}\rangle \propto \sum_{j_y=1}^{N_y} e^{-\frac{2\pi i}{N_y} n j_y} t^a_{1,j_y} |\psi_0\rangle. \tag{3.100}$$

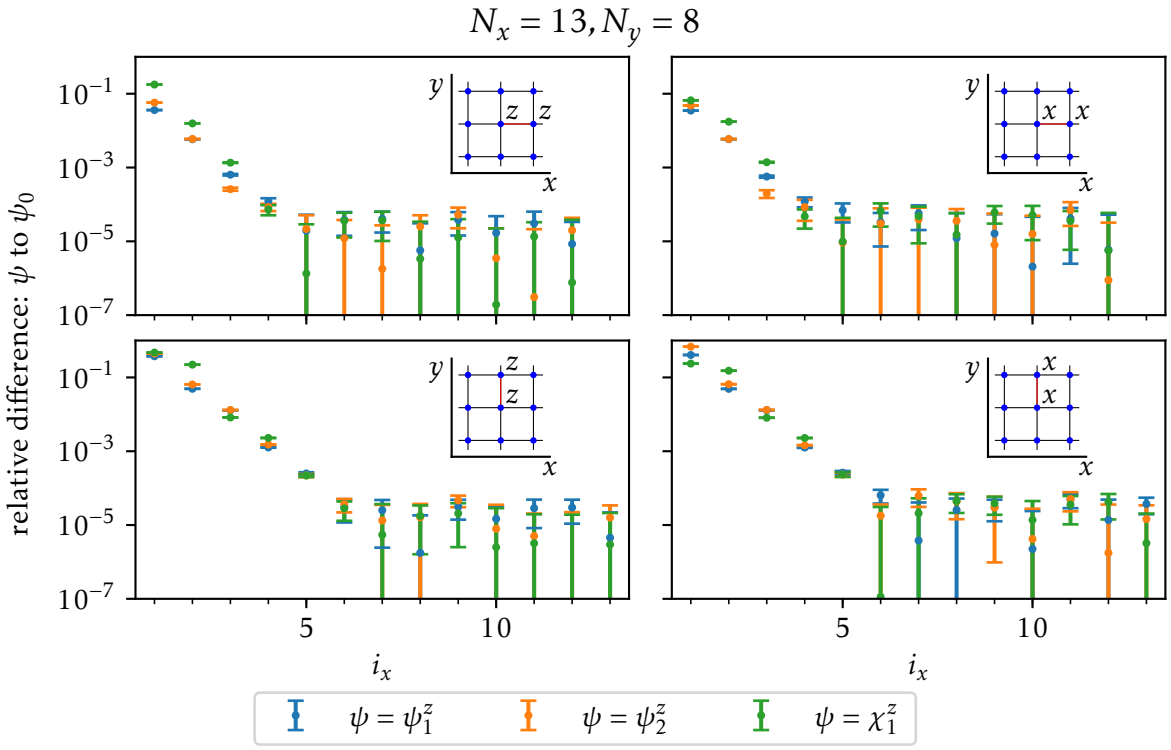

Figure 3.9: Relative difference $|S^{ab}_{\psi} - S^{ab}_{\psi_0}|/|S^{ab}_{\psi_0}|$ in nearest-neighbor correlators for $\psi \in \{\psi_1^z, \psi_2^z, \chi_1^z\}$ [cf. Eq. (3.100) for the definition of $|\chi_1^a\rangle$]. The position i_x in the x direction is varied along the horizontal axis. The plots in the left panels have $a = b = z$ and those in the right panels $a = b = x$. In the upper panels, the correlations along the x direction are shown [$j_x = i_x + 1$, $l = 0$] and the lower panels correspond to correlations along the y direction [$j_x = i_x, l = 1$].

Fig. 3.9 shows the difference in nearest-neighbor correlations relative to $|\psi_0\rangle$ for $N_x = 13$ and $N_y = 8$. The three colors correspond to the states $|\psi_1^z\rangle, |\psi_2^z\rangle$ and $|\chi_1^z\rangle$. As the position in the open direction is increased, the differences vanish exponentially for all three states. We note that the differences are large at the left edge ($i_x = 1$) and small at the right edge ($i_x = 13$). This agrees with the expectation that the operators u_{-n}^a are localized at the left edge. In contrast to the state $|\psi_0^{\mathrm{sgl}}\rangle$, the states $|\psi_n^a\rangle$ perturb $|\psi_0\rangle$ only at one edge and their behavior is, therefore, expected to approach that of $|\psi_0\rangle$ at the other edge. The results of Fig. 3.9 provide an indication that $|\psi_n^a\rangle$ describe edge states also for $n > 1$.

We note, however, that the linear span of $|\psi_n^a\rangle$ for $n \in \{1, \ldots, N-1\}$ contains not only edge states. The states $|\psi_n^a\rangle$ can even be linearly combined so that $|\psi_0\rangle$ is perturbed at an arbitrary position j:

$$t_j^a |\psi_0\rangle = \sum_{n=2}^{N} \left(Z^{-1}\right)_{jn} |\psi_{n-1}^a\rangle, \tag{3.101}$$

where Z is the matrix defined in Eq. (3.28). This observation can be understood from the fact that two states $|\psi_m^a\rangle$ and $|\psi_n^a\rangle$ are not necessarily orthogonal if $m - n = 0$ modulo N_y. In this case, $|\psi_m^a\rangle$ and $|\psi_n^a\rangle$ have the same momentum in the y direction, as discussed in Sec. 3.2. The linear combination

$$|\psi_n^a\rangle - e^{-2\pi \frac{N_x-1}{2}} |\psi_{n+N_y}^a\rangle = \sum_{j_x=1}^{N_x} \left(1 - e^{-2\pi(j_x-1)}\right) \sum_{j_y=1}^{N_y} \frac{1}{z_{j_x,j_y}^n} t_{j_x,j_y}^a |\psi_0\rangle, \tag{3.102}$$

for example, receives no contribution from spin operators at the left edge ($j_x = 1$). Even though both $|\psi_n^a\rangle$ and $|\psi_{n+N_y}^a\rangle$ are perturbed from $|\psi_0\rangle$ mostly at $j_x = 1$, this is not the case for the difference of Eq. (3.102).

3.4.4 Inner products of states from current operators

In this subsection, we discuss the relation of inner products between the states $|\psi_{n_l \ldots n_1}^{a_l \ldots a_1}\rangle$ on the level of the spin system and CFT inner products between states $(J_{-n_l}^{a_l} \ldots J_{-n_1}^{a_1})(0)|0\rangle$. For edge states in the continuum that are constructed from descendant states of a CFT, the authors of Ref. [99] come to the remarkable conclusion that, in the thermodynamic limit and under the assumption of exponentially decaying correlations in the bulk, the inner products between edge states are the same as the inner products between CFT states. We now consider inner products between states constructed from current operators to test if a similar correspondence holds for the lattice states $|\psi_{n_l \ldots n_1}^{a_l \ldots a_1}\rangle$ and the CFT states they are constructed from. The spin system inner products that we consider are given by

$$R^{k+k'} \frac{\langle \psi_{n_l \ldots n_1}^{a_l \ldots a_1} | \psi_{m_{l'} \ldots m_1}^{b_{l'} \ldots b_1} \rangle}{\langle \psi_0 | \psi_0 \rangle} \equiv R^{k+k'} \frac{\langle \psi_0 | \left(u_{-n_1}^{a_1}\right)^\dagger \ldots \left(u_{-n_l}^{a_l}\right)^\dagger u_{-m_{l'}}^{b_{l'}} \ldots u_{-m_1}^{b_1} | \psi_0 \rangle}{\langle \psi_0 | \psi_0 \rangle}, \tag{3.103}$$

where

$$R = \min_{j \in \{1,\ldots,N\}} |z_j| = e^{-\frac{\pi}{N_y}(N_x-1)} \tag{3.104}$$

is the minimal absolute value of the positions, $k = n_1 + \cdots + n_l$, and $k' = m_1 + \cdots + m_{l'}$. The factor $R^{k+k'}$ accounts for the scaling of the operators u_{-n}^a with respect to a rescaling of the positions.

The minimal value is chosen because the operators

$$u^a_{-n} = \sum_{j=1}^{N} \frac{t^a_j}{(z_j)^n} \tag{3.105}$$

have the highest contribution at the edge with $|z_j| = R$.

We compare the inner products of the lattice system (3.103) to the CFT inner products

$$\langle 0|J^{a_1}_{n_1} \dots J^{a_l}_{n_l} J^{b_{l'}}_{-m_{l'}} \dots J^{b_1}_{-m_1}|0\rangle. \tag{3.106}$$

If a correspondence similar to that of Ref. [99] also holds for lattice states, then the expressions of Eq. (3.103) should approach those of Eq. (3.106) in the thermodynamic limit.

Note that the inner products of the spin system are hard to evaluate for large system sizes, whereas the CFT inner product can be easily computed using the Kac-Moody algebra [Eq. (3.3)]. On the level of the spin system, the insertion of current operators corresponds to an application of spin operators to $|\psi_0\rangle$ [cf. Eq. (3.42)]. Therefore, the inner products can be determined numerically using a Monte Carlo method if the number of current operators is small.

We calculated the inner products for the states $|\psi^a_1\rangle$, $|\psi^a_2\rangle$ and $|\psi^{b\,b}_{1,1}\rangle$, which are all nonzero states at levels one and two. For these states, inner products between different states vanish because they have either a different spin or a different momentum. It is thus sufficient to compare the norm squared of a state to the norm squared of the corresponding CFT state, as summarized in Table 3.6.

Table 3.6: State of the spin system and corresponding CFT state up to level 2 in current operators. The third column shows the norm squared of the CFT state, which is expected to be approached by the spin-system inner product of Eq. (3.103).

Spin state	CFT state	Norm squared of CFT state
$\|\psi^a_1\rangle$	$J^a_{-1}\|0\rangle$	$\langle J^a_1 J^a_{-1}\rangle = \frac{1}{2}$ (no sum over a)
$\|\psi^a_2\rangle$	$J^a_{-2}\|0\rangle$	$\langle J^a_2 J^a_{-2}\rangle = 1$ (no sum over a)
$\|\psi^{b\,b}_{1,1}\rangle$	$J^b_{-1}J^b_{-1}\|0\rangle$	$\langle J^c_1 J^c_1 J^b_{-1} J^b_{-1}\rangle = \frac{9}{2}$

In Fig. 3.10, our numerical results are shown for the relative difference

$$\left| \frac{R^{2k} \dfrac{\langle\psi|\psi\rangle}{\langle\psi_0|\psi_0\rangle} - \langle\psi_{\mathrm{CFT}}|\psi_{\mathrm{CFT}}\rangle}{\langle\psi_{\mathrm{CFT}}|\psi_{\mathrm{CFT}}\rangle} \right| \tag{3.107}$$

as a function of the system size. Here, $\psi \in \{\psi^a_1, \psi^a_2, \psi^{b\,b}_{1,1}\}$ is one of the spin states, $k = 1$ for $|\psi\rangle = |\psi^a_1\rangle$, $k = 2$ for $|\psi\rangle \in \{|\psi^a_2\rangle, |\psi^{b\,b}_{1,1}\rangle\}$, and $|\psi_{\mathrm{CFT}}\rangle$ is the CFT state corresponding to $|\psi\rangle$.

For a given system size, we observe a smaller difference for the states at level $k = 1$ than for those at level $k = 2$. The computed inner products approach the CFT expectation if N_y is increased. The dependence on the number of spins in the x direction is, however, very weak for $N_x \geq 3$. In particular, the CFT result is not approached if N_x is increased and N_y kept fixed. For large enough N_y, our data suggest that the spin system inner products approach the CFT result with a power law in N_y.

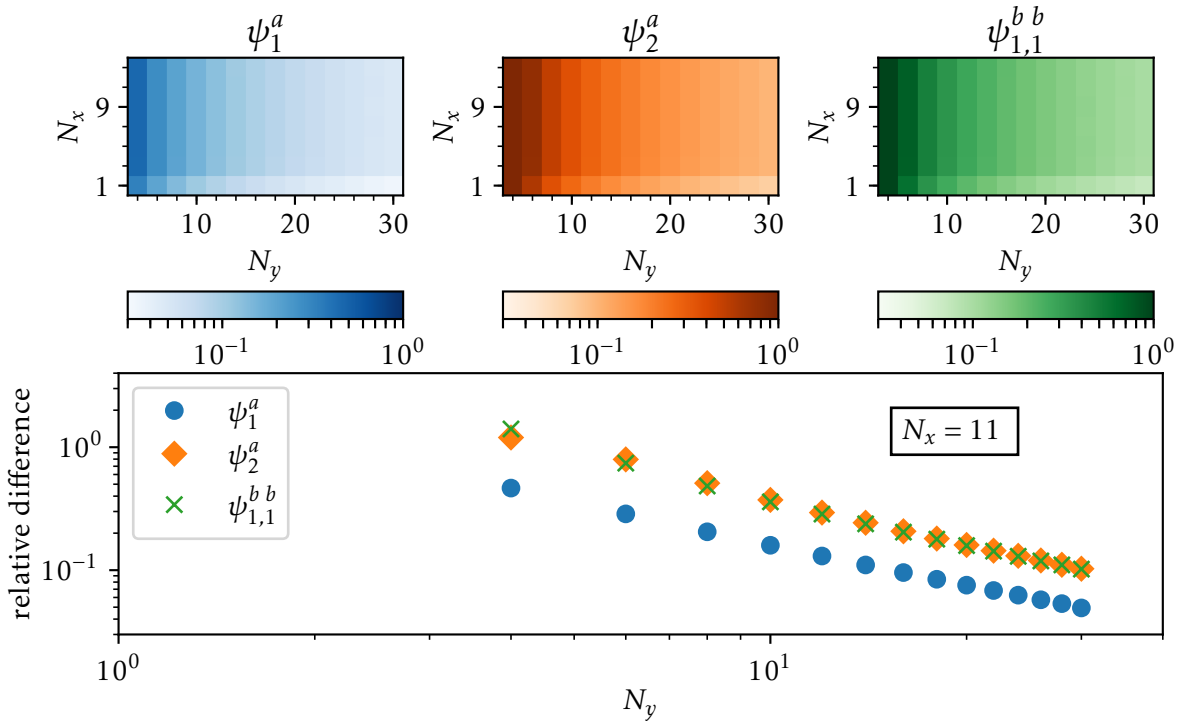

Figure 3.10: Inner product of spin system states: Relative difference to the CFT expectation [cf. Eq. (3.107)]. The colors correspond to the states $|\psi_1^a\rangle$ (blue), $|\psi_2^a\rangle$ (orange), and $|\psi_{1,1}^{b\,b}\rangle$ (green). The upper panels show the relative difference in a color plot as a function of N_x and N_y. We observe a very weak dependence on N_x for $N_x \geq 3$. The lower panel shows the dependence on N_y for $N_x = 11$. For large enough N_y, the data are consistent with a power-law behavior with an exponent of approximately -1.1. Monte Carlo error bars are not plotted because they are barely visible on the chosen scale. The maximal relative error of the shown data is 0.31 %.

3.4.5 Local model Hamiltonian

In the previous subsection, we provided numerical evidence that the states with one current operator insertion represent edge states with respect to $|\psi_0\rangle$. In this section, we study a set of local Hamiltonians on the cylinder. For a suitable choice of parameters, the ground state of the corresponding Hamiltonian has a good overlap with $|\psi_0\rangle$ and some of its low-energy excited states are well approximated by $|\psi_1^a\rangle$, the states with one current operator of order one.

We study the local Hamiltonians [118]

$$H = J_2 \sum_{\langle i,j\rangle} t_i^a t_j^a + J_2' \sum_{\langle\langle i,j\rangle\rangle} t_i^a t_j^a + J_3 \sum_{\langle i,j,k\rangle_\circlearrowleft} \varepsilon_{abc} t_i^a t_j^b t_k^c. \tag{3.108}$$

In these sums, the sites lie on a square lattice, $\langle i,j\rangle$ denotes all nearest neighbors, $\langle\langle i,j\rangle\rangle$ all next-to-nearest neighbors, and $\langle i,j,k\rangle_\circlearrowleft$ all triangles of nearest neighbors for which i,j, and k are oriented counter-clockwise. It was shown in a previous study [118] that the ground state of H on the plane (open boundary conditions in both directions) and on the torus has a good overlap with the Kalmeyer-Laughlin state for a range of parameters J_2, J_2', and J_3. Here, we study H on a cylinder of size $N_x \times N_y$, where N_x denotes the number of sites in the open direction and N_y the number of sites in the periodic direction. In the following, we

parameterize H in terms of two angles θ_1 and θ_2:

$$\begin{aligned} J_2 &= \cos(\theta_1)\cos(\theta_2), \\ J_2' &= \sin(\theta_1)\cos(\theta_2), \\ J_3 &= \sin(\theta_2). \end{aligned} \tag{3.109}$$

For $N_x = 5$ and $N_y = 4$, we studied the overlap between $|\psi_0\rangle$ and the ground state $|\psi_G\rangle$ of H as a function of θ_1 and θ_2 using an exact numerical diagonalization method (cf. Appendix A.1). We also computed the overlap of the states with one current operator insertion at level one $|\psi_1^a\rangle$ and the first excited states $|\psi_E^m\rangle$ of H that have spin one and the same momentum in the y direction as $|\psi_1^a\rangle$. Here, $m \in \{-1, 0, 1\}$ denotes the T^z eigenvalue of $|\psi_E^m\rangle$.

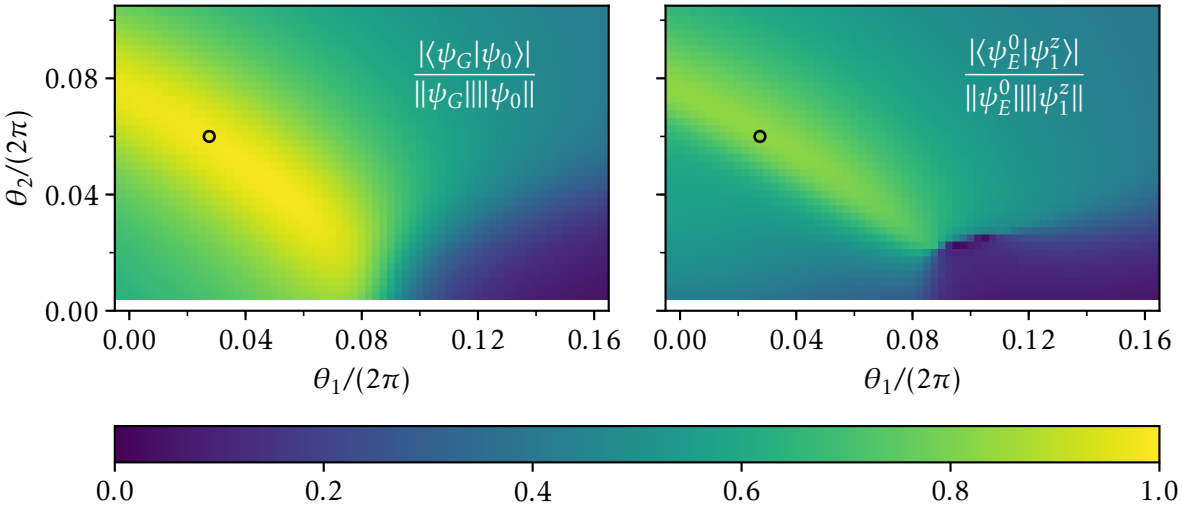

Figure 3.11: Overlaps of states constructed from CFT and eigenstates of the local Hamiltonian H of Eq. (3.108) for $N_x = 5$ and $N_y = 4$. The angles θ_1 and θ_2 parameterize the coupling constants of H according to Eq (3.109). In the left panel, the overlap $\Omega(\psi_G, \psi_0) \equiv |\langle\psi_G|\psi_0\rangle|/(\|\psi_G\|\|\psi_0\|)$ between $|\psi_0\rangle$ and the ground state $|\psi_G\rangle$ of H is plotted. The right panel shows the overlap between $|\psi_1^z\rangle$ and the first excited state $|\psi_E^0\rangle$ of H with the same spin and y momentum as $|\psi_1^z\rangle$ [spin one, $T^z = 0$, momentum $3/(8\pi)$]. The point marked with an open circle has $\theta_1 = 0.0275 \times 2\pi$ and $\theta_2 = 0.06 \times 2\pi$ and the highest combined overlap of $\sqrt{\Omega(\psi_G, \psi_0)^2 + \Omega\left(\psi_E^0, \psi_1^z\right)^2} \approx 1.2858$.

We denote the overlap between two states $|\phi_1\rangle$ and $|\phi_2\rangle$ as

$$\Omega(\phi_1, \phi_2) = \frac{|\langle\phi_1|\phi_2\rangle|}{\|\phi_1\|\|\phi_2\|}, \tag{3.110}$$

where $\|\phi\| = \sqrt{\langle\phi|\phi\rangle}$ is the norm of the state $|\phi\rangle$. In Fig. 3.11, the overlaps $\Omega(\psi_G, \psi_0)$ and $\Omega\left(\psi_G^0, \psi_1^z\right)$ are shown as a function of the parameters of the Hamiltonian. Due to SU(2) invariance, it is sufficient to consider the overlap between the states $|\psi_E^0\rangle$ and $|\psi_1^z\rangle$, which both have $T^z = 0$:

$$|\langle\psi_E^1|\psi_1^+\rangle| = |\langle\psi_E^{-1}|\psi_1^-\rangle| = |\langle\psi_E^0|\psi_1^z\rangle|, \tag{3.111}$$

where $\psi_1^\pm \equiv \psi_1^x \pm i\psi_1^y$. The best value for the combined overlap

$$\sqrt{\Omega(\psi_G, \psi_0)^2 + \Omega\left(\psi_E^0, \psi_1^z\right)^2} \tag{3.112}$$

was obtained for the angles $\theta_1 = 0.0275 \times 2\pi$ and $\theta_2 = 0.06 \times 2\pi$:

$\Omega(\psi_G, \psi_0)$	$\Omega\left(\psi_E^0, \psi_1^z\right)$	$\Omega(\psi_G, \psi_0)^{\frac{1}{N}}$	$\Omega\left(\psi_E^0, \psi_1^z\right)^{\frac{1}{N}}$
0.9829	0.8289	0.9991	0.9907

Since the size of the Hilbert space grows exponentially with the system size N, the overlaps are expected to scale exponentially in N. By taking the Nth root, one obtains a measure for the overlap per site, which takes into account this exponential scaling. Notice that the overlap per site is higher than 99 % for both the ground and the excited state.

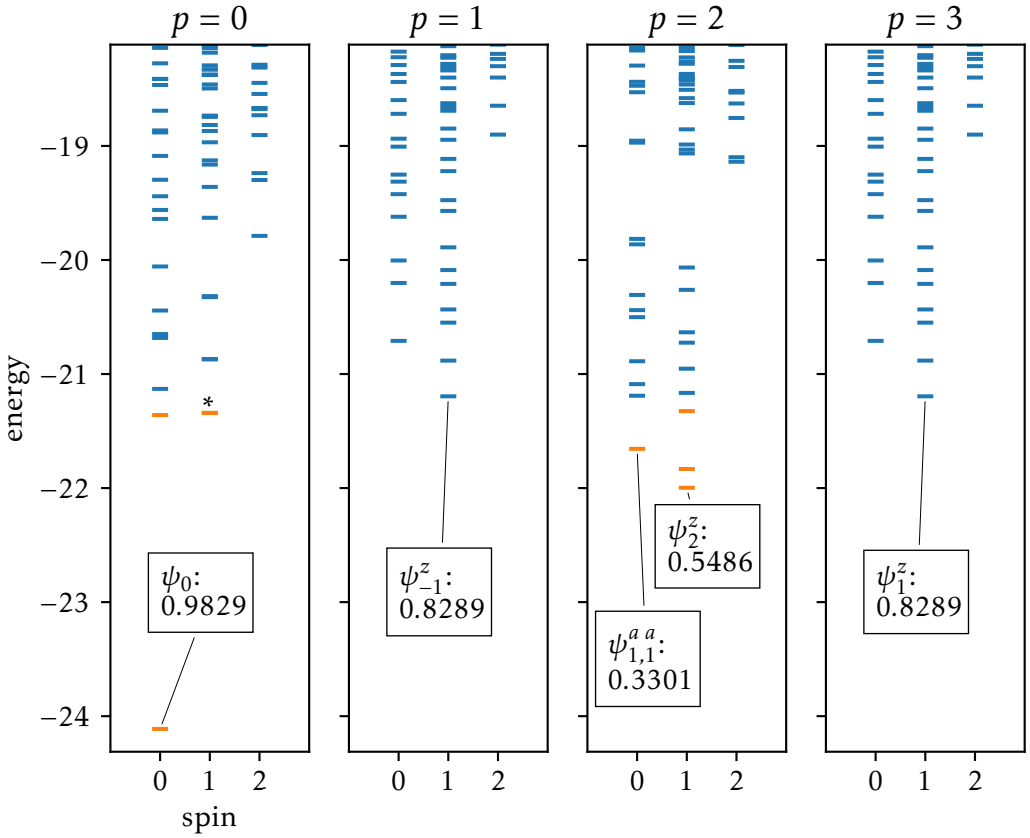

Figure 3.12: Low-energy spectrum of the Hamiltonian H of Eq. (3.108) for $N_x = 5, N_y = 4, \theta_1 = 0.0275 \times 2\pi$, and $\theta_2 = 0.06 \times 2\pi$. The four panels correspond to the four sectors of y momentum $p/(2\pi N_y)$ with $p \in \{0, 1, 2, 3\}$. Each shown level has a degeneracy of $2s + 1$ corresponding to the values of T^z. The labels show the ansatz state constructed from CFT and the value for its overlap with the corresponding eigenstate of H. The 8 energies shown in orange are those that are smaller than the lowest energy in the $p = 1$ and $p = 3$ sectors. [At the level marked with an asterisk (∗), there are two energies with a splitting of approximately 1.211×10^{-3}. This is not visible on the scale of the plot.]

The low-energy spectrum of H for the parameters with the best overlaps is plotted in Fig. 3.12. We find 8 energies below the energy of $|\psi_E^m\rangle$. The spectra plotted in Fig. 3.12 are separated into sectors of different y momentum $p/(2\pi N_y) = p/(8\pi)$ with $p \in \{0, 1, 2, 3\}$. Note that the states $|\psi_E^m\rangle$ are the first excited states with $p = 3$. The spectra for the momenta for $p = 1$ and $p = 3$ are the same because H is invariant under the inversion operator $\mathcal{I}$ introduced

in Sec. 3.2:

$$\mathcal{I}^{-1} H \mathcal{I} = H. \tag{3.113}$$

The relation

$$\mathcal{I}^{-1} \mathcal{T}_y \mathcal{I} = \mathcal{T}_y^{-1} \tag{3.114}$$

between $\mathcal{I}$ and translation operator in the y direction $\mathcal{T}_y$ follows directly from their definition (cf. Appendix B.3.2 and B.3.3). Therefore, if $|\psi\rangle$ is an eigenstate of H with momentum $p/(2\pi N_y)$, then $\mathcal{I}|\psi\rangle$ is also an eigenstate with momentum $(N_y - p)/(2\pi N_y)$. This means that for $|\psi_E^m\rangle$ with $p = 3$, there is a corresponding eigenstate $\mathcal{I}|\psi_E^m\rangle$ with $p = 1$, which satisfies

$$|\langle \psi_E^0 | \psi_1^z \rangle| = |\langle \mathcal{I} \psi_E^0 | \psi_{-1}^z \rangle|. \tag{3.115}$$

Here, $|\psi_{-1}^z\rangle = \mathcal{I}|\psi_1^z\rangle$ is the state obtained by inserting the current operator at $z_\infty = \infty$ instead of $z_0 = 0$ [cf. Eq. (3.52)].

Our results show that the state $|\psi_0\rangle$ and the states with one current operator of order one are good approximations of low-energy eigenstates of H for $N_x = 5$, $N_y = 4$, $\theta_1 = 0.0275 \times 2\pi$, and $\theta_2 = 0.06 \times 2\pi$. This raises the question if further eigenstates of H are effectively described by states constructed as CFT correlators. We also computed the overlaps of eigenstates of H with some additional states constructed from current operators for higher orders in current operators. At level two in current operators, the overlaps with the first excited states that have the same spin and momentum as our ansatz states are given by 0.5486 for $|\psi_2^a\rangle$ (0.9704 per site) and 0.3301 for $|\psi_{1,1}^{b\,b}\rangle$ (0.9461 per site). The corresponding energy levels are shown in Fig. 3.12.

In this subsection, we considered a local model and computed overlaps between ansatz states constructed from CFT and eigenstates of the model Hamiltonian. In Sec. 3.4.6, we also derive exact, SU(2) invariant parent Hamiltonians for some states constructed from current operators. These Hamiltonians are nonlocal with up to four-body interactions.

3.4.6 Exact parent Hamiltonians

As shown in Sec. 3.4.5, the edge states $|\psi_1^a\rangle$ have a good overlap with low-lying excited states of a local model, for which $|\psi_0\rangle$ approximates the ground state. We now analytically construct SU(2)-invariant, nonlocal parent Hamiltonians for some linear combinations of the states $|\psi_{n_l \dots n_1}^{a_l \dots a_1}\rangle$, i.e., Hamiltonians for which they are exact eigenstates with the lowest energy.

Construction of parent Hamiltonians

The starting point of our construction is the operator

$$\mathcal{C}'^a = \sum_{i \neq j}^{N} \frac{z_i + z_j}{z_i - z_j} \left(t_j^a + i \varepsilon_{abc} t_i^b t_j^c \right). \tag{3.116}$$

In Appendix B.1, we explicitly compute the action of $\mathcal{C}'^a$ on states constructed from $|\psi_0\rangle$ by insertion of current operators, and show that $\mathcal{C}'^a$ does not mix the states $|\psi_{n_l \dots n_1}^{a_l \dots a_1}\rangle$ with different levels $k = n_1 + \dots + n_l$ if $k < N_y$. This property is key to our construction of parent Hamiltonians: It allows us to treat the levels separately starting with the lower levels, which have fewer states. The action of $\mathcal{C}'^a$ on states at level k is described by a matrix. For low k, the dimension of this matrix is considerably smaller compared to that of an operator acting on the complete Hilbert

space. Moreover, the size of the matrix depends only on the level k rather than the number of spins N.

We next add a multiple of the total spin T^a to $\mathcal{C}'^a$ and define the operators

$$\mathcal{D}_n^a = \mathcal{C}'^a + (n+1-N)T^a, \tag{3.117}$$

where n is an integer. The operator $\mathcal{D}_n^a$ is also closed in the subspace of states of level k if $k < N_y$ since T^a does not mix states of different levels. For certain values of n, we managed to find states constructed from current operators that are annihilated by the three operators $\mathcal{D}_n^a$ for $a \in \{x, y, z\}$. These states are then ground states of the Hamiltonian

$$H_n = (\mathcal{D}_n^a)^\dagger \mathcal{D}_n^a, \tag{3.118}$$

where the index a is summed over. Note that the Hamiltonian H_n is positive semi-definite and SU(2) invariant. H_n is nonlocal and contains terms with up to four-body interactions since $\mathcal{D}_n^a$ has terms linear and quadratic in spin operators.

Before describing our results, we note that the condition $\mathcal{D}_n^a|\psi\rangle = 0$ for all $a \in \{x, y, z\}$ implies that the state $|\psi\rangle$ is part of the subspace on which $T^b T^b$ and $\mathcal{D}_n^a$ commute. To show this, we first note that

$$\left[\mathcal{D}_n^a, T^b\right] = i\varepsilon_{abc}\mathcal{D}_n^c, \tag{3.119}$$

which is a direct consequence of the definitions of Eqs. (3.116) and (3.117). It then follows that

$$\left[T^b T^b, \mathcal{D}_n^a\right]|\psi\rangle = \left(-i\varepsilon_{bac}T^b\mathcal{D}_n^c - i\varepsilon_{bac}\mathcal{D}_n^c T^b\right)|\psi\rangle = -i\varepsilon_{bac}\left[\mathcal{D}_n^c, T^b\right]|\psi\rangle = \varepsilon_{bac}\varepsilon_{cbd}\mathcal{D}_n^d|\psi\rangle = 0, \tag{3.120}$$

where we assumed that $\mathcal{D}_n^a|\psi\rangle = 0$ for all $a \in \{x, y, z\}$. The states satisfying $\mathcal{D}_n^a|\psi\rangle = 0$ can therefore be decomposed into sectors of different total spin.

We note that the condition $\left[T^b T^b, \mathcal{D}_n^a\right]|\psi\rangle = 0$ is equivalent to

$$\left[T^b T^b, \mathcal{C}'^a + (1-N)T^a\right]|\psi\rangle = 0, \tag{3.121}$$

since $T^b T^b$ and T^a commute. The operator $\mathcal{C}'^a + (1-N)T^a$ has the advantage that its matrix entries in terms of the states at level k do not depend on N and n [cf. Eq. (B.17) in Appendix B.1]. In our calculations, we found it technically easier to first determine the subspace of states on which $T^b T^b$ and $\mathcal{C}'^a + (1-N)T^a$ commute and then look for states that are annihilated by $\mathcal{D}_n^a$ for a suitable n within that subspace.

We summarize our analytical results in Table 3.7. The states with spin 2 and 3 appear as the symmetric-traceless parts of states with 2 and 3 open indices, respectively. For a two-index state $|\phi^{ab}\rangle$, the symmetric-traceless part is defined as

$$3\left(|\phi^{ab}\rangle + |\phi^{ba}\rangle\right) - 2\delta_{ab}|\phi^{dd}\rangle, \tag{3.122}$$

and for a three-index state $|\phi^{abc}\rangle$ as [157]

$$\begin{aligned} &5\Big(|\phi^{abc}\rangle + |\phi^{bca}\rangle + |\phi^{cab}\rangle + |\phi^{cba}\rangle + |\phi^{bac}\rangle + |\phi^{acb}\rangle\Big) \\ &-2\Big(\delta_{ab}(|\phi^{cdd}\rangle + |\phi^{dcd}\rangle + |\phi^{ddc}\rangle) + \delta_{ac}(|\phi^{bdd}\rangle + |\phi^{dbd}\rangle + |\phi^{ddb}\rangle) \\ &\quad + \delta_{bc}(|\phi^{add}\rangle + |\phi^{dad}\rangle + |\phi^{dda}\rangle)\Big). \end{aligned} \tag{3.123}$$

Table 3.7: States constructed from current operators that are annihilated by $\mathcal{D}_n^a$ for $a \in \{x, y, z\}$ on a cylinder with $N_y > k$ [cf. Eqs. (3.116) and (3.117) for the definition of $\mathcal{D}_n^a$]. For N_y sufficiently large ($N_y > k$), these states are ground states of the Hamiltonian $H_n = (\mathcal{D}_n^a)^\dagger \mathcal{D}_n^a$.

k	State	Spin	n
0	$\lvert\psi_0\rangle$	0	any
1	$\lvert\psi_1^a\rangle$	1	1
2	—	—	—
3	$\lvert\psi_3^a\rangle + i\varepsilon_{ade}\lvert\psi_{2,1}^{d\,e}\rangle$	1	5
4	Symmetric-traceless part of $\lvert\psi_{3,1}^{a\,b}\rangle$	2	3
5	$\lvert\psi_{3,1,1}^{a\,d\,d}\rangle + \frac{3}{2}i\varepsilon_{ade}\lvert\psi_{3,2}^{d\,e}\rangle + \frac{3}{2}i\varepsilon_{ade}\lvert\psi_{4,1}^{d\,e}\rangle + \frac{9}{4}\lvert\psi_5^a\rangle$	1	9
6	—	—	—
7	$\lvert\psi_{3,3,1}^{a\,d\,d}\rangle + 4\lvert\psi_{4,2,1}^{d\,a\,d}\rangle + \frac{5}{3}\lvert\psi_{4,2,1}^{a\,d\,d}\rangle + \frac{7}{3}\lvert\psi_{5,1,1}^{a\,d\,d}\rangle + i\varepsilon_{ade}\lvert\psi_{4,3}^{d\,e}\rangle$ $+\frac{5}{2}i\varepsilon_{ade}\lvert\psi_{5,2}^{d\,e}\rangle + \frac{9}{2}i\varepsilon_{ade}\lvert\psi_{6,1}^{d\,e}\rangle + \frac{21}{4}\lvert\psi_7^a\rangle$	1	13
8	Symmetric-traceless part of $i\varepsilon_{ade}\lvert\psi_{4,3,1}^{b\,d\,e}\rangle + \frac{1}{2}i\varepsilon_{ade}\lvert\psi_{5,2,1}^{b\,d\,e}\rangle - \frac{1}{2}\lvert\psi_{5,3}^{a\,b}\rangle - \lvert\psi_{6,2}^{a\,b}\rangle - 2\lvert\psi_{7,1}^{a\,b}\rangle$	2	7
9	Symmetric-traceless part of $\lvert\psi_{5,3,1}^{a\,b\,c}\rangle$	3	5
9	$i\varepsilon_{ade}\lvert\psi_{4,3,1,1}^{d\,e\,f\,f}\rangle - \frac{1}{2}\lvert\psi_{4,3,2}^{a\,d\,d}\rangle - \frac{3}{2}\lvert\psi_{5,2,2}^{a\,d\,d}\rangle - \frac{1}{2}\lvert\psi_{4,4,1}^{a\,d\,d}\rangle$ $+3\lvert\psi_{5,3,1}^{d\,d\,a}\rangle - \frac{9}{2}\lvert\psi_{5,3,1}^{d\,a\,d}\rangle - \frac{9}{2}\lvert\psi_{5,3,1}^{a\,d\,d}\rangle - \frac{9}{2}\lvert\psi_{6,2,1}^{d\,a\,d}\rangle$ $-\frac{7}{2}\lvert\psi_{6,2,1}^{a\,d\,d}\rangle - 3\lvert\psi_{7,1,1}^{a\,d\,d}\rangle - \frac{27}{8}i\varepsilon_{ade}\lvert\psi_{5,4}^{d\,e}\rangle - \frac{21}{8}i\varepsilon_{ade}\lvert\psi_{6,3}^{d\,e}\rangle$ $-\frac{45}{8}i\varepsilon_{ade}\lvert\psi_{7,2}^{d\,e}\rangle - \frac{63}{8}i\varepsilon_{ade}\lvert\psi_{8,1}^{d\,e}\rangle - \frac{105}{8}\lvert\psi_9^a\rangle$	1	17

Except for the levels 2 and 6, we find states and corresponding parent Hamiltonians for all levels that were considered. Note that the singlet $\lvert\psi_0\rangle$ is a ground state of H_n for any value of n. For the additional ground states, we observe that the value of n tends to be larger at higher levels k. This means that the ground state space of the Hamiltonians H_n with lower n contains states of a lower level in current operators. For example, we only find the ground states $\lvert\psi_0\rangle$ and $\lvert\psi_1^a\rangle$ for H_1. Similarly, the only appearing ground states of H_3 at levels $k \leq 9$ are ψ_0 and the symmetric-traceless part of $\lvert\psi_{3,1}^{a\,b}\rangle$.

Ground-state degeneracies

In the previous subsection, we explicitly constructed analytical ground states of the Hamiltonians H_n with $n \in \{1, 3, 5, 7, 9, 13, 17\}$ in terms of linear combinations of states $\lvert\psi_{n_l \ldots n_1}^{a_l \ldots a_1}\rangle$ with levels $k \leq 9$. We now study the ground state spaces of the Hamiltonians H_n numerically and provide evidence for $n \in \{1, 3, 5\}$ that the complete ground state space is spanned by the states given in Table 3.7.

By an exact diagonalization, we numerically determined the ground state multiplets of the Hamiltonians H_n for $n \leq 13$ and systems with $N = N_x N_y \leq 14$ and N even. Our results are summarized in Table 3.8. We observe that states with spin s occur in the ground state spaces only in systems with $N_y \geq 2s$. Furthermore, we find that the ground state degeneracy does not grow anymore if N_y reaches a certain value $N_y^{\min}$. This statement is most conclusive for the lower values n, where $N_y^{\min}$ is smaller and we are thus able to probe more systems with $N_y \geq N_y^{\min}$. For $n \in \{1, 3, 5\}$, this implies that all ground states are given by the corresponding states of Table 3.7.

Table 3.8: Numerically determined ground state multiplets of the Hamiltonians H_n for $n \leq 13$ and an even number of spins N with $N \leq 14$. The second column indicates the minimal number of spins $N_y^{\min}$ in the periodic direction for which the complete shown multiplet was observed in all system with $N_y^{\min} \leq N_y \leq 14$. For a lower number of spins in the y direction, the observed ground state space is smaller. For even n, we only find a singlet ground state.

n	$N_y^{\min}$	Ground-state multiplet
1	2	$0 \oplus 1$
3	4	$0 \oplus 2$
5	6	$0 \oplus 1 \oplus 3$
7	8	$0 \oplus 2 \oplus 4$
9	10	$0 \oplus 1 \oplus 3 \oplus 5$
11	12	$0 \oplus 2 \oplus 4 \oplus 6$
13	14	$0 \oplus 1 \oplus 3 \oplus 5 \oplus 7$

Finally, let us formulate a conjecture about the structure of the states annihilated by $\mathcal{D}_n^a$, which are ground states of H_n. Our analytical results are consistent with the following rule: For each spin sector $s \in \{1, 2, \dots\}$, there is a series of states at levels $k = s^2 + 2sj$ with $j \in \{0, 1, 2, \dots\}$. These states are annihilated by $\mathcal{D}_n^a$ with $n = 2s - 1 + 4j$. As one can show by induction, the second rule implies that the ground state space of H_n with $n = 2s - 1$ contains the multiplet

$$0 \oplus \begin{cases} 1 \oplus 3 \oplus \cdots \oplus s & \text{if } s \text{ is odd,} \\ 2 \oplus 4 \oplus \cdots \oplus s & \text{if } s \text{ is even.} \end{cases}$$

The numerical results of Table 3.8 are consistent with this multiplet structure and thus support the conjecture that the values of n are given by $n = 2s - 1 + 4j$.

3.5 Conclusion

In this chapter, we defined a map from excitations of the $\mathrm{SU}(2)_1$ WZW CFT to states of a spin-$\frac{1}{2}$ system. In 1D, we constructed eigenstates of the Haldane-Shastry model in terms of these states, while we investigated their properties as tentative edge modes in 2D.

The spin-$\frac{1}{2}$ wave functions studied in this chapter were defined through CFT correlators. Earlier studies [102, 109] showed that the ground state of the Haldane-Shastry model in 1D and the Kalmeyer-Laughlin spin liquid state in 2D correspond to a CFT correlator of *primary* fields. In this chapter, we inserted additional CFT *descendant* fields to obtain excited states in 1D and edge modes in 2D.

For an even number of spins, we showed analytically that the Haldane-Shastry model is block-diagonal in the states $|\psi_{n_l \dots n_1}^{a_l \dots a_1}\rangle$, which have modes of the current operator inserted at $z_0 = 0$. We showed that these states span the complete Hilbert space. Thus, all eigenstates of the Haldane-Shastry model can be obtained as linear combinations of $|\psi_{n_l \dots n_1}^{a_l \dots a_1}\rangle$. We diagonalized the Hamiltonian analytically for levels up to $k = 8$ in current operators. Depending on N, we identified certain states that are null but correspond to non-null CFT states. These additional null states occur due to the finite size of the spin system's Hilbert space. Our method of detecting them is based on a sufficient criterion for a state to be null. In order to test if a given state is not null, one could use the known algebraic equations for spin correlation functions [103] in $|\psi_0\rangle$ to compute the needed inner products numerically, even for large system sizes.

We provided numerical evidence that a similar construction is possible for an odd number of spins and for the tower of states corresponding to the sector of the CFT Hilbert space that is built on top of the $h = \frac{1}{4}$ primary field.

Our manifestly SU(2) invariant ansatz is compatible with the construction of eigenstates of the Haldane-Shastry model as multiplets of the Yangian algebra in the sense that the Yangian operator does not change the number of current operators. This allowed us to explicitly relate the excited states constructed from current operators to the highest weight states of the Yangian operator.

In the case of the SU(2)$_1$ WZW model, which we studied here, the resulting spin system is equivalent to the Haldane-Shastry model. Thus, our method provides an alternative way of constructing the excited states of the Haldane-Shastry model, which emphasizes its close relation to the underlying CFT. We expect that this method could be generalized to the SU(n)$_1$ WZW model, which is related to the SU(n) Haldane-Shastry spin chain [158]. We provided numerical evidence that a construction of excited states in terms of WZW currents is also possible for the open Haldane-Shastry model. It would be interesting to also construct these eigenstates analytically.

The second part of this chapter studied trial wave functions for lattice FQH states constructed as chiral correlators of the SU(2)$_1$ WZW CFT. In 2D, we investigated states obtained from descendant CFT fields as tentative edge modes of the Kalmeyer-Laughlin state. For continuous systems, analogous states constructed from CFT were proposed as FQH edge states previously [99, 129]. Here, we worked on the lattice and applied Monte Carlo techniques to test a central expectation for edge states: That the local, bulk properties of different edge states should be the same.

For a system on the cylinder, we compared spin correlation functions in the states with one current operator ($|\psi_1^a\rangle$) to the state with no current operators ($|\psi_0\rangle$). Our numerical results show that the nearest-neighbor bulk correlations approach each other exponentially as the number of spins in the open direction (N_x) is increased. On the other hand, the states $|\psi_1^a\rangle$ and $|\psi_0\rangle$ are different globally since their spin and momentum are different. This supports the assumption that they describe edge states.

We compared inner products of lattice states at levels one and two in current operators to CFT inner products of the corresponding descendant states. For large enough N_y (periodic direction), the computed inner products approach the CFT expectation with a power law in N_y. This suggests that there is a correspondence between inner products of states $|\psi_{n_l \dots n_1}^{a_l \dots a_1}\rangle$ and CFT inner products in the thermodynamic limit. Such a correspondence was found for continuous wave functions in Ref. [99].

Furthermore, we compared nearest-neighbor bulk correlations in $|\psi_0^{\mathrm{sgl}}\rangle$ to those in $|\psi_0\rangle$, where $|\psi_0^{\mathrm{sgl}}\rangle$ is the singlet component of the state obtained by insertion of two extra primary fields. In contrast to $|\psi_1^a\rangle$, we find that the correlations do not approach each other if the thermodynamic limit is taken only in the open direction. However, if N_x is chosen large enough, the difference in correlation functions vanishes exponentially as a function of N_y.

We showed by an exact diagonalization that $|\psi_0\rangle$ has a good overlap with the ground state of a local Hamiltonian and $|\psi_1^a\rangle$ with the first excited states that have the same spin and momentum as $|\psi_1^a\rangle$. This could be an indication that further low-energy excitations of that local Hamiltonian are edge states described by the SU(2)$_1$ WZW CFT. It would be interesting to investigate this relation in more detail for larger system sizes and different topologies.

We showed that the complete Hilbert space is covered by the linear span of the states $|\psi_{n_l \dots n_1}^{a_l \dots a_1}\rangle$ and, therefore, only a subset of these states are edge states. For the states with one current operator, we argued that not all linear combinations of states $|\psi_m^a\rangle$ describe edge modes because states with the same y momentum can be non-orthogonal. It is possible to restrict the

space of states to an orthogonal subset given by $|\psi^a_m\rangle$ with $m \in \{1, \ldots, N_y\}$.

Taking the limit of large mode numbers could be another possibility of removing bulk states for the linear span of $|\psi^{a_l \ldots a_1}_{n_l \ldots n_1}\rangle$. More precisely, one can replace n_i by $n_i + m_i N_y$ and then take $m_i \to \infty$. In this limit, the sum in the operators $u^a_{-n_i - m_i N_y}$ only extends over the edge sites because all other positions are exponentially suppressed. The fact that this class of states (and also linear combinations of such states) is obtained from $|\psi_0\rangle$ by application of edge spin operators only, suggests that their complete span represents edge states. For one of these states, $|\chi^a_1\rangle$, we did numerical tests that indeed indicated that $|\chi^a_1\rangle$ is an edge state.

4 Approximation of correlations for states obtained from conformal field theory

This chapter considers wave functions obtained as chiral correlators of the CFT of a massless, free boson introduced in Sec. 2.1.1. In 1D, these are good approximations of the ground state of the spin-$\frac{1}{2}$ XXZ model [102], and they are equivalent to lattice Laughlin states in 2D [109].

The purpose of this chapter is to investigate how the properties of these states are related to the CFT they are constructed from. We focus on correlation functions since they encode central characteristics of a state: At the edge of a 2D system, Laughlin states exhibit polynomially decaying correlations, which reflect the existence of gapless excitations. The bulk of a FQH system, on the other hand, is gapped and correlations thus decay exponentially, which is known as the screening property.

Correlations of FQH states can be computed numerically through Monte Carlo simulations [109, 120] (cf. also Appendix A.2). Even though large system sizes can be achieved through this method, it does not provide conceptual insight into how the correlations follow from the CFT that defines the states. In Ref. [99], such a link between CFT and properties of states was established by showing that the edge correlations follow from those of the CFT. This derivation, however, assumes exponentially decaying correlation functions in the bulk.

In this chapter, we derive an exact path integral representation of spin-spin correlation functions in the states obtained from the free-boson CFT. This provides a relation between a property of the states and the CFT they are constructed from. Through an approximation of this exact expression, we arrive at a representation of the correlations in terms of a quadratic effective action that is a modification of the CFT. It differs from the latter by an additional mass-like term inserted at the positions of the lattice. This mass-like term in the effective action causes exponentially decaying bulk correlations. Thus, we provide a conceptual argument for the screening property.

A similar construction in terms of an action that is a perturbation of the CFT was made in Refs. [99, 141] for general FQH states with continuous spatial degrees of freedom. The distinct contribution of our work is twofold. First, we provide an argument through our exact path integral representation in favor of doing this approximation. Second, we explicitly compute the correlations within the approximation and provide extensive tests of its accuracy.

Our approximation can be understood as a transition from discrete spins to continuous ones. This breaks the invariance under a rescaling of the lattice. Thus, the approximation depends on a new scale parameter, which we fix by minimizing the subleading term in the approximation. Taking an additional continuum limit of the lattice, we derive analytical expressions for the approximate correlations.

In this chapter, we study correlations of lattice Laughlin states and corresponding approximations. In the past years, entanglement properties [83, 84, 159] have been used as a tool to characterize quantum many-body states. In particular, entanglement entropies and spectra were shown to exhibit properties of the underlying CFT [159–163]. This direction is pursued in Chapter 5 of this thesis, where we compute entanglement properties of states with continuous spins that have the same correlations as that of the approximation studied in this chapter.

This chapter is structured as follows.

- Sec. 4.1 introduces the spin-$\frac{1}{2}$ states studied in this chapter.

- We derive an exact path integral representation of correlations in Sec. 4.2, where we also introduce the approximation through a truncation of the exact expression.
- Sec. 4.3 explains how we solve the approximation on lattices and by taking an additional continuum limit for the positions.
- The accuracy of the approximation is tested in Sec. 4.4.
- Sec. 4.5 contains an outlook and a discussion of how the approximation could be improved by keeping the periodicity of the original expressions.
- Sec. 4.6 concludes this chapter.

Most of the rest of this chapter and the corresponding appendices are adaptations of the following previously published work:

- B. Herwerth, G. Sierra, J. I. Cirac, and A. E. B. Nielsen, "Effective description of correlations for states obtained from conformal field theory", Phys. Rev. B **96**, 115139 (2017), ©2017 American Physical Society (Ref. [164]).

4.1 Spin states from conformal fields

We consider a free, massless bosonic field $\varphi(z,\bar{z})$ in one spatial dimension with the Euclidean action $S_0[\varphi]$ given in Eq. (2.6). This theory was used in Sec. 2.3 to define spin-$\frac{1}{2}$ states $|\psi_\alpha\rangle$, where $\alpha > 0$ is a real parameter. In this chapter, we study spin-spin correlations of the states $|\psi_\alpha\rangle$.

For a 2D system, $|\psi_\alpha\rangle$ is similar to the Laughlin lattice state with $\nu = \frac{1}{4\alpha}$ particles per flux [109], cf. also Sec. 2.2. In particular, $\alpha = \frac{1}{4}$ corresponds to an integer quantum Hall state with one particle per flux and $\alpha = \frac{1}{2}$ to the Kalmeyer-Laughlin FQH state with $\frac{1}{2}$ particle per flux, which was studied in Chapter 3 of this thesis. When 4α is not an integer, the states $|\psi_\alpha\rangle$ can be thought of as generalizations of FQH lattice states.

4.2 Effective description of correlations

In this section, we derive an effective description of the zz correlations in the states $|\psi_\alpha\rangle$ in terms of a free field theory. The zz correlations between lattice points i and j are defined as

$$\langle \sigma_i^z \sigma_j^z \rangle \equiv 4 \frac{\langle \psi_\alpha | t_i^z t_j^z | \psi_\alpha \rangle}{\langle \psi_\alpha | \psi_\alpha \rangle} = \frac{\sum_{s_1,\dots,s_N} s_i s_j |\psi_\alpha(s_1,\dots,s_N)|^2}{\sum_{s_1,\dots,s_N} |\psi_\alpha(s_1,\dots,s_N)|^2}. \tag{4.1}$$

In the following, it is assumed that the sites i and j are distinct since the correlator for $i = j$ can be evaluated trivially, $\langle \sigma_i^z \sigma_i^z \rangle = 1$. We first derive an exact representation of $\langle \sigma_i^z \sigma_j^z \rangle$, which we then truncate to an effective, quadratic theory.

4.2.1 Exact field theory representation of correlations

Let us first consider the normalization $\langle \psi_\alpha | \psi_\alpha \rangle$ in Eq. (4.1). Using the form of the wave function [Eq. (2.25)], $\langle \sigma_i^z \sigma_j^z \rangle$ can be written as a vacuum expectation value of vertex operators

in the complete free-boson theory (chiral and antichiral):

$$\langle\psi_\alpha|\psi_\alpha\rangle = \sum_{s_1,\ldots,s_N} |\psi_\alpha(s_1,\ldots,s_N)|^2 = \sum_{s_1,\ldots,s_N} \delta_{\mathbf{s}} \prod_{i<j} |z_i - z_j|^{2\alpha s_i s_j} \tag{4.2}$$

$$= \sum_{s_1,\ldots,s_N} \langle : e^{i\sqrt{\alpha}s_1\varphi(z_1,\bar{z}_1)} : \cdots : e^{i\sqrt{\alpha}s_N\varphi(z_N,\bar{z}_N)} : \rangle, \tag{4.3}$$

where $\delta_{\mathbf{s}} \prod_{i<j} |z_i - z_j|^{2\alpha s_i s_j}$ was written as the correlation function of N vertex operators $: e^{i\sqrt{\alpha}s_j\varphi(z_j,\bar{z}_j)} :$. Note that the condition imposed by $\delta_{\mathbf{s}}$ is implicitly contained in Eq. (4.3) since the correlator of vertex operators vanishes unless $s_1 + \cdots + s_N = 0$.

Carrying out each of the sums over s_j,

$$\sum_{s_j\in\{-1,1\}} : e^{i\sqrt{\alpha}s_j\varphi(z_j,\bar{z}_j)} : = 2 : \cos\left(\sqrt{\alpha}\varphi(z_j,\bar{z}_j)\right) :, \tag{4.4}$$

we obtain

$$\langle\psi_\alpha|\psi_\alpha\rangle = 2^N \langle \prod_{k=1}^{N} : \cos\left(\sqrt{\alpha}\varphi(z_k,\bar{z}_k)\right) : \rangle. \tag{4.5}$$

For the numerator in Eq. (4.1), we additionally use

$$\sum_{s_j\in\{-1,1\}} s_j : e^{i\sqrt{\alpha}s_j\varphi(z_j,\bar{z}_j)} : = 2i : \sin\left(\sqrt{\alpha}\varphi(z_j,\bar{z}_j)\right) : \tag{4.6}$$

and obtain

$$4\langle\psi_\alpha|t_i^z t_j^z|\psi_\alpha\rangle = \sum_{s_1,\ldots,s_N} s_i s_j \langle : e^{i\sqrt{\alpha}s_1\varphi(z_1,\bar{z}_1)} : \cdots : e^{i\sqrt{\alpha}s_N\varphi(z_N,\bar{z}_N)} : \rangle \tag{4.7}$$

$$= -2^N \langle : \sin\left(\sqrt{\alpha}\varphi(z_i,\bar{z}_i)\right) :: \sin\left(\sqrt{\alpha}\varphi(z_j,\bar{z}_j)\right) : \prod_{k(\neq i,j)}^{N} : \cos\left(\sqrt{\alpha}\varphi(z_k,\bar{z}_k)\right) : \rangle, \tag{4.8}$$

where $k(\neq i,j)$ denotes all indices k that are distinct from i and j. Therefore, the expression for the zz correlations becomes

$$\langle\sigma_i^z\sigma_j^z\rangle = -\frac{\langle : \sin\left(\sqrt{\alpha}\varphi(z_i,\bar{z}_i)\right) :: \sin\left(\sqrt{\alpha}\varphi(z_j,\bar{z}_j)\right) : \prod_{k(\neq i,j)}^{N} : \cos\left(\sqrt{\alpha}\varphi(z_k,\bar{z}_k)\right) : \rangle}{\langle \prod_{k=1}^{N} : \cos\left(\sqrt{\alpha}\varphi(z_k,\bar{z}_k)\right) : \rangle}. \tag{4.9}$$

As we show in Appendix C.1, one can drop the normal ordering in this expression since this changes the numerator and denominator by the same constant factor. Thus, the path integral representation of Eq. (4.9) is given by

$$\langle\sigma_i^z\sigma_j^z\rangle = -\frac{\int \mathcal{D}\varphi \tan\left(\sqrt{\alpha}\varphi(z_i,\bar{z}_i)\right)\tan\left(\sqrt{\alpha}\varphi(z_j,\bar{z}_j)\right)\cos\left(\sqrt{\alpha}\varphi(z_1,\bar{z}_1)\right)\ldots\cos\left(\sqrt{\alpha}\varphi(z_N,\bar{z}_N)\right)e^{-S_0[\varphi]}}{\int \mathcal{D}\varphi \cos\left(\sqrt{\alpha}\varphi(z_1,\bar{z}_1)\right)\ldots\cos\left(\sqrt{\alpha}\varphi(z_N,\bar{z}_N)\right)e^{-S_0[\varphi]}}. \tag{4.10}$$

This expression determines the exact zz correlations in $|\psi_\alpha\rangle$.

4.2.2 Effective theory for correlations

The starting point of our approximation is to expand the path integral representation of Eq. (4.10) to quadratic order in $\varphi(z,\bar{z})$ around 0. This is motivated by the following observation: For large N, the contribution of the integrand in Eq. (4.10) is only significant for field configurations that have $\cos(\sqrt{\alpha}\varphi(z_j,\bar{z}_j)) \approx \pm 1$ at all positions z_j. At the same time, the massless, free-boson action $S_0[\varphi]$ suppresses field configurations that change rapidly through the derivative term. Therefore, the fields dominating the path integral are those for which $\sqrt{\alpha}\varphi(z,\bar{z})$ is near the same extremum of cosine for all positions z. Since $S_0[\varphi]$ is invariant under a constant shift of the field value, $\varphi(z,\bar{z}) \to \varphi(z,\bar{z}) + \text{const.}$, we can focus on the case $\varphi(z,\bar{z}) \approx 0$. The expansion around the extremum of the cosine function is analogous to Kosterlitz and Thouless's treatment of the XY model [71, 72]. We are, however, not taking into account terms that would correspond to vortex configurations in the XY model.

Hence, we expand $\cos(\sqrt{\alpha}\varphi(z,\bar{z})) \sim e^{-\frac{\alpha}{2}\varphi(z,\bar{z})^2}$ and $\tan(\sqrt{\alpha}\varphi(z,\bar{z})) \sim \sqrt{\alpha}\varphi(z,\bar{z})$ in Eq. (4.10) and obtain

$$\langle \sigma_i^z \sigma_j^z \rangle \approx -\alpha \frac{\int \mathcal{D}\varphi\, \varphi(z_i,\bar{z}_i)\varphi(z_j,\bar{z}_j) e^{-S_\alpha[\varphi]}}{\int \mathcal{D}\varphi e^{-S_\alpha[\varphi]}}, \tag{4.11}$$

where

$$S_\alpha[\varphi] = \frac{1}{4\pi}\int dz d\bar{z}\, \partial_z\varphi(z,\bar{z})\partial_{\bar{z}}\varphi(z,\bar{z}) + \frac{\alpha}{2}\sum_{j=1}^{N}\varphi(z_j,\bar{z}_j)^2. \tag{4.12}$$

The quadratic action $S_\alpha[\varphi]$ provides an effective theory that approximately describes the zz correlations in the state $|\psi_\alpha\rangle$. Compared to the action of the free, massless boson, it has an additional mass-like term at the positions of the lattice as illustrated in Fig. 1.4.

4.3 Solution schemes for 1D and 2D lattices

In the following, we describe two solution schemes to the quadratic action $S_\alpha[\varphi]$ of Eq. (4.12), which determines the approximate zz correlations in the state $|\psi_\alpha\rangle$. The first scheme consists of taking a continuum limit of the lattice. This further simplification allows us to derive analytical results for the approximate zz correlations. The second scheme keeps the structure of the lattice and is solved numerically.

4.3.1 Continuum approximation

We apply an additional approximation to the action $S_\alpha[\varphi]$ by writing the sum over the positions z_j as an integral. We replace the sum over positions $\sum_{j=1}^{N}\varphi(z_j,\bar{z}_j)^2$ in Eq. (4.12) by a term proportional to the integral $\int_D dz d\bar{z}\varphi(z,\bar{z})^2$, where D is the region in the complex plane in which the spins are located. For this continuum approximation, we consider the systems illustrated in Fig. 4.1: a 1D system (infinite line and circle), a 2D system without a boundary (sphere), and a 2D system with a boundary (half plane and half-infinite cylinder). The resulting approximation for the zz correlations are summarized in Table 4.1. Most of the computations leading to the results of Table 4.1 for the case of the infinite line, the circle, the half-plane, and the cylinder were done by Germán Sierra and can be found in the Appendix of Ref. [164]. The calculation on the sphere is carried out in Appendix C.3.1.

Note that the continuum approximation predicts a power law decay of the long-range correlations in a 1D and at the edge of a 2D system with the power being -2 independent of α. In the bulk of a 2D system, we find an exponential decay of the correlations at large distances.

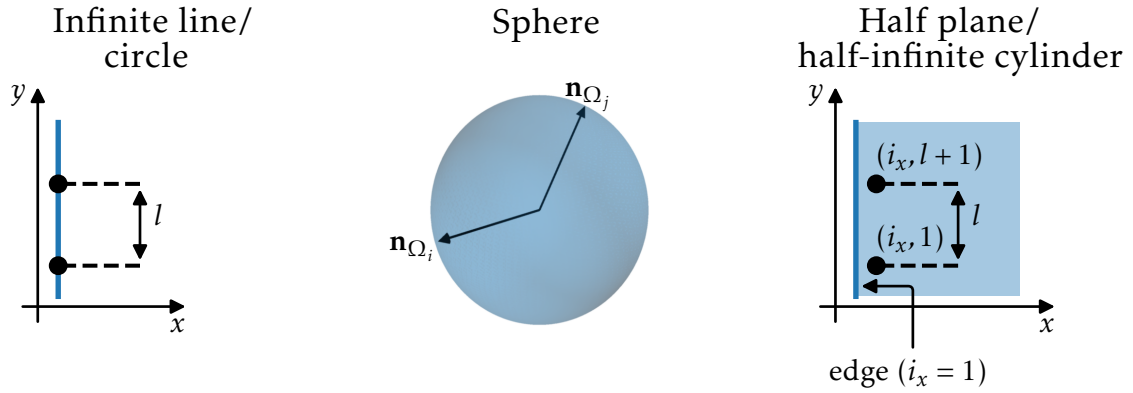

Figure 4.1: Systems for the computation of the zz correlations in the continuum approximation. The spins are located in the blue regions. In the case of the circle and the half-infinite cylinder, periodic boundary conditions are imposed along the y direction. The two points shown in each of the panels are the sites for which the zz correlations were computed.

4.3.2 Discrete approximation

The continuum approximation of the previous subsection does not take into account the lattice structure of the states $|\psi_\alpha\rangle$. In order to test this simplification and to obtain a better approximation of the exact zz correlations, we now discuss an approximation scheme that keeps the lattice. Specifically, we discuss the three types of lattices introduced in Sec. 2.3.1: a uniform lattice on a circle, an approximately uniform lattice on the sphere, and a square lattice on the cylinder. Thus, we can study both a 1D system and 2D systems with and without edges.

In the discrete case, we do not work with the path integral representation of the approximate zz correlations of Eq. (4.12) since it contains short-distance divergences at the lattice positions z_j. Taking the continuum limit as done above is one way to remove these divergences. In the discrete case, we choose to work with normal ordered fields and thus avoid divergences. This corresponds to taking the normal ordered expression of Eq. (4.9) as the starting point of the approximation instead of the path integral representation of Eq. (4.10). The approximation of the zz correlation then becomes

$$\langle \sigma_i^z \sigma_j^z \rangle \approx -\alpha \frac{\langle : \varphi(z_i,\bar{z}_i) e^{-\frac{\alpha}{2}\varphi(z_i,\bar{z}_i)^2} :: \varphi(z_j,\bar{z}_j) e^{-\frac{\alpha}{2}\varphi(z_j,\bar{z}_j)^2} : \prod_{k(\neq i,j)}^{N} : e^{-\frac{\alpha}{2}\varphi(z_k,\bar{z}_k)^2} : \rangle}{\langle \prod_{k=1}^{N} : e^{-\frac{\alpha}{2}\varphi(z_k,\bar{z}_k)^2} : \rangle}. \tag{4.13}$$

In Appendix C.3.2, we compute this expression and find

$$\langle \sigma_i^z \sigma_j^z \rangle \approx \Gamma_{ij}, \tag{4.14}$$

where

$$\Gamma_{ij} = \left[T_r \left(T_r^t M T_r + \mathbf{e}_r \mathbf{e}_r^t \right)^{-1} T_r^t - \mathbb{I} \right]_{ij}, \tag{4.15}$$

$r \in \{1, \ldots, N\}$ is an arbitrary index, M and T_r are the $N \times N$ with entries

$$M_{mn} = \delta_{mn} - 2\alpha \log(d_{mn} + \delta_{mn}), \qquad (T_r)_{mn} = \delta_{mn} - \delta_{mr}, \tag{4.16}$$

$\mathbf{e}_r$ is the rth unit vector, and $\mathbb{I}$ is the identity matrix. The $N \times N$ matrix d_{ij} contains the distances between sites i and j. It is given by $d_{ij} = |z_i - z_j|$ for positions in the complex plane. We note that the matrix Γ is independent of the choice of r.

Table 4.1: Approximation of the zz correlations in $|\psi_\alpha\rangle$ in the continuum approximation, cf. Fig. 4.1 for an illustration of the different systems. $\Phi(z,s,a) = \sum_{m=0}^{\infty} z^m/(a+m)^s$ denotes the Lerch transcendent function, Si and Ci are the sine and cosine integral functions, respectively. The position on the sphere $\mathbf{n}_{\Omega_i} \in S^2$ is defined in Eq. (2.31).

System	zz correlations	Large distances ($l \gg 1$)
Infinite line ($l = 0,1,2,\dots$)	$\langle\sigma^z_{l+1}\sigma^z_1\rangle \approx 2\alpha\left[\cos(r)\,\mathrm{Ci}(r) + \sin(r)\left(\mathrm{Si}(r) - \frac{\pi}{2}\right)\right]$, with $r = 2\pi\alpha l$	$-\frac{1}{2\pi^2\alpha}\frac{1}{l^2}$
Circle ($l = 0,1,\dots,N-1$)	$\langle\sigma^z_{l+1}\sigma^z_1\rangle \approx \frac{1}{N} - 2\alpha\,\mathrm{Re}\left[\Phi\left(e^{2\pi i\frac{l}{N}},1,N\alpha\right)\right]$	
Sphere $\left(\mathbf{n}_{\Omega_i},\mathbf{n}_{\Omega_j} \in S^2\right)$	$\langle\sigma^z_i\sigma^z_j\rangle \approx -\alpha\int_0^\infty dq\,\frac{2\cos\left(\sqrt{N\alpha-\frac{1}{4}}q\right)}{\sqrt{2\cosh(q)-2+\lvert\mathbf{n}_{\Omega_i}-\mathbf{n}_{\Omega_j}\rvert^2}}$	
Half-plane ($i_x = 1,2,\dots$; $l = 0,1,2,\dots$)	$\langle\sigma^z_{i_x,l+1}\sigma^z_{i_x,1}\rangle \approx \int_{-\infty}^{\infty}\frac{dq}{2\pi}e^{-iql}g(q)$, with $g(q) = -\frac{2\pi\alpha}{\sqrt{4\pi\alpha+q^2}}\left[1 + \frac{4\pi\alpha e^{-2(i_x-1)\sqrt{4\pi\alpha+q^2}}}{\left(\lvert q\rvert+\sqrt{4\pi\alpha+q^2}\right)^2}\right]$	edge ($i_x = 1$): $-\frac{1}{\pi l^2}$; bulk ($i_x \to \infty$): $-\pi^{\frac{1}{4}}\alpha^{\frac{3}{4}}\frac{e^{-2\sqrt{\pi\alpha}l}}{\sqrt{l}}$
Half-infinite cylinder ($i_x = 1,2,\dots$; $l = 0,1,\dots,N_y-1$)	$\langle\sigma^z_{i_x,l+1}\sigma^z_{i_x,1}\rangle \approx \frac{1}{N_y}\sum_{m=-\infty}^{\infty} e^{-\frac{2\pi iml}{N_y}} g(\frac{2\pi m}{N_y})$, with $g(q)$ as for the half-plane	

Lattices symmetries for the discrete approximation

Let us now explain how we ensure that the approximation retains the symmetries of the lattice.

The positions on the sphere are given by the unit vectors $\mathbf{n}_{\Omega_j}$ of Eq. (2.31), where $\Omega_j = (\theta_j,\phi_j)$ in terms of the polar angle θ_j and the azimuthal angle ϕ_j. When computing the exact zz correlations, the positions $\mathbf{n}_{\Omega_j}$ on the sphere can be mapped to the complex plane using the stereographic projection $z_j = \tan(\theta_j/2)e^{-i\phi_j}$, cf. Sec. 2.3.1. For the approximate zz correlations, however, it is better not to do this projection but to work directly on the sphere. The reason is that the differences in the complex plane, $|z_m - z_n| = |e^{-i\phi_m}\tan(\theta_m/2) - e^{-i\phi_n}\tan(\theta_n/2)|$, are not invariant under general rotations of the sphere. Note that this is not a problem for the exact zz correlations since

$$\langle\sigma^z_i\sigma^z_j\rangle = \frac{\sum_{s_1,\dots,s_N} s_i s_j \delta_{\mathbf{s}} \prod_{m<n}|z_m - z_n|^{2\alpha s_m s_n}}{\sum_{s_1,\dots,s_N}\delta_{\mathbf{s}}\prod_{m<n}|z_m - z_n|^{2\alpha s_m s_n}} = \frac{\sum_{s_1,\dots,s_N} s_i s_j \delta_{\mathbf{s}} \prod_{m<n}|\mathbf{n}_{\Omega_m} - \mathbf{n}_{\Omega_n}|^{2\alpha s_m s_n}}{\sum_{s_1,\dots,s_N}\delta_{\mathbf{s}}\prod_{m<n}|\mathbf{n}_{\Omega_m} - \mathbf{n}_{\Omega_n}|^{2\alpha s_m s_n}}, \tag{4.17}$$

where $|\mathbf{n}_{\Omega_m} - \mathbf{n}_{\Omega_n}|$ is invariant under sphere rotations. [Eq. (4.17) follows from $|\mathbf{n}_{\Omega_m} - \mathbf{n}_{\Omega_n}| = 2\cos(\theta_m/2)\cos(\theta_n/2)|z_m - z_n|$ and $s_1 + \cdots + s_N = 0$.] As we show in Appendix (C.2.1), the replacement of $|z_m - z_n|$ by $|\mathbf{n}_{\Omega_m} - \mathbf{n}_{\Omega_n}|$ corresponds to working directly on the sphere instead of the complex plane. Doing our approximation for the free-boson field $\varphi(\theta,\phi)$ instead of $\varphi(z,\bar z)$ thus leads us to an approximation that keeps the rotation invariance on the sphere. It is given by the expressions following Eq. (4.14) with $d_{mn} = |\mathbf{n}_{\Omega_m} - \mathbf{n}_{\Omega_n}|$.

The positions on the cylinder with N_x sites in the open direction and N_y sites in the periodic direction are defined as

$$w_j = \frac{2\pi}{N_y}(j_x + i j_y), \tag{4.18}$$

where $j_x \in \{1,\dots,N_x\}$ and $j_y \in \{1,\dots,N_y\}$ are the x and y components of the index j, respectively. The positions w_{j_x,j_y+N_y} and $w_{j_x j_y}$ are identified to impose periodicity in the y direction. In Sec. 2.3.1, the coordinates w_j on the cylinder were projected onto the complex plane through $z_j = e^{w_j}$. As for the stereographic projection in the case of the sphere, this mapping is a symmetry of the exact but not of the approximate zz correlations. Even though $|z_i - z_j|$ does not change under rotations of the cylinder, it distorts distances. As we show in Appendix C.2.2, working with coordinates w_j instead of $z_j = e^{w_j}$ corresponds to the replacement $|z_i - z_j| \to d_{ij}$ with

$$d_{ij} = \left|2\sinh\left(\frac{1}{2}(w_i - w_j)\right)\right|. \tag{4.19}$$

Our approximation on the cylinder is thus obtained by expanding in the field $\varphi(w,\bar{w})$ on the cylinder instead of $\varphi(z,\bar{z})$ on the plane. The resulting approximation of $\langle\sigma_i^z\sigma_j^z\rangle$ is given by using d_{ij} of Eq. (4.19) in the expressions following Eq. (4.14).

Choice of the lattice scale

The exact zz correlations are invariant under rescaling transformations of the lattice due to the conformal symmetry of the correlator of Eq. (2.25). These change the distances according to

$$d_{mn} \to \lambda d_{mn}, \tag{4.20}$$

where $\lambda > 0$. The quadratic, discrete approximation of $\langle\sigma_i^z\sigma_j^z\rangle$ is, however, not invariant under such rescalings since the matrix M of Eq. (4.16) varies under a change of the lattice scale λ. Thus, different choices of λ lead to different values of the approximation, and we need a criterion to uniquely determine the value of λ. We note that this problem does not occur in the continuum approximation since the replacement of the sum over lattice positions by an integral restores scale invariance, cf. the Appendix of Ref. [164]. In order to fix λ in the discrete case, we computed the subleading term of the expansion for the zz correlations in Appendix C.3.2:

$$\langle\sigma_i^z\sigma_j^z\rangle \approx \Gamma_{ij} - \Gamma_{ij}(\Gamma_{ii} + \Gamma_{jj}). \tag{4.21}$$

For two given indices i and j, we define the optimal scale λ by requiring that it minimizes the subleading term of the expansion, i.e., it is a minimum of

$$|\Gamma_{ii} + \Gamma_{jj}|. \tag{4.22}$$

Instead of choosing different scales for the different values of i and j, we also considered the following simpler approach: For a given set of positions and value of α, we determine a single optimal scale λ by minimizing the expression

$$\sqrt{\sum_{j=1}^{N}\Gamma_{jj}^2}. \tag{4.23}$$

In addition to minimizing expression (4.22) or (4.23), we require that λ is chosen such that eigenvalues of the matrix $T_r^t M T_r + \mathbf{e}_r \mathbf{e}_r^t$ appearing in Eq. (4.15) are all positive. This condition ensures the convergence of an N-dimensional Gaussian integral, cf. the derivation in Appendix C.3.2. As our numerical calculations show, these requirements uniquely determine the value of λ. In Fig. 4.2, we show plots for the determination of the minimal scale in two exemplary cases.

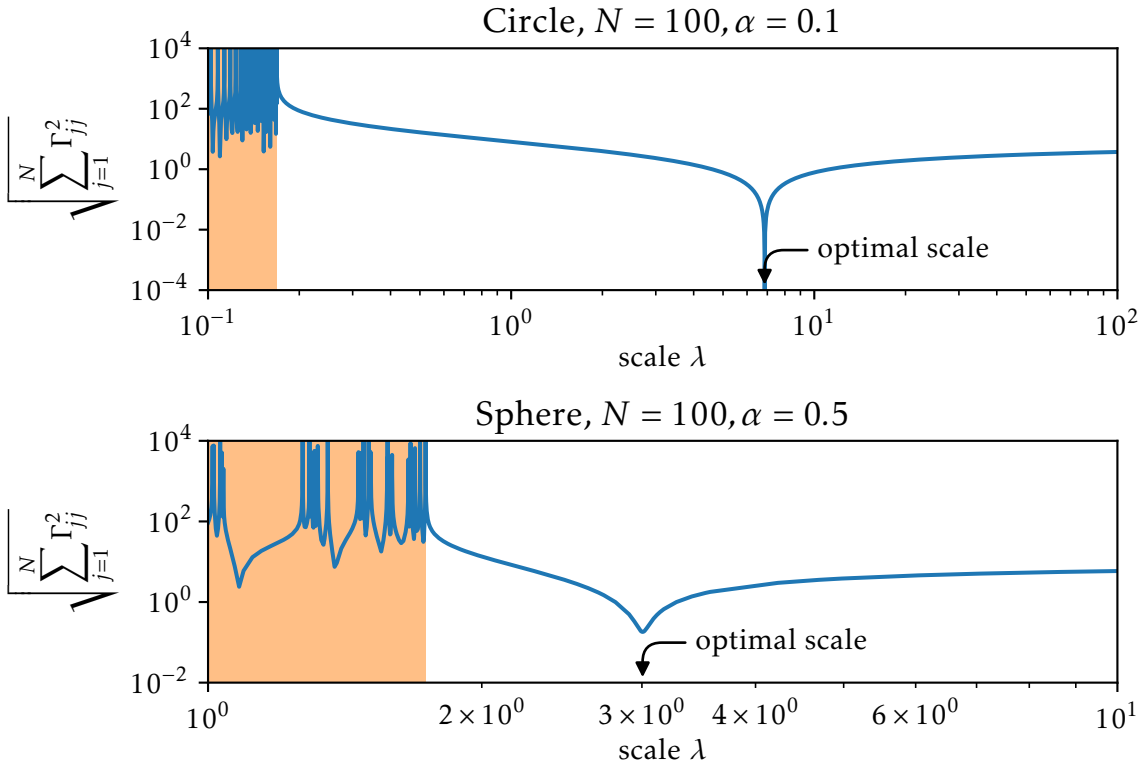

Figure 4.2: Determination of the optimal scale λ by minimizing the subleading term in the approximation. Values of λ below a minimal scale are excluded from the optimization since the approximation does not converge there (orange regions).

We did computations with multiple optimizations, i.e., minimizing expression (4.22), and a single optimization of expression (4.23). We found that doing multiple optimizations does not result in a substantial improvement of our results. Therefore, the data shown in the following correspond to a single optimization for a given lattice and value of α.

4.4 Quality of approximation for different systems

In this section, we test the validity of our approximation by comparing the obtained zz correlations to their actual value. Our aim in doing this analysis is to test whether the simple picture of the effective, quadratic theory is accurate. In two special cases, the actual zz correlations can be computed exactly, namely for $\alpha = \frac{1}{4}$, where $\psi_\alpha(s_1, \ldots, s_N)$ is the wave function of $\frac{N}{2}$ free fermions [109], and for $\alpha = \frac{1}{2}$ on the circle, where the exact correlations are known analytically [103, 165]. For all other cases, we used a Metropolis Monte Carlo method explained in Appendix A.2 to obtain estimates of the exact zz correlations in $|\psi_\alpha\rangle$. The approximation data in the following plots was computed using the discrete scheme described

in Sec. 4.3.2. We restrict ourselves to the four values of $\alpha = 0.125, 0.25, 0.375$, and $\alpha = 0.5$ here. Plots for additional values of α as well as for the continuum approximation can be found in the Supplementary Material of Ref. [164].

4.4.1 One-dimensional system

We first consider a 1D system. In this case, we can compare our results to bosonization studies of the XXZ model

$$H_{XXZ} = \sum_{j=1}^{N} \left(t_j^x t_{j+1}^x + t_j^y t_{j+1}^y + \Delta t_j^z t_{j+1}^z \right), \tag{4.24}$$

where $t_{N+1}^a = t_1^a$ for periodic boundary conditions. This model is in a critical phase for anisotropies $-1 < \Delta \leq 1$. The wave function $\psi_\alpha(s_1, \ldots, s_N)$ was used previously [102] as a variational ansatz for H_{XXZ} in the half-filled sector ($t_1^z + \cdots + t_N^z = 0$). More precisely, the positions z_j were taken to be uniformly distributed on a circle and α was determined for a given value of Δ such that the variational energy in $|\psi_\alpha\rangle$ is minimal. In the critical phase, the optimal value of α approximately satisfies $\Delta = -\cos(2\pi\alpha)$ and the overlap between the exact ground state $|\psi_0\rangle$ and the optimal $|\psi_\alpha\rangle$ is large [102]. Using the relation $\Delta = -\cos(2\pi\alpha)$, the results for the long-range zz correlations obtained using bosonization [97, 136] are given by

$$\frac{\langle \psi_0 | \sigma_{l+1}^z \sigma_1^z | \psi_0 \rangle}{\langle \psi_0 | \psi_0 \rangle} \sim -\frac{1}{2\pi^2 \alpha} \frac{1}{l^2} + A \frac{(-1)^l}{l^{\frac{1}{2\alpha}}}, \tag{4.25}$$

where A is the α-dependent amplitude that was determined in Ref. [136]. In the bosonization formalism, the local Pauli matrix σ_i^z has two contributions: A smooth term proportional to the U(1) current $\partial_y \varphi(y)$ and a second, rapidly varying term proportional to $\cos(\pi y + \sqrt{2\pi}\varphi(y))$ [166]. The decay of correlations with a power of -2 originates from the correlator of two U(1) currents, while the rapidly varying term in the representation of σ_i^z causes the staggered contribution to Eq. (4.25).

For small values of α, the first term in Eq. (4.25) is dominant. Our analytical results for the long-range correlations in an infinite 1D system of Table 4.1 correctly reproduce this term. As α approaches $\frac{1}{4}$, however, the second, alternating term in Eq. (4.25) becomes relevant and eventually dominates for $\alpha > \frac{1}{4}$. In this regime, the state develops quasi-long-range antiferromagnetic order. This behavior is not captured by the results of our continuum approximation. In contrast to bosonization, our representation of the zz correlations neglects rapid changes with position by assuming that the boson field is close to the same extremum of cosine at all positions, cf. Sec. 4.2.2. Furthermore, our approximation assumes that $\sqrt{\alpha}\varphi(z, \bar{z})$ is small and therefore we do not expect to obtain the second term in Eq. (4.25), which is relevant for large α.

Let us now discuss our numerical results for the discrete approximation. These are shown for $N = 100$ spins uniformly distributed on the circle in Fig. 4.3. At large distances, we observe a polynomial decay in the correlations. (Both axes in Fig. 4.3 are scaled logarithmically.) We find good agreement between the Monte Carlo estimate of the exact correlator and the approximation for $\alpha = 0.125$. The results differ substantially from the exact correlator for $\alpha \geq 0.25$ and the deviation grows with α. In particular, the oscillating behavior of $\langle \sigma_{l+1}^z \sigma_1^z \rangle$ for $\alpha > 0.25$ is not reproduced by our approximation.

To further emphasize that the approximation captures the smooth part of the correlator but not the alternating one, we consider the average $a_l = \frac{1}{2}(\langle \sigma_{l+2}^z \sigma_1^z \rangle + \langle \sigma_{l+1}^z \sigma_1^z \rangle)$ between the

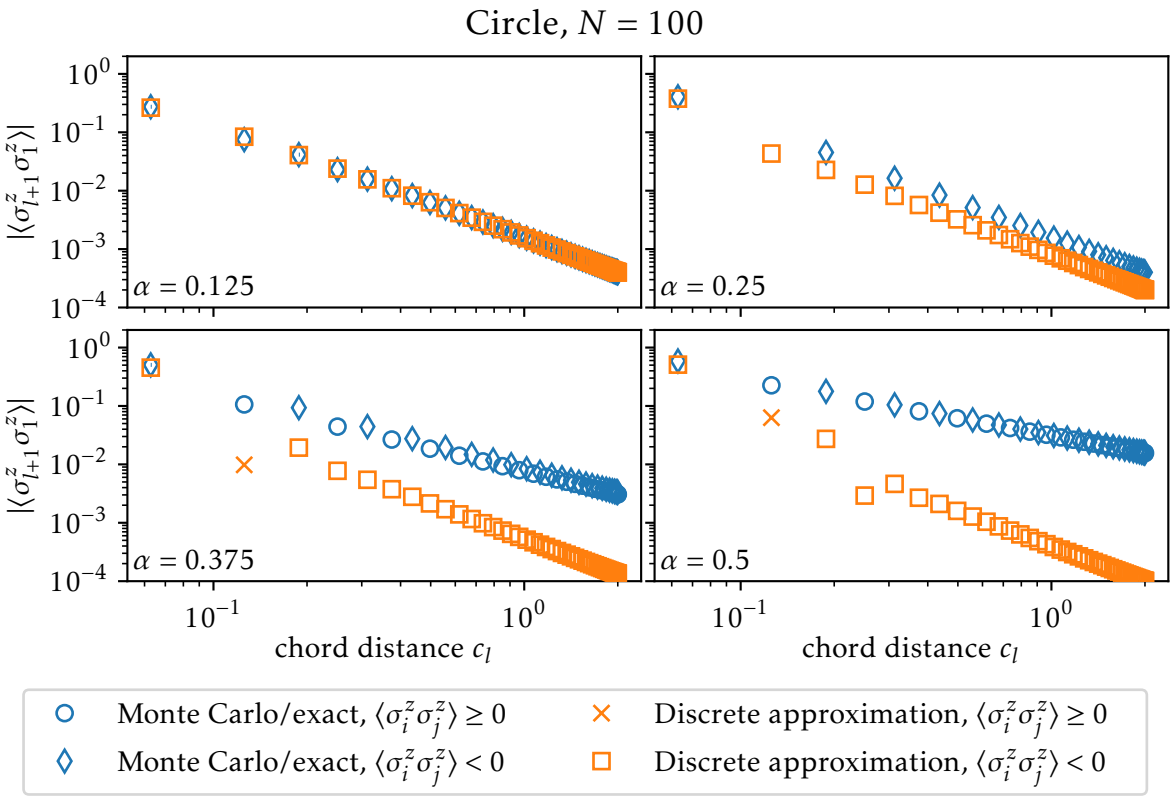

Figure 4.3: zz correlations in $|\psi_\alpha\rangle$ for $N = 100$ spins uniformly distributed on the circle. The data shown in blue are Monte Carlo estimates ($\alpha = 0.125$ and $\alpha = 0.375$) or exact ($\alpha = 0.25$ and $\alpha = 0.5$). The Monte Carlo errors are of the order of 10^{-6} and are thus not visible. The horizontal axes show the chord distance $c_l = |2\sin(\pi l/N)|$. At $\alpha = 0.25$, every second value of the actual correlator (blue symbols) is zero within numerical error and thus not visible.

correlator at distances $l+1$ and l. This combination suppresses the oscillating term at large distances:

$$\frac{1}{2}\left(\frac{\langle\psi_0|\sigma^z_{l+2}\sigma^z_1|\psi_0\rangle}{\langle\psi_0|\psi_0\rangle} + \frac{\langle\psi_0|\sigma^z_{l+1}\sigma^z_1|\psi_0\rangle}{\langle\psi_0|\psi_0\rangle}\right) \sim -\frac{1}{2\pi^2\alpha l^2} + A\frac{(-1)^l}{4\alpha l^{1+\frac{1}{2\alpha}}} \tag{4.26}$$

for the correlator obtained through bosonization. The average a_l is plotted in Fig. 4.4 for the actual zz correlations in $|\psi_\alpha\rangle$ and those obtained within the discrete approximation. Indeed, the agreement for a_l is better also for larger values of α. [The value of $\alpha = \frac{1}{2}$ is special in the sense that a_l still oscillates as a function of the distance. The reason is that both terms in Eq. (4.26) for $\alpha = \frac{1}{2}$ decay with the same power and the amplitude of the oscillating term dominates. While this oscillation is absent in the approximation, the power of the decay of a_l agrees with the actual one.]

In summary, both the comparison to bosonization and to the exact correlator lead to the conclusion that our approximation is only valid for small values of α in 1D.

4.4.2 Two-dimensional system without a boundary (sphere)

We next discuss the case of a 2D system without a boundary. The results of the discrete approximation are compared to the exact zz correlations in Fig. 4.5 for $N = 100$ spins on the

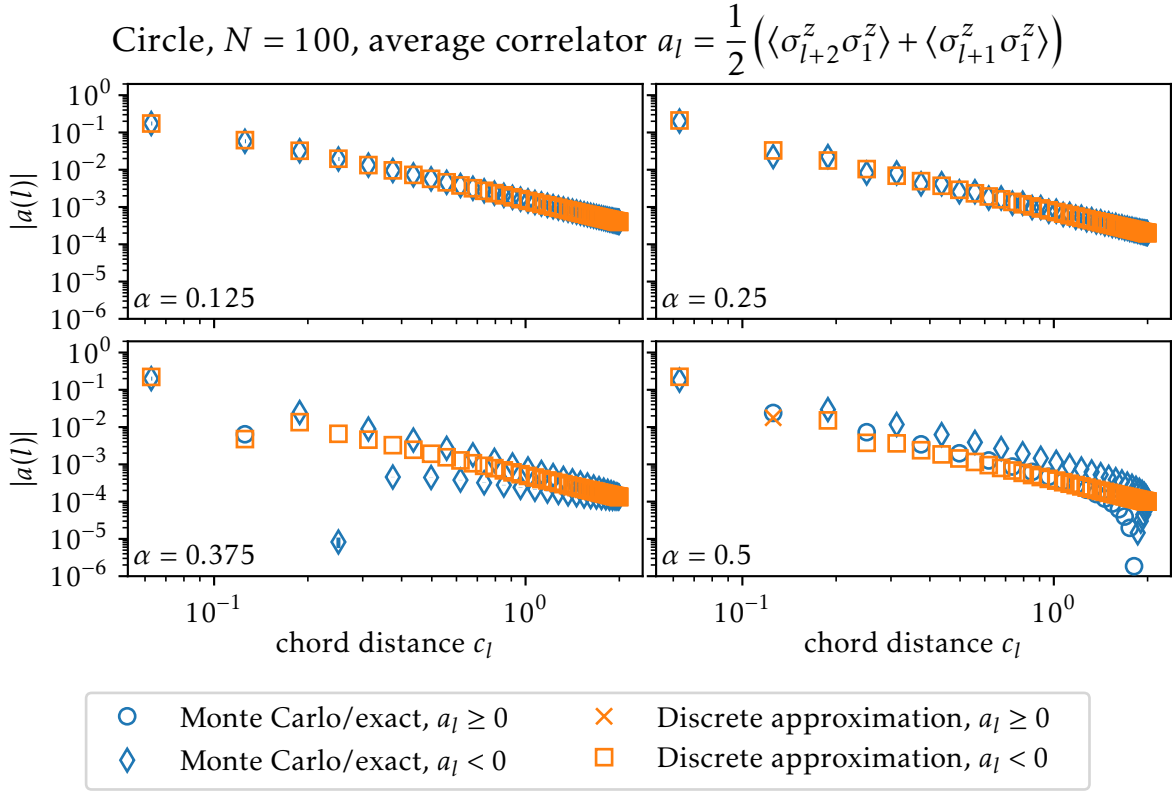

Figure 4.4: Average $a_l = \frac{1}{2}(\langle\sigma^z_{l+2}\sigma^z_1\rangle + \langle\sigma^z_{l+1}\sigma^z_1\rangle)$ between in the zz correlations in $|\psi_\alpha\rangle$ at distances l and $l+1$ for $N = 100$ spins on the circle. The blue symbols correspond to numerically exact data for $\alpha = 0.25$ and $\alpha = 0.5$ and to Monte Carlo estimates for $\alpha = 0.125$ and $\alpha = 0.375$. The horizontal axes show the chord distance $c_l = |2\sin(\pi l/N)|$.

sphere. The distribution of sites on the sphere was chosen to be approximately uniform. In Fig. 4.5, the vertical axis is scaled logarithmically, while the horizontal axis is linear.

Both the approximate correlations and the actual ones decay exponentially. Furthermore, a similar transition in the behavior of the zz correlations appears at $\alpha = \frac{1}{4}$ as in 1D: For $\alpha \leq \frac{1}{4}$, the correlations between distinct sites are negative whereas for $\alpha > \frac{1}{4}$ they change sign as a function of the distance. As in 1D, we find the best agreement for the smallest value of α and large deviations at the transition point $\alpha = \frac{1}{4}$. However, in contrast to the 1D case, the approximation captures the qualitative behavior of the correlations for larger values of α. In particular, we observe that the sign changes are reproduced correctly.

A reason for the better performance of the approximation in 2D could be as follows: Due to the cosine factors in Eq. (4.10), we assumed field configurations around 0 mainly contribute to the path integral. In the case of a 1D system, however, these cosine factors only depend on the field configuration along a 1D path and therefore they do not restrict contributions to the path integral as strongly as for a 2D system. Furthermore, the oscillations in the actual correlations are much stronger in 1D, where they decay polynomially, than in 2D, where the decay is exponential and there is no quasi-long-range antiferromagnetic order.

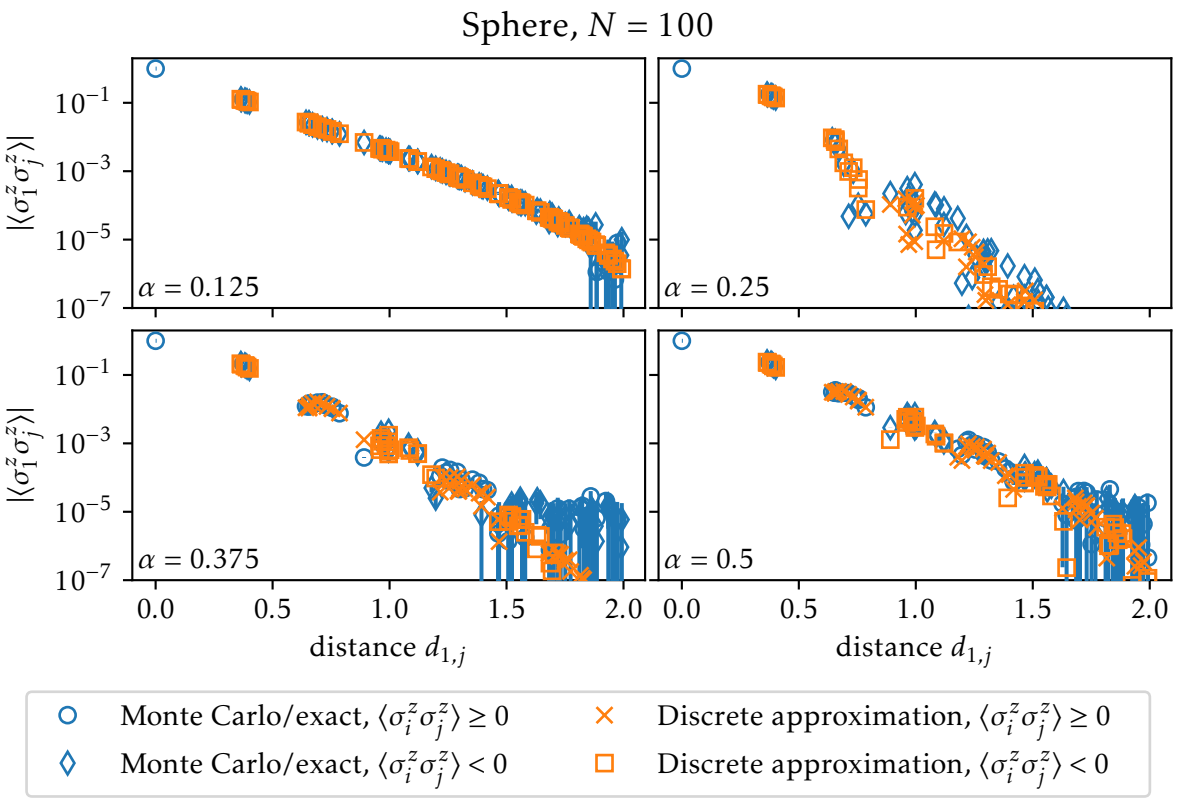

Figure 4.5: zz correlations in $|\psi_\alpha\rangle$ for $N = 100$ spins with an approximately uniform distribution on the sphere. The blue data points are Monte Carlo estimates ($\alpha = 0.125, 0.375, 0.5$) or exact ($\alpha = 0.25$). The horizontal axes show the distance $d_{1,j} = |\mathbf{n}_{\Omega_1} - \mathbf{n}_{\Omega_j}|$, cf. Eq. (2.31) for the definition of $\mathbf{n}_{\Omega_j}$.

4.4.3 Two-dimensional system with a boundary (cylinder)

Let us now consider a 2D system with an edge. Our results for the edge correlations of a cylinder of size $N_x = 14$ and $N_y = 160$ are shown in Fig. 4.6. (The large number of spins $N_y = 160$ is chosen so that we can study the long-range decay of edge correlations.) For $\alpha = 0.125$, we observe a good agreement at all length scales. As α becomes larger, the approximation deviates from the exact result at short distances but follows the decay at larger ones to good accuracy. The plots in Fig 4.6 are logarithmically scaled on both axes and therefore show an algebraic decay of long-range correlations with a power of -2 as predicted by our continuum approximation (cf. Table 4.1). This behavior corresponds to the decay of a current-current correlator of a U(1) theory at the edge.

Our results for the correlator in the bulk of the cylinder are shown in Fig. 4.7. The agreement between the approximate and the actual correlator is similar to that on the sphere: The approximation is best for $\alpha = 0.125$, fails to describe the transition at $\alpha = 0.25$, and is qualitatively right for $\alpha > 0.25$. The approximate correlations and the actual ones decay exponentially. (The horizontal axes in Fig. 4.7 are scaled linearly.)

4.4.4 Comparison of continuum and discrete approximation

Finally, we note that the discrete approximation generally yields better results than the continuum approximation, especially for larger values of α in 2D. (Corresponding plots are shown

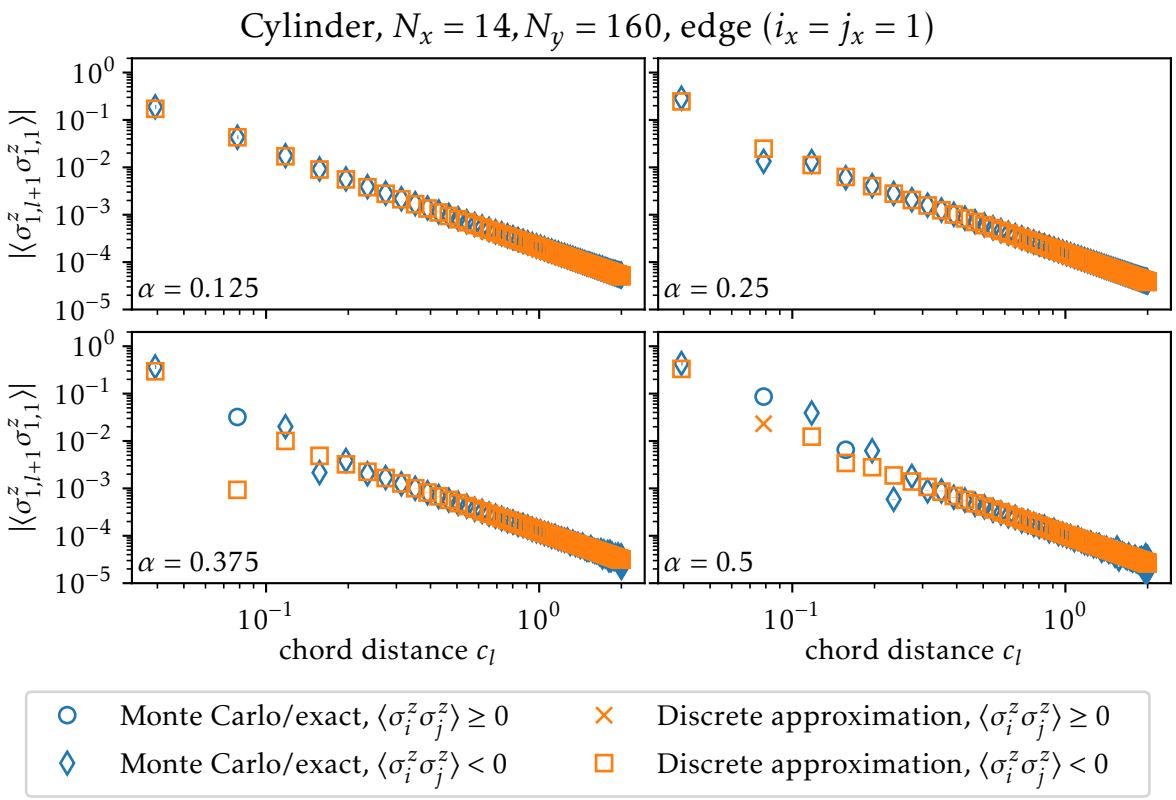

Figure 4.6: zz correlations in $|\psi_\alpha\rangle$ on the edge of a cylinder with $N_x = 14$ sites in the open direction and $N_y = 160$ sites in the periodic direction. The shown correlations are those along the y direction. The blue data points are Monte Carlo estimates ($\alpha = 0.125, 0.375, 0.5$) or exact ($\alpha = 0.25$). The horizontal axes show the chord distance $c_l = |2\sin(\pi l/N_y)|$.

in the Supplementary Material of Ref. [164].) In particular, the continuum approximation does not reproduce the alternating behavior of the correlations for $\alpha > \frac{1}{4}$. At the edge of the 2D system, the continuum approximation agrees with the exact correlation in the power of the long-range decay but not in the prefactor, which is, however, reproduced correctly by the discrete approximation. In order to get a better agreement at larger values of α, it is therefore necessary to keep the lattice structure and to optimize the approximation by choosing the scale as described in Sec. 4.3.2.

4.5 Outlook: Approximation through a periodic function

Our approximation of the spin-spin correlations in $|\psi_\alpha\rangle$ is based on replacing $\cos(\sqrt{\alpha}\varphi(z,\bar{z}))$ by the Gaussian $e^{-\frac{\alpha}{2}\varphi(z,\bar{z})^2}$. The latter is non-periodic and positive everywhere.

We thus expect that the approximation can be improved by replacing $\cos(\sqrt{\alpha}\varphi(z,\bar{z}))$ by a periodic function that assumes positive and negative values. Let us thus consider the following approximate representations of $\cos(x)$ and $\sin(x)$:

$$\cos(x) \approx \sum_{\mu\in\mathbb{Z}} e^{-\frac{1}{2}(x-\pi\mu)^2 - i\pi\mu}, \qquad \sin(x) \approx i \sum_{\mu\in\mathbb{Z}+\frac{1}{2}} e^{-\frac{1}{2}(x-\pi\mu)^2 - i\pi\mu}. \tag{4.27}$$

An approximation of this kind was done by Villain [167] in the context of the classical XY

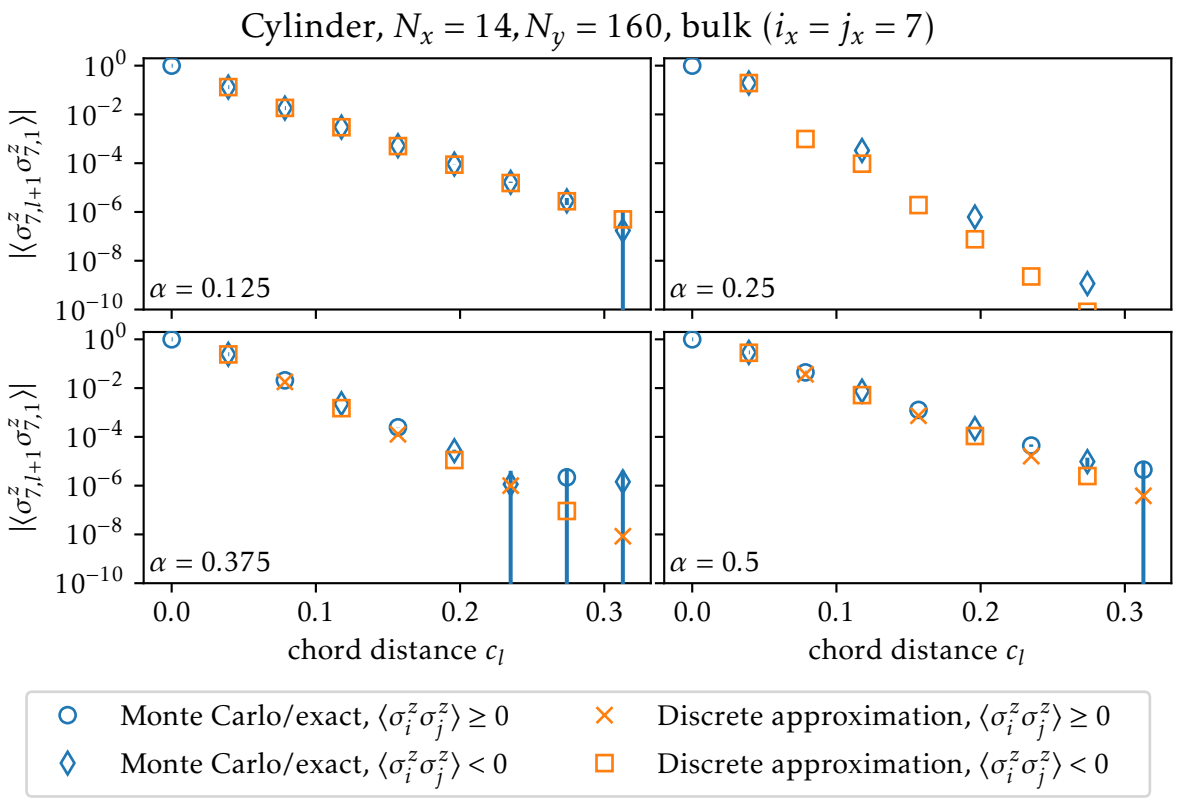

Figure 4.7: zz correlations in $|\psi_\alpha\rangle$ in the bulk of a cylinder with $N_x = 14$ sites in the open direction and $N_y = 160$ sites in the periodic direction. The shown correlations are those along the y direction. The blue data points are Monte Carlo estimates ($\alpha = 0.125, 0.375, 0.5$) or exact ($\alpha = 0.25$). The horizontal axes show the chord distance $c_l = |2\sin(\pi l/N_y)|$. We only plot the data at short distances since the correlations decay exponentially and good Monte Carlo estimates cannot be obtained at larger distances. At $\alpha = 0.25$, every second data point of the actual correlator (blue symbols) assumes a value below the lower boundary of the plot and is thus not visible.

model in 2D. Using Eq. (4.9), this leads to the following approximation of zz correlations for $i \neq j$:

$$\langle\sigma^z_i\sigma^z_j\rangle \approx \frac{\mathcal{Z}_\alpha(i,j)}{\mathcal{Z}_\alpha()}, \qquad \text{where } \mathcal{Z}_\alpha(i_1,\ldots,i_k) = \sum_{\mu_1,\ldots,\mu_N} \langle \prod_{j=1}^{N} : e^{-\frac{1}{2}\left(\sqrt{\alpha}\varphi(z_j,\bar{z}_j)-\pi\mu_j\right)^2 - i\pi\mu_j} :\rangle, \tag{4.28}$$

and μ_j is summed over

$$\mu_j \in \begin{cases} \mathbb{Z}+\frac{1}{2} & \text{if } j \in \{i_1,\ldots i_k\}, \\ \mathbb{Z} & \text{otherwise.} \end{cases} \tag{4.29}$$

Let us evaluate the function

$$\zeta(\boldsymbol{\mu}) = \langle \prod_{j=1}^{N} : e^{-\frac{1}{2}\left(\sqrt{\alpha}\varphi(z_j,\bar{z}_j)-\pi\mu_j\right)^2} :\rangle = e^{-\frac{\pi^2}{2}\boldsymbol{\mu}^2} \langle \prod_{j=1}^{N} : e^{-\frac{\alpha}{2}\varphi(z_j,\bar{z}_j)^2 + \pi\sqrt{\alpha}\mu_j\varphi(z_j,\bar{z}_j)} :\rangle. \tag{4.30}$$

In Appendix C.3.2, we show that

$$\Big\langle \prod_{j=1}^{N} :e^{-\frac{\alpha}{2}\varphi(z_j,\bar{z}_j)^2 + i\sqrt{\alpha}J_j\varphi(z_j,\bar{z}_j)}: \Big\rangle \propto e^{\frac{1}{2}\boldsymbol{J}^t\Gamma\boldsymbol{J}}, \tag{4.31}$$

where Γ was defined in Eq. (4.15), and $\boldsymbol{J} \in \mathbb{R}^N$. By analytical continuation of Eq. (4.31) with $\boldsymbol{J} = -i\pi\boldsymbol{\mu}$, it follows that

$$\zeta(\boldsymbol{\mu}) \propto e^{-\frac{1}{2}\boldsymbol{\mu}^t\left[\pi^2(\Gamma+\mathbb{I})\right]\boldsymbol{\mu}}. \tag{4.32}$$

Therefore, the approximate zz correlations based on the replacements of Eq. (4.27) are given by

$$\langle \sigma_i^z \sigma_j^z \rangle \approx \frac{\sum\limits_{\substack{\mu_i,\mu_j\in\mathbb{Z}+\frac{1}{2},\\ \mu_k\in\mathbb{Z}\text{ for }k\notin\{i,j\}}} (-1)^{\sum_{k=1}^N \mu_k} e^{-\frac{1}{2}\boldsymbol{\mu}^t\left[\pi^2(\Gamma+\mathbb{I})\right]\boldsymbol{\mu}}}{\sum_{\mu_1,\ldots,\mu_N\in\mathbb{Z}} (-1)^{\sum_{k=1}^N \mu_k} e^{-\frac{1}{2}\boldsymbol{\mu}^t\left[\pi^2(\Gamma+\mathbb{I})\right]\boldsymbol{\mu}}}. \tag{4.33}$$

[Note that writing $(-1)^{\mu_i+\mu_j}$ is not ambiguous for both μ_i and μ_j being a half-integer.] This expression resembles an expectation value in a statistical model of integer spins $\mu_j \in \mathbb{Z}$ and an effective Hamiltonian $H_{\text{eff}}(\boldsymbol{\mu}) = \frac{\pi^2}{2}\boldsymbol{\mu}^t(\Gamma+\mathbb{I})\boldsymbol{\mu}$. The factor $\exp\left(-\frac{\pi^2}{2}\boldsymbol{\mu}^2\right)$ suppresses terms with high values of μ_j and could thus justify a restriction to $\mu_j \in \{-1,0,1\}$.

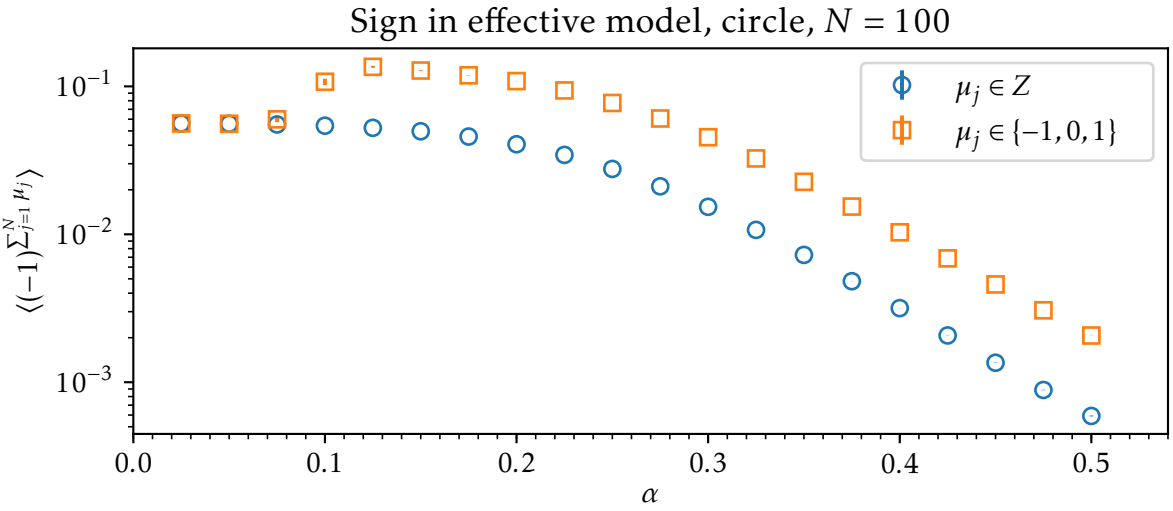

Figure 4.8: Sign factor in the approximate correlations of Eq. (4.33), cf. Eq. (4.34) for the definition of $\langle(-1)^{\sum_{j=1}^N \mu_j}\rangle$. The blue circles correspond to the unrestricted case of $\mu_j \in \mathbb{Z}$. The points shown as orange squares were obtained by restricting to $\mu_j \in \{-1,0,1\}$.

However, the factor $(-1)^{\sum_{k=1}^N \mu_j}$ can become negative and it is thus not possible to incorporate it into the effective Hamiltonian. In Fig. 4.8, we plot the quantity

$$\langle(-1)^{\sum_{j=1}^N \mu_j}\rangle \equiv \frac{\sum_{\mu_1,\ldots,\mu_N} (-1)^{\sum_{j=1}^N \mu_j} e^{-\frac{1}{2}\boldsymbol{\mu}^t\left[\pi^2(\Gamma+\mathbb{I})\right]\boldsymbol{\mu}}}{\sum_{\mu_1,\ldots,\mu_N} e^{-\frac{1}{2}\boldsymbol{\mu}^t\left[\pi^2(\Gamma+\mathbb{I})\right]\boldsymbol{\mu}}} \tag{4.34}$$

determined through Monte Carlo simulations for a circle of size $N = 100$. Both in the unrestricted case of $\mu_j \in \mathbb{Z}$ and for $\mu_j \in \{-1,0,1\}$, we find small values for $\langle(-1)^{\sum_{j=1}^N \mu_j}\rangle$. This indicates

that there is a cancellation between configurations with positive and negative values of $(-1)^{\sum_j \mu_j}$. A computation of Eq. (4.33) through Monte Carlo simulations and an interpretation in terms of an average in a statistical model is thus complicated by a sign problem.

In principle, Eq. (4.33) can be transformed to another representation that is free of the sign problem through Poisson's formula

$$\sum_{n\in\mathbb{Z}} f(n) = \sum_{n\in\mathbb{Z}} \int_{-\infty}^{\infty} dy e^{-2\pi i n y} f(y), \tag{4.35}$$

where $f(y)$ is a function of a real argument y. However, the result is very similar to the original, exact expression. Applying Eq. (4.35) to the approximation of Eq. (4.27), we obtain

$$\cos(x) \approx \sum_{\mu\in\mathbb{Z}} e^{-\frac{1}{2}(x-\pi\mu)^2 - i\pi\mu} = \sum_{\mu\in\mathbb{Z}} \int_{-\infty}^{\infty} dy e^{-2\pi i y\mu - i\pi y} e^{-\frac{1}{2}(x-\pi y)^2} = \sqrt{\frac{2}{\pi}} \sum_{\sigma\in 2\mathbb{Z}+1} e^{-\frac{1}{2}\sigma^2} e^{-ix\sigma}. \tag{4.36}$$

The factor $e^{-i\pi\mu}$ that causes the sign problem in Eq. (4.33) is not present anymore after applying the Poisson summation. However, the right-hand side of Eq. (4.36) is similar to the exact equation $\cos(x) = \frac{1}{2}(e^{ix} + e^{-ix})$. Thus, it does not yield a useful simplification: The dominating terms are those that have $\sigma = -1$ or $\sigma = 1$ since the remaining terms are exponentially suppressed. Restricting the sum to $\sigma \in \{-1, 1\}$, one obtains the cosine up to the factor $2\sqrt{2/(\pi e)} \approx 0.968$.

4.6 Conclusion

In this chapter, we studied correlations in states $|\psi_\alpha\rangle$ of N spins on a lattice. The wave functions $\psi_\alpha(s_1, \ldots, s_N)$ are constructed as chiral correlators of the CFT of a free, massless boson. In 1D, they are approximate ground states of the XXZ spin chain, and they are similar to Laughlin lattice states in 2D.

We derived an exact representation of the zz correlations in $|\psi_\alpha\rangle$ in terms of a path integral expression. By truncating it to quadratic order, we obtained an effective description in terms of a solvable, quadratic action. Our effective theory differs from the original massless boson by an additional mass-like term, which depends on the field configuration at the lattice sites. Thus, we establish an analytical connection between physical properties of a state, namely its correlations, and the underlying CFT.

By solving the free field theory, we obtained an approximation of the zz correlations in $|\psi_\alpha\rangle$. The mass-like term in our effective theory gives rise to an exponential decay of correlations in the bulk of a 2D system, whereas our approximation predicts a power-law decay in 1D and at the edge of a 2D system. We compared our results for the approximate correlations to Monte Carlo estimates of the exact value. Our analysis shows that the approximation is most reliable for small values of α, where it yields good results in the case of a 1D and a 2D system, both in the bulk and at the edge. The long-range decay of the correlations at the edge of a 2D system is reproduced correctly by the approximation for all considered values of α. Furthermore, we find qualitative agreement between the exact result and our approximating in the bulk of a 2D system for values of $\alpha > \frac{1}{4}$, whereas it fails to describe this regime in 1D.

The reason that the approximation is better in 2D than in 1D is presumably due to the fact that field configurations away from 0 are more relevant in 1D than in 2D. We thus expect to obtain the oscillating term for larger values of α in 1D by taking into account these field configurations. Following Ref. [167], we considered such an approximation but found that the resulting expressions suffer from a sign problem.

In this chapter, we focused on approximating the zz correlations in terms of a free field theory. It would be interesting to extend this method to other quantities.

5 States with continuous spins obtained from conformal field theory

This chapter investigates nonchiral states with continuous spins on lattices obtained as correlators of the CFT of a massless, free boson introduced in Sec. 2.1.1. This approach is distinct from the case of continuous positional degrees of freedom [7], but also from the lattice wave functions defined on a discrete Hilbert space consisting of spins or occupation numbers [102], which was studied in Chapter 3 and 4 of this thesis.

Opposed to the case of discrete spins, the wave functions with continuous spins of this chapter can be treated as bosonic Gaussian states. This implies that their properties can be computed efficiently, whereas Monte Carlo simulations are necessary for states with discrete spins. Besides this technical advantage, a motivation for considering Gaussian states is given by the fact that the underlying CFT is also Gaussian. It is thus interesting to study how this case differs from that of non-Gaussian states derived from the same CFT.

The purpose of this chapter is to characterize the continuous-spin states derived from the free-boson CFT for systems in 1D and in 2D. To do so, we compute and analyze entanglement properties. In 1D, these can be used to identify CFT behavior in quantum-many body states [160, 168, 169]. Furthermore, topological properties in 2D can be characterized through the entanglement entropy [83, 84] and entanglement spectra [159, 161–163].

In 1D, we find that the continuous-spin states are closely related to the free-boson CFT they are constructed from. Both the entanglement entropies and spectra agree with the CFT expectation. Furthermore, we find a parent Hamiltonian with low-energy eigenvalues that are consistent with a massless, free boson.

For systems in 2D, we investigate topological properties encoded in entanglement entropies and spectra. Our results indicate that the topological entanglement entropy vanishes. This means that the continuous-spin states do not exhibit intrinsic topological order, which is expected for Gaussian states and distinct from the case of discrete spins. However, an analysis of entanglement spectra reveals nonchiral states that are exponentially localized at the edge created by the entanglement cut. This is an indication that the states support edge modes.

The continuous-spin wave functions studied in this chapter have the same spin-spin correlations as the approximation of Chapter 4. In this sense, this chapter, which studies entanglement properties, is an extension of Chapter 4, which considered spin-spin correlations. Here, however, we focus on investigating and characterizing model wave functions with continuous spins instead of approximating properties of discrete, spin-$\frac{1}{2}$ states. In this chapter, we examine nonchiral, real wave functions, which is distinct from the case of chiral states studied in Chapters 3 and 4 of this thesis. We provide an outlook on the case of chiral wave functions with continuous spins at the end of this chapter.

This chapter is organized as follows.

- Sec. 5.1 defines nonchiral states with continuous spins from the free-boson CFT, relates them to the approximation of Chapter 4, represents them as bosonic Gaussian states, and summarizes how we compute entanglement properties for them.
- Sec. 5.2 considers these states in 1D, compares their entanglement entropies and spectra to those of the CFT, and studies a parent Hamiltonian.

- In Sec. 5.3, we study the states on a cylinder, show that they have a vanishing topological entanglement entropy, and find indications of edge modes in the entanglement spectrum.
- Sec. 5.4 discusses the chiral wave function.
- Sec. 5.5 concludes this chapter.

Most of the rest of this chapter and the corresponding appendices are adaptations of the following preprint:

- B. Herwerth, G. Sierra, J. I. Cirac, and A. E. B. Nielsen, "Bosonic Gaussian states from conformal field theory", arXiv:1807.01943 (2018), submitted to Phys. Rev. B (Ref. [170]).

5.1 Spin states from conformal field theory

This section defines states with a continuous spin as correlators of the free-boson CFT, represents them as bosonic Gaussian states, and explains how we compute entanglement properties.

5.1.1 Definition of states

We consider the CFT of a massless, free bosonic field $\varphi(z,\bar{z})$ for $z \in \mathbb{C}$ introduced in Sec. 2.1.1. This theory has a series of conformal primary fields $:e^{is\varphi(z,\bar{z})}:$ for $s \in \mathbb{R}$, where the colons denote normal ordering. We define spin wave functions as the correlator of primary fields:

$$\begin{aligned}\psi_\beta(\boldsymbol{s}) &= e^{-\frac{1}{4}(\beta+\beta_0)\boldsymbol{s}^2}\langle : e^{\frac{i}{\sqrt{2}}s_1\varphi(z_1,\bar{z}_1)} : \cdots : e^{\frac{i}{\sqrt{2}}s_N\varphi(z_N,\bar{z}_N)} :\rangle \\ &= e^{-\frac{1}{4}(\beta+\beta_0)\boldsymbol{s}^2}\,\delta(s_1+\cdots+s_N)\prod_{m<n}|z_m-z_n|^{s_m s_n},\end{aligned} \tag{5.1}$$

where z_j for $j \in \{1,\ldots,N\}$ defines a lattice of positions in the complex plane, $\boldsymbol{s} \in \mathbb{R}^N$ is a vector of N continuous spin variables, δ is the Dirac delta function originating from the charge neutrality condition, and $\beta > 0$ is a real parameter. We define the real number β_0 through a normalizability criterion and introduce β_0 separately from β for convenience so that β is always positive, cf. Sec. 5.1.4 below. The parametric dependence of $\psi_\beta(\boldsymbol{s})$ on the lattice positions z_j is suppressed for simplicity of notation.

The prefactor $e^{-\frac{1}{4}(\beta+\beta_0)s^2}$ in Eq. (5.1) corresponds to a rescaling $(z_j,\bar{z}_j) \to (\lambda z_j, \lambda\bar{z}_j)$ with $\lambda > 0$, under which the correlation function of primary fields $:e^{\frac{i}{\sqrt{2}}s_j\varphi(z_j,\bar{z}_j)}:$ changes by a factor $\lambda^{-\frac{1}{2}s^2}$. Comparing to the form of the wave function of Eq. (5.1), we have $\beta+\beta_0 = 2\log\lambda$ in terms of the scale parameter λ of the lattice. In the definition of $\psi_\beta(\boldsymbol{s})$, we do not include an additional parameter in the exponent of the vertex operators as in the case of the spin-$\frac{1}{2}$ states defined in Sec. 2.3. The reason is that such a parameter can be removed by a rescaling of the continuous spins $s_j \in \mathbb{R}$.

5.1.2 Relation to approximation of spin-$\frac{1}{2}$ states

In Chapter 4, we considered continuous-spin approximations for correlations of spin-$\frac{1}{2}$ states $|\psi_\alpha\rangle$ defined in Eq. (2.24). The wave functions $\psi_\beta(\boldsymbol{s})$ have the same correlations as the approximation that was made in Chapter 4, as we shall now show.

In Chapter 4, we considered zz correlations C_{ij} in $|\psi_\alpha\rangle$,

$$C_{ij} \equiv 4\frac{\langle\psi_\alpha|t_i^z t_j^z|\psi_\alpha\rangle}{\langle\psi_\alpha|\psi_\alpha\rangle} = \frac{\sum_{s_1,\ldots,s_N} s_i s_j \delta_{\boldsymbol{s}} \prod_{m<n}|z_m-z_n|^{2\alpha s_m s_n}}{\sum_{s_1,\ldots,s_N}\delta_{\boldsymbol{s}}\prod_{m<n}|z_m-z_n|^{2\alpha s_m s_n}}, \tag{5.2}$$

and approximated them for $i \neq j$ by a continuous integral of the form

$$C_{ij}^{(\text{approx})} = \frac{\int d^N \boldsymbol{s} s_i s_j \delta(s_1 + \cdots + s_N) e^{-\frac{1}{2}\boldsymbol{s}^2} \prod_{m<n} |\lambda(z_m - z_n)|^{2\alpha s_m s_n}}{\int d^N \boldsymbol{s} \delta(s_1 + \cdots + s_N) e^{-\frac{1}{2}\boldsymbol{s}^2} \prod_{m<n} |\lambda(z_m - z_n)|^{2\alpha s_m s_n}}, \tag{5.3}$$

where $\lambda > 0$ is a scale parameter that we fixed by requiring that the subleading term of the approximation is minimal (cf. Sec. 4.3.2).

The expression $C_{ij}^{(\text{approx})}$ of Eq. (5.3) follows from Eqs. (C.51), (C.54), and (C.61) of Appendix C.3.2. It corresponds to what we called the *discrete* approximation in Chapter 4. We note that the word *discrete* does not refer to the spins in the approximation (which are *continuous*) but to the lattice of positions. The term *discrete* is used in Chapter 4 to emphasize the difference to the case where an additional continuum limit of the lattice is taken (cf. Sec. 4.3.1).

Rescaling $s_j \to s_j/\sqrt{\alpha}$ in $C_{ij}^{(\text{approx})}$ and using $\prod_{m<n} \lambda^{s_m s_n} = e^{-\frac{1}{2}\boldsymbol{s}^2 \log \lambda}$ for $s_1 + \cdots + s_N = 0$, we find

$$C_{ij}^{(\text{approx})} = \frac{1}{\alpha} \frac{\int d^N \boldsymbol{s} s_i s_j \delta(s_1 + \cdots + s_N) e^{-\frac{1}{2}\boldsymbol{s}^2 \left(\frac{1}{\alpha} + 2\log\lambda\right)} \prod_{m<n} |z_m - z_n|^{2 s_m s_n}}{\int d^N \boldsymbol{s} \delta(s_1 + \cdots + s_N) e^{-\frac{1}{2}\boldsymbol{s}^2 \left(\frac{1}{\alpha} + 2\log\lambda\right)} \prod_{m<n} |z_m - z_n|^{2 s_m s_n}} \tag{5.4}$$

$$= \frac{1}{\alpha} \frac{\int d^N \boldsymbol{s} s_i s_j |\psi_\beta(\boldsymbol{s})|^2}{\int d^N \boldsymbol{s} |\psi_\beta(\boldsymbol{s})|^2}, \tag{5.5}$$

where we identified $\beta + \beta_0 = \frac{1}{\alpha} + 2\log\lambda$. Thus, the approximation $C_{ij}^{(\text{approx})}$ made in Chapter 4 corresponds to the spin-spin correlations of the wave function $\psi_\beta(\boldsymbol{s})$ up to a total factor of $\frac{1}{\alpha}$.

Having realized that the approximate correlations of $|\psi_\alpha\rangle$ are precisely those of $\psi_\beta(\boldsymbol{s})$, we now study and characterize the model wave functions $\psi_\beta(\boldsymbol{s})$ in their own right. We note, however, that there is an important difference between $\psi_\alpha(s_1, \ldots, s_N)$ and $\psi_\beta(\boldsymbol{s})$: The former is chiral while the latter is not. We comment on the case of a chiral wave function with continuous spins in Sec. 5.4 below.

5.1.3 Representation as a Gaussian state

We now represent $\psi_\beta(\boldsymbol{s})$ as a bosonic Gaussian state, which implies that its properties can be computed efficiently for large systems. To this end, we replace the delta function $\delta(s_1 + \cdots + s_N)$ in $\psi_\beta(\boldsymbol{s})$ [cf. Eq. (5.1)] by a Gaussian of width proportional to $\sqrt{\epsilon}$ for $\epsilon > 0$. This leads to the wave function

$$\psi_{\beta,\epsilon}(\boldsymbol{s}) = e^{-\frac{1}{2}\boldsymbol{s}^t \left(\frac{1}{2\epsilon}\boldsymbol{e}\boldsymbol{e}^t + X_\beta\right)\boldsymbol{s}}, \tag{5.6}$$

where

$$\left(X_\beta\right)_{mn} = \frac{1}{2}(\beta + \beta_0)\delta_{mn} + X_{mn}, \tag{5.7}$$

$$X_{mn} = -\log(|z_m - z_n| + \delta_{mn}), \tag{5.8}$$

and $\boldsymbol{e} = (1, \ldots, 1)^t$ is the vector with all entries being equal to one. Then,

$$\psi_\beta(\boldsymbol{s}) = \lim_{\epsilon \to 0} \frac{1}{2\sqrt{\pi\epsilon}} \psi_{\beta,\epsilon}(\boldsymbol{s}). \tag{5.9}$$

Defining

$$X_{\beta,\epsilon} = \frac{1}{2\epsilon}\boldsymbol{e}\boldsymbol{e}^t + X_\beta \equiv \frac{1}{2\epsilon}\boldsymbol{e}\boldsymbol{e}^t + \frac{1}{2}(\beta + \beta_0)\mathbb{I} + X, \tag{5.10}$$

where $\mathbb{I}$ is the $N \times N$ identity matrix, $\psi_{\beta,\epsilon}(\boldsymbol{s})$ assumes the standard form of a pure, bosonic Gaussian state:

$$\psi_{\beta,\epsilon}(\boldsymbol{s}) = e^{-\frac{1}{2}\boldsymbol{s}^t X_{\beta,\epsilon}\boldsymbol{s}}. \tag{5.11}$$

We refer to Appendix D.1 for a review of properties of bosonic Gaussian states. In short, a pure bosonic Gaussian state is quasifree since it is the ground state of a quadratic Hamiltonian. It is completely characterized by its covariance matrix, which contains the expectation values of all pairs of bosonic annihilation and creation operators a_j and $a_j^\dagger$. In particular, the covariance matrix determines the entanglement properties under a bipartition of the system. The covariance matrix of $\psi_{\beta,\epsilon}(\boldsymbol{s})$ can be computed efficiently from the matrix $X_{\beta,\epsilon}$ in Eq. (5.11).

The representation of $\psi_\beta(\boldsymbol{s})$ in terms of $\psi_{\beta,\epsilon}(\boldsymbol{s})$ also regularizes divergences. These are due to the delta function $\delta(s_1 + \cdots + s_N)$, which implies that the state is infinitely localized along the "center of mass" coordinate $s_1 + \cdots + s_N$. By introducing ϵ as a regularization parameter, we can isolate and subtract divergences. These occur, for example, in the entanglement entropies computed below.

5.1.4 Definition of β_0

We define β_0 by requiring that $\psi_{\beta,\epsilon}(\boldsymbol{s})$ is normalizable for all $\beta > 0$. According to Eq. (5.7), we have

$$\beta_0 = -2\min\{\lambda_\epsilon^{(1)}, \ldots, \lambda_\epsilon^{(N)}\}, \tag{5.12}$$

where $\{\lambda_\epsilon^{(1)}, \ldots, \lambda_\epsilon^{(N)}\}$ are the eigenvalues of $\frac{1}{2\epsilon}\boldsymbol{e}\boldsymbol{e}^t + X$.

In the limit $\epsilon \to 0$, the matrix $\frac{1}{2\epsilon}\boldsymbol{e}\boldsymbol{e}^t + X$ becomes divergent, and we determine $\{\lambda_\epsilon^{(1)}, \ldots, \lambda_\epsilon^{(N)}\}$ as the inverse eigenvalues of

$$\left[\frac{1}{2\epsilon}\boldsymbol{e}\boldsymbol{e}^t + X\right]^{-1} = X^{-1} - \frac{X^{-1}\boldsymbol{e}\boldsymbol{e}^t X^{-1}}{2\epsilon + \boldsymbol{e}^t X^{-1}\boldsymbol{e}}, \tag{5.13}$$

where we used a general formula for the inverse of a matrix that is changed by a term of rank one [171].

5.1.5 Entanglement properties

The representation of $\psi_\beta(\boldsymbol{s})$ as a Gaussian state allows us to efficiently compute its entanglement properties under partition of the system into parts A and B, cf. Appendix D.2 for details.

In summary, we find that the Rényi entanglement entropies $S_a(A)$ of order a are given by

$$S_a(A) = -\frac{1}{2}\log\epsilon + S_a'(A) + \mathcal{O}(\epsilon), \tag{5.14}$$

where $S_a'(A)$ is independent of ϵ. The divergence in $S_a(A)$ for $\epsilon \to 0$ is a consequence of the delta function $\delta(s_1 + \cdots + s_N)$ in $\psi_\beta(\boldsymbol{s})$. By subtracting it, we obtain the finite entropies $S_a'(A)$. The entanglement Hamiltonian can be brought into the diagonal form $\sum_{j=1}^{|A|} \tilde{\omega}_j b_j^\dagger b_j$ in a suitable basis of annihilation and creation operators b_j and $b_j^\dagger$. The single-particle energies $\tilde{\omega}_j$ determine the entanglement spectrum.

5.1.6 States on the cylinder

For the rest of this chapter, we study a system on a cylinder with a square lattice of N_x sites in the open and N_y sites in the periodic direction:

$$w_m \equiv w_{m_x m_y} = \frac{2\pi}{N_y}\left(m_x + i m_y\right), \tag{5.15}$$

where m_x is the x and m_y the y component of the index m [$m = (m_x - 1)N_y + m_y$], and we identify $w_{m_x m_y}$ with $w_{m_x, m_y + N_y}$. This includes a uniform lattice in 1D with periodic boundary conditions as the special case $N_x = 1$.

The wave function $\psi_\beta(\boldsymbol{s})$ was defined for positions z_j in the complex plane in Eq. (5.1). For positions w_j on the cylinder, we use the map $z_j = e^{w_j}$ from the cylinder to the plane and define the wave function by evaluating the CFT correlator on the cylinder:

$$\begin{aligned}\psi_\beta(\boldsymbol{s}) &= e^{-\frac{1}{4}(\beta+\beta_0)s^2}\left\langle : e^{\frac{i}{\sqrt{2}}s_1\varphi(w_1,\bar{w}_1)} : \cdots : e^{\frac{i}{\sqrt{2}}s_N\varphi(w_N,\bar{w}_N)} :\right\rangle \\ &= e^{-\frac{1}{4}(\beta+\beta_0)s^2}\,\delta(s_1 + \cdots + s_N)\prod_{m<n}\left|2\sinh\left(\frac{1}{2}(w_m - w_n)\right)\right|^{s_m s_n},\end{aligned} \tag{5.16}$$

where we used Eq. (5.1) and the transformation rule for primary fields [5] under $z_j = e^{w_j}$ (cf. Sec. 2.1.2). The definition of $\psi_{\beta,\epsilon}(\boldsymbol{s})$ introduced in Sec. 5.1.3 changes accordingly on the cylinder.

In the spin-$\frac{1}{2}$ case of Sec. 2.3, we projected the cylinder onto the plane and then defined the wave function as a correlator in terms of coordinates in the complex plane. In the spin-$\frac{1}{2}$ case, this is possible since the correlator on the cylinder differs from that on the plane only by a spin-independent constant. For the continuous spins $s_j \in \mathbb{R}$ studied in this chapter, this is not the case, and it is necessary use the CFT correlator on the cylinder. This is similar to the approximation of Chapter 4, where we used CFT correlators on the cylinder and on the sphere since the approximation is not invariant under a projection onto the complex plane.

5.2 Properties of states in 1D

In this section, we study properties of $\psi_\beta(\boldsymbol{s})$ for a 1D system with periodic boundary conditions. We show that the correlations, entanglement properties, and a parent Hamiltonian exhibit signatures of the underlying CFT of a free, massless boson.

5.2.1 Correlations

A plot of spin-spin correlations in $\psi_\beta(\boldsymbol{s})$ and a fit to the CFT expectation are shown in Fig. 5.1 for $\beta \in \{0.5, 2, 4, 8\}$. We observe a long-range power-law decay that is consistent with a power of -2 independent of β and find that the correlator is negative at large distances. This agrees with the term in the bosonization result for the XXZ model [97] that originates from the current-current correlator. The correlations in $\psi_\beta(\boldsymbol{s})$ do, however, not have the staggered contribution observed for the XXZ model. We interpret this as a smoothing effect due to the transition from discrete to continuous spins. A similar behavior was found in Chapter 4 in the context of approximating correlations for spin-$\frac{1}{2}$ lattice states (cf. Fig. 4.3).

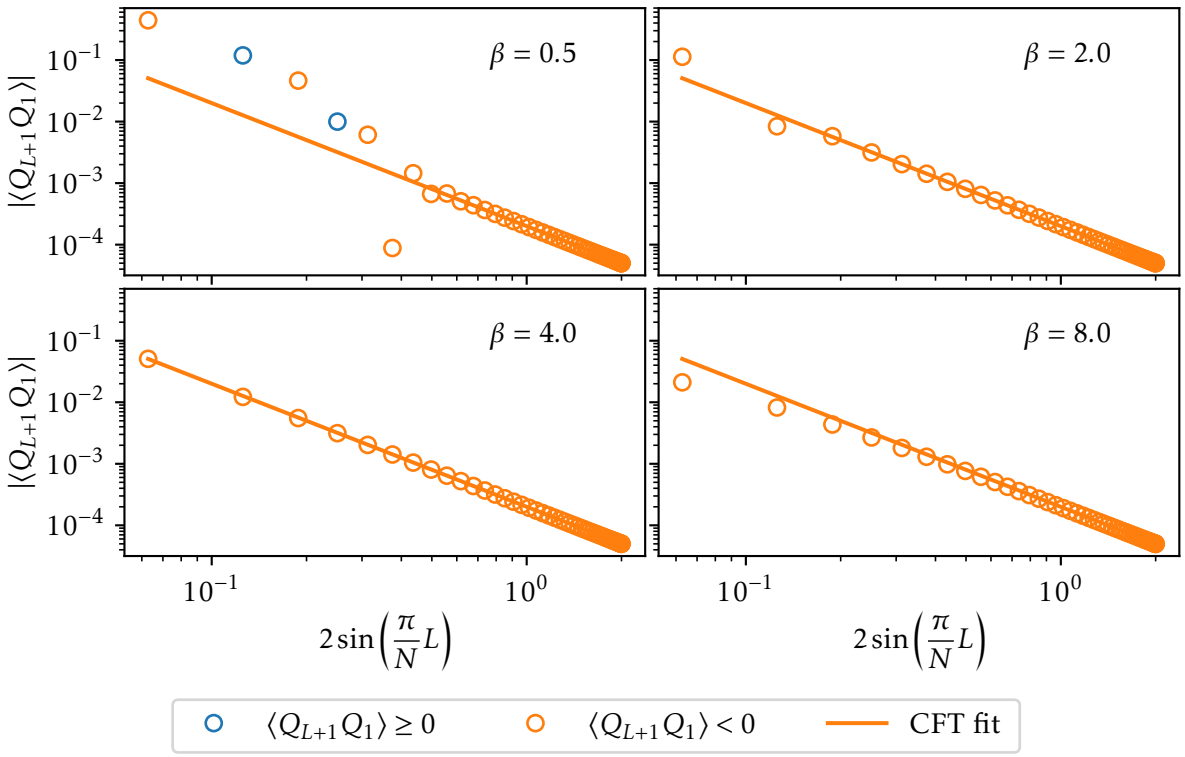

Figure 5.1: Spin-Spin correlations $\langle Q_{L+1} Q_1 \rangle$ in $\psi_\beta(\boldsymbol{s})$ in 1D with periodic boundary conditions for $N = 100$ sites. The operator Q_m is defined as $(Q_m \psi_\beta)(\boldsymbol{s}) = s_m \psi_\beta(\boldsymbol{s})$. The long-range decay is consistent with the CFT expectation of an algebraic decay with a power of -2. The fit was done for the 10 data points with the largest value of L.

5.2.2 Entanglement entropies

For a partition of the system into two connected regions of length L and $N - L$, respectively, the CFT entanglement entropy is given by [169, 172, 173]

$$S_a^{\mathrm{CFT}}(L) = \frac{c}{6}\left(1 + \frac{1}{a}\right) \log\left[\frac{N}{\pi} \sin\left(\frac{\pi}{N} L\right)\right] + c'_a, \tag{5.17}$$

where c is the central charge, a the order of the Rényi entropy, and c'_a a non-universal constant. As shown in Fig. 5.2, we find good agreement between the entropy of $\psi_\beta(\boldsymbol{s})$ and $S_a^{\mathrm{CFT}}(L)$ for larger values of L.

For a system that has a low-energy description in terms of a Luttinger liquid, one expects [174] subleading, oscillatory corrections to the CFT behavior of Eq. (5.17). For the XXZ model, for example, these oscillations were found [174] in Rényi entropies S_a for $a \neq 1$. From Fig. 5.2, we conclude that such oscillations around the CFT expectation are absent for the state $\psi_\beta(\boldsymbol{s})$. This is in agreement with our findings about the correlations, and we interpret it as a result of the transition from discrete to continuous spins, which has a smoothing effect and thus removes the oscillatory components.

To characterize the correction of the entropy to CFT in the case of $\psi_\beta(\boldsymbol{s})$, we define

$$\begin{aligned} \Delta_L &= S_a(L) - S_a\left(\frac{N}{2}\right) - \left[S_a^{\mathrm{CFT}}(L) - S_a^{\mathrm{CFT}}\left(\frac{N}{2}\right)\right] \\ &= S_a(L) - S_a\left(\frac{N}{2}\right) - \frac{c}{6}\left(1 + \frac{1}{a}\right) \log\left[\sin\left(\frac{\pi}{N} L\right)\right]. \end{aligned} \tag{5.18}$$

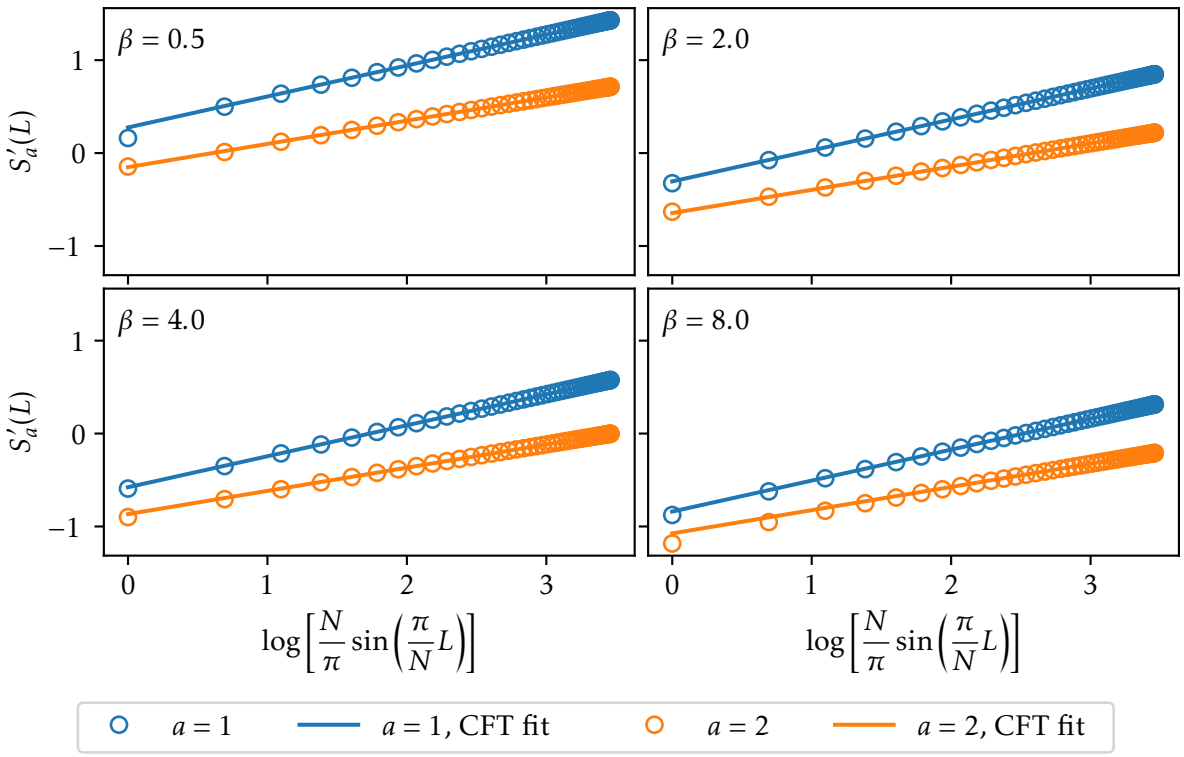

Figure 5.2: Entanglement entropies of $\psi_\beta(\boldsymbol{s})$ in 1D with periodic boundary conditions and $N = 100$ sites. The long-range behavior is consistent with the CFT expectation of Eq. (5.17). The quantities S'_a can become negative since they differ from the Rényi entropies S_a by a divergent term, cf. Eq. (5.14). For the fit to the CFT formula, we chose $c = 1$ and used the 10 data points with the largest value of L.

As shown in Fig. 5.3, we find that Δ_L becomes smaller for increasing system sizes and larger values of L, i.e., the agreement with CFT is better is these regimes. For $L \gtrsim 3N/8$, the computed behavior of Δ_L is consistent with a linear dependence on $\log\left[\sin\left(\frac{\pi}{N}L\right)\right]$. From the definition of Eq. (5.18), it thus follows that $S_a(L) - S_a\left(\frac{N}{2}\right)$ is also proportional to $\log\left[\sin\left(\frac{\pi}{N}L\right)\right]$ for $L \gtrsim 3N/8$. The deviation from CFT is thus a correction to the CFT proportionality constant $\frac{c}{6}\left(1 + \frac{1}{a}\right)$. We emphasize that this correction can be considered to be a finite size effect since it becomes smaller for larger system sizes. This distinguishes it from the parity effects observed in Ref. [174] for the XXZ model.

5.2.3 Entanglement spectrum

To further substantiate the close connection between $\psi_\beta(\boldsymbol{s})$ and the free-boson CFT, we computed the entanglement spectrum for a partition in momentum space. This choice makes it possible to trace out the negative momenta, thus retaining only the chiral components [175, 176]. The details of the computation can be found in Appendix D.2.3. In summary, we find an entanglement Hamiltonian $\sum_{k=1}^{\lfloor \frac{N-1}{2} \rfloor} \tilde{\omega}_k b_k^\dagger b_k$, where b_k and $b_k^\dagger$ are bosonic annihilation and creation operators, k is the momentum, and $\tilde{\omega}_k$ are single-particle entanglement energies. We plot the low-lying part of the spectrum in Fig. 5.4. For large systems, we observe a linear behavior $\tilde{\omega}_k = k\tilde{\omega}_1$, where $\tilde{\omega}_1$ is the energy at momentum $k = 1$. The entanglement spectrum is thus consistent with a chiral, massless, free boson.

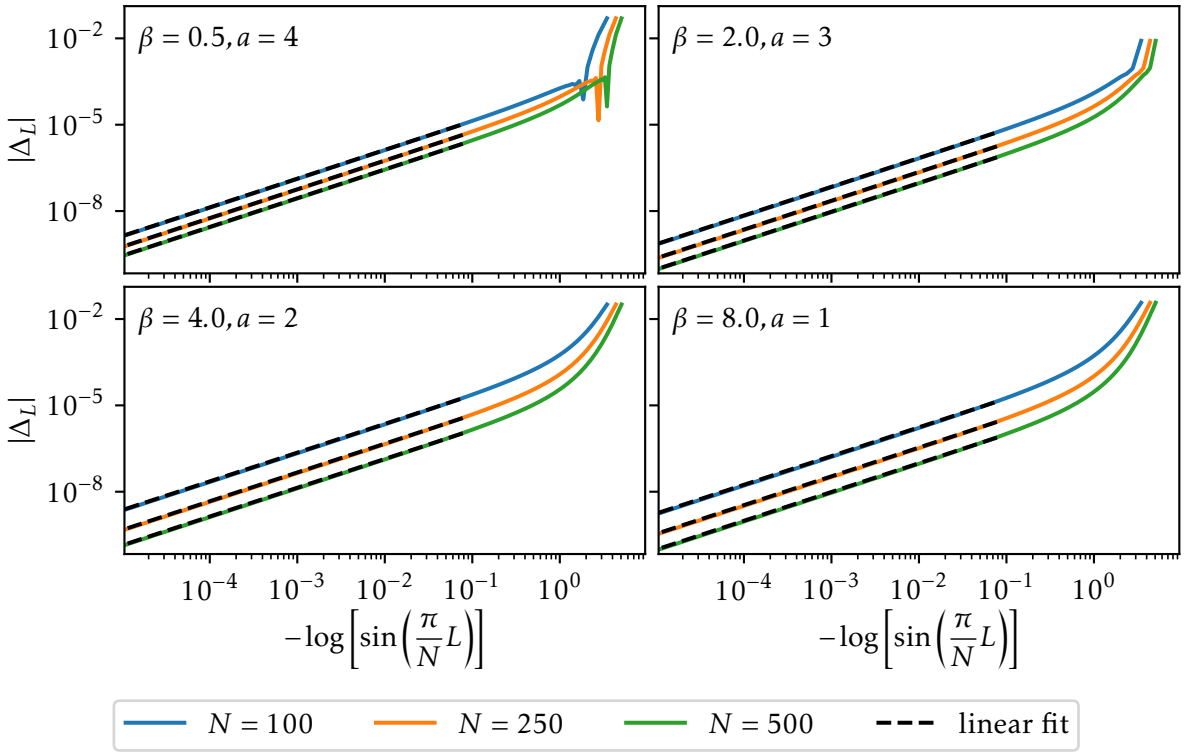

Figure 5.3: Differences Δ_L between the computed entropy and the CFT expectation for a uniform 1D lattice with periodic boundary conditions [cf. Eq. (5.18) for the definition of Δ_L]. Dashed black lines: Linear fits $\Delta_L = -A \log\left[\sin\left(\frac{\pi}{N}L\right)\right]$ done for $L \geq 3N/8$.

5.2.4 Parent Hamiltonian

We now show that $\psi_\beta(\boldsymbol{s})$ in 1D has a parent Hamiltonian whose low-lying energies are in agreement with the underlying CFT. The precise form of this Hamiltonian is derived in Appendix D.3, where we also show that it can be brought into the diagonal form $\sum_{k=1}^{N} \omega_k b_k^\dagger b_k$ in a suitable basis of annihilation and creation operators b_k and $b_k^\dagger$. Due to translational invariance, k in the single-particle energies ω_k has the meaning of a momentum variable in 1D.

The low-lying part of the single-particle spectrum is shown in Fig. 5.5. The observed linear behavior $\omega_k = \omega_1 |k|$ is consistent with CFT and our findings about the momentum-space entanglement spectra. In the latter case, however, the spectrum has only chiral components since the negative momenta were traced out.

5.3 Properties of states in 2D

In this section, we consider a cylinder of size $N_x \times N_y$ as defined in Sec. 5.1.6. Through a determination of the topological entanglement entropy and entanglement spectra, we provide evidence that $\psi_\beta(\boldsymbol{s})$ exhibits edge modes.

5.3.1 Correlations

Since the spin-spin correlations do not depend on the phase of the wave function, the correlators in $\psi_\beta(\boldsymbol{s})$ agree with those of the approximation made in Chapter 4, cf. Sec. 5.1.2. In

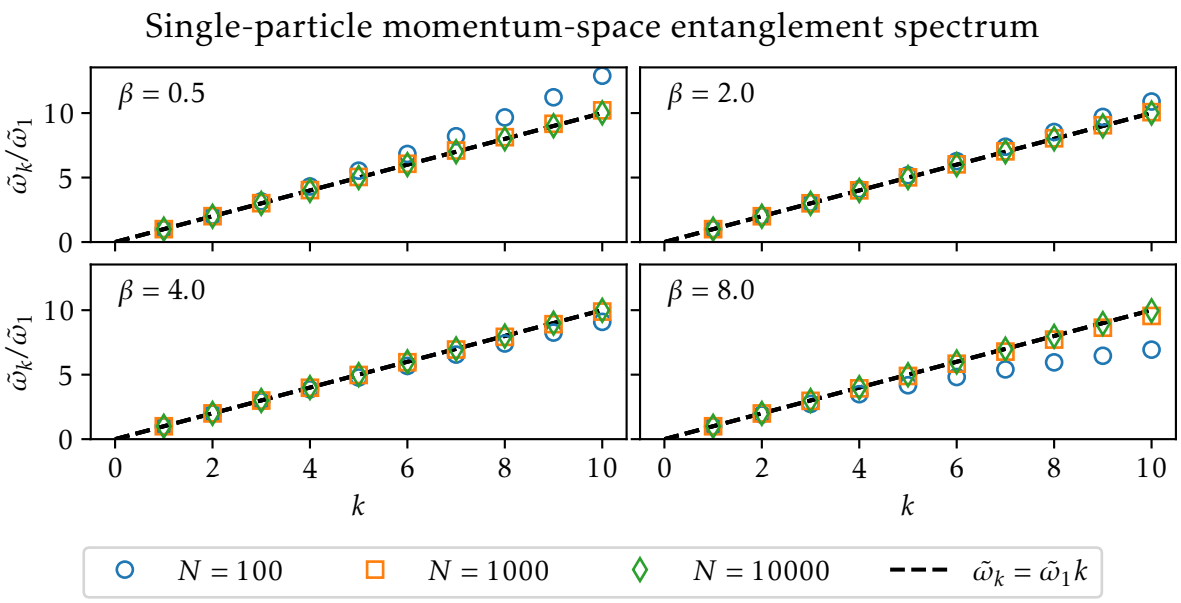

Figure 5.4: Single-particle entanglement spectrum in 1D with periodic boundary conditions for a partition in momentum space. The low-lying part of the spectrum is shown for various system sizes and values of β.

agreement with Chapter 4, we find an exponential decay of spin-spin correlations in the bulk of a 2D system. The long-range edge correlations decay with a power of -2 independent of β, which agrees with the decay of a current-current correlator of the underlying CFT.

The exponential decay of bulk correlations is characterized by the correlation length ξ. For a cylinder of size $N_x \times N_x = 60 \times 60$, we fitted exponential functions $Ae^{-l/\xi}$ to the bulk spin-spin correlations, where l is the distance along the y direction and A a fit parameter. The inverse correlation length ξ^{-1} is plotted in Fig. 5.6.

5.3.2 Absence of intrinsic topological order

The topological order of a state can be characterized by the topological entanglement entropy [83, 84] γ_{top}, which occurs in the dependence of the entanglement entropy $S_a(A)$ on the region A:

$$S_a(A) = -\gamma_{\text{top}} + b\, \partial A + \ldots, \tag{5.19}$$

where ∂A is the perimeter of A, b is a non-universal constant, and the dots stand for terms that vanish for $\partial A \to \infty$. A nonzero value of γ_{top} indicates that a state exhibits intrinsic topological order.

The topological entanglement entropy can be computed as a linear combination of entropies for geometries that are chosen so that the terms dependent on ∂A in Eq. (5.19) drop out [83, 84]. Here, we consider the construction of Levin and Wen [84] with regions as defined in the left panel of Fig. 5.7. For geometries that are large compared to the correlation length, γ_{top} is equal to

$$S_{\text{Levin–Wen}} = \frac{1}{2}\Big[(S_1(ABC) - S_1(AC)) - (S_1(ABCD) - S_1(ADC))\Big], \tag{5.20}$$

where the Rényi index $a = 1$ was chosen.

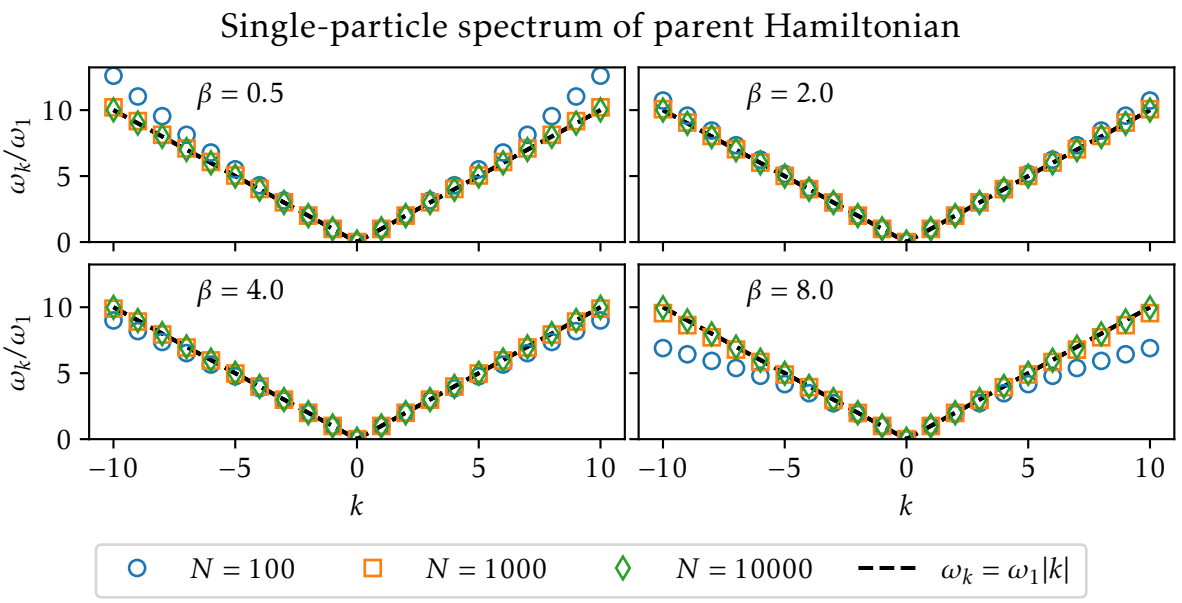

Figure 5.5: Low-lying energies of the single-particle spectrum for the parent Hamiltonian of $\psi_\beta(\boldsymbol{s})$ in 1D with periodic boundary conditions.

We plot $S_{\text{Levin–Wen}}$ for $\psi_\beta(\boldsymbol{s})$ in Fig. 5.8. For all considered system sizes and values of β, we observe that $S_{\text{Levin–Wen}}$ is below 0.002. Furthermore, $S_{\text{Levin–Wen}}$ tends to decrease for larger systems. This indicates that the state has a vanishing topological entanglement entropy, $\gamma_{\text{top}} = 0$, and thus no intrinsic topological order. A similar observation of a vanishing topological entanglement entropy was made for BCS states with a $p_x + ip_y$ symmetry in Refs. [177, 178].

5.3.3 Entanglement spectrum and edge states

In the previous subsection, we provided evidence that $\psi_\beta(\boldsymbol{s})$ does not have intrinsic topological order. We now study the entanglement spectrum and show that it contains indications of edge states.

We consider a partition of the cylinder into two pieces of equal size, where we choose the cut perpendicular to the open direction as illustrated in the right panel of Fig. 5.7. The low-lying part of the single-particle entanglement spectrum is shown in Fig. 5.9. Since the cut preserves translational symmetry, the spectrum can be ordered according to the momentum k_y in the periodic direction. The dependence of the low-lying single-particle energies $\tilde{\omega}_{k_y}$ is consistent with

$$\tilde{\omega}_{k_y} = A\sqrt{\frac{2\pi}{N_y}|k_y|} + B\frac{2\pi}{N_y}|k_y|, \tag{5.21}$$

where A and B are fit constants. For large systems, we find that A and B are independent of the system size within variations that are due to the chosen fit range. Thus, $\omega_{k_y} \propto \sqrt{|k_y|}$ for the smallest momenta. A similar dispersion relation was recently found in the entanglement spectra of coupled Luttinger liquids [179].

Next, we investigate whether the low-lying excited states in the entanglement spectrum are localized at the boundary created by the cut and thus represent edge excitations. To this end, we compute the basis change that makes the entanglement Hamiltonian diagonal. To exploit

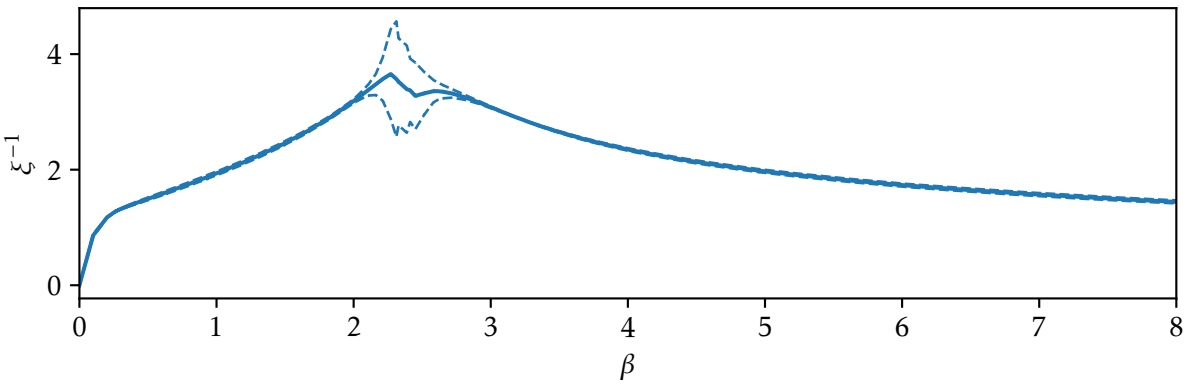

Figure 5.6: Inverse correlation length ξ^{-1} (solid line) for bulk spin-spin correlations of $\psi_\beta(\boldsymbol{s})$ along the periodic direction of a cylinder of size $N_x \times N_y = 60 \times 60$. The dashed lines are error estimates, which were determined by varying the fit range. At $\beta \approx 2.4$, the correlations change from alternating in sign (small values of β) to having a stationary, negative sign (large values of β).

translational symmetry, we use Fourier transformed annihilation and creation operators $\tilde{a}_{i_x k_y}$ and $\tilde{a}^\dagger_{i_x k_y}$, where i_x is the x index and k_y the y momentum. As shown in Appendix D.2.4, the entanglement Hamiltonian is diagonal in annihilation and creation operators $b_{i_x l_y \sigma}$ and $b^\dagger_{i_x l_y \sigma}$, where l_y is an index of non-negative momenta and σ a sign index ($\sigma \in \{+,-\}$ for $l_y \notin \{0, \frac{N_y}{2}\}$ and $\sigma = +$ for $l_y \in \{0, \frac{N_y}{2}\}$). For $l_y \notin \{0, \frac{N_y}{2}\}$, the transformation to the diagonal basis assumes the form

$$\begin{pmatrix} \boldsymbol{b}_{l_y,\sigma=+} \\ \boldsymbol{b}^\dagger_{l_y,\sigma=+} \end{pmatrix} = R_{l_y} \frac{1}{\sqrt{2}} \begin{pmatrix} \tilde{\boldsymbol{a}}_{l_y} + \tilde{\boldsymbol{a}}_{-l_y} \\ \tilde{\boldsymbol{a}}^\dagger_{l_y} + \tilde{\boldsymbol{a}}^\dagger_{-l_y} \end{pmatrix}, \qquad \begin{pmatrix} \boldsymbol{b}_{l_y,\sigma=-} \\ \boldsymbol{b}^\dagger_{l_y,\sigma=-} \end{pmatrix} = R_{l_y} \frac{1}{\sqrt{2}} \begin{pmatrix} -i\tilde{\boldsymbol{a}}_{l_y} + i\tilde{\boldsymbol{a}}_{-l_y} \\ i\tilde{\boldsymbol{a}}^\dagger_{l_y} - i\tilde{\boldsymbol{a}}^\dagger_{-l_y} \end{pmatrix}, \tag{5.22}$$

where $\boldsymbol{b}_{l_y\sigma} = (b_{i_x=1,l_y,\sigma}, \ldots, b_{i_x=\frac{N_x}{2},l_y,\sigma})^t$ and analogously for the other annihilation and creation operators. The $N_x \times N_x$ matrix R_{l_y} is a symplectic basis transformation in the complex representation,

$$R_{l_y} = \begin{pmatrix} R^{(1)}_{l_y} & R^{(2)}_{l_y} \\ \left(R^{(2)}_{l_y}\right)^* & \left(R^{(1)}_{l_y}\right)^* \end{pmatrix}. \tag{5.23}$$

We order the spectrum so that $(R^{(r)}_{l_y})_{i_x j_x}$ with $i_x = 1$ and $r \in \{1,2\}$ corresponds to the lowest energy state in the sector of momentum l_y. According to Eq. (5.22), $\boldsymbol{b}_{l_y\sigma}$ are linear combinations of modes with momenta l_y and $-l_y$. The two choices $\sigma \in \{+,-\}$ have the same energy and correspond to the degeneracies in Fig. 5.9.

Fig. 5.10 shows $(R^{(r)}_{l_y})_{i_x j_x}$ for $i_x = 1$ and $l_y \in \{1,2,3\}$. We observe that $(R^{(r)}_{l_y})_{i_x j_x}$ falls off exponentially in j_x for large distances to the position of the cut ($j_x = 50$). Thus, the corresponding states are exponentially localized at the edge created by the cut. This observation provides evidence that $\psi_\beta(\boldsymbol{s})$ indeed supports gapless edge states.

We also did analogous computations for the local parent Hamiltonian of Appendix D.3 to test whether its low-lying excited states are localized at the physical edges. Compared to the entanglement spectrum, we observed the following differences. First, the low-lying single-particle spectrum of the parent Hamiltonian does not consist of a single branch as the

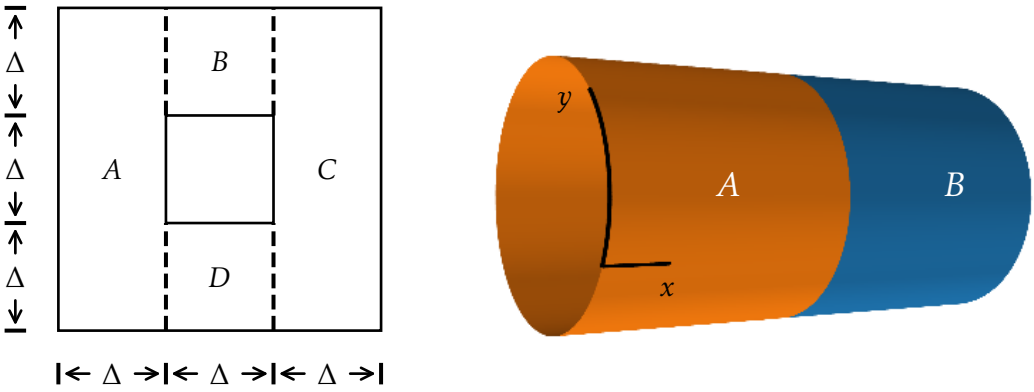

Figure 5.7: Left panel: Definition of regions for the computation of the topological entanglement entropy according to Levin and Wen [84]. The regions A and C are of size $\Delta \times 3\Delta$ and the regions B and D of size $\Delta \times \Delta$. We place the region $ABCD$ into the center of a cylinder of size $N_x \times N_y$. Right panel: Cut of the cylinder into two pieces A and B for the computation of the entanglement spectrum.

entanglement spectrum of Fig. 5.9. Second, we find eigenstates of the Hamiltonian with low energies that are not localized at the edge. This raises the question whether there is another parent Hamiltonian with the same low-energy behavior as observed in the entanglement spectrum.

5.4 Outlook: Chiral state

In this chapter, we focus on the case of a real wave function $\psi_\beta(\boldsymbol{s})$ defined through operators $:e^{is_j\varphi(z_j,\bar{z}_j)/\sqrt{2}}:$ with chiral and antichiral components. In this section, we comment on the corresponding chiral wave function, demonstrate its equivalence to $\psi_\beta(\boldsymbol{s})$ for the case of a uniform 1D lattice, and explain some difficulties we encountered in studying the chiral state for 2D systems.

The chiral analog of $\psi_\beta(\boldsymbol{s})$ has the form

$$\begin{aligned}\tilde{\psi}_\beta(\boldsymbol{s}) &= e^{-\frac{1}{4}(\beta+\beta_0)s^2}\langle :e^{is_1\varphi(z_1)}:\cdots:e^{is_N\varphi(z_N)}:\rangle \\ &= e^{-\frac{1}{4}(\beta+\beta_0)s^2}\,\delta(s_1+\cdots+s_N)\prod_{m<n}(z_m-z_n)^{s_ms_n},\end{aligned} \tag{5.24}$$

where $\varphi(z)$ is the chiral part of the free boson according to the decomposition $\varphi(z,\bar{z}) = \varphi(z)+\bar{\varphi}(\bar{z})$.

On the cylinder introduced in Sec. 5.1.6, the chiral wave function becomes

$$\begin{aligned}\tilde{\psi}_\beta(\boldsymbol{s}) &= e^{-\frac{1}{4}(\beta+\beta_0)s^2}\langle :e^{is_1\varphi(w_1)}:\cdots:e^{is_N\varphi(w_N)}:\rangle \\ &= e^{-\frac{1}{4}(\beta+\beta_0)s^2}\,\delta(s_1+\cdots+s_N)\prod_{m<n}\left[2\sinh\left(\frac{1}{2}(w_m-w_n)\right)\right]^{s_ms_n}.\end{aligned} \tag{5.25}$$

Since $\tilde{\psi}_\beta(\boldsymbol{s})$ differs from $\psi_\beta(\boldsymbol{s})$ only by a phase, it has the same spin-spin correlations. As explained in Sec. 5.1.2, these agree with those of the approximation made in Chapter 4.

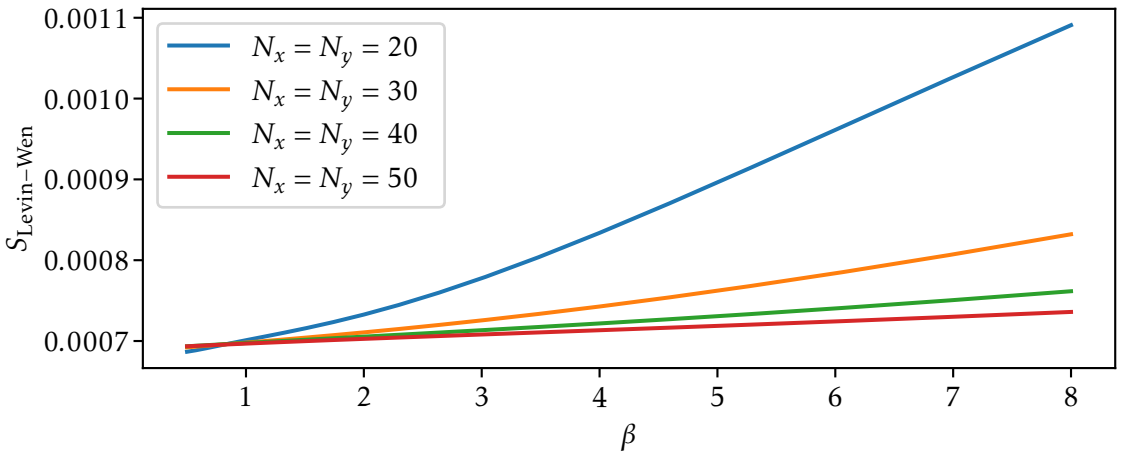

Figure 5.8: Linear combination $S_{\text{Levin–Wen}}$ of Eq. (5.20) for different system sizes and values of β. The size of Δ was chosen as $\Delta = N_x/5$.

5.4.1 Equivalence to nonchiral state in 1D

We now show that $\psi_\beta(\boldsymbol{s})$ is equivalent to $\tilde{\psi}_\beta(\boldsymbol{s})$ for a uniform lattice in 1D with periodic boundary conditions. Setting $N_x = 1$ in Eqs. (5.15) and (5.25), we have

$$\begin{aligned}\tilde{\psi}_\beta(\boldsymbol{s}) &= \delta(s_1 + \cdots + s_N)\, e^{-\frac{1}{4}(\beta+\beta_0)\boldsymbol{s}^2} \prod_{m<n}^{N} \left[2i \sin\left(\frac{\pi}{N}(m-n)\right)\right]^{s_m s_n} \\ &= e^{i\frac{\pi}{4}\boldsymbol{s}^2}\, \delta(s_1 + \cdots + s_N)\, e^{-\frac{1}{4}(\beta+\beta_0)\boldsymbol{s}^2} \prod_{m<n}^{N} \left[2 \sin\left(\frac{\pi}{N}(n-m)\right)\right]^{s_m s_n} \\ &= e^{i\frac{\pi}{4}\boldsymbol{s}^2}\, \psi_\beta(\boldsymbol{s}),\end{aligned}$$

where we used that $s_1 + \cdots + s_N = 0$. Up to the phase factor $e^{i\frac{\pi}{4}\boldsymbol{s}^2}$, the wave function $\tilde{\psi}_\beta(\boldsymbol{s})$ thus coincides with $\psi_\beta(\boldsymbol{s})$. Since $e^{i\frac{\pi}{4}\boldsymbol{s}^2}$ is a product of local phase factors, it does not influence the spin-spin correlations and entanglement entropies. Furthermore, it can be transformed away through the symplectic transformation

$$\begin{pmatrix} \boldsymbol{Q} \\ \boldsymbol{P} \end{pmatrix} \to \begin{pmatrix} \mathbb{I} & 0 \\ -\frac{\pi}{2}\mathbb{I} & \mathbb{I} \end{pmatrix} \begin{pmatrix} \boldsymbol{Q} \\ \boldsymbol{P} \end{pmatrix}. \tag{5.26}$$

5.4.2 Dependence on lattice ordering

For generic lattice configurations, however, an important difference between the real wave function $\psi_\beta(\boldsymbol{s})$ and the chiral $\tilde{\psi}_\beta(\boldsymbol{s})$ is that the former is independent of the lattice ordering while the latter is not. More precisely, $\psi_\beta(\boldsymbol{s})$ is symmetric under a simultaneous permutation σ of both the spins s_j and the positions z_j:

$$\psi_\beta^{(z_{\sigma(1)},\ldots,z_{\sigma(N)})}(s_{\sigma(1)},\ldots,s_{\sigma(N)}) = \psi_\beta^{(z_1,\ldots,z_N)}(s_1,\ldots,s_N), \tag{5.27}$$

where we explicitly wrote the parametric dependence of $\psi_\beta(\boldsymbol{s})$ on the lattice positions. This symmetry does, however, not hold in the chiral case. The permutation $\sigma(j) = N - j + 1$, for

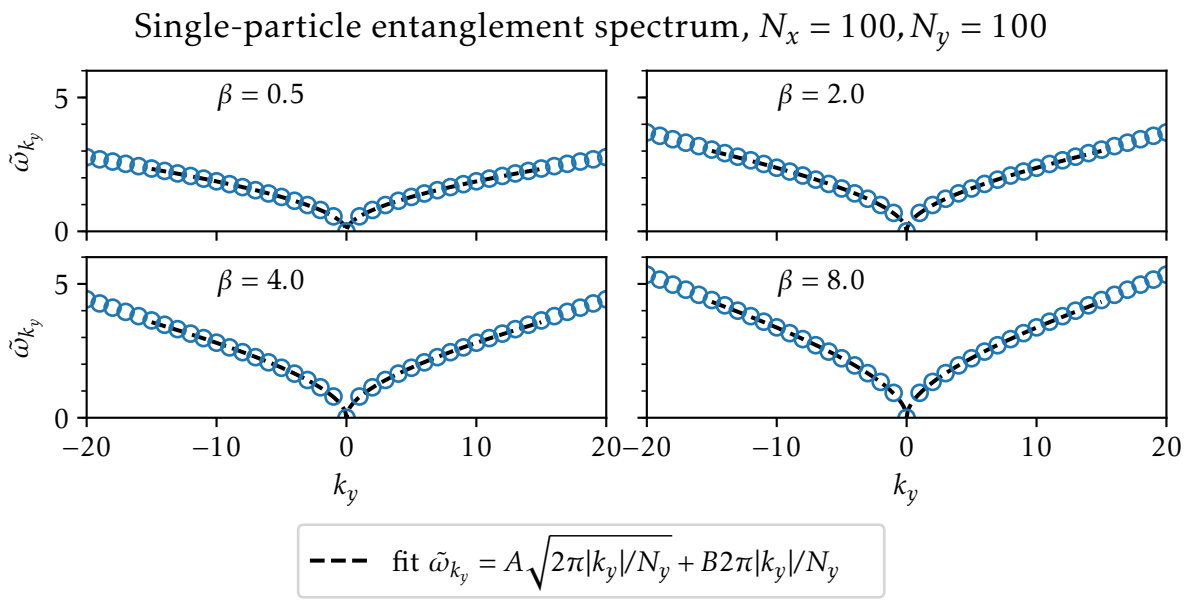

Figure 5.9: Low-lying part of the single-particle entanglement spectrum in 2D for a cut of the cylinder into two pieces as shown in the right panel of Fig. 5.7.

example, changes the wave function according to

$$\tilde{\psi}_\beta^{(z_{\sigma(1)},\ldots,z_{\sigma(N)})}(s_{\sigma(1)},\ldots,s_{\sigma(N)}) = \prod_{m<n} e^{\pi i s_m s_n \Phi_{nm}} \tilde{\psi}_\beta^{(z_1,\ldots,z_N)}(s_1,\ldots,s_N), \tag{5.28}$$

where $\Phi_{mn} = \frac{1}{\pi}[\arg(z_m - z_n) - \arg(z_n - z_m)]$, and we explicitly wrote the parametric dependence on z_j. The phase $\prod_{m<n} e^{\pi i s_m s_n \Phi_{nm}}$ does not change the spin-spin correlations in $\tilde{\psi}_\beta(\boldsymbol{s})$, but it influences entanglement properties since it is in general not a product of single-particle phase factors.

To illustrate this point, let us compare the entanglement entropy of $\tilde{\psi}_\beta(\boldsymbol{s})$ defined on the cylinder in Eq. (5.25) to the entropy of

$$\begin{aligned}\phi_\beta(\boldsymbol{s}) &= e^{-\frac{1}{4}(\beta+\beta_0)\boldsymbol{s}^2} \langle : e^{i s_N \phi(w_N)} : \cdots : e^{i s_1 \phi(w_1)} : \rangle \\ &= e^{-\frac{1}{4}(\beta+\beta_0)\boldsymbol{s}^2} \delta(s_1 + \cdots + s_N) \prod_{m<n} \left[-2\sinh\left(\frac{1}{2}(w_m - w_n)\right)\right]^{s_m s_n},\end{aligned} \tag{5.29}$$

which is the permuted wave function of Eq. (5.28) for $\sigma(j) = N - j + 1$. In Fig. 5.11, we plot the von Neumann entropy $S_1'(L)$ for subsystems $A = \{1,\ldots,L\}$ and $B = \{L+1,\ldots,N\}$ for the cylinder coordinates of Eq. (5.15). The entropy of $\phi_\beta(\boldsymbol{s})$ differs considerably from that of $\tilde{\psi}_\beta(\boldsymbol{s})$. We observe that $S_1'(L)$ for $\psi_\beta(\boldsymbol{s})$ and for $\phi_\beta(\boldsymbol{s})$ is consistent with an area law in the bulk of the system. There, $S_1'(L)$ is approximately constant except where L is an integer multiple of N_y. (These configurations have a shorter boundary length and thus a smaller entropy.) For $\tilde{\psi}_\beta(\boldsymbol{s})$, on the other hand, $S_1'(L)$ bends in the bulk of the system, which is in contrast to the area law.

The lower entropy consistent with an area law seems to suggest that $\phi_\beta(\boldsymbol{s})$ rather than $\tilde{\psi}_\beta(\boldsymbol{s})$ provides the natural choice of the wave function. However, we encountered additional issues when computing the entropy of $\phi_\beta(\boldsymbol{s})$ for subsystems different from $A = \{1,\ldots,L\}$ and $B = \{L+1,\ldots,N\}$. More precisely, we determined the entropies for Levin-Wen regions AC and $ABCD$ defined in the left panel of Fig. 5.7 for different sizes Δ. As shown in Fig. 5.12, both entropies are consistent with a linear dependence on the boundary length for large values of Δ.

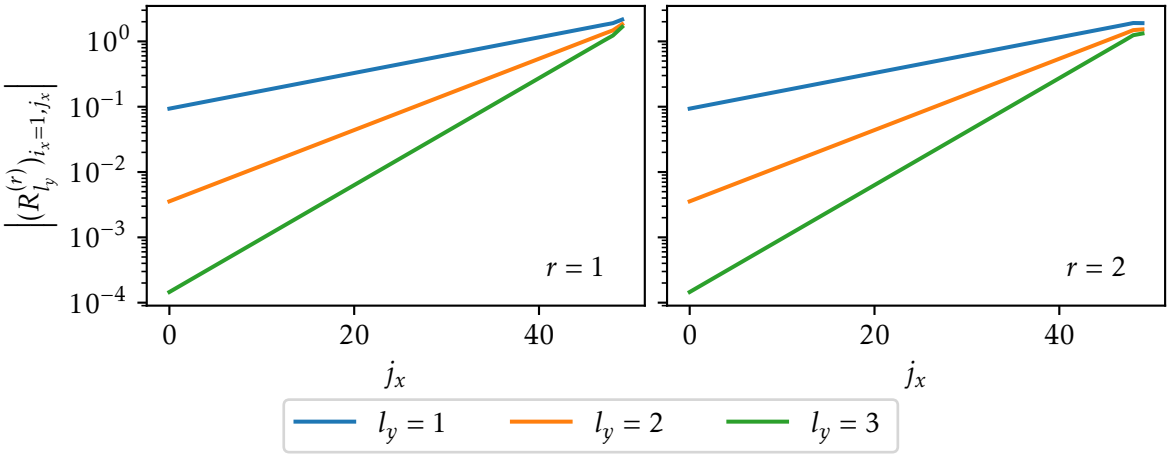

Figure 5.10: Amplitude of the basis transformation for the first excited states in the entanglement spectrum of Fig. 5.9 for a cylinder of size $N_x \times N_y = 100 \times 100$. The shown data have $\beta = 2.0$. (The corresponding amplitudes for $\beta \in \{0.5, 4, 8\}$ have the same qualitative behavior.) The lowest energy in the sector of momentum l_y corresponds to $i_x = 1$, cf. the explanation below Eq. (5.22). The value $j_x = 50$ is the position of the cut.

However, the slopes are different for the two regions $ABCD$ and AC. This is a contradiction to the area law, where the coefficient of the linear term is independent of the choice of the region.

The dependence of the chiral state on the lattice ordering and the violation of the area law for Levin-Wen regions $ABCD$ and AC could mean that a consistent treatment as a bosonic Gaussian state is not possible. Perhaps the chiral state has some additional structure, similar to the anyonic states in the case discrete spins [143], which needs to be taken into account to obtain a consistent definition that is independent of the lattice ordering.

5.5 Conclusion

This chapter considered continuous-spin wave functions $\psi_\beta(\boldsymbol{s})$ on lattices that are constructed as correlators of the massless, free boson CFT. In contrast to the case of discrete spins or continuous positional degrees of freedom, the wave functions $\psi_\beta(\boldsymbol{s})$ are Gaussian and their properties can be computed efficiently using the formalism of bosonic Gaussian states.

Through an analysis of entanglement entropies and spectra, we found that $\psi_\beta(\boldsymbol{s})$ is closely related to the underlying CFT in 1D. More precisely, we observed a good agreement between the entanglement entropy of $\psi_\beta(\boldsymbol{s})$ and the CFT expectation. In contrast to some lattice systems like the XXZ model [174], we do not find subleading oscillatory corrections to the CFT behavior. At small energies, we recovered the underlying CFT of a free, massless boson, in the momentum space entanglement spectrum and also in the spectrum of a parent Hamiltonian.

In 2D, we probed possible topological properties of $\psi_\beta(\boldsymbol{s})$ through an analysis of entanglement entropies and spectra. Although our results are consistent with a vanishing topological entanglement entropy, we found evidence for edge states in the entanglement spectrum. The absence of intrinsic topological order is distinct from the chiral case with discrete spins.

The wave function $\psi_\beta(\boldsymbol{s})$ is real since it is constructed from the full bosonic field $\varphi(z, \bar{z})$. As a consequence, the entanglement Hamiltonian in 2D has eigenstates that are linear combinations of left- and right-moving modes. Together with our observation of states localized at the edge

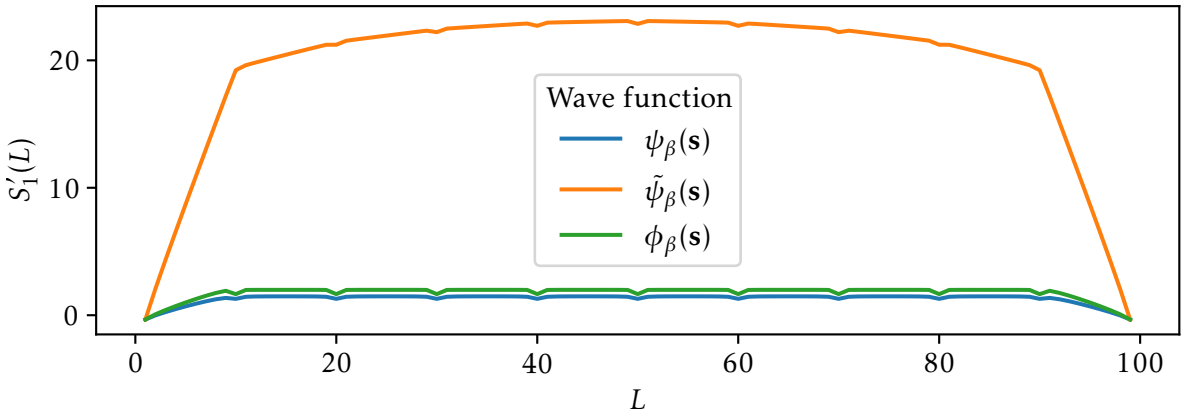

Figure 5.11: Von Neumann entanglement entropy for subsystems $A = \{1,\dots,L\}$ and $B = \{L+1,\dots,N\}$ on a cylinder of size $N_x \times N_y = 10 \times 10$ and $\beta = 2$. The three curves correspond to the wave functions $\psi_\beta(\boldsymbol{s})$ [Eq. (5.16)], $\tilde{\psi}_\beta(\boldsymbol{s})$ [Eq. (5.25)] and $\phi_\beta(\boldsymbol{s})$ [Eq. (5.29)]. The vertical axis shows $S_1'(L)$, which can become negative since it differs from the von Neumann entropy $S_1(L)$ by the subtraction of a divergent term [cf. Eq. (5.14)].

in the low-lying entanglement spectrum, this is an indication that $\psi_\beta(\boldsymbol{s})$ could describe a state that is similar to a quantum spin Hall effect.

We found a local parent Hamiltonian whose low-lying energy levels in 1D are consistent with the corresponding entanglement spectrum. In 2D, however, this parent Hamiltonian has low-lying excited states that are not localized at the edge, which is in contrast to the entanglement spectrum. It would be interesting to investigate if there is another local parent Hamiltonian with the same low-energy properties as observed in the entanglement spectrum.

In 1D, the real wave function $\psi_\beta(\boldsymbol{s})$ is equivalent to the analogously defined chiral wave function, which is constructed from the chiral part of the free-boson field. For general lattice configurations, however, $\psi_\beta(\boldsymbol{s})$ differs from its chiral counterpart. In contrast to the real case, we found that the chiral state depends on the ordering of the lattice positions. It could, therefore, be that another framework than that of bosonic Gaussian states is necessary to consistently treat the chiral state, and it would be interesting to investigate this question in a future study.

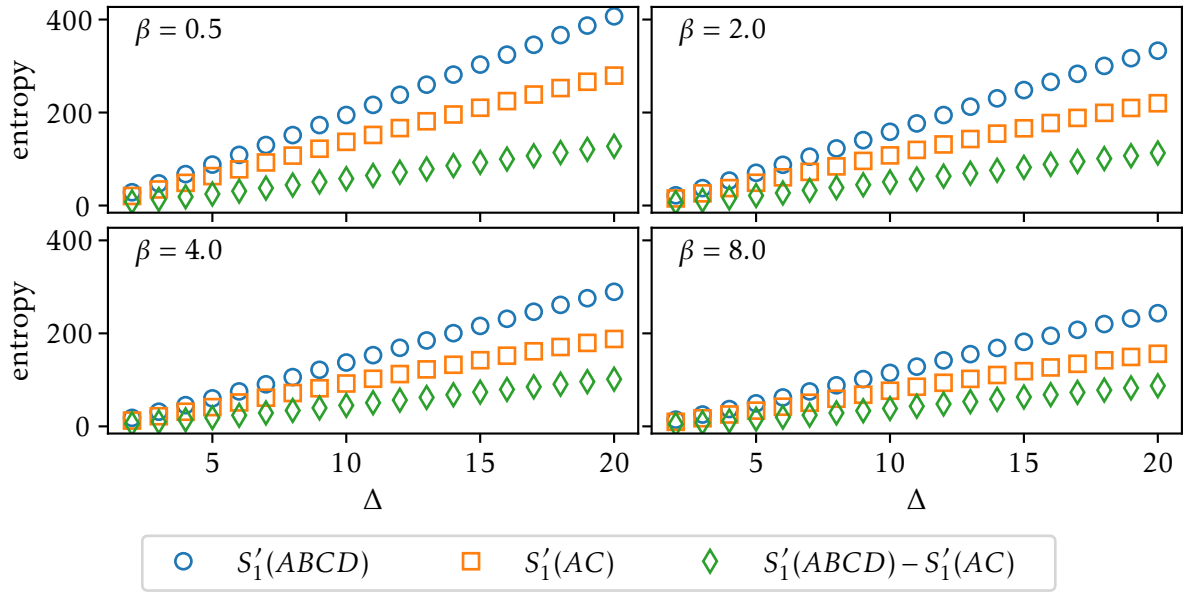

Figure 5.12: Entropies of the chiral state $\phi_\beta(s)$ [Eq. (5.29)] for Levin-Wen regions $ABCD$ and AC defined in the left panel of Fig. 5.7. The regions $ABCD$ and AC have a boundary length of 16Δ. Both $S_1'(ABCD)$ and $S_1'(AC)$ are consistent with a leading linear dependence on Δ, however with different slopes.

6 Conclusion and outlook

This thesis uses 1(+1)-dimensional CFT to describe states of quantum many-body systems. We adopted the approach introduced by Moore and Read [7] to construct wave functions of quantum states as correlators of CFT primary fields. Following a recent development [102], the wave functions studied here describe spin systems on lattices.

From the $SU(2)_1$ WZW CFT, we obtained a wave function $\psi_0(s_1,\dots,s_N)$ of N spin-$\frac{1}{2}$ degrees of freedom. In 1D, $\psi_0(s_1,\dots,s_N)$ is the ground state of the Haldane-Shastry model, an SU(2) invariant spin chain with inverse-square two-body interactions. For lattices in 2D, $\psi_0(s_1,\dots,s_N)$ is equivalent to Kalmeyer and Laughlin's chiral spin liquid.

By adding descendant fields to the correlator that defines $\psi_0(s_1,\dots,s_N)$, we constructed excited states of the Haldane-Shastry model. This shows that there is a correspondence between the excited states of the underlying CFT and those of the Haldane-Shastry spin chain. Our approach is SU(2) invariant and differs from previous studies that solved the Haldane-Shastry model by exploiting its hidden Yangian symmetry.

For systems in 2D, we then studied states with additional CFT descendant fields as tentative edge modes with respect to $\psi_0(s_1,\dots,s_N)$. We found that their nearest-neighbor spin-spin correlations become indistinguishable from those of $\psi_0(s_1,\dots,s_N)$ as the system size is increased. This provides evidence that these states indeed describe edge modes. These findings confirm the bulk-edge correspondence: The CFT associated with the gapless edge of the system can be used to obtain a description of the bulk. Through Monte Carlo simulations, we also provided numerical evidence supporting another aspect of the bulk-edge correspondence, namely that inner products of the CFT approach those of the spin system in the thermodynamic limit [99], cf. also Ref. [180] for a recent study of the case of continuous wave functions.

Using exact diagonalization for a cylinder with 4 sites in the periodic and 5 sites in the open direction, we studied a local model Hamiltonian with nearest-neighbor two- and three-body interactions, the ground state of which is known to be well-approximated by $\psi_0(s_1,\dots,s_N)$. We found that the low-lying excited states of that model have a good overlap with some edge states constructed from CFT. This local model could provide a way of experimentally realizing these states since an implementation scheme with ultracold atoms was proposed in Refs. [118, 119].

We then studied the larger class of states $\psi_\alpha(s_1,\dots,s_N)$ with $\alpha > 0$ obtained from vertex operators of the free-boson CFT. In 2D, these correspond to Laughlin states on a half-filled lattice and a Landau level filling of $\nu = \frac{1}{4\alpha}$, so that the Kalmeyer-Laughlin state corresponds to $\alpha = \frac{1}{2}$. For systems in 1D, $\psi_\alpha(s_1,\dots,s_N)$ is a good description of the ground state of the XXZ spin-$\frac{1}{2}$ model.

We derived a path integral representation of the spin-spin correlations in $\psi_\alpha(s_1,\dots,s_N)$, from which we proposed an approximation in terms of an effective field theory. The action of that model is a modification of the free-boson CFT, which underlies $\psi_\alpha(s_1,\dots,s_N)$. It has an additional mass-like term at the positions of the lattice. Our approximation of spin-spin correlations is given by the two-point function in the effective action. The mass-like term in the effective model leads to an exponential decay of correlations in the bulk of a 2D system. This screening property is central to a state describing a FQH system since it reflects the bulk gap. In deriving an effective action for the correlations, we provided an analytical argument supporting the screening property of the Laughlin states.

Through Monte Carlo simulations, we determined the actual spin-spin correlations in $\psi_\alpha(s_1,\ldots,s_N)$, and compared them to those obtained within the approximation. We found good quantitative agreement for small values of α ($\alpha \lesssim 0.1$) both in 1D and in 2D. Furthermore, qualitative agreement was observed between the approximation and the actual spin-spin correlations also for larger values of α. In 1D and at the edge of 2D systems, the approximate correlations decay with a power of -2 independent of α. This corresponds to a current-current correlator of the free-boson CFT.

The last part of this thesis investigates states $\psi_\beta(\boldsymbol{s})$ with continuous spins $\boldsymbol{s} \in \mathbb{R}^N$ constructed from the CFT of a free boson. These states have the spin-spin correlations that we used before to approximate those of $\psi_\alpha(s_1,\ldots,s_N)$. We characterized the continuous-spin states $\psi_\beta(\boldsymbol{s})$ through a determination of entanglement entropies and spectra. Opposed to the case of discrete spins, the wave functions $\psi_\beta(\boldsymbol{s})$ are Gaussian, and thus their properties can be computed efficiently.

In 1D, the continuous-spin states $\psi_\beta(\boldsymbol{s})$ exhibit signatures of the underlying CFT, where the entanglement entropies and spectra were found to agree with the CFT expectation. Furthermore, we derived a parent Hamiltonian that has power-law decaying interactions in 1D. For large system sizes, the low-energy part of its spectrum was found to agree with that of the CFT.

Through an investigation of entanglement entropies and spectra, we characterized topological properties of $\psi_\beta(\boldsymbol{s})$ in 2D. Opposed to the FQH Laughlin states, we found a vanishing topological entanglement entropy, and thus no long-range entanglement characteristic of states with intrinsic topological order. On the other hand, an analysis of the entanglement spectrum revealed low-lying states that are exponentially localized at the edge created by the cut.

Our construction of excited states of the Haldane-Shastry model emphasizes the close relationship between the $\mathrm{SU}(2)_1$ WZW model and the spin chain. Recently, the Haldane-Shastry model with open boundary conditions was obtained using boundary CFT [108]. We provided numerical evidence that a similar construction of excited states is possible in this case if the current operators are inserted at infinity. It would be interesting to extend our analytical method to the case of open boundary conditions. Further generalizations could be possible for the SU(n) spin chains of Refs. [106–108], or the ladder models of Ref. [181].

An advantage of the Laughlin states studied here is the simple form of their wave function. By modifying it, localized bulk excitations, as well as edge modes, can be described. On the other hand, the simplicity of Laughlin-type wave functions implies that they have limited variational degrees of freedom. The Kalmeyer-Laughlin state is known to have a good overlap with the ground state of a local Hamiltonian [118], and here we showed that edge modes derived from it are also good descriptions of low-lying excited states of that model. Recently, the ground state of that local Hamiltonian was approximated through projected entangled pair states [182] and neural network states [183]. In both cases, lower variational energies than that of the Kalmeyer-Laughlin state were achieved. Furthermore, the study of Ref. [182] indicates that the true ground state may have long-range rather than short-range correlations observed in Laughlin states. To clarify the nature of the local model, more refined variational ansatz states are thus necessary than those provided by the Laughlin wave functions studied in this thesis.

Our approximation of correlations is based on a truncation to quadratic order which is similar to the expansion made by Kosterlitz and Thouless in their study on the classical XY model [71, 72]. It would be interesting to investigate if one can also incorporate vortex-like configurations into our approximation. We did some first steps in this direction by adopting Villain's approximation [167]. Opposed to the case of the XY model, however, we applied the approximation to the integrand of the partition function, whereas Kosterlitz and Thouless

approximate a Hamiltonian. This caused a non-positive factor in the partition function's integrand, which prevented us from incorporating it into an effective, statistical Hamiltonian.

Our investigation of continuous-spin states $\psi_\beta(\boldsymbol{s})$ constructed from CFT focused on nonchiral wave functions. In the entanglement spectrum, we observed indications of low-lying edge states. The local parent Hamiltonian, on the other hand, was found to have low-lying excited states that have significant bulk components and thus cannot be considered to be edge states. It would be interesting to find another local parent Hamiltonian whose low-energy states represent edge modes similar to those of the entanglement spectrum.

The nonchiral nature of $\psi_\beta(\boldsymbol{s})$ is an important difference to the Laughlin states. We also defined chiral wave functions with continuous spins. Unlike in the nonchiral case, we found that these depend on the ordering of the lattice positions. This could indicate that they cannot be consistently treated as bosonic Gaussian states but require another formalism. It would be interesting to investigate this question in a future study.

Acknowledgments

I want to thank Ignacio Cirac for his supervision, the many things I have been able to learn from him, the opportunity to be part of his research group and to work in the exciting field of quantum many-body and quantum Hall systems.

I am grateful to Anne Nielsen for supervising me, for her help, and the many discussions we had, including the technical parts of my work. I also want to thank her for the opportunity to visit her group at the Max Planck Institute for the Physics of Complex Systems in Dresden, which was very beneficial for our project and my work.

I have been very fortunate in being able to work with Germán Sierra and Hong-Hao Tu and want to thank them for their productive collaboration, many inspiring discussions, and the opportunity to learn from them. I profited from a visit of Germán Sierra's research group in Madrid and am grateful for that opportunity.

All members of the theory group at the Max Planck Institute of Quantum Optics created this unique and inspiring atmosphere for which I am very thankful. I had many opportunities to discuss with and learn from others. In particular, I want to express my gratitude to Tao Shi for introducing me to Gaussian states and for his help in preparing seminar talks. I want to thank Thorsten Wahl, Stefan Kühn, Julian Ross, and Shin-Liang Chen for the time we had together as office mates and the friendly environment I have been able to work in. Stefan Kühn helped me many times regarding technical questions about the computing cluster, and he advised me on the administrative process of submitting the thesis. Regarding the many stimulating discussions with members of the theory group, I particularly want to mention those I had with Stefan Kühn and Ivan Glasser.

This thesis would not have been possible without the support from the non-scientific staff at the Max Planck Institute of Quantum Optics. In particular, I would like to thank Andrea Kluth for her kindness and the help she provided on numerous occasions. I am also grateful to the IT staff for setting up and maintaining the computing facilities that were used in the numerical part of this work.

Finally, I want to express my gratitude to my family for the help and love I have been receiving. I am deeply grateful to my wife Marina for her enduring support and unconditional love. I thank my daughter Sophia who brings great joy into every day of my life. My parents Christa and Wolfgang supported and guided me in my educational path from the beginning to this day, and I am indebted to them.

A Numerical methods

A.1 Exact diagonalization

A quantum many-body state $|\psi\rangle$ of N participants with local Hilbert spaces of dimension d is defined in terms of d^N coefficients $\psi(s_1,\ldots,s_N)$:

$$|\psi\rangle = \sum_{s_1,\ldots,s_N} \psi(s_1,\ldots,s_N)|s_1,\ldots,s_N\rangle, \tag{A.1}$$

were $|s_1,\ldots,s_N\rangle = |s_1\rangle\otimes\cdots\otimes|s_N\rangle$ is the product basis. Similarly, an operator acting on this many-body space has $d^N \times d^N$ coefficients. For a state of N spin-$\frac{1}{2}$ degrees of freedom, $d = 2$ and the local Hilbert space is spanned by the basis states $|s\rangle$ with $s \in \{-1, 1\}$. In the following, we focus on this case, which relevant for Chapters 3 and 4 of this thesis.

Conceptually, the simplest way to treat states $|\psi\rangle$ numerically and compute their properties is to construct them as vectors of dimension 2^N with coefficients given by $\psi(s_1,\ldots,s_N)$. Operators acting on states $|\psi\rangle$ are then represented by matrices of size $2^N \times 2^N$. In particular, eigenstates and spectra of Hamiltonians can be computed numerically using standard numerical tools for diagonalizing matrices [184, 185]. This method is known as exact diagonalization [186], where the word *exact* refers to the fact that a Hamiltonian is represented completely without truncating its dimensionality.

Physical Hamiltonians are often sparse, i.e., they only have few non-zero entries. If one is only interested in the lowest part of the spectrum, methods for solving sparse eigensystems can be used, and thus larger system sizes can be achieved. In this thesis, we use the SciPy [184] interface to the ARPACK library [187] of sparse eigensolvers. These are based on a variant of the Lanczos algorithm [188].

Due to the exponential dependence of the dimension 2^N on N, this procedure is, however, limited to small system sizes. With 16 GB of memory, for example, it is possible to store a complex vector of size 2^N with $N = 30$, where we assumed that 64-bit floating points are used. Increasing N by just one additional site already requires twice the amount of memory.

In some cases, a given Hamiltonian or state can be decomposed into different sectors according to symmetries. By restricting to these sectors, one can work with Hilbert spaces of a lower dimension than that of the full problem and thus treat larger systems with limited computational resources. A Hamiltonian that commutes with the total spin T^z, for example, can be diagonalized block-wise in the eigenspaces of T^z.

Current state-of-the-art techniques exploit symmetries and make use of parallelization. In this way, system sizes with up to $N = 50$ sites for a spin-$\frac{1}{2}$ system [189] were recently achieved.

Despite the exponential dependence on N, exact diagonalization techniques are an indispensable tool for studying many-body physics. This is particularly true in 1D, where systems with moderate values of N can already be close to the thermodynamic limit. Furthermore, exact diagonalization is used to test and benchmark other methods and approximation techniques.

In Chapter 3 of this thesis, we make use of exact diagonalization to test an analytical construction of eigenstates of the Haldane-Shastry model and also to extend the construction to cases not covered by the analytical computations. Furthermore, exact diagonalization is

used to compute eigenstates of a local 2D model in Chapter 3 and to determine ground state spaces of analytically determined parent Hamiltonians.

A.2 The Metropolis-Hastings Monte Carlo algorithm

As discussed in the previous subsection, the method of exact diagonalization is limited to small systems due to an exponential dependence on N. Similarly, an exact determination of properties like correlations in states of Eq. (A.1) is only possible for small systems. As explained in the following, this thesis uses the Metropolis-Hastings Monte Carlo method [190–193] to obtain estimates of a state's properties for large system sizes.

For computing the expectation value of some operator $\widehat{\mathcal{O}}$ in the state $|\psi\rangle$, we write it in the form

$$\langle\widehat{\mathcal{O}}\rangle \equiv \frac{\langle\psi|\widehat{\mathcal{O}}|\psi\rangle}{\langle\psi|\psi\rangle} = \frac{\sum_{s_1,\ldots,s_N} \mathcal{O}(s_1,\ldots,s_N)\rho(s_1,\ldots,s_N)}{\sum_{s_1,\ldots,s_N} \rho(s_1,\ldots,s_N)}, \tag{A.2}$$

where $\rho(s_1,\ldots,s_N) \geq 0$ is a (not necessarily normalized) probability density in the space of configurations $(s_1,\ldots,s_N)$ with $s_i \in \{-1,1\}$. For the case of zz correlations, for example, $\widehat{\mathcal{O}} = \sigma_i^z\sigma_j^z$, where σ_i^z and σ_j^z are local Pauli-z matrices. Then, $\mathcal{O}(s_1,\ldots,s_N) = s_i s_j$ and $\rho(s_1,\ldots,s_N) = |\psi(s_1,\ldots,s_N)|^2$.

The key idea of the algorithm is to evaluate Eq. (A.2) for a set of relevant configurations with a high value of $\rho(s_1,\ldots,s_N)$ instead of computing the complete sums of 2^N terms. Let

$$C_i = \left(s_1^{(i)},\ldots,s_N^{(i)}\right) \tag{A.3}$$

with $i \in \{1,\ldots,n_s\}$ denote these configurations. Then, an estimate for $\langle\widehat{\mathcal{O}}\rangle$ is given by

$$\mathcal{O}_{\text{est}} = \frac{1}{n_s}\sum_{i=1}^{n_s} \mathcal{O}(C_i). \tag{A.4}$$

Algorithm 1 Metropolis-Hastings algorithm for computing expectation values of the form of Eq. (A.2).

Input: Probability density ρ, proposal distribution q, configuration C_i
Output: Next configuration C_{i+1}

- Generate a proposal configuration C' according to $q(C'|C_i)$.
- Draw a random number r with $0 \leq r < 1$ from a uniform distribution.
- If $\frac{\rho(C')}{\rho(C_i)}\frac{q(C_i|C')}{q(C'|C_i)} > r$, set $C_{i+1} = C'$ (acceptance), otherwise set $C_{i+1} = C_i$ (rejection).

The configurations C_i are generated through a pseudorandom process according to the following algorithm. First, a candidate C' for the next configuration C_{i+1} is generated from C_i according to a given proposal distribution $q(C'|C_i)$. This candidate is then either accepted ($C_{i+1} = C'$) or rejected ($C_{i+1} = C_i$) with a certain probability that takes into account the values $\rho(C_i)$, $\rho(C')$, and the transition probabilities under q. The details are given in Algorithm 1, see also Refs. [194, 195]. An initial configuration C_1 can be found by starting from a random

configuration and then running the algorithm for a certain number of iterations without measuring the observable value (warm up).

A useful feature of the algorithm is that it only depends on the ratio of probability densities, and thus unnormalized distributions $\rho(s_1,\dots,s_N)$ can be used. The states considered in this thesis have a fixed number of the total spin, i.e., $\rho(s_1,\dots,s_N)$ vanishes unless $s_1+\dots+s_N$ is equal to a constant. In this case, it is useful to generate proposal configurations by exchanging the positions of a down spin with an up spin in C_i. When choosing these up and down spins from C_i randomly with a uniform distribution, q is symmetric, i.e., $q(C'|C_i) = q(C_i|C')$. The acceptance probability in Algorithm 1 is thus independent of q and determined by the ratio of probabilities $\frac{\rho(C')}{\rho(C_i)}$. As a further advantage, this ratio can be computed more efficiently than the probability of generic configurations since C' and C_i only differ by the value of two spins.

Given an estimate of the operator expectation value as in Eq. (A.4), it is important to determine the accuracy of this value. To this end, we determine n_t statistically independent estimates $\mathcal{O}^{(j)}_{\text{est}}$, $j\in\{1,\dots,n_t\}$, by running the algorithm n_t times. The true value $\langle\widehat{\mathcal{O}}\rangle$ is then expected to lie in $\overline{\mathcal{O}}_{\text{est}}\pm\Delta\overline{\mathcal{O}}_{\text{est}}$ with approximately 68% confidence, where

$$\overline{\mathcal{O}}_{\text{est}} = \frac{1}{n_t}\sum_{j=1}^{n_t}\mathcal{O}^{(j)}_{\text{est}} \qquad \text{and } \Delta\overline{\mathcal{O}}_{\text{est}} = \sqrt{\frac{1}{n_t(n_t-1)}\sum_{j=1}^{n_t}\left(\overline{\mathcal{O}}_{\text{est}}-\mathcal{O}^{(j)}_{\text{est}}\right)^2} \tag{A.5}$$

are the mean of the n_t estimates and the standard error of the mean, respectively.

The Monte Carlo methods described in this section are used in Chapter 3 to study and compare correlation functions of a FQH lattice state and candidate states for its edge excitations. Chapter 4 computes approximations for correlations of states constructed from CFT and compares these approximations to Monte Carlo estimates of the actual correlations.

B Details on excited and edge states

B.1 Decoupling equation for states obtained from current operators

In this section, we derive the decoupling equation for the states $|\psi^{a_k\dots a_1}_{1\dots 1}\rangle$ defined through the wave function

$$\psi^{a_k\dots a_1}_{1\dots 1}(s_1,\dots,s_N) = \langle \phi_{s_1}(z_1)\dots\phi_{s_N}(z_N)\left(J^{a_k}_{-1}\dots J^{a_1}_{-1}\right)(0)\rangle, \tag{B.1}$$

where $\phi_s(z)$ is the $h=\frac{1}{4}$ WZW primary field and J^a_n are modes of the current $J^a(z)$ introduced in Sec. 3.1 of the main text.

The decoupling equation describes the action of the operator $\mathcal{C}^a_i$ of Eq. (3.55) on a state $|\psi^{a_k\dots a_1}_{1\dots 1}\rangle$ and was used to construct excited states of the Haldane-Shastry model in Sec. 3.3. Note that it is enough to consider states $|\psi^{a_k\dots a_1}_{1\dots 1}\rangle$, where all mode numbers are equal to one, to describe the action of $\mathcal{C}^a_i$ on general states $|\psi^{a_l\dots a_1}_{n_l\dots n_1}\rangle$ with $k=n_1+\dots+n_l$ since the latter can be rewritten in terms $|\psi^{a_k\dots a_1}_{1\dots 1}\rangle$ by repeated application of the Kac-Moody algebra [cf. Eq. (3.60)].

The starting point of our derivation is the CFT operator

$$\sum_{s'\in\{-1,1\}} \left(K^a_b\right)_{ss'} (J^b_{-1}\varphi_{s'})(z_i), \tag{B.2}$$

where $K^a_b = \frac{2}{3}(\delta_{ab} - i\varepsilon_{abc}t^c)$. The operator of Eq. (B.2) is a *null field*, i.e., when inserting it into the correlation function of conformal primary fields, the resulting expression vanishes [103]. Therefore,

$$0 = \sum_s \left(K^a_b\right)_{s_i s} \langle \phi_{s_1}(z_1)\dots\phi_{s_{i-1}}(z_{i-1})\left(J^b_{-1}\phi_s\right)(z_i)\phi_{s_{i+1}}(z_{i+1})\dots\phi_{s_N}(z_N)\left(J^{a_k}_{-1}J^{a_{k-1}}_{-1}\dots J^{a_1}_{-1}\right)(0)\rangle. \tag{B.3}$$

To simplify the notation, we write $\left(K^a_b\right)_i \phi_{s_i}(z_i)$ instead of $\sum_s \left(K^a_b\right)_{s_i s}\phi_s(z_i)$ and similarly $t^a_i\phi_{s_i}(z_i)$ instead of $\sum_s t^a_{s_i s}\phi_s(z_i)$ in the following. This notation is motivated by the fact that we treat the spin variables $s_1,\dots,s_N$ as arguments of a wave function $\psi(s_1,\dots,s_N)$ and that the wave function of the state $t^a_i|\psi\rangle$ is given by

$$\sum_s t^a_{s_i s}\psi(s_1,\dots,s_{i-1},s,s_{i+1},\dots,s_N). \tag{B.4}$$

Then,

$$\begin{aligned} 0 &= \left(K^a_b\right)_i \oint_0 \frac{dw_k}{2\pi i w_k}\dots\oint_0 \frac{dw_1}{2\pi i w_1}\langle \phi_{s_1}(z_1)\dots\left(J^b_{-1}\phi_{s_i}\right)(z_i)\dots\phi_{s_N}(z_N)J^{a_k}(w_k)\dots J^{a_1}(w_1)\rangle \\ &= \left(K^a_b\right)_i \oint_0 \frac{dw_k}{2\pi i w_k}\dots\oint_0 \frac{dw_1}{2\pi i w_1}\oint_{z_i}\frac{dz}{2\pi i(z-z_i)} \\ &\quad\times\langle \phi_{s_1}(z_1)\dots J^b(z)\phi_{s_i}(z_i)\dots\phi_{s_N}(z_N)J^{a_k}(w_k)\dots J^{a_1}(w_1)\rangle. \end{aligned} \tag{B.5}$$

Through a deformation of the integration contour, the integral around z_i can be transformed into a sum over integrals encircling the positions z_j for $j \neq i$ and the positions w_q in the clockwise direction. Therefore,

$$\begin{aligned}0 = &-\left(K_b^a\right)_i \sum_{j=1,j\neq i}^{N} \oint_0 \frac{dw_k}{2\pi i w_k} \dots \oint_0 \frac{dw_1}{2\pi i w_1} \oint_{z_j} \frac{dz}{2\pi i (z-z_i)} \\ &\times \langle \phi_{s_1}(z_1) \dots J^b(z) \phi_{s_i}(z_i) \dots \phi_{s_N}(z_N) J^{a_k}(w_k) \dots J^{a_1}(w_1) \rangle \\ &-\left(K_b^a\right)_i \sum_{q=1}^{k} \oint_0 \frac{dw_k}{2\pi i w_k} \dots \oint_0 \frac{dw_1}{2\pi i w_1} \oint_{w_q} \frac{dz}{2\pi i (z-z_i)} \\ &\times \langle \phi_{s_1}(z_1) \dots J^b(z) \phi_{s_i}(z_i) \dots \phi_{s_N}(z_N) J^{a_k}(w_k) \dots J^{a_1}(w_1) \rangle .\end{aligned} \tag{B.6}$$

Next, we apply the OPE between a primary fields and a WZW current of Eq. (3.4) and the OPE between two currents [151],

$$J^a(z) J^b(w) \sim \frac{\delta_{ab}}{2(z-w)^2} + i\varepsilon_{abc} \frac{J^c(w)}{z-w}. \tag{B.7}$$

Introducing the notation $\mathbf{\Phi}_{\boldsymbol{s}}(\boldsymbol{z}) = \phi_{s_1}(z_1) \dots \phi_{s_N}(z_N)$, we have

$$\begin{aligned}0 = &\left(K_b^a\right)_i \sum_{j=1,j\neq i}^{N} \oint_0 \frac{dw_k}{2\pi i w_k} \dots \oint_0 \frac{dw_1}{2\pi i w_1} \oint_{z_j} \frac{dz}{2\pi i (z-z_i)} \frac{t_j^b}{z-z_j} \langle \mathbf{\Phi}_{\boldsymbol{s}}(\boldsymbol{z}) J^{a_k}(w_k) \dots J^{a_1}(w_1) \rangle \\ &-\left(K_b^a\right)_i \sum_{q=1}^{k} \oint_0 \frac{dw_k}{2\pi i w_k} \dots \oint_0 \frac{dw_1}{2\pi i w_1} \oint_{w_q} \frac{dz}{2\pi i (z-z_i)} \frac{\delta_{ba_q}}{2(z-w_q)^2} \\ &\times \langle \mathbf{\Phi}_{\boldsymbol{s}}(\boldsymbol{z}) J^{a_k}(w_k) \dots J^{a_{q+1}}(w_{q+1}) J^{a_{q-1}}(w_{q-1}) \dots J^{a_1}(w_1) \rangle \\ &-\left(K_b^a\right)_i \sum_{q=1}^{k} \oint_0 \frac{dw_k}{2\pi i w_k} \dots \oint_0 \frac{dw_1}{2\pi i w_1} \oint_{w_q} \frac{dz}{2\pi i (z-z_i)} \frac{i\varepsilon_{ba_qc}}{z-w_q} \\ &\times \langle \mathbf{\Phi}_{\boldsymbol{s}}(\boldsymbol{z}) J^{a_k}(w_k) \dots J^{c}(w_q) \dots J^{a_1}(w_1) \rangle \\ = &-\left(K_b^a\right)_i \sum_{j=1,j\neq i}^{N} \frac{t_j^b}{z_i - z_j} \oint_0 \frac{dw_k}{2\pi i w_k} \dots \oint_0 \frac{w_1}{2\pi i w_1} \langle \mathbf{\Phi}_{\boldsymbol{s}}(\boldsymbol{z}) J^{a_k}(w_k) \dots J^{a_1}(w_1) \rangle \\ &+\sum_{q=1}^{k} \left(K_{a_q}^a\right)_i \oint_0 \frac{dw_k}{2\pi i w_k} \dots \oint_0 \frac{dw_1}{2\pi i w_1} \frac{1}{2(w_q - z_i)^2} \\ &\times \langle \mathbf{\Phi}_{\boldsymbol{s}}(\boldsymbol{z}) J^{a_k}(w_k) \dots J^{a_{q+1}}(w_{q+1}) J^{a_{q-1}}(w_{q-1}) \dots J^{a_1}(w_1) \rangle \\ &-\left(K_b^a\right)_i \sum_{q=1}^{k} \oint_0 \frac{dw_k}{2\pi i w_k} \dots \oint_0 \frac{dw_1}{2\pi i w_1} \frac{i\varepsilon_{ba_qc}}{w_q - z_i} \langle \mathbf{\Phi}_{\boldsymbol{s}}(\boldsymbol{z}) J^{a_k}(w_k) \dots J^{c}(w_q) \dots J^{a_1}(w_1) \rangle .\end{aligned} \tag{B.8}$$

With $J_{-1}^a = \oint \frac{dw}{2\pi i w} J^a(w)$ and Eq. (B.1), we thus get

$$\begin{aligned}0 = &-\left(K_b^a\right)_i \sum_{j=1,j\neq i}^{N} \frac{t_j^a}{z_i - z_j} |\psi_{1\ \dots 1}^{a_k \dots a_1}\rangle + \sum_{q=1}^{k} \frac{\left(K_{a_q}^a\right)_i}{2z_i^2} |\psi_{1\ \dots 1\ 1\ \dots 1}^{a_k \dots a_{q+1}\ a_{q-1} \dots a_1}\rangle \\ &-\left(K_b^a\right)_i \sum_{q=1}^{k} \sum_{s_1,\dots,s_N} i\varepsilon_{ba_qc} \oint_0 \frac{dw_k}{2\pi i w_k} \dots \oint_0 \frac{dw_q}{2\pi i w_q} \frac{1}{w_q - z_i} \\ &\times \langle \mathbf{\Phi}_{\boldsymbol{s}}(\boldsymbol{z}) J^{a_k}(w_k) \dots J^{c}(w_q) \left(J_{-1}^{a_{q-1}} \dots J_{-1}^{a_1}\right)(0) \rangle |s_1, \dots, s_N\rangle\end{aligned} \tag{B.9}$$

$$
\begin{aligned}
&= -\left(K_b^a\right)_i \sum_{j=1,j\neq i}^{N} \frac{t_j^a}{z_i - z_j} |\psi_{1\ \ldots 1}^{a_k \ldots a_1}\rangle + \sum_{q=1}^{k} \frac{\left(K_{a_q}^a\right)_i}{2z_i^2} |\psi_{1\ \ldots 1\ 1\ \ldots 1}^{a_k \ldots a_{q+1} a_{q-1} \ldots a_1}\rangle \\
&\quad - \left(K_b^a\right)_i \sum_{q=1}^{k} \sum_{n=-1}^{q-1} \sum_{s_1,\ldots,s_N} i\varepsilon_{ba_qc} \oint_0 \frac{dw_k}{2\pi i w_k} \ldots \oint_0 \frac{dw_q}{2\pi i w_q} \frac{w_q^{-n-1}}{w_q - z_i} \\
&\qquad \times \langle \mathbf{\Phi}_{\boldsymbol{s}}(\boldsymbol{z}) J^{a_k}(w_k) \ldots J^{a_{q+1}}(w_{q+1}) \left(J_n^c J_{-1}^{a_{q-1}} \ldots J_{-1}^{a_1}\right)(0)\rangle |s_1, \ldots, s_N\rangle \\
&= -\left(K_b^a\right)_i \sum_{j=1,j\neq i}^{N} \frac{t_j^a}{z_i - z_j} |\psi_{1\ \ldots 1}^{a_k \ldots a_1}\rangle + \sum_{q=1}^{k} \frac{\left(K_{a_q}^a\right)_i}{2z_i^2} |\psi_{1\ \ldots 1\ 1\ \ldots 1}^{a_k \ldots a_{q+1} a_{q-1} \ldots a_1}\rangle \\
&\quad + \left(K_b^a\right)_i \sum_{q=1}^{k} \sum_{n=-1}^{q-1} \sum_{s_1,\ldots,s_N} \frac{i\varepsilon_{ba_qc}}{z_i^{n+2}} \langle \mathbf{\Phi}_{\boldsymbol{s}}(\boldsymbol{z}) \left(J_{-1}^{a_k} \ldots J_{-1}^{a_{q+1}} J_n^c J_{-1}^{a_{q-1}} \ldots J_{-1}^{a_1}\right)(0)\rangle |s_1, \ldots, s_N\rangle.
\end{aligned}
$$

Next, we multiply this equation by $2z_i$ and use $w_{ij} \equiv (z_i + z_j)/(z_i - z_j)$ to obtain

$$
\begin{aligned}
\left(K_b^a\right)_i \sum_{j=1,j\neq i}^{N} (w_{ij} + 1) t_j^b |\psi_{1\ \ldots 1}^{a_k \ldots a_1}\rangle &= \sum_{q=1}^{k} \frac{\left(K_{a_q}^a\right)_i}{z_i} |\psi_{1\ \ldots 1\ 1\ \ldots 1}^{a_k \ldots a_{q+1} a_{q-1} \ldots a_1}\rangle + 2\left(K_b^a\right)_i \sum_{q=1}^{k} \sum_{n=-1}^{q-1} \sum_{s_1,\ldots,s_N} \frac{i\varepsilon_{ba_qc}}{z_i^{n+1}} \\
&\quad \times \langle \mathbf{\Phi}_{\boldsymbol{s}}(\boldsymbol{z}) \left(J_{-1}^{a_k} \ldots J_{-1}^{a_{q+1}} J_n^c J_{-1}^{a_{q-1}} \ldots J_{-1}^{a_1}\right)(0)\rangle |s_1, \ldots s_N\rangle
\end{aligned}
\tag{B.10}
$$

Using

$$
T^b |\psi_{1\ \ldots 1}^{a_k \ldots a_1}\rangle = i \sum_{q=1}^{k} \varepsilon_{ba_qc} |\psi_{1\ \ldots 1\ 1\ 1\ \ldots 1}^{a_k \ldots a_{q+1} c a_{q-1} \ldots a_1}\rangle, \tag{B.11}
$$

$$
\left(K_b^a\right)_i t_i^b = 0, \tag{B.12}
$$

and

$$
\mathcal{C}_i^a = \left(K_b^a\right)_i \sum_{j=1,j\neq i}^{N} w_{ij} t_j^b, \tag{B.13}
$$

we get the final decoupling equation

$$
\begin{aligned}
\mathcal{C}_i^a |\psi_{1\ \ldots 1}^{a_k \ldots a_1}\rangle &= \sum_{q=1}^{k} \frac{\left(K_{a_q}^a\right)_i}{z_i} |\psi_{1\ \ldots 1\ 1\ \ldots 1}^{a_k \ldots a_{q+1} a_{q-1} \ldots a_1}\rangle + \left(K_b^a\right)_i T^b |\psi_{1\ \ldots 1}^{a_k \ldots a_1}\rangle \\
&\quad + 2\left(K_b^a\right)_i \sum_{q=2}^{k} \sum_{n=0}^{q-1} \sum_{s_1,\ldots,s_N} \frac{i\varepsilon_{ba_qc}}{z_i^{n+1}} \langle \mathbf{\Phi}_{\boldsymbol{s}}(\boldsymbol{z}) \left(J_{-1}^{a_k} \ldots J_{-1}^{a_{q+1}} J_n^c J_{-1}^{a_{q-1}} \ldots J_{-1}^{a_1}\right)(0)\rangle |s_1, \ldots, s_N\rangle.
\end{aligned}
\tag{B.14}
$$

Let us now specialize the positions z_j to those of a square lattice on the cylinder,

$$
z_j \propto e^{\frac{2\pi}{N_y}(j_x + i j_y)}, \tag{B.15}
$$

and consider the action of $\sum_{i=1}^{N} \mathcal{C}_i^a$ on a state $|\psi_{1\ \ldots 1}^{a_k \ldots a_1}\rangle$. For $n \bmod N_y \neq 0$, we have

$$
\sum_{j=1}^{N} \left(z_j\right)^{-n} = 0 \tag{B.16}
$$

on the cylinder. Summing over i in Eq. (B.14) and introducing $\mathcal{C}'^a = \frac{3}{2}\sum_{i=1}^N \mathcal{C}_i^a$, we therefore obtain for $k < N_y$

$$\mathcal{C}'^a|\psi_{1\ \ldots 1}^{a_k\ldots a_1}\rangle = (N-1)T^a|\psi_{1\ \ldots 1}^{a_k\ldots a_1}\rangle + \sum_{q=1}^{k} i\varepsilon_{a_q ac}|\psi_{11\ \ldots 1\ \ 1\ \ \ldots 1}^{ca_k\ldots a_{q+1}a_{q-1}\ldots a_1}\rangle \tag{B.17}$$
$$+ \sum_{s_1,\ldots,s_N}\sum_{q=2}^{k}\sum_{n=0}^{q-1} G_{a_k\ldots a_1}^{q,n}(s_1,\ldots,s_N)|s_1,\ldots,s_N\rangle,$$

where

$$G_{a_k\ldots a_1}^{q,n}(s_1,\ldots,s_N) = 2\langle \mathbf{\Phi}_{\boldsymbol{s}}(z)\left(J_{-n-1}^{a_q}J_{-1}^{a_k}\ldots J_{-1}^{a_{q+1}}J_n^a J_{-1}^{a_{q-1}}\ldots J_{-1}^{a_1}\right)(0)\rangle \tag{B.18}$$
$$- 2\delta_{a_q a}\langle \mathbf{\Phi}_{\boldsymbol{s}}(z)\left(J_{-n-1}^{c}J_{-1}^{a_k}\ldots J_{-1}^{a_{q+1}}J_n^c J_{-1}^{a_{q-1}}\ldots J_{-1}^{a_1}\right)(0)\rangle.$$

We now argue that all terms in Eq. (B.17) can be written in terms of states $|\psi_{1\ \ldots 1}^{a_k\ldots a_1}\rangle$, which have k current operators modes J_{-1}^a. Using Eq. (B.11), the first term can be brought into the desired form. In the term containing $G_{a_k\ldots,a_q}^{q,n}(s_1,\ldots,s_N)$, the modes J_n^a and J_n^c can be commuted to the right since $J_n^a|0\rangle = 0$ for $n \geq 0$:

$$\left(J_n^a J_{-1}^{a_{q-1}}\ldots J_{-1}^{a_1}\right)(0)|0\rangle = \sum_{r=1}^{q-1} i\varepsilon_{aa_r d}\left(J_{-1}^{a_{q-1}}\ldots J_{-1}^{a_{r+1}}J_{n-1}^d J_{-1}^{a_{r-1}}\ldots J_{-1}^{a_1}\right)(0)|0\rangle, \tag{B.19}$$

and similarly for $\left(J_n^c J_{-1}^{a_{q-1}}\ldots J_{-1}^{a_1}\right)(0)|0\rangle$. Iterating this step, the current operator modes with a positive mode number can be eliminated. The resulting terms only have negative mode numbers and are all of order k in current operators.

B.2 Commutator of Haldane-Shastry Hamiltonian and u_{-1}^a

In this section we derive an expression for the commutator $\left[\mathcal{H}, u_{-1}^a\right]$, where $\mathcal{H}$ is the Haldane-Shastry Hamiltonian defined in Sec. 3.3.1. This commutator was used in Sec. 3.3.3 to determine the action of $\mathcal{H}$ on a state $|\psi_{n_l\ldots n_1}^{a_l\ldots a_1}\rangle$.

As a first step, we compute the Fourier transforms of $w_{ij} = (z_i + z_j)/(z_i - z_j)$ and w_{ij}^2, see also Ref. [196], where these Fourier sums were evaluated using contour integrals. Due to translational invariance, the Fourier transforms can be reduced to one sum,

$$\sum_{i\neq j}\frac{w_{ij}}{z_i^k z_j^l} = N\tilde{\delta}_{k+l}\sum_{i(\neq N)}\frac{w_{iN}}{z_i^k}, \qquad \sum_{i\neq j}\frac{w_{ij}^2}{z_i^k z_j^l} = N\tilde{\delta}_{k+l}\sum_{i(\neq N)}\frac{w_{iN}^2}{z_i^k}, \tag{B.20}$$

where $\sum_{i(\neq j)}$ denotes the sum over all $i \in \{1,\ldots,N\}\setminus\{j\}$, and z_j is given in Eq. (3.53) of the main text.

In order to evaluate the remaining sums, it is useful to compute the Fourier sums

$$\sum_{k=0}^{N-1} k^n z_k^j \tag{B.21}$$

for $n = 1$ and $n = 2$. For $j = 0$, we have

$$\sum_{k=0}^{N-1} k = \frac{N(N-1)}{2}, \qquad \sum_{k=0}^{N-1} k^2 = \frac{N(N-1)(2N-1)}{6}. \tag{B.22}$$

For $j = 1, 2, \ldots, N-1$, we use the generating function

$$f(\omega) = \sum_{k=0}^{N-1} e^{i\omega k} = \frac{1-e^{i\omega N}}{1-e^{i\omega}}, \qquad \sum_{k=0}^{N-1} k^n z_k^j = \left(\frac{d}{id\omega}\right)^n f(\omega)\Big|_{\omega=\frac{2\pi j}{N}}. \tag{B.23}$$

Taking the first and the second derivative, we find

$$\sum_{k=0}^{N-1} k z_k^j = \frac{N}{2}(w_{jN} - 1), \qquad \sum_{k=0}^{N-1} k^2 z_k^j = \frac{N}{2}\left(1 - N + N w_{jN} - w_{jN}^2\right). \tag{B.24}$$

Taking the inverse Fourier transforms of these equations and solving for $\sum_{j(\neq N)} w_{jN}/z_j^k$ and $\sum_{j(\neq N)} w_{jN}^2/z_j^k$, we arrive at

$$\begin{aligned}
\sum_{i\neq j} \frac{w_{ij}}{z_i^k z_j^l} &= \begin{cases} 0, & \text{if } k = 0 \\ (2k-N)\tilde{\delta}_{k+l} N, & \text{if } k = 1, 2, \ldots, N-1 \end{cases} \\
\sum_{i\neq j} \frac{w_{ij}^2}{z_i^k z_j^l} &= \begin{cases} \left(N - \frac{N^2}{3} - \frac{2}{3}\right)\tilde{\delta}_l N & \text{if } k = 0 \\ \left(\frac{N^2}{6} - 2(k - \frac{N}{2})^2 - \frac{2}{3}\right)\tilde{\delta}_{k+l} N & \text{if } k = 1, 2, \ldots, N-1, \end{cases}
\end{aligned} \tag{B.25}$$

where $\tilde{\delta}_m = 1$ if $m \bmod N = 0$ and $\tilde{\delta}_m = 0$ otherwise.

The explicit form of the Haldane-Shastry Hamiltonian in terms of spin operators is [103]

$$\mathcal{H} = -\frac{1}{6}\sum_{k,j}\sum_{i\neq(k,j)} w_{ij} w_{ik} t_j^b t_k^b - \frac{1}{6}\sum_{i\neq j} w_{ij}^2 t_i^b t_j^b + \frac{1}{6}(N+1) T^b T^b. \tag{B.26}$$

We use the Fourier transforms of Eq. (B.25) to rewrite $\mathcal{H}$ in terms of u_k^a. According to the definition of Eq. (3.25), the operators u_k^a are Fourier transforms of t_j^a on the circle with periodic boundary conditions. Therefore, the expansions of $\mathcal{H}$ in terms of u_k^a corresponds to a Fourier transform. We find

$$\mathcal{H} = \sum_{k=0}^{N-1} \frac{1 + 2N^2 - 9Nk + 9k^2}{9N} u_{-k}^b u_k^b. \tag{B.27}$$

Starting from this expansion, we next compute the commutator between $\mathcal{H}$ and u_{-1}^a. Using

$$\left[u_m^a, u_n^b\right] = i\varepsilon_{abc} u_{n+m}^c, \tag{B.28}$$

which directly follows from the commutator algebra of the spin operators t_i^a, we obtain

$$[\mathcal{H}, u_{-1}^a] = 2i\varepsilon_{abc} u_{-1}^b T^c - \frac{2i}{N}\varepsilon_{abc}\sum_{m=1}^{N-1} m u_{-m}^b u_{m-1}^c + (3-N) u_{-1}^a. \tag{B.29}$$

It is possible to rewrite the sum over Fourier transformed spin operators in terms of the operator $\mathcal{C}_i^a$, which was defined in Eq. (3.55). To this end, we computed the Fourier expansion of $\mathcal{C}_i^a$. The result is

$$\frac{3}{2}\sum_{j=1}^{N} \frac{\mathcal{C}_j^a}{z_j^p} = i\varepsilon_{abc} u_{-p}^b T^c + (2p + 2 - 2N) u_{-p}^a - \frac{2i}{N}\varepsilon_{abc}\sum_{m=1}^{N-1} m u_{-m}^b u_{m-p}^c \tag{B.30}$$

for $p \in \{1, \ldots, N-1\}$. For $p = 1$, we find the same sum over Fourier transformed spin operators that occurs in the above expansion of the Hamiltonian [Eq. (B.29)]. Inserting the $p = 1$ Fourier mode of $\mathcal{C}_i^a$, we arrive at Eq. (3.61) of the main text.

B.3 Translation and inversion of states on the cylinder

B.3.1 Transformation under a permutation of the spins

Both the translation operator $\mathcal{T}_y$ and the inversion operator $\mathcal{I}$ act on a product state as a permutation of the spins. Such a permutation operator $\mathcal{O}_\tau$ is defined for the permutation τ of N elements as

$$\mathcal{O}_\tau |s_1,\dots,s_N\rangle = |s_{\tau(1)},\dots,s_{\tau(N)}\rangle. \tag{B.31}$$

The action of $\mathcal{O}_\tau$ on $|\psi_0\rangle$ and $|\psi_0^{s_0,s_\infty}\rangle$ can be rewritten in terms of a permutation of the positions z_i, which will facilitate our calculations for $\mathcal{T}_y$ and $\mathcal{I}$. Our derivation of this transformation rule follows Ref. [156].

We consider the wave function

$$\tilde{\psi}_0^{z_1,\dots,z_N}(s_1,\dots,s_N) = \delta_{\mathbf{s}}\chi_{\mathbf{s}}\prod_{i<j}^{N}(z_i-z_j)^{\frac{1}{2}(s_is_j+1)}, \tag{B.32}$$

which is equivalent to $\psi_0(s_1,\dots,s_N)$ because it only differs by a spin-independent constant [cf. Eq. (3.12)]. We have also explicitly written out the parametric dependence on the positions z_i. Similarly, the wave function

$$\tilde{\psi}_0^{s_0,s_\infty,z_1,\dots,z_N}(s_1,\dots,s_N) = \delta_{\tilde{\mathbf{s}}}(-1)^{\frac{1}{2}(1-s_\infty)}\chi_{\mathbf{s}}\prod_{n=1}^{N} z_n^{\frac{1}{2}(s_0s_n+1)}\prod_{n<m}^{N}(z_n-z_m)^{\frac{1}{2}(s_ns_m+1)} \tag{B.33}$$

is equivalent to $\psi_0^{s_0,s_\infty}(s_1,\dots,s_N)$. Let us first calculate the transformation of $\tilde{\psi}_0^{z_1,\dots,z_N}(s_1,\dots,s_N)$ under a simultaneous permutation of both the spins and the coordinates. Since every permutation can be decomposed into a series of transpositions, we consider the case that τ is a transposition:

$$\tau(i) = \begin{cases} i & \text{if } i \notin \{m,n\}, \\ n & \text{if } i = m, \\ m & \text{if } i = n \end{cases} \tag{B.34}$$

for $m,n \in \{1,\dots,N\}$ and $m<n$. It follows that

$$\begin{aligned}\frac{\tilde{\psi}_0^{z_{\tau(1)},\dots,z_{\tau(N)}}(s_{\tau(1)},\dots,s_{\tau(N)})}{\tilde{\psi}_0^{z_1,\dots,z_N}(s_1,\dots,s_N)} &= \underbrace{(-1)^{\frac{1}{2}(n-m)(s_m-s_n)}}_{\text{transformation of }\chi_{\mathbf{s}}}\prod_{\substack{i<j,\\ \tau(i)>\tau(j)}}^{N}(-1)^{\frac{1}{2}(s_{\tau(i)}s_{\tau(j)}+1)} \\ &= (-1)^{\frac{1}{2}(n-m)(s_m-s_n)}(-1)^{\frac{1}{2}(s_ms_n+1)}\prod_{j=m+1}^{n-1}(-1)^{\frac{1}{2}(s_j(s_m+s_n)+2)} \\ &= -1. \end{aligned} \tag{B.35}$$

Therefore, if τ is a general permutation corresponding to $\mathcal{N}_\tau$ subsequent transpositions,

$$\tilde{\psi}_0^{z_{\tau(1)},\dots,z_{\tau(N)}}(s_{\tau(1)},\dots,s_{\tau(N)}) = \operatorname{sign}(\tau)\tilde{\psi}_0^{z_1,\dots,z_N}(s_1,\dots,s_N), \tag{B.36}$$

where $\operatorname{sign}(\tau) = (-1)^{\mathcal{N}_\tau}$ is the signature of the permutation. Substituting s_i by $s_{\tau^{-1}(i)}$ in Eq. (B.36), we arrive at the final transformation rule:

$$\tilde{\psi}_0^{z_1,\dots,z_N}(s_{\tau^{-1}(1)},\dots,s_{\tau^{-1}(N)}) = \operatorname{sign}(\tau)\tilde{\psi}_0^{z_{\tau(1)},\dots,z_{\tau(N)}}(s_1,\dots,s_N). \tag{B.37}$$

The transformation under a permutation of the spins can therefore be calculated by considering the corresponding transformation of the coordinates and taking into account the signature of the permutation.

We note that Eq. (B.37) is not valid for the original wave function $\psi_0(s_1,\dots,s_N)$ but only for $\tilde{\psi}_0^{z_1,\dots,z_N}(s_1,\dots,s_N)$, which differs from $\psi_0(s_1,\dots,s_N)$ by a factor depending on z_i. However, this factor does not depend on the spins. Therefore, if $|\tilde{\psi}_0^{z_1,\dots,z_N}\rangle$ is an eigenstate of $\mathcal{O}_\tau$, then this is also the case for $|\psi_0\rangle$.

Compared to $\tilde{\psi}_0(s_1,\dots,s_N)$, there are some an additional factors present the wave function $\tilde{\psi}_0^{s_0,s_\infty,z_1,\dots,z_N}(s_1,\dots,s_N)$. Since these are invariant under a permutation of both the spins and the coordinates, a formula analogous to Eq. (B.37) holds for $\tilde{\psi}_0^{s_0,s_\infty,z_1,\dots,z_N}(s_1,\dots,s_N)$.

B.3.2 Translation in the periodic direction

The translation operator $\mathcal{T}_y$ is defined through the permutation $\tilde{\mathcal{T}}_y$:

$$\tilde{\mathcal{T}}_y\left(i_x,i_y\right)=\begin{cases}(i_x,i_y+1) & \text{if } i_y\neq N_y,\\ (i_x,1) & \text{if } i_y=N_y,\end{cases} \tag{B.38}$$

where i_x is the x component and i_y the y component of an index i.

The signature of this permutation is given by

$$\operatorname{sign}(\tilde{\mathcal{T}}_y)=(-1)^{N_x(N_y-1)}=(-1)^{N_x}, \tag{B.39}$$

where we used that $N=N_yN_x$ is even. In terms of the positions, the transformation corresponds to a multiplication by a phase, $z_{\tilde{\mathcal{T}}_y(j)}=e^{2\pi i/N_y}z_j$. Therefore,

$$\begin{aligned}\tilde{\psi}_0^{z_1,\dots,z_N}(s_{\tilde{\mathcal{T}}_y^{-1}(1)},\dots,s_{\tilde{\mathcal{T}}_y^{-1}(N)})&=\operatorname{sign}(\tilde{\mathcal{T}}_y)\tilde{\psi}_0^{z_{\tilde{\mathcal{T}}_y(1)},\dots,z_{\tilde{\mathcal{T}}_y(N)}}(s_1,\dots,s_N)\\&=(-1)^{N_x}\delta_{\mathbf{s}}\chi_{\mathbf{s}}\prod_{i<j}^{N}\left(e^{\frac{2\pi i}{N_y}}(z_i-z_j)\right)^{\frac{1}{2}(s_is_j+1)}\\&=(-1)^{\frac{1}{2}N_xN}\tilde{\psi}_0^{z_1,\dots,z_N}(s_1,\dots,s_N).\end{aligned} \tag{B.40}$$

Here, we have used that

$$\prod_{i<j}^{N}e^{\frac{\pi i}{N_y}(s_is_j+1)}=(-1)^{N_x\frac{N}{2}+N_x}, \tag{B.41}$$

which follows from $s_1+\dots+s_N=0$. The eigenvalue of $|\psi_0\rangle$ with respect to $\mathcal{T}_y$ is therefore $(-1)^{N_xN/2}$. With

$$\mathcal{T}_y u^a_{-n}\mathcal{T}_y^{-1}=e^{-\frac{2\pi i}{N_y}n}u^a_{-n} \tag{B.42}$$

it follows that the eigenvalue of $|\psi^{a_l\dots a_1}_{n_l\dots n_1}\rangle$ is $e^{-2\pi ik/N_y}(-1)^{N_xN/2}$, where $k=n_1+\dots+n_l$.

For $|\tilde{\psi}_0^{s_0,s_\infty,z_1,\dots,z_N}\rangle$, we obtain

$$\begin{aligned}&\tilde{\psi}_0^{s_0,s_\infty,z_1,\dots,z_N}(s_{\tilde{\mathcal{T}}_y^{-1}(1)},\dots,s_{\tilde{\mathcal{T}}_y^{-1}(N)})\\&=(-1)^{N_x}\prod_{n=1}^{N}e^{\frac{\pi i}{N_y}(s_ns_0+1)}\prod_{n<m}^{N}e^{\frac{\pi i}{N_y}(s_ns_m+1)}\tilde{\psi}_0^{s_0,s_\infty,z_1,\dots,z_N}(s_1,\dots,s_N)\\&=(-1)^{N_x+N_x\frac{N}{2}}\tilde{\psi}_0^{s_0,s_\infty,z_1,\dots,z_N}(s_1,\dots,s_N).\end{aligned} \tag{B.43}$$

In the last equation, we have used that $s_1+\dots+s_N+s_0+s_\infty=0$.

B.3.3 Inversion

We require that the inversion $\mathcal{I}$ acts on the positions defined in Eq. (3.51) as

$$z_{\tilde{\mathcal{I}}(i_x),\tilde{\mathcal{I}}(i_y)} = \frac{1}{z_{i_x,i_y}}. \tag{B.44}$$

This leads to the definition

$$\tilde{\mathcal{I}}\left(i_x, i_y\right) = \begin{cases} (N_x + 1 - i_x, N_y - i_y) & \text{if } i_y \neq N_y, \\ (N_x + 1 - i_x, N_y) & \text{if } i_y = N_y. \end{cases} \tag{B.45}$$

We note that in our choice of z_i, the center of the cylinder is at the unit circle. If this is not the case, then the definition of Eq. (B.45) leads to an additional factor when $\tilde{\mathcal{I}}$ is applied to z_i.

In order to determine the sign of the permutation, we arrange the state $|s_1, \ldots, s_N\rangle$ in a matrix:

$$|s_{1,1}, \ldots, s_{N_x,N_y}\rangle \cong \begin{pmatrix} s_{1,1} & \cdots & s_{1,N_y} \\ s_{2,1} & \cdots & s_{2,N_y} \\ \vdots & \vdots & \vdots \\ s_{N_x,1} & \cdots & s_{N_x,N_y} \end{pmatrix}. \tag{B.46}$$

The transformed state is then given by

$$\mathcal{I}|s_{1,1}, \ldots, s_{N_x,N_y}\rangle \cong \begin{pmatrix} s_{N_x,N_y-1} & s_{N_x,N_y-2} & \cdots & s_{N_x,1} & s_{N_x,N_y} \\ s_{N_x-1,N_y-1} & s_{N_x-1,N_y-2} & \cdots & s_{N_x-1,1} & s_{N_x-1,N_y} \\ \vdots & \vdots & \vdots & \vdots & \vdots \\ s_{1,N_y-1} & s_{1,N_y-2} & \cdots & s_{1,1} & s_{1,N_y} \end{pmatrix}. \tag{B.47}$$

To bring the transformed matrix back to the original form, we first reverse all N_y columns and then reverse all N_x rows excluding the last element of each row. A single sequence of L elements can be reversed in $\frac{1}{2}L(L-1)$ steps. Therefore, the sign of the permutation is given by

$$\operatorname{sign}(\tilde{\mathcal{I}}) = (-1)^{N_y \frac{1}{2} N_x (N_x - 1) + N_x \frac{1}{2}(N_y - 1)(N_y - 2)}. \tag{B.48}$$

We next determine the contribution from the coordinate part of $\psi_0(s_1, \ldots, s_N)$. Using Eq. (B.44), we have

$$\begin{aligned} \tilde{\psi}_0^{z_{\tilde{\mathcal{I}}(1)}, \ldots, z_{\tilde{\mathcal{I}}(N)}}(s_1, \ldots, s_N) &= \tilde{\psi}_0^{z_1, \ldots, z_N}(s_1, \ldots, s_N) \prod_{m<n}^{N} (-z_m z_n)^{-\frac{1}{2}(s_m s_n + 1)} \\ &= \tilde{\psi}_0^{z_1, \ldots, z_N}(s_1, \ldots, s_N) e^{-\frac{1}{4}\sum_{m \neq n}(s_m s_n + 1)(\log(z_m z_n) + \pi i)} \\ &= \tilde{\psi}_0^{z_1, \ldots, z_N}(s_1, \ldots, s_N) e^{-\frac{1}{4}\sum_{m,n}(s_m s_n + 1)(\log(z_m z_n) + \pi i)} e^{\frac{1}{2}\sum_i (2\log(z_i) + \pi i)} \\ &= \tilde{\psi}_0^{z_1, \ldots, z_N}(s_1, \ldots, s_N)(-1)^{\frac{N}{2} N_x + N_x}. \end{aligned} \tag{B.49}$$

In the last step, we have used that $s_1 + \cdots + s_N = 0$ and

$$\sum_{n=1}^{N} \log(z_n) = \pi i \, (N + N_x). \tag{B.50}$$

Therefore, the eigenvalue of $|\psi_0\rangle$ with respect to $\mathcal{I}$ is

$$\mathrm{sign}(\tilde{\mathcal{I}})(-1)^{\frac{N}{2}N_x+N_x} = (-1)^{\frac{N}{2}N_y}. \tag{B.51}$$

The states $|\psi^{a_l\dots a_1}_{n_l\dots n_1}\rangle$ are not eigenstates of $\mathcal{I}$, but transform as

$$\mathcal{I}|\psi^{a_l\dots a_1}_{n_l\dots n_1}\rangle = \mathcal{I}u^{a_l}_{-n_l}\mathcal{I}^{-1}\dots\mathcal{I}u^{a_1}_{-n_1}\mathcal{I}^{-1}\mathcal{I}|\psi_0\rangle = (-1)^{\frac{N}{2}N_y}u^{a_l}_{n_l}\dots u^{a_1}_{n_1}|\psi_0\rangle. \tag{B.52}$$

Here, we have used that

$$\mathcal{I}u^{a_j}_{-n_j}\mathcal{I}^{-1} = \sum_{i=1}^{N}\frac{1}{(z_i)^{n_j}}\mathcal{I}t_i^{a_j}\mathcal{I}^{-1} = \sum_{i=1}^{N}\frac{1}{(z_i)^{n_j}}t^{a_j}_{\tilde{\mathcal{I}}^{-1}(i)} = \sum_{i=1}^{N}(z_i)^{n_j}\,t_i^{a_j} = u^{a_j}_{n_j}, \tag{B.53}$$

if the center of the cylinder is at the unit circle. In terms of the states $|\psi^{a_l\dots a_1}_{-n_l\cdots-n_1}\rangle$ defined in Eq. (3.52), we therefore have

$$\mathcal{I}|\psi^{a_l\dots a_1}_{n_l\dots n_1}\rangle = (-1)^{\frac{N}{2}N_y}|\psi^{a_l\dots a_1}_{-n_l\cdots-n_1}\rangle. \tag{B.54}$$

For the transformed states $\mathcal{I}|\psi^{a_l\dots a_1}_{n_l\dots n_1}\rangle$, the current operators are therefore inserted at $z_\infty=\infty$ instead of at $z_0=0$. Eigenstates of $\mathcal{I}$ with eigenvalues $(\pm1)(-1)^{\frac{N}{2}N_y}$ are then given by

$$|\psi^{a_l\dots a_1}_{n_l\dots n_1}\rangle \pm |\psi^{a_l\dots\ a_1}_{-n_l\cdots-n_1}\rangle. \tag{B.55}$$

Finally, we determine the transformation of $|\tilde{\psi}_0^{s_0,s_\infty,z_1,\dots,z_N}\rangle$ with respect to $\mathcal{I}$. As for $|\psi_0\rangle$, there is a contribution from the sign of the permutation and from the transformation of the coordinates. The calculation is similar to that for $|\psi_0\rangle$, only that now $s_1+\dots+s_N+s_0+s_\infty=0$. We find

$$\mathcal{I}|\tilde{\psi}_0^{s_0,s_\infty,z_1,\dots,z_N}\rangle = \mathrm{sign}(\tilde{\mathcal{I}})|\tilde{\psi}_0^{s_0,s_\infty,z_{\tilde{\mathcal{I}}(1)},\dots,z_{\tilde{\mathcal{I}}(N)}} = (-1)^{N_y\frac{N}{2}+N_x+1}|\tilde{\psi}_0^{s_\infty,s_0,z_1,\dots,z_N}\rangle. \tag{B.56}$$

Since $\psi_0^{s_0,s_\infty}(s_1,\dots,s_N)$ and $\tilde{\psi}_0^{s_0,s_\infty,z_1,\dots,z_N}(s_1,\dots,s_N)$ only differ by a spin-independent factor, we also have

$$\mathcal{I}|\psi_0^{s_0,s_\infty}\rangle = (-1)^{N_y\frac{N}{2}+N_x+1}|\psi_0^{s_\infty,s_0}\rangle. \tag{B.57}$$

Note that $\mathcal{I}$ exchanges the spins s_0 and s_∞ in $|\psi_0^{s_0,s_\infty}\rangle$.

C Details on approximations of correlations

C.1 Vertex operators and normal ordering

In this section, we derive the following relation between the exponential of the boson field $\varphi(z,\bar{z})$ and the normal ordered exponential of $\varphi(z,\bar{z})$:

$$e^{i\sqrt{\alpha}s\varphi(z,\bar{z})} = e^{-\frac{1}{2}\alpha s^2\langle\varphi(z,\bar{z})\varphi(z,\bar{z})\rangle} : e^{i\sqrt{\alpha}s\varphi(z,\bar{z})} :, \tag{C.1}$$

where $\alpha > 0$ and $s \in \mathbb{R}$.

The field $\varphi(z,\bar{z})$ satisfies Wick's theorem [5], i.e., $\varphi(z,\bar{z})^n$ for $n \in \{0,1,\dots\}$ is equal to the sum of all possible contractions of $:\varphi(z,\bar{z})^n:$. Any contraction of k pairs of fields from $:\varphi(z,\bar{z})^n:$ results in the expression

$$\langle\varphi(z,\bar{z})\varphi(z,\bar{z})\rangle^k : \varphi(z,\bar{z})^{n-2k} :, \tag{C.2}$$

and there are

$$\frac{n(n-1)\dots(n-2k+1)}{k!2^k} = \frac{n!}{k!(n-2k)!2^k} \tag{C.3}$$

of such contractions.

The reason for this combinatorial factor is as follows: The numerator $n(n-1)\dots(n-2k+1)$ counts the number of possibilities of taking $2k$ fields from n fields. The factor $k!$ in the denominator corresponds to the number of permutations of the factors $\langle\varphi(z,\bar{z})\varphi(z,\bar{z})\rangle^k$ and the factor 2^k corresponds to the freedom to interchange two fields within a correlator $\langle\varphi(z,\bar{z})\varphi(z,\bar{z})\rangle$. Since these operators do not change the contraction, we divide by $k!2^k$.

Therefore,

$$\varphi(z,\bar{z})^n = \sum_{k=0}^{[n/2]} \frac{n!}{k!(n-2k)!2^k}\langle\varphi(z,\bar{z})\varphi(z,\bar{z})\rangle^k : \varphi(z,\bar{z})^{n-2k} :, \tag{C.4}$$

where $[n/2] = n/2$ for n even and $[n/2] = (n-1)/2$ for n odd. ($[n/2]$ is the maximal number of pairs that can be contracted from $:\varphi(z,\bar{z})^n:$.) Multiplying Eq. (C.4) by $(i\sqrt{\alpha}s)^n/n!$ and summing over n, we obtain

$$e^{is\sqrt{\alpha}\varphi(z,\bar{z})} = \sum_{n=0}^{\infty}\sum_{k=0}^{[n/2]} \frac{1}{k!(n-2k)!2^k}(i\sqrt{\alpha}s)^n\langle\varphi(z,\bar{z})\varphi(z,\bar{z})\rangle^k : \varphi(z,\bar{z})^{n-2k} : \tag{C.5}$$

$$= \sum_{n=0}^{\infty}\sum_{k=0}^{[n/2]} \frac{\left(-\alpha s^2\langle\varphi(z,\bar{z})\varphi(z,\bar{z})\rangle\right)^k}{k!2^k} \frac{\left(is\sqrt{\alpha} : \varphi(z,\bar{z}) :\right)^{n-2k}}{(n-2k)!}. \tag{C.6}$$

This double sum can be rearranged into a double sum with both summation indices ranging from 0 to ∞ (cf. Ref. [197]),

$$e^{is\sqrt{\alpha}\varphi(z,\bar{z})} = \sum_{n=0}^{\infty}\sum_{k=0}^{\infty} \frac{\left(-s^2\alpha\langle\varphi(z,\bar{z})\varphi(z,\bar{z})\rangle\right)^k}{k!2^k} \frac{\left(is\sqrt{\alpha} : \varphi(z,\bar{z}) :\right)^n}{n!} \tag{C.7}$$

$$= e^{-\frac{1}{2}\alpha s^2\langle\varphi(z,\bar{z})\varphi(z,\bar{z})\rangle} : e^{i\sqrt{\alpha}s\varphi(z,\bar{z})} :. \tag{C.8}$$

It follows that

$$\cos\left(\sqrt{\alpha}\varphi(z,\bar{z})\right) = e^{-\frac{1}{2}\alpha\langle\varphi(z,\bar{z})\varphi(z,\bar{z})\rangle} : \cos\left(\sqrt{\alpha}\varphi(z,\bar{z})\right) : \tag{C.9}$$

and

$$\sin\left(\sqrt{\alpha}\varphi(z,\bar{z})\right) = e^{-\frac{1}{2}\alpha\langle\varphi(z,\bar{z})\varphi(z,\bar{z})\rangle} : \sin\left(\sqrt{\alpha}\varphi(z,\bar{z})\right) : . \tag{C.10}$$

Therefore, the normal ordering can be left out in the exact expression for the zz correlations of Eq. (4.9).

C.2 Free boson on the sphere and on the cylinder

In this section, we consider a free boson on the sphere and on the cylinder. We explicitly work with coordinates $\Omega = (\theta, \phi)$ on the sphere and $(w, \bar{w})$ on the cylinder and do not project onto the plane. This is not necessary when computing the exact correlations in $|\psi_\alpha\rangle$, which are invariant under a projection of the positions onto the complex plane. However, different approximations of the correlations are obtained depending on whether one expands in the field $\varphi(z,\bar{z})$ or $\varphi(\Omega)$ and $\varphi(w,\bar{w})$, respectively.

C.2.1 Sphere

The free boson on the sphere has the action

$$S_{\text{sphere}}[\varphi] = \frac{1}{8\pi}\int_{S^2} d\Omega \left[(\partial_\theta\varphi(\Omega))^2 + \frac{1}{\sin^2(\theta)}(\partial_\phi\varphi(\Omega))^2 + \tilde{m}^2\varphi(\Omega)^2\right], \tag{C.11}$$

where $\Omega = (\theta,\phi)$ in terms of the polar angle θ and the azimuthal angle ϕ, $d\Omega = d\theta d\phi \sin(\theta)$, and $\tilde{m}$ is a mass regulator. We will take $\tilde{m}$ to be 0 eventually.

After two integrations by part with vanishing boundary terms,

$$S_{\text{sphere}} = \frac{1}{8\pi}\int_{S^2} d\Omega\varphi(\Omega)\left[L^2 + \tilde{m}^2\right]\varphi(\Omega), \tag{C.12}$$

where

$$L^2 = -\frac{1}{\sin(\theta)}\partial_\theta\left[\sin(\theta)\partial_\theta\right] - \frac{1}{\sin^2(\theta)}\partial_\phi^2 \tag{C.13}$$

is the square of the orbital angular momentum operator ($L^2 = L_x^2 + L_y^2 + L_z^2$).

The two-point correlator $\langle\varphi(\Omega)\varphi(\Omega')\rangle$ is determined by

$$\frac{1}{4\pi}\left(L^2 + \tilde{m}^2\right)\langle\varphi(\Omega)\varphi(\Omega')\rangle = \delta(\Omega - \Omega'), \tag{C.14}$$

where the δ function is defined with respect to the measure $d\Omega$ [$\int_{S^2} d\Omega\delta(\Omega) = 1$].

Since the spherical harmonics Y_l^m are eigenfunctions of L^2 with eigenvalues $l(l+1)$, we expand

$$\langle\varphi(\Omega)\varphi(\Omega')\rangle = \sum_{l,l'=0}^{\infty}\sum_{m=-l}^{l}\sum_{m'=-l'}^{l'} c_{ll'}^{mm'} Y_l^m(\Omega)Y_{l'}^{m'*}(\Omega'). \tag{C.15}$$

Using $\delta(\Omega-\Omega') = \sum_{l=0}^{\infty}\sum_{m=-l}^{l} Y_l^m(\Omega)Y_l^{m*}(\Omega')$ and Eq. (C.14), we obtain

$$c_{ll'}^{mm'} = \frac{4\pi}{l(l+1)+\tilde{m}^2}\delta_{ll'}\delta_{mm'}, \tag{C.16}$$

$$\langle\varphi(\Omega)\varphi(\Omega')\rangle = \sum_{l=0}^{\infty}\frac{4\pi}{l(l+1)+\tilde{m}^2}\sum_{m=-l}^{l} Y_l^m(\Omega)Y_l^{m*}(\Omega'). \tag{C.17}$$

The sum over m is given by [197]

$$\sum_{m=-l}^{l} Y_l^m(\Omega)Y_l^{m*}(\Omega') = \frac{2l+1}{4\pi}P_l(x), \tag{C.18}$$

where P_l is the lth Legendre polynomial, $x = 1-\frac{1}{2}|\mathbf{n}_\Omega - \mathbf{n}_{\Omega'}|^2$, and $\mathbf{n}_\Omega$ and $\mathbf{n}_{\Omega'}$ are unit vectors on S^2 embedded in $\mathbb{R}^3$ [cf. Eq. (2.31)].

Let us first consider the case of a finite mass $\tilde{m} > 0$, which is needed in Appendix C.3.1 for the computation of the continuum approximation on the sphere:

$$\langle\varphi(\Omega)\varphi(\Omega')\rangle = \sum_{l=0}^{\infty}\frac{2l+1}{l(l+1)+\tilde{m}^2}P_l(x) = \sum_{l=0}^{\infty}\left(\frac{1}{l+\frac{1}{2}+\sqrt{\frac{1}{4}-\tilde{m}^2}} + \frac{1}{1+\frac{1}{2}-\sqrt{\frac{1}{4}-\tilde{m}^2}}\right)P_l(x). \tag{C.19}$$

Using the generating function of $P_l(x)$,

$$\frac{1}{\sqrt{1-2xz+z^2}} = \sum_{l=0}^{\infty}P_l(x)z^l, \tag{C.20}$$

Eq. (C.19) can be transformed into an integral. To this end, we multiply the generating function (C.20) by $z^{\gamma-1}$ with $\mathrm{Re}(\gamma) > 0$ and then integrate z from 0 to 1:

$$\int_0^1 dz\frac{z^{\gamma-1}}{\sqrt{1-2xz+z^2}} = \sum_{l=0}^{\infty}\frac{1}{l+\gamma}P_l(x). \tag{C.21}$$

Applying this identity to Eq. (C.19), we find

$$\langle\varphi(\Omega)\varphi(\Omega')\rangle = \int_0^1 dz\frac{2\cosh\left[\sqrt{\frac{1}{4}-\tilde{m}^2}\log(z)\right]}{\sqrt{z\left[(z-1)^2+|\mathbf{n}_\Omega-\mathbf{n}_{\Omega'}|^2 z\right]}} = \int_0^\infty dq\frac{2\cosh\left(\sqrt{\frac{1}{4}-\tilde{m}^2}q\right)}{\sqrt{2\cosh(q)-2+|\mathbf{n}_\Omega-\mathbf{n}_{\Omega'}|^2}}, \tag{C.22}$$

where $q = -\log z$ was substituted in the integral.

Let us now consider the case of $\tilde{m} \to 0$. Since the $l = 0$ term is divergent for $\tilde{m} \to 0$, we separate it from the sum of Eq. (C.19) and expand the remaining terms to leading order in $\tilde{m}$:

$$\langle\varphi(\Omega)\varphi(\Omega')\rangle = \frac{1}{\tilde{m}^2} + \sum_{l=1}^{\infty}\left(\frac{1}{l}+\frac{1}{l+1}\right)P_l(x) + \mathcal{O}(\tilde{m}^2), \tag{C.23}$$

where $(2l+1)/(l(l+1)) = 1/l + 1/(l+1)$ and $P_0(x) = 1$ was used.

As a last step, we apply the identities

$$\sum_{l=0}^{\infty}\frac{P_l(x)}{l+1} = \log\frac{1+\sqrt{2-2x}-x}{1-x}, \tag{C.24}$$

$$\sum_{l=1}^{\infty}\frac{P_l(x)}{l} = \log\frac{2}{1+\sqrt{2-2x}-x}, \tag{C.25}$$

which can be derived from the generating function of $P_l(x)$: Eq. (C.24) follows from Eq. (C.20) by integrating z from 0 to 1. To obtain Eq. (C.25), one can first bring the $l = 0$ term in Eq. (C.20) to the left-hand side, then divide by z, and finally integrate z from 0 to 1.

Using Eqs. (C.24, C.25) in Eq. (C.23), we obtain

$$\langle\varphi(\Omega)\varphi(\Omega')\rangle = \frac{1}{\tilde{m}^2} - 1 + \log\frac{4}{|\mathbf{n}_\Omega - \mathbf{n}_{\Omega'}|^2} + \mathcal{O}(\tilde{m}^2). \tag{C.26}$$

Taking $\tilde{m} \to 0$,

$$\langle\varphi(\Omega)\varphi(\Omega')\rangle = -\log|\mathbf{n}_\Omega - \mathbf{n}_{\Omega'}|^2 + \text{constant}. \tag{C.27}$$

Next, we define vertex operators on the sphere as $:e^{i\sqrt{\alpha}s\varphi(\Omega)}:$, where $\alpha > 0$, $s \in \mathbb{R}$, and normal ordering is defined by subtracting vacuum expectation values on the sphere:

$$:\varphi(\Omega_1)\varphi(\Omega_2): = \varphi(\Omega_1)\varphi(\Omega_2) - \langle\varphi(\Omega_1)\varphi(\Omega_2)\rangle, \tag{C.28}$$

and similarly for more fields.

Let us now relate the vertex operator on the sphere to the vertex operator on the plane. The bosonic field on the plane is related to that on the sphere through the stereographic projection:

$$\varphi(z,\bar{z}) = \varphi(\Omega), \tag{C.29}$$

with $z = \tan(\theta/2)e^{-i\phi}$ and $\bar{z} = \tan(\theta/2)e^{i\phi}$. Correspondingly, we have

$$e^{i\sqrt{\alpha}s\varphi(z,\bar{z})} = e^{i\sqrt{\alpha}s\varphi(\Omega)}. \tag{C.30}$$

Note that this equation only holds without normal ordering since the normal ordering prescription depends on subtracting vacuum expectation values on the plane and sphere, respectively. However, we can use Eq. (C.1) relating the exponential of φ to the normal ordered exponential of φ. [The computation leading to Eq. (C.1) was formulated on the plane but it also applies to the sphere since we only made use of the relation between normal ordering and subtractions of vacuum expectation values.] Therefore,

$$e^{-\frac{1}{2}\alpha s^2\langle\varphi(\Omega)\varphi(\Omega)\rangle} :e^{i\sqrt{\alpha}s\varphi(\Omega)}: = e^{-\frac{1}{2}\alpha s^2\langle\varphi(z,\bar{z})\varphi(z,\bar{z})\rangle} :e^{i\sqrt{\alpha}s\varphi(z,\bar{z})}: \tag{C.31}$$

or

$$:e^{i\sqrt{\alpha}s\varphi(\Omega)}: =: e^{i\sqrt{\alpha}s\varphi(z,\bar{z})}: \lim_{\substack{\Omega'\to\Omega\\ z'\to z}} e^{-\frac{1}{2}\alpha s^2(\langle\varphi(z,\bar{z})\varphi(z',\bar{z}')\rangle - \langle\varphi(\Omega)\varphi(\Omega')\rangle)} \tag{C.32}$$

$$=: e^{i\sqrt{\alpha}s\varphi(z,\bar{z})}: \lim_{\substack{\Omega'\to\Omega\\ z'\to z}} \left(\frac{|z-z'|}{|\mathbf{n}_\Omega - \mathbf{n}_{\Omega'}|}\right)^{\alpha s^2} \tag{C.33}$$

$$=: e^{i\sqrt{\alpha}s\varphi(z,\bar{z})}: \left[2\cos\left(\frac{\theta}{2}\right)^2\right]^{-\alpha s^2}. \tag{C.34}$$

In the last step, it was used that

$$|\mathbf{n}_\Omega - \mathbf{n}_{\Omega'}| = 2\cos\left(\frac{\theta}{2}\right)\cos\left(\frac{\theta'}{2}\right)|z - z'|. \tag{C.35}$$

We can now determine the correlator of N vertex operators on the sphere from the corresponding correlator on the plane:

$$\langle : e^{i\sqrt{\alpha}s_1\varphi(\Omega_1)}\cdots : e^{i\sqrt{\alpha}s_N\varphi(\Omega_N)} : \rangle = \delta_{\mathbf{s}}\left(\prod_{m=1}^{N}\left[2\cos\left(\frac{\theta_m}{2}\right)^2\right]^{-\alpha s_m^2}\right)\prod_{m<n}^{N}|z_m - z_n|^{2\alpha s_m s_n} \tag{C.36}$$

$$= \delta_{\mathbf{s}}\prod_{m<n}^{N}\left[2\cos\left(\frac{\theta_m}{2}\right)\cos\left(\frac{\theta_n}{2}\right)|z_m - z_n|\right]^{2\alpha s_m s_n} \tag{C.37}$$

$$= \delta_{\mathbf{s}}\prod_{m<n}^{N}|\mathbf{n}_{\Omega_m} - \mathbf{n}_{\Omega_n}|^{2\alpha s_m s_n}, \tag{C.38}$$

where we used that

$$\delta_{\mathbf{s}}\prod_{m<n}^{N}\left[2\cos\left(\frac{\theta_m}{2}\right)\cos\left(\frac{\theta_n}{2}\right)\right]^{2\alpha s_m s_n} = \delta_{\mathbf{s}}e^{\alpha\sum_{m\neq n}s_m s_n\log[2\cos(\theta_m/2)\cos(\theta_n/2)]} \tag{C.39}$$

$$= \delta_{\mathbf{s}}e^{-\alpha\sum_{m=1}^{N}s_m^2\log\left[2\cos(\theta_m/2)^2\right]} \tag{C.40}$$

$$= \delta_{\mathbf{s}}\prod_{m=1}^{N}\left[2\cos(\theta_m/2)^2\right]^{-\alpha s_m^2}. \tag{C.41}$$

C.2.2 Cylinder

In the case of the cylinder, we can use the conformal transformation $z = e^w$ to transform the known correlator of vertex operators on the plane to that on the cylinder:

$$\langle : e^{is_1\sqrt{\alpha}\varphi(w_1,\bar{w}_1)} : \cdots : e^{i\sqrt{\alpha}s_N\varphi(w_N,\bar{w}_N)} : \rangle = \left|\prod_{j=1}^{N}e^{\frac{\alpha}{2}w_j s_j^2}\right|^2 \langle : e^{is_1\sqrt{\alpha}\varphi(z_1,\bar{z}_1)} : \cdots : e^{is_N\sqrt{\alpha}\varphi(z_N,\bar{z}_N)} : \rangle \tag{C.42}$$

$$= \delta_{\mathbf{s}}\left|\prod_{j=1}^{N}e^{\frac{\alpha}{2}w_j s_j^2}\right|^2\prod_{i<j}^{N}\left|e^{w_i} - e^{w_j}\right|^{2\alpha s_i s_j} \tag{C.43}$$

$$= \delta_{\mathbf{s}}\prod_{i<j}^{N}\left|2\sinh\left(\frac{1}{2}(w_i - w_j)\right)\right|^{2\alpha s_i s_j}. \tag{C.44}$$

In the last step, it was used that

$$\delta_{\mathbf{s}}\left|\prod_{j=1}^{N}e^{\frac{\alpha}{2}w_j s_j^2}\right|^2 = \delta_{\mathbf{s}}\left|\prod_{i<j}^{N}e^{-\frac{\alpha}{2}s_i s_j(w_i + w_j)}\right|^2. \tag{C.45}$$

C.3 Solution of the quadratic theory

C.3.1 Continuum approximation on the sphere

On the sphere, the quadratic action that provides an approximation of the zz correlations is given by

$$S_\alpha[\varphi] = \frac{1}{8\pi}\int_{S^2}d\Omega\varphi(\Omega)L^2\varphi(\Omega) + \frac{\alpha}{2}\sum_{j=1}^{N}\varphi(\Omega_j)^2, \tag{C.46}$$

where L^2 is the square of the orbital angular momentum operator (cf. Appendix C.2.1).

We consider an approximately uniform distribution of positions $\Omega_j = (\theta_j, \phi_j)$ on the sphere. As a consequence, each solid angle element $\Delta\Omega$ contains approximately the same number of points Ω_j and we approximate

$$\frac{4\pi}{N}\sum_{j=1}^{N}\varphi(\Omega_j)^2 \approx \int_{S^2} d\Omega\,\varphi(\Omega)^2, \tag{C.47}$$

$$S_\alpha[\varphi] \approx \frac{1}{8\pi}\int_{S^2} d\Omega\,\varphi(\Omega)(L^2+\alpha N)\varphi(\Omega). \tag{C.48}$$

Using the result for the propagator of the massive boson on the sphere of Eq. (C.22), the following approximation for the zz correlations is obtained:

$$\langle\sigma_i^z\sigma_j^z\rangle \approx -\alpha\int_0^\infty dq\,\frac{2\cos\left(\sqrt{N\alpha-\frac{1}{4}}q\right)}{\sqrt{2\cosh(q)-2+|\mathbf{n}_{\Omega_i}-\mathbf{n}_{\Omega_j}|^2}}. \tag{C.49}$$

C.3.2 Discrete approximation

Discrete approximation from CFT operators

Let us define the two-point Green's function of the discrete approximation as

$$G^\alpha_{i,j} = \frac{\langle :\varphi(y_i)e^{-\frac{\alpha}{2}\varphi(y_i)^2}::\varphi(y_j)e^{-\frac{\alpha}{2}\varphi(y_j)^2}:\prod_{k(\neq i,j)}^{N}:e^{-\frac{\alpha}{2}\varphi(y_k)^2}:\rangle}{\langle\prod_{k=1}^{N}:e^{-\frac{\alpha}{2}\varphi(y_k)^2}:\rangle}, \tag{C.50}$$

where the expectation value is taken with respect to action of the massless boson. The generalized coordinate y_j is assumed to be one of the following: $y_j = (z_j, \bar{z}_j)$ for positions in the complex plane, $y_j = \Omega_j = (\theta_j, \phi_j)$ on the sphere, and $y_j = (w_j, \bar{w}_j)$ on the cylinder. The zz correlation in the discrete approximation is then given by

$$\langle\sigma_i^z\sigma_j^z\rangle \approx -\alpha G^\alpha_{i,j}. \tag{C.51}$$

The following computation makes use of the correlator of N vertex operators given by

$$\langle\prod_{j=1}^{N}:e^{i\sqrt{\alpha}s_j\varphi(y_j)}:\rangle = \delta_{\mathbf{s}}\prod_{m<n}^{N} d_{mn}^{2\alpha s_m s_n}, \tag{C.52}$$

where

$$d_{mn} = \begin{cases} |z_m - z_n| & \text{(complex plane)},\\ |\mathbf{n}_{\Omega_m} - \mathbf{n}_{\Omega_n}| & \text{(sphere)},\\ |2\sinh(\frac{1}{2}(w_m - w_n))| & \text{(cylinder)}, \end{cases} \tag{C.53}$$

cf. Appendix C.2 for the computation on the sphere and on the cylinder. For the calculation below, it is important to note that Eq. (C.52) holds not only for $s_j \in \{-1, 1\}$ but for general $s_j \in \mathbb{R}$.

We define higher order Green's functions $G^{\alpha}_{i_1,\ldots,i_{2n}}$ analogously to Eq. (C.50). Let us denote the generating function of $G^{\alpha}_{i_1,\ldots,i_{2n}}$ by $\mathcal{Z}_\alpha(\mathbf{J})$, where $\mathbf{J}$ is an N-dimensional, real vector:

$$G^{\alpha}_{i_1,\ldots,i_{2n}} = \left(-\frac{1}{\alpha}\right)^n \frac{1}{\mathcal{Z}_\alpha(\mathbf{J})} \frac{\partial}{\partial J_1}\frac{\partial}{\partial J_2}\cdots\frac{\partial}{\partial J_{2n}} \mathcal{Z}_\alpha(\mathbf{J})\Big|_{\mathbf{J}=0}, \tag{C.54}$$

$$\mathcal{Z}_\alpha(\mathbf{J}) = \langle \prod_{j=1}^{N} : e^{-\frac{\alpha}{2}\varphi(y_j)^2 + i\sqrt{\alpha}J_j\varphi(y_j)} : \rangle. \tag{C.55}$$

The generating function $\mathcal{Z}_\alpha(\mathbf{J})$ will now be evaluated using the N-dimensional Gaussian integral [5]

$$\int d^N\mathbf{x} e^{-\frac{1}{2}\mathbf{x}^t A\mathbf{x} + \mathbf{b}^t\mathbf{x}} = \left(\frac{(2\pi)^N}{\det A}\right)^{\frac{1}{2}} e^{\frac{1}{2}\mathbf{b}^t A^{-1}\mathbf{b}}, \tag{C.56}$$

where A is a symmetric, real $N\times N$ matrix with positive eigenvalues and $\mathbf{b}$ a real vector of length N. By Fourier transforming

$$: e^{-\frac{1}{2}\alpha\varphi(y_j)^2} : = \frac{1}{\sqrt{2\pi}} \int_{-\infty}^{\infty} ds_j e^{-\frac{1}{2}s_j^2} : e^{i\sqrt{\alpha}s_j\varphi(y_j)} :, \tag{C.57}$$

we obtain

$$\mathcal{Z}_\alpha(\mathbf{J}) \propto \int d^N\mathbf{s} e^{-\frac{1}{2}\mathbf{s}^2} \langle \prod_{j=1}^{N} : e^{i\sqrt{\alpha}(s_j+J_j)\varphi(y_j)} : \rangle. \tag{C.58}$$

Using Eq. (C.52) results in

$$\mathcal{Z}_\alpha(\mathbf{J}) \propto \int d^N\mathbf{s} e^{-\frac{1}{2}\mathbf{s}^2} \delta\left(\sum_{j=1}^{N} s_j + \sum_{j=1}^{N} J_j\right) \prod_{m<n}^{N} d_{m,n}^{2\alpha(s_m+J_m)(s_n+J_n)} \tag{C.59}$$

$$= \int d^N\mathbf{s} e^{-\frac{1}{2}(\mathbf{s}-\mathbf{J})^2} \delta\left(\sum_{j=1}^{N} s_j\right) \prod_{m<n} d_{m,n}^{2\alpha s_m s_n} \tag{C.60}$$

$$= e^{-\frac{1}{2}\mathbf{J}^2} \int d^N\mathbf{s} \delta\left(\sum_{j=1}^{N} s_j\right) e^{-\frac{1}{2}\mathbf{s}^t M\mathbf{s} + \mathbf{J}^t\mathbf{s}}, \tag{C.61}$$

where

$$M_{mn} = \delta_{mn} - 2\alpha\log(d_{mn} + \delta_{mn}). \tag{C.62}$$

One of the N integrals can be evaluated due to the δ function. To this end, we choose some index $r \in \{1,\ldots,N\}$ and introduce the $N\times N$ matrix T_r by the linear transformation

$$T_r\mathbf{s} = \left(s_1,\ldots,s_{r-1},-\sum_{j(\neq r)} s_j, s_{r+1},\ldots,s_N\right)^t, \tag{C.63}$$

i.e., the matrix entries of T_r are given by

$$(T_r)_{mn} = \delta_{mn} - \delta_{mr}. \tag{C.64}$$

Carrying out the integral over s_r results in

$$\mathcal{Z}_\alpha(\mathbf{J}) \propto e^{-\frac{1}{2}\mathbf{J}^2} \int \left(\prod_{j(\neq r)} ds_j \right) e^{-\frac{1}{2}\mathbf{s}^t T_r^t M T_r \mathbf{s} + \mathbf{J}^t T_r \mathbf{s}}. \tag{C.65}$$

Using

$$\sqrt{2\pi} = \int_{-\infty}^{\infty} ds_r e^{-\frac{1}{2}s_r^2} = \int_{-\infty}^{\infty} ds_r e^{-\frac{1}{2}\mathbf{s}^t \mathbf{e}_r \mathbf{e}_r^t \mathbf{s}}, \tag{C.66}$$

where $\mathbf{e}_r$ denotes the rth unit vector, we reintroduce an integral over s_r and obtain

$$\mathcal{Z}_\alpha(\mathbf{J}) \propto e^{-\frac{1}{2}\mathbf{J}^2} \int d^N\mathbf{s} e^{-\frac{1}{2}\mathbf{s}^t (T_r^t M T_r + \mathbf{e}_r \mathbf{e}_r^t)\mathbf{s} + \mathbf{J}^t T_r \mathbf{s}}. \tag{C.67}$$

With the N-dimensional Gaussian integral of Eq. (C.56), we arrive at

$$\mathcal{Z}_\alpha(\mathbf{J}) \propto e^{\frac{1}{2}\mathbf{J}^t \Gamma \mathbf{J}}, \tag{C.68}$$

where

$$\Gamma = T_r \left(T_r^t M T_r + \mathbf{e}_r \mathbf{e}_r^t \right)^{-1} T_r^t - \mathbb{I}. \tag{C.69}$$

Note that Γ is independent of the choice of the index r since it does not matter which of the integrals is evaluated using the δ function.

It follows that

$$G_{i,j}^\alpha = -\frac{1}{\alpha} \frac{\partial}{\partial J_i} \frac{\partial}{\partial J_j} e^{\frac{1}{2}\mathbf{J}^t \Gamma \mathbf{J}} \Big|_{\mathbf{J}=0} = -\frac{1}{\alpha} \Gamma_{ij} \qquad \text{and } \langle \sigma_i^z \sigma_j^z \rangle \approx \Gamma_{ij}. \tag{C.70}$$

Let us now compute the subleading term in the expansion of $\langle \sigma_i^z \sigma_j^z \rangle$. To this end, we write the exact zz correlations as

$$\langle \sigma_i^z \sigma_j^z \rangle = -\frac{\langle \prod_{k\in\{i,j\}} : \tan(\sqrt{\alpha}\varphi(y_k)) C(\sqrt{\alpha}\varphi(y_k)) e^{-\frac{\alpha}{2}\varphi(y_k)^2} : \prod_{k(\neq i,j)}^N : C(\sqrt{\alpha}\varphi(y_k)) e^{-\frac{\alpha}{2}\varphi(y_k)^2} : \rangle}{\langle \prod_{k=1}^N : C(\sqrt{\alpha}\varphi(y_k)) e^{-\frac{\alpha}{2}\varphi(y_k)^2} : \rangle}, \tag{C.71}$$

where $C(x) = \cos(x) e^{\frac{1}{2}x^2}$. In terms of the generating function $\mathcal{Z}_\alpha$ of Eq. (C.55),

$$\langle \sigma_i^z \sigma_j^z \rangle = -\frac{\tan(-i\partial_i)\tan(-i\partial_j) \prod_{k=1}^N C(-i\partial_k) \mathcal{Z}_\alpha(\mathbf{J}) \big|_{\mathbf{J}=0}}{\prod_{k=1}^N C(-i\partial_k) \mathcal{Z}_\alpha(\mathbf{J}) \big|_{\mathbf{J}=0}}, \tag{C.72}$$

where $\partial_k = \frac{\partial}{\partial J_k}$. Expanding to fourth order in derivatives,

$$\tan(-i\partial_i)\tan(-i\partial_j) \prod_{k=1}^N C(-i\partial_k) = -\partial_i\partial_j + \frac{1}{3}(\partial_i^3\partial_j + \partial_i\partial_j^3) + \ldots, \tag{C.73}$$

$$\prod_{k=1}^N C(-i\partial_k) = 1 - \frac{1}{12} \sum_{k=1}^N \partial_k^4 + \ldots, \tag{C.74}$$

we obtain

$$\langle \sigma_i^z \sigma_j^z \rangle = \Gamma_{i,j} - \Gamma_{i,j}(\Gamma_{i,i} + \Gamma_{j,j}) + \ldots. \tag{C.75}$$

Alternative derivation of discrete approximation

We now demonstrate that the discrete approximation can be obtained directly from the expression of the exact zz correlations in $|\psi_\alpha\rangle$ without using CFT operators.

Let us first consider the norm squared of $|\psi_\alpha\rangle$:

$$\langle\psi_\alpha|\psi_\alpha\rangle = \sum_{s_1,\ldots,s_N} \delta_{\mathbf{s}} \prod_{m<n} d_{mn}^{2\alpha s_m, s_n} = \sum_{s_1,\ldots,s_N} \delta_{\mathbf{s}} e^{-\frac{1}{2}\mathbf{s}^t(M-\mathbb{I})\mathbf{s}}, \tag{C.76}$$

where d_{mn} is defined in Eq. (C.53) and M in Eq. (C.62).

Writing the sums over each s_j as an integral,

$$\sum_{s_j\in\{-1,1\}} \to \int_{-\infty}^{\infty} ds_j \Big(\delta(s_j+1)+\delta(s_j-1)\Big), \tag{C.77}$$

we obtain

$$\langle\psi_\alpha|\psi_\alpha\rangle \propto \int d^N\mathbf{s}\left[\prod_{m=1}^{N}(\delta(s_m+1)+\delta(s_m-1))\right]\delta\left(\sum_{m=1}^{N} s_m\right) e^{-\frac{1}{2}\mathbf{s}^t(M-\mathbb{I})\mathbf{s}} \tag{C.78}$$

$$\propto \int d^N\mathbf{x}\left[\prod_{m=1}^{N}\cos(x_m)\right]\int d^N\mathbf{s} e^{-i\mathbf{x}^t\mathbf{s}}\delta\left(\sum_{m=1}^{N} s_m\right) e^{-\frac{1}{2}\mathbf{s}^t(M-\mathbb{I})\mathbf{s}}, \tag{C.79}$$

where it was used that

$$\delta(s_m+1)+\delta(s_m-1) = \int_{-\infty}^{\infty}\frac{dx_m}{\pi}\cos(x_m)e^{-ix_m s_m}. \tag{C.80}$$

For the expectation value $4\langle\psi_\alpha|t_i^z t_j^z|\psi_\alpha\rangle$, we additionally replace

$$\sum_{s_j\in\{-1,1\}} s_j \to \int_{-\infty}^{\infty} ds_j\Big(\delta(s_j-1)-\delta(s_j+1)\Big) \tag{C.81}$$

and use

$$\delta(s_j-1)-\delta(s_j+1) = i\int_{-\infty}^{\infty}\frac{dx_j}{\pi}\sin(x_j)e^{-ix_j s_j} \tag{C.82}$$

so that

$$4\langle\psi_\alpha|t_i^z t_j^z|\psi_\alpha\rangle \propto -\int d^N\mathbf{x}\tan(x_i)\tan(x_j)\left[\prod_{m=1}^{N}\cos(x_m)\right]\int d^N\mathbf{s} e^{-i\mathbf{x}^t\mathbf{s}}\delta\left(\sum_{m=1}^{N} s_m\right)e^{-\frac{1}{2}\mathbf{s}^t(M-\mathbb{I})\mathbf{s}}. \tag{C.83}$$

Let us introduce the generating function

$$\mathcal{Z}'_\alpha(\mathbf{J}) = \int d^N\mathbf{x} e^{-\frac{1}{2}\mathbf{x}^2+i\mathbf{J}^t\mathbf{x}}\int d^N\mathbf{s} e^{-i\mathbf{x}^t\mathbf{s}}\delta\left(\sum_{j=1}^{N} s_j\right)e^{-\frac{1}{2}\mathbf{s}^t(M-\mathbb{I})\mathbf{s}}, \tag{C.84}$$

which is defined in such a way that the exact zz correlations $\langle\sigma_i^z\sigma_j^z\rangle = 4\frac{\langle\psi_\alpha|t_i^z t_j^z|\psi_\alpha\rangle}{\langle\psi_\alpha|\psi_\alpha\rangle}$ are given by Eq. (C.72) with $\mathcal{Z}_\alpha(\mathbf{J})$ replaced by $\mathcal{Z}'_\alpha(\mathbf{J})$. In particular, the zz correlations in the quadratic approximation are given by

$$\langle\sigma_i^z\sigma_j^z\rangle \approx \frac{1}{\mathcal{Z}'_\alpha(\mathbf{J})}\frac{\partial}{\partial J_i}\frac{\partial}{\partial J_j}\mathcal{Z}'_\alpha(\mathbf{J})\Big|_{\mathbf{J}=0}. \tag{C.85}$$

We now show that $\mathcal{Z}'_\alpha(\mathbf{J})$ is equivalent to the generating function $\mathcal{Z}_\alpha(\mathbf{J})$ of the previous derivation. Carrying out the integral over $\mathbf{x}$ in Eq. (C.84),

$$\mathcal{Z}'_\alpha(\mathbf{J}) \propto \int d^N\mathbf{s} e^{-\frac{1}{2}(\mathbf{J}-\mathbf{s})^2} \delta\left(\sum_{j=1}^N s_j\right) e^{-\frac{1}{2}\mathbf{s}^t(M-\mathbb{I})\mathbf{s}} = e^{-\frac{1}{2}\mathbf{J}^2} \int d^N\mathbf{s}\delta\left(\sum_{j=1}^N s_j\right) e^{-\frac{1}{2}\mathbf{s}^t M\mathbf{s}+\mathbf{J}^t\mathbf{s}}. \tag{C.86}$$

Comparing to $\mathcal{Z}_\alpha(\mathbf{J})$ in Eq. (C.61), we conclude that $\mathcal{Z}'_\alpha(\mathbf{J}) \propto \mathcal{Z}_\alpha(\mathbf{J}) \propto e^{\frac{1}{2}\mathbf{J}^t\Gamma\mathbf{J}}$.

D Details on continuous-spin wave functions

D.1 Bosonic Gaussian states

This section provides a short introduction to the formalism of bosonic Gaussian states and discusses how their entanglement properties can be computed.

In the following, we consider N bosonic modes with annihilation and creation operators a_m and $a_m^\dagger$ for $m \in \{1,\dots,N\}$. These satisfy the commutation relations

$$\left[a_m, a_n^\dagger\right] = \delta_{mn}. \tag{D.1}$$

The corresponding position and momentum operators are defined as

$$Q_m = \frac{1}{\sqrt{2}}\left(a_m + a_m^\dagger\right), \qquad P_m = \frac{1}{\sqrt{2}}\left(-ia_m + ia_m^\dagger\right), \tag{D.2}$$

and satisfy the canonical commutation relations

$$[Q_m, P_n] = i\delta_{mn}. \tag{D.3}$$

They can be represented on wave functions $\psi(\boldsymbol{s})$ with $\boldsymbol{s} \in \mathbb{R}^N$ as

$$(Q_m\psi)(\boldsymbol{s}) = s_m\psi(\boldsymbol{s}) \qquad \text{and } (P_m\psi)(\boldsymbol{s}) = -i\frac{\partial\psi}{\partial s_m}(\boldsymbol{s}). \tag{D.4}$$

Arranging the operators Q_m and P_m in a vector $\boldsymbol{R} = (Q_1,\dots,Q_N,P_1,\dots,P_N)^t$ of length $2N$, the commutation relations of Eq. (D.3) can be formulated as

$$[R_m, R_n] = i\Omega_{mn}, \tag{D.5}$$

where Ω is the $2N \times 2N$ matrix

$$\Omega = \begin{pmatrix} 0 & \mathbb{I} \\ -\mathbb{I} & 0 \end{pmatrix} \tag{D.6}$$

and $\mathbb{I}$ the $N \times N$ identity matrix. Symplectic matrices are defined as $2N \times 2N$ real matrices S that satisfy $S\Omega S^t = \Omega$ [198]. A symplectic matrix S defines a transformation of operators that preserves the commutation relations:

$$[R'_m, R'_n] = [R_m, R_n] = i\Omega_{mn} \qquad \text{for } \boldsymbol{R}' = S\boldsymbol{R}. \tag{D.7}$$

A general quadratic Hamiltonian assumes the form [199]

$$\mathcal{H} = \frac{1}{2}\boldsymbol{R}^t H \boldsymbol{R} = \frac{1}{2}\sum_{m,n=1}^{2N} R_m H_{mn} R_n, \tag{D.8}$$

where H is a real and positive semidefinite $2N \times 2N$ matrix. These conditions on H ensure that $\mathcal{H}$ is Hermitian and bounded from below. Gaussian states are ground and thermal states of such Hamiltonians [130, 199, 200].

For a given normalized density matrix ρ, the covariance matrix γ is defined through the expectation values

$$\gamma_{mn} = \langle\{\Delta R_m, \Delta R_n\}\rangle, \qquad \Delta R_m = R_m - \langle R_m\rangle, \tag{D.9}$$

where $\{\bullet,\bullet\}$ is the anticommutator, $\langle\bullet\rangle = \mathrm{tr}\,(\bullet\rho)$, and $\langle R_m\rangle$ are the first moments. Gaussian states are completely characterized by their covariance matrix γ and their first moments $\langle R_m\rangle$, i.e., all other properties can be derived from γ and $\langle R_m\rangle$.

In this thesis, we focus on the special case of a pure Gaussian state. Its covariance matrix assumes the form [201]

$$\gamma = \begin{pmatrix} X^{-1} & -X^{-1}Y \\ -YX^{-1} & X + YX^{-1}Y \end{pmatrix} \tag{D.10}$$

in terms of real, symmetric $N \times N$ matrices X and Y with X being positive definite. The (unnormalized) wave function corresponding to this covariance matrix is given by [202]

$$\psi(\boldsymbol{s}) = e^{-\frac{1}{2}\boldsymbol{s}^t(X+iY)\boldsymbol{s}}. \tag{D.11}$$

Let us now discuss how to compute entanglement properties of the state $\psi(\boldsymbol{s})$. To this end, we consider a bipartition of the system into disjoint parts $A = \{i_1,\ldots,i_L\}$ and $B = \{j_1,\ldots,j_{N-L}\}$ with $A \cup B = \{1,\ldots,N\}$. The reduced density matrix ρ_A is defined by tracing out the modes B from the pure-state density matrix corresponding to $\psi(\boldsymbol{s})$:

$$\rho_A = \mathrm{tr}_B \frac{|\psi\rangle\langle\psi|}{\langle\psi|\psi\rangle}. \tag{D.12}$$

The Rényi entropies of order a are then defined as [203]

$$S_a(A) = \frac{1}{1-a}\log \mathrm{tr}\left[(\rho_A)^a\right], \tag{D.13}$$

and the von Neumann entropy

$$S_{\text{von Neumann}}(A) = -\mathrm{tr}\,(\rho_A \log \rho_A). \tag{D.14}$$

It can be obtained as the limit $a \to 1$ of Rényi entropies, $S_{\text{von Neumann}}(A) = \lim_{a\to 1} S_a(A)$. The entanglement Hamiltonian H_A is defined through $\rho_A = e^{-H_A}$ and its eigenvalues form the entanglement spectrum [159, 204].

For Gaussian states, the partial trace of Eq. (D.12) assumes a particularly simple form in terms of the covariance matrix. Namely, the covariance matrix γ_A of the reduced density matrix ρ_A can be obtained from γ by removing the rows and columns corresponding to the subsystem B from γ [205]. The entanglement entropies and spectra can then be computed from the symplectic eigenvalues of ρ_A. These are defined through Williamson's decomposition [202, 206], which states that any real, positive definite $2N\times 2N$ matrix M can be factorized according to

$$S^t M S = \mathrm{diag}(\nu_1,\ldots,\nu_N,\nu_1,\ldots,\nu_N), \tag{D.15}$$

where S is symplectic and $\nu_1,\ldots,\nu_N$ are positive real numbers that define the sympletic spectrum of M. We note that $\nu_1,\ldots,\nu_N$ are equal to the positive eigenvalues of $i\Omega M$ [130].

Applying Williamson's theorem to the covariance matrix γ_A corresponds to a decomposition in to thermal modes [130]. To see this, we note that a single harmonic oscillator with modes b and $b^\dagger$ and thermal density matrix

$$\rho_{\text{thermal}} = \frac{1}{Z}e^{-\omega b^\dagger b}, \qquad Z = \mathrm{tr}\left(e^{-\omega b^\dagger b}\right), \tag{D.16}$$

has a covariance matrix

$$\gamma_{\text{thermal}} = \text{diag}(\nu, \nu), \tag{D.17}$$

where the oscillator energy ω and ν are related through

$$\omega = \log \frac{\nu + 1}{\nu - 1}. \tag{D.18}$$

The decomposition $S^t \gamma_A S = \text{diag}(\nu_1, \ldots, \nu_L, \nu_1, \ldots, \nu_L)$ thus corresponds to a basis change of the reduced density matrix ρ_A to a product state ρ_A' of thermal oscillators [130, 204]:

$$\rho_A' = \frac{1}{Z} e^{-\sum_{j=1}^{L} \omega_j b_j^\dagger b_j}, \tag{D.19}$$

where b_j are bosonic modes in the new basis and ω_j is related to the symplectic eigenvalue ν_j through Eq. (D.18). The single-particle entanglement spectrum is thus given by $\omega_1, \ldots, \omega_L$, and the entanglement Hamiltonian in its diagonalized form follows from Eq. (D.19).

The Rényi entanglement entropies can be computed from the symplectic eigenvalues $\nu_1, \ldots, \nu_L$ of ρ_A according to [207, 208]

$$S_a(A) = \sum_{j=1}^{L} g_a(\nu_j), \tag{D.20}$$

where

$$g_a(y) = \frac{1}{a-1} \log \left[\left(\frac{y+1}{2} \right)^a - \left(\frac{y-1}{2} \right)^a \right] \tag{D.21}$$

In particular, the limit $a \to 1$ yields the von Neumann entropy with

$$\lim_{a \to 1} g_a(y) = \frac{y+1}{2} \log \left(\frac{y+1}{2} \right) - \frac{y-1}{2} \log \left(\frac{y-1}{2} \right). \tag{D.22}$$

D.2 Entanglement properties of $\psi_\beta(\boldsymbol{s})$

This section explains how we compute entanglement properties for the Gaussian wave function $\psi_\beta(\boldsymbol{s})$ defined in Sec. 5.1. With respect to the case of generic bosonic Gaussian states discussed in Appendix D.1, we now have to take into account the delta function in $\psi_\beta(\boldsymbol{s})$, which leads to divergences. The regularization explained in Sec. 5.1.3 leads to the wave function $\psi_{\beta,\epsilon}(\boldsymbol{s})$ with covariance matrix [cf. Eq. (D.10)]

$$\gamma_{\beta,\epsilon} = \frac{1}{2\epsilon} \begin{pmatrix} 0 & 0 \\ 0 & \boldsymbol{e}\boldsymbol{e}^t \end{pmatrix} + \gamma'_{\beta,\epsilon}, \tag{D.23}$$

where

$$\gamma'_{\beta,\epsilon} = \begin{pmatrix} X_{\beta,\epsilon}^{-1} & 0 \\ 0 & X_\beta \end{pmatrix}. \tag{D.24}$$

For the chiral wave function $\tilde{\psi}_\beta(\boldsymbol{s})$ discussed in Sec. 5.4, we introduce a regularized wave function $\tilde{\psi}_{\beta,\epsilon}(\boldsymbol{s})$ analogously to $\psi_{\beta,\epsilon}(\boldsymbol{s})$ and write it in the form

$$\tilde{\psi}_{\beta,\epsilon}(\boldsymbol{s}) = e^{-\frac{1}{2}\boldsymbol{s}^t (X_{\beta,\epsilon} + iY)\boldsymbol{s}}, \tag{D.25}$$

where Y is real and symmetric. [The matrix $X_{\beta,\epsilon}$ is the same as in the real case since $\tilde{\psi}_\beta(\boldsymbol{s})$ differs from $\psi_\beta(\boldsymbol{s})$ only by a phase.] This leads to a covariance matrix as in Eq. (D.23) but with

$$\gamma'_{\beta,\epsilon} = \begin{pmatrix} X^{-1}_{\beta,\epsilon} & -X^{-1}_{\beta,\epsilon} Y \\ -Y X^{-1}_{\beta,\epsilon} & X_\beta + Y X^{-1}_{\beta,\epsilon} Y \end{pmatrix}. \tag{D.26}$$

The calculations of Secs. D.2.1 and D.2.2 below are then also valid for $\tilde{\psi}_\beta(\boldsymbol{s})$ with $\gamma'_{\beta,\epsilon}$ of Eq. (D.26).

Using [171]

$$X^{-1}_{\beta,\epsilon} = X^{-1}_\beta - \frac{1}{2\epsilon + \boldsymbol{e}^t X^{-1}_\beta \boldsymbol{e}} X^{-1}_\beta \boldsymbol{e}\boldsymbol{e}^t X^{-1}_\beta, \tag{D.27}$$

we find that $\gamma'_{\beta,\epsilon}$ is finite in the limit $\epsilon \to 0$. In particular, the QQ, QP, and PQ blocks of the covariance matrix $\gamma_{\beta,\epsilon}$ are finite, while the PP block has a divergent term.

D.2.1 Symplectic eigenvalues of the reduced state's covariance matrix

Let us write the covariance matrix of Eq. (D.23) as

$$\gamma_{\beta,\epsilon} = \frac{1}{2\epsilon} v v^t + \gamma'_{\beta,\epsilon}, \qquad \text{where } v = \begin{pmatrix} 0 \\ \boldsymbol{e} \end{pmatrix}. \tag{D.28}$$

In the following, we consider a bipartition into disjoint subsystems $A = \{i_1, \ldots, i_L\}$ and $B = \{j_1, \ldots, j_{N-L}\}$, where $A \cup B = \{1, \ldots, N\}$ and $L \in \{1, \ldots, N-1\}$. The covariance matrix after tracing out the subsystem B is given by $\mathcal{D}_A \gamma_{\beta,\epsilon} \mathcal{D}_A^t$, where

$$\mathcal{D}_A = \begin{pmatrix} D_A & 0 \\ 0 & D_A \end{pmatrix} \tag{D.29}$$

with the $L \times N$ matrix

$$D_A = \begin{pmatrix} — \boldsymbol{e}^t_{i_1} — \\ \vdots \\ — \boldsymbol{e}^t_{i_L} — \end{pmatrix} \tag{D.30}$$

and $\boldsymbol{e}_i$ being the ith unit vector. The matrix $\mathcal{D}_A$ removes the rows and columns corresponding to B from $\gamma_{\beta,\epsilon}$.

The entanglement entropies and spectra follow directly from the symplectic eigenvalues of $\mathcal{D}_A \gamma_{\beta,\epsilon} \mathcal{D}_A^t$, which are the positive eigenvalues of $i\Omega \mathcal{D}_A \gamma_{\beta,\epsilon} \mathcal{D}_A^t$. However, the covariance matrix $\gamma_{\beta,\epsilon}$ is divergent in the limit $\epsilon \to 0$, which leads to an infinity in the symplectic eigenvalues and thus in the entropies. To handle this divergence, we compute the inverse $\left[\mathcal{D}_A \gamma_{\beta,\epsilon} \mathcal{D}_A^t\right]^{-1}$ since it is finite for $\epsilon \to 0$:

$$\left[\mathcal{D}_A \gamma_{\beta,\epsilon} \mathcal{D}_A^t\right]^{-1} = \left[\mathcal{D}_A \gamma'_{\beta,\epsilon} \mathcal{D}_A^t\right]^{-1} - \frac{\left[\mathcal{D}_A \gamma'_{\beta,\epsilon} \mathcal{D}_A^t\right]^{-1} \mathcal{D}_A v v^t \mathcal{D}_A^t \left[\mathcal{D}_A \gamma'_{\beta,\epsilon} \mathcal{D}_A^t\right]^{-1}}{2\epsilon + v^t \mathcal{D}_A^t \left[\mathcal{D}_A \gamma'_{\beta,\epsilon} \mathcal{D}^t\right]^{-1} \mathcal{D}_A v}, \tag{D.31}$$

where we used the formula of Ref. [171] to compute the inverse of a matrix that is changed by a term of rank one. With $\mu^{(1)}_{\beta,\epsilon} \le \mu^{(2)}_{\beta,\epsilon} \cdots \le \mu^{(L)}_{\beta,\epsilon}$ being the ordered positive eigenvalues of

$-i\left[\mathcal{D}_A\gamma_{\beta,\epsilon}\mathcal{D}_A^t\right]^{-1}\Omega$, the symplectic spectrum of $\mathcal{D}_A\gamma_{\beta,\epsilon}\mathcal{D}_A^t$ is then given by $\{\nu_{\beta,\epsilon}^{(j)} = 1/\mu_{\beta,\epsilon}^{(j)}\}_{1\leq j\leq L}$. For $\epsilon\to 0$, we have $\mu_{\beta,\epsilon}^{(1)}\to 0$ so that $\nu_{\beta,\epsilon}^{(1)}\to\infty$.

Let us now compute how $\nu_{\beta,\epsilon}^{(1)}$ scales with ϵ for $\epsilon\to 0$. This will be needed to subtract the divergence from the resulting entanglement entropy. With $\det\Omega = 1$, we have

$$\log\det\mathcal{D}_A\gamma_{\beta,\epsilon}\mathcal{D}_A^t = \log\det\Omega\mathcal{D}_A\gamma_{\beta,\epsilon}\mathcal{D}_A^t = \sum_{j=1}^{L}\log\left[\left(\nu_{\beta,\epsilon}^{(j)}\right)^2\right] \tag{D.32}$$

and therefore

$$\log\nu_{\beta,\epsilon}^{(1)} = \frac{1}{2}\log\det\mathcal{D}_A\gamma_{\beta,\epsilon}\mathcal{D}_A^t - \sum_{j=2}^{L}\log\left[\nu_{\beta,\epsilon}^{(j)}\right]. \tag{D.33}$$

The matrix determinant lemma allows to express the determinant of $\mathcal{D}_A\gamma_{\beta,\epsilon}\mathcal{D}_A^t$ in terms of $\mathcal{D}_A\gamma'_{\beta,\epsilon}\mathcal{D}_A^t$, which differs from $\mathcal{D}_A\gamma_{\beta,\epsilon}\mathcal{D}_A^t$ only by a term of rank one. Thus, we obtain

$$\log\nu_{\beta,\epsilon}^{(1)} = \frac{1}{2}\log\left[\left(1+\frac{1}{2\epsilon}v^t\mathcal{D}_A^t\left(\mathcal{D}_A\gamma'_{\beta,\epsilon}\mathcal{D}_A^t\right)^{-1}\mathcal{D}_A v\right)\det\left(\mathcal{D}_A\gamma'_{\beta,\epsilon}\mathcal{D}_A^t\right)\right] - \sum_{j=2}^{L}\log\nu_{\beta,\epsilon}^{(j)} \tag{D.34}$$

$$= -\frac{1}{2}\log\epsilon + \log\tilde{\nu}_\beta + \mathcal{O}(\epsilon), \tag{D.35}$$

where

$$\log\tilde{\nu}_\beta = \frac{1}{2}\log\left[\frac{\det\left(\mathcal{D}_A\gamma'_{\beta,\epsilon=0}\mathcal{D}_A^t\right)}{2}v^t\mathcal{D}_A^t\left(\mathcal{D}_A\gamma'_{\beta,\epsilon=0}\mathcal{D}_A^t\right)^{-1}\mathcal{D}_A v\right] - \sum_{j=2}^{L}\log\nu_{\beta,\epsilon=0}^{(j)}. \tag{D.36}$$

D.2.2 Entanglement entropies and spectra

Having computed the symplectic spectrum $\{\nu_{\beta,\epsilon}^{(1)},\ldots,\nu_{\beta,\epsilon}^{(L)}\}$ of the reduced state's covariance matrix, we can now determine the entanglement properties in $\psi_\beta(\boldsymbol{s})$.

The divergent symplectic eigenvalue assumes the form $\log\nu_{\beta,\epsilon}^{(1)} = -\frac{1}{2}\log\epsilon + \log\tilde{\nu}_\beta + \mathcal{O}(\epsilon)$ [cf. Eq. (D.35)], and thus we find

$$g_a(\nu_{\beta,\epsilon}^{(1)}) = -\frac{1}{2}\log(\epsilon) + \frac{1}{a-1}\log(a) - \log(2) + \log\tilde{\nu}_\beta + \mathcal{O}(\epsilon), \tag{D.37}$$

where $g_a(y)$ was defined in Eq. (D.21). From Eq. (D.20), the entanglement entropies then follow as

$$S_a(A) = -\frac{1}{2}\log\epsilon + S'_a(A) + \mathcal{O}(\epsilon), \tag{D.38}$$

where

$$S'_a(A) = \frac{1}{a-1}\log(a) - \log(2) + \log\tilde{\nu}_\beta + \sum_{j=2}^{L} g_a\left(\nu_{\beta,\epsilon=0}^{(j)}\right). \tag{D.39}$$

The entropy $S'_a(A)$ differs from $S_a(A)$ by the subtraction of the divergent term $-\frac{1}{2}\log\epsilon$.

Given the symplectic eigenvalues $\nu^{(j)}_{\beta,\epsilon}$, one can also compute the entanglement spectrum. According to Eq. (D.18), we find the single-particle entanglement energies

$$\tilde{\omega}_j = \begin{cases} 0 & \text{if } j = 1, \\ \log \frac{\nu^{(j)}_{\beta,\epsilon=0}+1}{\nu^{(j)}_{\beta,\epsilon=0}-1} & \text{if } j \neq 1 \end{cases} \tag{D.40}$$

in the limit $\epsilon \to 0$. Since $\nu^{(1)}_{\beta,\epsilon} \to \infty$ for $\epsilon \to 0$, the energy $\tilde{\omega}_1$ vanishes. The entanglement Hamiltonian thus assumes the form $\sum_{j=1}^{L} \tilde{\omega}_j b_j^\dagger b_j$, where b_j and $b_j^\dagger$ are annihilation and creation operators in a suitable basis. The precise relation between the original operators $(a_j, a_j^\dagger)$ and $(b_j, b_j^\dagger)$ can be determined by computing Williamson's normal form [202, 206] of the covariance matrix corresponding to the state's reduced density matrix.

D.2.3 Momentum-space entanglement spectrum in 1D with periodic boundary conditions

We now consider the state $\psi_\beta(\boldsymbol{s})$ in 1D with periodic boundary conditions. For this choice, the matrix $\left(X_{\beta,\epsilon}\right)_{i,j}$ only depends on the difference $i-j$ modulo N, and thus we write $\left(X_{\beta,\epsilon}\right)_{i,j} = \left(X_{\beta,\epsilon}\right)_{i-j}$.

We consider the discrete Fourier transform

$$F_{kj} = \frac{1}{\sqrt{N}} e^{-2\pi i \frac{kj}{N}}, \tag{D.41}$$

where the normalization was chosen so that F is unitary.

Writing $F = F_x + iF_y$ with F_x and F_y real, we define the symplectic transformation

$$\mathcal{F} = \begin{pmatrix} F_x & -F_y \\ F_y & F_x \end{pmatrix}, \tag{D.42}$$

which corresponds to a unitary rotation of creation and annihilation operators of the form

$$\begin{pmatrix} \boldsymbol{a} \\ \boldsymbol{a}^\dagger \end{pmatrix} \to \begin{pmatrix} F & 0 \\ 0 & F^* \end{pmatrix} \begin{pmatrix} \boldsymbol{a} \\ \boldsymbol{a}^\dagger \end{pmatrix}. \tag{D.43}$$

Therefore, $\mathcal{F}$ is the symplectic matrix that transforms to momentum space.

The covariance matrix of Eq. (D.23) transformed to momentum space then becomes

$$\mathcal{F} \gamma_{\beta,\epsilon} \mathcal{F}^t = \begin{pmatrix} \gamma^{(1)}_{\beta,\epsilon} & 0 \\ 0 & \gamma^{(2)}_{\beta,\epsilon} \end{pmatrix}, \tag{D.44}$$

where

$$\left(\gamma^{(1)}_{\beta,\epsilon}\right)_{k,l} = \frac{1}{2}\left[\tilde{\delta}_{k-l}\left(\left(\hat{X}_{\beta,\epsilon}\right)_k + \frac{1}{\left(\hat{X}_{\beta,\epsilon}\right)_k}\right) - \tilde{\delta}_{k+l}\left(\left(\hat{X}_{\beta,\epsilon}\right)_k - \frac{1}{\left(\hat{X}_{\beta,\epsilon}\right)_k}\right)\right], \tag{D.45}$$

$$\left(\gamma^{(2)}_{\beta,\epsilon}\right)_{k,l} = \frac{1}{2}\left[\tilde{\delta}_{k-l}\left(\left(\hat{X}_{\beta,\epsilon}\right)_k + \frac{1}{\left(\hat{X}_{\beta,\epsilon}\right)_k}\right) + \tilde{\delta}_{k+l}\left(\left(\hat{X}_{\beta,\epsilon}\right)_k - \frac{1}{\left(\hat{X}_{\beta,\epsilon}\right)_k}\right)\right], \tag{D.46}$$

$$\left(\hat{X}_{\beta,\epsilon}\right)_k = \sum_{j=0}^{N-1} e^{-2\pi i \frac{kj}{N}} \left(X_{\beta,\epsilon}\right)_j, \tag{D.47}$$

and

$$\tilde{\delta}_k = \begin{cases} 1 & \text{if } k \bmod N = 0, \\ 0 & \text{otherwise.} \end{cases} \tag{D.48}$$

Next, we trace out the momenta $k \notin A$ where $A = \{1, \ldots, \lfloor \frac{N-1}{2} \rfloor\}$, i.e., we remove the negative momenta and the momenta $k \in \{0, \frac{N}{2}\}$. The resulting covariance matrix is diagonal:

$$\mathcal{D}_A \mathcal{F} \gamma_{\beta,\epsilon} \mathcal{F}^t \mathcal{D}_A^t = \bigoplus_{k=1}^{\lfloor \frac{N-1}{2} \rfloor} \frac{1}{2} \left[\left(\hat{X}_\beta\right)_k + \frac{1}{\left(\hat{X}_\beta\right)_k} \right] \oplus \bigoplus_{k=1}^{\lfloor \frac{N-1}{2} \rfloor} \frac{1}{2} \left[\left(\hat{X}_\beta\right)_k + \frac{1}{\left(\hat{X}_\beta\right)_k} \right], \tag{D.49}$$

where we replaced $\left(\hat{X}_{\beta,\epsilon}\right)_k$ by

$$\left(\hat{X}_\beta\right)_k = \sum_{j=0}^{N-1} e^{-2\pi i \frac{kj}{N}} \left(X_\beta\right)_j \tag{D.50}$$

since $\left(\hat{X}_\beta\right)_k = \left(\hat{X}_{\beta,\epsilon}\right)_k$ for $k \neq 0$. In Eq. (D.49), we can directly read off the symplectic eigenvalues of the reduced state's covariance matrix as

$$\nu_k = \frac{1}{2} \left[\left(\hat{X}_\beta\right)_k + \frac{1}{\left(\hat{X}_\beta\right)_k} \right]. \tag{D.51}$$

In a suitable basis, the entanglement Hamiltonian is thus given by $\sum_{k=1}^{\lfloor \frac{N-1}{2} \rfloor} \tilde{\omega}_k b_k^\dagger b_k$, where b_k and $b_k^\dagger$ are bosonic annihilation and creation operators, and the entanglement energies are given by

$$\tilde{\omega}_k = \log\left(\frac{\nu_k + 1}{\nu_k - 1}\right) = 2 \log \left| \frac{\left(\hat{X}_\beta\right)_k + 1}{\left(\hat{X}_\beta\right)_k - 1} \right|. \tag{D.52}$$

Since we traced out the mode $k = 0$, all entanglement energies are independent of ϵ.

D.2.4 Entanglement spectrum on the cylinder

The entanglement cut of the cylinder made in Sec. 5.3.3 preserves translational symmetry. Therefore, it is convenient to express the eigenbasis of the entanglement Hamiltonian in terms of Fourier modes as explained in the following. The entanglement Hamiltonian is diagonal in the basis that transforms the reduced state's covariance matrix into Williamson's normal form.

For a cylinder of size $N_x \times N_y$ with N_x even and coordinates defined in Eq. (5.15), we consider the bipartition $A = \{1, \ldots, \frac{N}{2}\}$, $B = \{\frac{N}{2} + 1, \ldots, N\}$ corresponding to the right panel of Fig. 5.7. The Fourier transform of the reduced state's covariance matrix is given by

$$\mathcal{F}_y \gamma^{(A)}_{\beta,\epsilon} \mathcal{F}_y^\dagger = \bigoplus_{k_y=0}^{N_y-1} \gamma^{(A)}_{k_y,\beta,\epsilon}, \tag{D.53}$$

where $\gamma^{(A)}_{\beta,\epsilon} = \mathcal{D}_A \gamma_{\beta,\epsilon} \mathcal{D}_A^t$, and

$$\mathcal{F}_y = \begin{pmatrix} F_y & 0 \\ 0 & F_y^* \end{pmatrix} \tag{D.54}$$

with

$$\left(F_y\right)_{i_x k_y, j_x j_y} = \frac{\delta_{i_x j_x}}{\sqrt{N_y}} e^{-\frac{2\pi i}{N_y} k_y j_y}. \tag{D.55}$$

The $N_x \times N_x$ matrices $\gamma^{(A)}_{k_y,\beta,\epsilon}$ are the blocks of the reduced state's covariance matrix in momentum space. We note that $\gamma^{(A)}_{k_y,\beta,\epsilon}$ is real and $\gamma^{(A)}_{k_y,\beta,\epsilon} = \gamma^{(A)}_{-k_y,\beta,\epsilon}$. This is a consequence of $X_{\beta,\epsilon}$ being symmetric under $i_y - j_y \to N_y - (i_y - j_y)$ for y indices $i_y, j_y \in \{1,\dots,N_y\}$.

The matrix $\mathcal{F}_y$ is complex and does therefore not define a real symplectic transformation. However, we can construct a real matrix from it by combining the Fourier modes of momentum k_y and $-k_y$. After this transformation, we have a description in terms of positive momenta $l_y \in \{0,\dots,\lfloor \frac{N_y}{2} \rfloor\}$ and an additional index $\sigma \in \{+,-\}$ for $l_y \notin \{0, \frac{N_y}{2}\}$ and $\sigma = +$ for $l_y \in \{0, \frac{N_y}{2}\}$. More precisely, we define the unitary matrix T_y through its action on a vector $c_{i_x k_y}$ in Fourier space as

$$\left(T_y c\right)_{i_x l_y \sigma} = \begin{cases} c_{i_x l_y} & \text{if } l_y \in \{0, \frac{N_y}{2}\}, \\ \frac{1}{\sqrt{2}}\left(c_{i_x l_y} + c_{i_x, -l_y}\right) & \text{if } l_y \notin \{0, \frac{N_y}{2}\} \text{ and } \sigma = +, \\ \frac{1}{\sqrt{2}}\left(-i c_{i_x l_y} + i c_{i_x, -l_y}\right) & \text{if } l_y \notin \{0, \frac{N_y}{2}\} \text{ and } \sigma = -. \end{cases} \tag{D.56}$$

Introducing

$$\mathcal{T}_y = \begin{pmatrix} T_y & 0 \\ 0 & T_y^* \end{pmatrix}, \tag{D.57}$$

it follows that $\mathcal{T}_y \mathcal{F}_y$ is real and symplectic. Furthermore,

$$\mathcal{T}_y \mathcal{F}_y \gamma^{(A)}_{\beta,\epsilon} \left(\mathcal{T}_y \mathcal{F}_y\right)^t = \bigoplus_{l_y=0}^{\lfloor \frac{N_y}{2} \rfloor} \bigoplus_{\sigma} \gamma^{(A)}_{l_y,\beta,\epsilon}, \tag{D.58}$$

which follows from $\gamma^{(A)}_{l_y,\beta,\epsilon} = \gamma^{(A)}_{-l_y,\beta,\epsilon}$. Using Williamson's decomposition [202, 206, 209], we next construct symplectic matrices $R'_{l_y,\beta,\epsilon}$ to that

$$R'_{l_y,\beta,\epsilon} \gamma^{(A)}_{l_y,\beta,\epsilon} R'^{t}_{l_y,\beta,\epsilon} = \operatorname{diag}\left(\nu^{(1)}_{l_y,\beta,\epsilon}, \dots, \nu^{(\frac{N_x}{2})}_{l_y,\beta,\epsilon}, \nu^{(1)}_{l_y,\beta,\epsilon}, \dots, \nu^{(\frac{N_x}{2})}_{l_y,\beta,\epsilon}\right). \tag{D.59}$$

The reduced state's covariance matrix $\gamma^{(A)}_{l_y,\beta,\epsilon}$ is thus brought into Williamson's normal form through the transformation

$$\begin{pmatrix} \boldsymbol{Q}' \\ \boldsymbol{P}' \end{pmatrix} = R'_{\beta,\epsilon} \mathcal{T}_y \mathcal{F}_y \begin{pmatrix} \boldsymbol{Q} \\ \boldsymbol{P} \end{pmatrix}, \tag{D.60}$$

where

$$R'_{\beta,\epsilon} = \bigoplus_{l_y=0}^{\lfloor \frac{N_y}{2} \rfloor} \bigoplus_{\sigma} R'_{l_y,\beta,\epsilon}. \tag{D.61}$$

In terms of creation and annihilation operators, this transformation is given by

$$\begin{pmatrix} \boldsymbol{b} \\ \boldsymbol{b}^\dagger \end{pmatrix} = R_{\beta,\epsilon} \mathcal{T}_y \mathcal{F}_y \begin{pmatrix} \boldsymbol{a} \\ \boldsymbol{a}^\dagger \end{pmatrix}, \tag{D.62}$$

where $R_{\beta,\epsilon} = \mathcal{U} R'_{\beta,\epsilon} \mathcal{U}^\dagger$,

$$\mathcal{U} = \frac{1}{\sqrt{2}} \begin{pmatrix} \mathbb{I} & i\mathbb{I} \\ \mathbb{I} & -i\mathbb{I} \end{pmatrix}, \tag{D.63}$$

and we used $\mathcal{U} \mathcal{T}_y \mathcal{F}_y \mathcal{U}^\dagger = \mathcal{T}_y \mathcal{F}_y$.

For the blocks with momenta $l_y \notin \{0, \frac{N_y}{2}\}$, the transformation of Eq. (D.62) is given by

$$\begin{pmatrix} \boldsymbol{b}_{l_y,\sigma=+} \\ \boldsymbol{b}^\dagger_{l_y,\sigma=+} \end{pmatrix} = R_{l_y,\beta,\epsilon} \frac{1}{\sqrt{2}} \begin{pmatrix} \tilde{\boldsymbol{a}}_{l_y} + \tilde{\boldsymbol{a}}_{-l_y} \\ \tilde{\boldsymbol{a}}^\dagger_{l_y} + \tilde{\boldsymbol{a}}^\dagger_{-l_y} \end{pmatrix}, \qquad \begin{pmatrix} \boldsymbol{b}_{l_y,\sigma=-} \\ \boldsymbol{b}^\dagger_{l_y,\sigma=-} \end{pmatrix} = R_{l_y,\beta,\epsilon} \frac{1}{\sqrt{2}} \begin{pmatrix} -i\tilde{\boldsymbol{a}}_{l_y} + i\tilde{\boldsymbol{a}}_{-l_y} \\ i\tilde{\boldsymbol{a}}^\dagger_{l_y} - i\tilde{\boldsymbol{a}}^\dagger_{-l_y} \end{pmatrix}, \tag{D.64}$$

where $\boldsymbol{b}_{l_y,\sigma}$ and $\tilde{\boldsymbol{a}}_{l_y}$ are vectors of length $\frac{N_x}{2}$ corresponding to $i_x \in \{1, \ldots, \frac{N_x}{2}\}$, $R_{l_y,\beta,\epsilon}$ are the blocks of $R_{\beta,\epsilon}$ defined analogously to Eq. (D.61), and

$$\tilde{a}_{i_x k_y} = \frac{1}{\sqrt{N_y}} \sum_{j_y=1}^{N_y} e^{-\frac{2\pi i}{N_y} j_y k_y} a_{i_x j_y} \tag{D.65}$$

are the Fourier transformed annihilation operators.

For $k_y \neq 0$, the blocks $\gamma^{(A)}_{\beta,\epsilon}$ and thus $R_{l_y,\beta,\epsilon}$ do not depend on ϵ, which follows from the definition of $X_{\beta,\epsilon}$ in Eq. (5.10). Thus, Eq. (D.64) leads to to Eq. (5.22) of Chapter 5, where we suppressed the dependence of $R_{l_y,\beta,\epsilon}$ on β for better readability.

D.3 Parent Hamiltonian

The covariance matrix of $\psi_{\beta,\epsilon}(\boldsymbol{s})$ is given by

$$\begin{pmatrix} X^{-1}_{\beta,\epsilon} & 0 \\ 0 & X_{\beta,\epsilon} \end{pmatrix}, \tag{D.66}$$

cf. Eq. (D.10). The following Hamiltonians have a ground state with the same covariance matrix and are thus parent Hamiltonians of $\psi_{\beta,\epsilon}(\boldsymbol{s})$:

$$\mathcal{H}_\eta = \frac{1}{2} \sum_{i,j=1}^{2N} \begin{pmatrix} \boldsymbol{Q} \\ \boldsymbol{P} \end{pmatrix}_i \left(H_\eta\right)_{ij} \begin{pmatrix} \boldsymbol{Q} \\ \boldsymbol{P} \end{pmatrix}_j, \tag{D.67}$$

where

$$H_\eta = \begin{pmatrix} X^{1+\eta}_{\beta,\epsilon} & 0 \\ 0 & X^{-1+\eta}_{\beta,\epsilon} \end{pmatrix}, \tag{D.68}$$

η is a real parameter, and we used a general result [199] about the relationship between a block-diagonal Hamiltonian and the corresponding ground-state covariance matrix.

To diagonalize $\mathcal{H}_\eta$, we choose an orthonormal eigenbasis V_ϵ of $X_{\beta,\epsilon}$:

$$V_\epsilon^t X_{\beta,\epsilon} V_\epsilon = \chi_{\beta,\epsilon}, \tag{D.69}$$

where

$$\chi_{\beta,\epsilon} = \mathrm{diag}\left(c_{\beta,\epsilon}^{(1)},\dots,c_{\beta,\epsilon}^{(N)}\right). \tag{D.70}$$

[The eigenbasis V_ϵ is independent of β since $X_{\beta,\epsilon}$ depends on β through a term proportional to the identity, cf. Eq. (5.10).] The symplectic matrix

$$S_{\beta,\epsilon} = \begin{pmatrix} X_{\beta,\epsilon}^{-\frac{1}{2}} V_\epsilon & 0 \\ 0 & X_{\beta,\epsilon}^{\frac{1}{2}} V_\epsilon \end{pmatrix} \tag{D.71}$$

transforms H_η into

$$S_{\beta,\epsilon}^t H_\eta S_{\beta,\epsilon} = \mathrm{diag}\left[\left(c_{\beta,\epsilon}^{(1)}\right)^\eta,\dots,\left(c_{\beta,\epsilon}^{(N)}\right)^\eta,\left(c_{\beta,\epsilon}^{(1)}\right)^\eta,\dots,\left(c_{\beta,\epsilon}^{(N)}\right)^\eta\right].$$

Thus, the symplectic eigenvalues of H_η are given by $\left(c_{\beta,\epsilon}^{(k)}\right)^\eta$. Defining single-particle energies as

$$\omega_k = \left(c_{\beta,\epsilon}^{(k)}\right)^\eta, \tag{D.72}$$

we thus find a parent Hamiltonian $\sum_{k=1}^N \omega_k b_k^\dagger b_k$ of $\psi_{\beta,\epsilon}(\boldsymbol{s})$, where the new creation and annihilation operators $\boldsymbol{b}$ and $\boldsymbol{b}^\dagger$ are related to the original ones ($\boldsymbol{a}$ and $\boldsymbol{a}^\dagger$) through

$$\begin{pmatrix} \boldsymbol{b} \\ \boldsymbol{b}^\dagger \end{pmatrix} = \frac{1}{2}\begin{pmatrix} \chi_{\beta,\epsilon}^{\frac{1}{2}} + \chi_{\beta,\epsilon}^{-\frac{1}{2}} & \chi_{\beta,\epsilon}^{\frac{1}{2}} - \chi_{\beta,\epsilon}^{-\frac{1}{2}} \\ \chi_{\beta,\epsilon}^{\frac{1}{2}} - \chi_{\beta,\epsilon}^{-\frac{1}{2}} & \chi_{\beta,\epsilon}^{\frac{1}{2}} + \chi_{\beta,\epsilon}^{-\frac{1}{2}} \end{pmatrix}\begin{pmatrix} V_\epsilon^t & 0 \\ 0 & V_\epsilon^t \end{pmatrix}\begin{pmatrix} \boldsymbol{a} \\ \boldsymbol{a}^\dagger \end{pmatrix}. \tag{D.73}$$

With $-i\frac{\partial\psi}{\partial s_k}(\boldsymbol{s}) = i(XQ)_k\psi(\boldsymbol{s})$, it follows that the excited states with a single mode assume the form

$$b_k^\dagger|\psi_\beta\rangle = \sqrt{2}\left(\chi_{\beta,\epsilon}^{\frac{1}{2}} V_\epsilon^t \boldsymbol{Q}\right)_k |\psi_\beta\rangle. \tag{D.74}$$

Chapter 5 discusses the case $\eta = -1$, where the parent Hamiltonian becomes

$$\mathcal{H}_{\eta=-1} = \frac{1}{2}\left(\sum_{m=1}^N Q_m^2 + \sum_{m,n=1}^N C_{mn}P_mP_n\right) \tag{D.75}$$

with

$$C = X_{\beta,\epsilon}^{-2}\big|_{\epsilon=0} = \left[X_\beta^{-1} - \frac{X_\beta^{-1}\boldsymbol{e}\boldsymbol{e}^t X_\beta^{-1}}{\boldsymbol{e}^t X_\beta^{-1}\boldsymbol{e}}\right]^2. \tag{D.76}$$

We did numerical computations for a uniform lattice on the circle and a square lattice on the cylinder and found that the matrix C_{mn} decays with the distance between the sites m and n. At large distances, the decay is consistent with a power law on the circle and on the edge of the cylinder and with an exponential in the bulk of the cylinder.

List of Figures

List of Tables

Bibliography

[1] P. W. Anderson, "More Is Different", Science **177**, 393 (1972).

[2] R. B. Laughlin, "Nobel Lecture: Fractional quantization", Rev. Mod. Phys. **71**, 863 (1999).

[3] R. B. Laughlin and D. Pines, "The Theory of Everything", PNAS **97**, 28 (2000).

[4] P. Ginsparg, "Applied Conformal Field Theory", arXiv:hep-th/9108028 (1991).

[5] P. Di Francesco, P. Mathieu, and D. Sénéchal, *Conformal Field Theory*, Graduate Texts in Contemporary Physics (Springer, New York, 1997).

[6] A. O. Gogolin, A. A. Nersesyan, and A. M. Tsvelik, *Bosonization and Strongly Correlated Systems* (Cambridge University Press, Cambridge, 1998).

[7] G. Moore and N. Read, "Nonabelions in the fractional quantum Hall effect", Nucl. Phys. B **360**, 362 (1991).

[8] K. v. Klitzing, G. Dorda, and M. Pepper, "New Method for High-Accuracy Determination of the Fine-Structure Constant Based on Quantized Hall Resistance", Phys. Rev. Lett. **45**, 494 (1980).

[9] D. C. Tsui, H. L. Stormer, and A. C. Gossard, "Two-Dimensional Magnetotransport in the Extreme Quantum Limit", Phys. Rev. Lett. **48**, 1559 (1982).

[10] R. B. Laughlin, "Anomalous Quantum Hall Effect: An Incompressible Quantum Fluid with Fractionally Charged Excitations", Phys. Rev. Lett. **50**, 1395 (1983).

[11] J. P. Eisenstein and H. L. Stormer, "The Fractional Quantum Hall Effect", Science **248**, 1510 (1990).

[12] H. L. Stormer, "Nobel Lecture: The fractional quantum Hall effect", Rev. Mod. Phys. **71**, 875 (1999).

[13] R. B. Laughlin, "Quantized Hall conductivity in two dimensions", Phys. Rev. B **23**, 5632 (1981).

[14] D. J. Thouless, M. Kohmoto, M. P. Nightingale, and M. den Nijs, "Quantized Hall Conductance in a Two-Dimensional Periodic Potential", Phys. Rev. Lett. **49**, 405 (1982).

[15] F. Wilczek, "Magnetic Flux, Angular Momentum, and Statistics", Phys. Rev. Lett. **48**, 1144 (1982).

[16] F. Wilczek, "Quantum Mechanics of Fractional-Spin Particles", Phys. Rev. Lett. **49**, 957 (1982).

[17] D. Arovas, J. R. Schrieffer, and F. Wilczek, "Fractional Statistics and the Quantum Hall Effect", Phys. Rev. Lett. **53**, 722 (1984).

[18] B. I. Halperin, "Statistics of Quasiparticles and the Hierarchy of Fractional Quantized Hall States", Phys. Rev. Lett. **52**, 2390 (1984).

[19] L. Landau, "Theory of the Superfluidity of Helium II", Phys. Rev. **60**, 356 (1941).

[20] L. D. Landau, "The Theory of a Fermi Liquid", J. Exp. Theor. Phys. **30**, 1058 (1956).

[21] A. A. Abrikosov and I. M. Khalatnikov, "The theory of a fermi liquid (the properties of liquid ^{3}He at low temperatures)", Rep. Prog. Phys. **22**, 329 (1959).

[22] L. D. Landau, E. M. Lifshitz, and L. P. Pitaevskii, *Statistical Physics*, trans. by J. B. Sykes and M. J. Kearsley, Course of Theoretical Physics (Butterworth-Heinemann, Oxford, 1980).

[23] A. A. Abrikosov, L. P. Gorkov, and I. E. Dzyaloshinski, *Methods of quantum field theory in statistical physics*, ed. and trans. by R. A. Silverman (Prentice Hall, Englewood Cliff, 1963).

[24] D. Tong, "Lectures on the Quantum Hall Effect", arXiv:1606.06687 (2016).

[25] F. D. M. Haldane, "Fractional Quantization of the Hall Effect: A Hierarchy of Incompressible Quantum Fluid States", Phys. Rev. Lett. **51**, 605 (1983).

[26] J. K. Jain, "Composite-fermion approach for the fractional quantum Hall effect", Phys. Rev. Lett. **63**, 199 (1989).

[27] J. K. Jain, "Theory of the fractional quantum Hall effect", Phys. Rev. B **41**, 7653 (1990).

[28] X. G. Wen, "Non-Abelian statistics in the fractional quantum Hall states", Phys. Rev. Lett. **66**, 802 (1991).

[29] N. Read and E. Rezayi, "Beyond paired quantum Hall states: Parafermions and incompressible states in the first excited Landau level", Phys. Rev. B **59**, 8084 (1999).

[30] A. Y. Kitaev, "Fault-tolerant quantum computation by anyons", Ann. Phys. **303**, 2 (2003).

[31] C. Nayak, S. H. Simon, A. Stern, M. Freedman, and S. Das Sarma, "Non-Abelian anyons and topological quantum computation", Rev. Mod. Phys. **80**, 1083 (2008).

[32] F. D. M. Haldane, "Model for a Quantum Hall Effect without Landau Levels: Condensed-Matter Realization of the 'Parity Anomaly'", Phys. Rev. Lett. **61**, 2015 (1988).

[33] E. Tang, J.-W. Mei, and X.-G. Wen, "High-Temperature Fractional Quantum Hall States", Phys. Rev. Lett. **106**, 236802 (2011).

[34] T. Neupert, L. Santos, C. Chamon, and C. Mudry, "Fractional Quantum Hall States at Zero Magnetic Field", Phys. Rev. Lett. **106**, 236804 (2011).

[35] K. Sun, Z. Gu, H. Katsura, and S. Das Sarma, "Nearly Flatbands with Nontrivial Topology", Phys. Rev. Lett. **106**, 236803 (2011).

[36] A. G. Grushin, J. Motruk, M. P. Zaletel, and F. Pollmann, "Characterization and stability of a fermionic $\nu = 1/3$ fractional Chern insulator", Phys. Rev. B **91**, 035136 (2015).

[37] V. Kalmeyer and R. B. Laughlin, "Equivalence of the resonating-valence-bond and fractional quantum Hall states", Phys. Rev. Lett. **59**, 2095 (1987).

[38] V. Kalmeyer and R. B. Laughlin, "Theory of the spin liquid state of the Heisenberg antiferromagnet", Phys. Rev. B **39**, 11879 (1989).

[39] M. Greiter and R. Thomale, "Non-Abelian Statistics in a Quantum Antiferromagnet", Phys. Rev. Lett. **102**, 207203 (2009).

[40] P. W. Anderson, "Resonating valence bonds: A new kind of insulator?", Mater. Res. Bull. **8**, 153 (1973).

[41] P. W. Anderson, "The Resonating Valence Bond State in La_2CuO_4 and Superconductivity", Science **235**, 1196 (1987).

[42] J. G. Bednorz and K. A. Müller, "Possible High T_c Superconductivity in the Ba-La-Cu-O System", Z. Phys. B Con. Mat. **64**, 189 (1986).

[43] I. Bloch, J. Dalibard, and W. Zwerger, "Many-body physics with ultracold gases", Rev. Mod. Phys. **80**, 885 (2008).

[44] N. Goldman, J. C. Budich, and P. Zoller, "Topological quantum matter with ultracold gases in optical lattices", Nat. Phys. **12**, 639 (2016).

[45] A. S. Sørensen, E. Demler, and M. D. Lukin, "Fractional Quantum Hall States of Atoms in Optical Lattices", Phys. Rev. Lett. **94**, 086803 (2005).

[46] M. Hafezi, A. S. Sørensen, E. Demler, and M. D. Lukin, "Fractional quantum Hall effect in optical lattices", Phys. Rev. A **76**, 023613 (2007).

[47] N. R. Cooper and J. Dalibard, "Reaching Fractional Quantum Hall States with Optical Flux Lattices", Phys. Rev. Lett. **110**, 185301 (2013).

[48] N. Y. Yao, A. V. Gorshkov, C. R. Laumann, A. M. Läuchli, J. Ye, and M. D. Lukin, "Realizing Fractional Chern Insulators in Dipolar Spin Systems", Phys. Rev. Lett. **110**, 185302 (2013).

[49] D. R. Hofstadter, "Energy levels and wave functions of Bloch electrons in rational and irrational magnetic fields", Phys. Rev. B **14**, 2239 (1976).

[50] M. Aidelsburger, M. Atala, M. Lohse, J. T. Barreiro, B. Paredes, and I. Bloch, "Realization of the Hofstadter Hamiltonian with Ultracold Atoms in Optical Lattices", Phys. Rev. Lett. **111**, 185301 (2013).

[51] H. Miyake, G. A. Siviloglou, C. J. Kennedy, W. C. Burton, and W. Ketterle, "Realizing the Harper Hamiltonian with Laser-Assisted Tunneling in Optical Lattices", Phys. Rev. Lett. **111**, 185302 (2013).

[52] P. W. Anderson, *Concepts in Solids: Lectures on the Theory of Solids* (World Scientific, Singapore, 1997).

[53] P. W. Anderson, "Plasmons, Gauge Invariance, and Mass", Phys. Rev. **130**, 439 (1963).

[54] F. Englert and R. Brout, "Broken Symmetry and the Mass of Gauge Vector Mesons", Phys. Rev. Lett. **13**, 321 (1964).

[55] P. W. Higgs, "Broken Symmetries and the Masses of Gauge Bosons", Phys. Rev. Lett. **13**, 508 (1964).

[56] P. Kapitza, "Viscosity of Liquid Helium below the λ-Point", Nature **141**, 74 (1938).

[57] J. F. Allen and A. D. Misener, "Flow of Liquid Helium II", Nature **141**, 75 (1938).

[58] X. G. Wen and Q. Niu, "Ground-state degeneracy of the fractional quantum Hall states in the presence of a random potential and on high-genus Riemann surfaces", Phys. Rev. B **41**, 9377 (1990).

[59] C. W. J. Beenakker, "Edge channels for the fractional quantum Hall effect", Phys. Rev. Lett. **64**, 216 (1990).

[60] A. H. MacDonald, "Edge states in the fractional-quantum-Hall-effect regime", Phys. Rev. Lett. **64**, 220 (1990).

[61] B. I. Halperin, "Quantized Hall conductance, current-carrying edge states, and the existence of extended states in a two-dimensional disordered potential", Phys. Rev. B **25**, 2185 (1982).

[62] X. G. Wen, "Chiral Luttinger liquid and the edge excitations in the fractional quantum Hall states", Phys. Rev. B **41**, 12838 (1990).

[63] X. G. Wen, "Electrodynamical properties of gapless edge excitations in the fractional quantum Hall states", Phys. Rev. Lett. **64**, 2206 (1990).

[64] X. G. Wen, "Gapless boundary excitations in the quantum Hall states and in the chiral spin states", Phys. Rev. B **43**, 11025 (1991).

[65] X.-G. Wen, "Theory of the edge states in fractional quantum Hall effects", Int. J. Mod. Phys. B **6**, 1711 (1992).

[66] X. G. Wen, "Vacuum degeneracy of chiral spin states in compactified space", Phys. Rev. B **40**, 7387 (1989).

[67] X. G. Wen, "Topological Orders in Rigid States", Int. J. Mod. Phys. B **4**, 239 (1990).

[68] V. L. Berezinskii, "Destruction of long-range order in one-dimensional and two-dimensional systems having a continuous symmetry group I. Classical systems", J. Exp. Theor. Phys. **32**, 493 (1971).

[69] V. L. Berenzinskii, "Destruction of long-range order in one-dimensional and two-dimensional systems possessing a continuous symmetry group. II. Quantum systems", J. Exp. Theor. Phys. **34**, 610 (1972).

[70] J. M. Kosterlitz and D. J. Thouless, "Long range order and metastability in two dimensional solids and superfluids. (Application of dislocation theory)", J. Phys. C: Solid State Phys. **5**, L124 (1972).

[71] J. M. Kosterlitz and D. J. Thouless, "Ordering, metastability and phase transitions in two-dimensional systems", J. Phys. C: Solid State Phys. **6**, 1181 (1973).

[72] J. M. Kosterlitz, "The critical properties of the two-dimensional xy model", J. Phys. C: Solid State Phys. **7**, 1046 (1974).

[73] J. M. Kosterlitz, "Nobel Lecture: Topological defects and phase transitions", Rev. Mod. Phys. **89**, 040501 (2017).

[74] F. D. M. Haldane, "Ground State Properties of Antiferromagnetic Chains with Unrestricted Spin: Integer Spin Chains as Realisations of the O(3) Non-Linear Sigma Model", arXiv:1612.00076 (1981).

[75] F. D. M. Haldane, "Continuum dynamics of the 1-D Heisenberg antiferromagnet: Identification with the O(3) nonlinear sigma model", Phys. Lett. A **93**, 464 (1983).

[76] F. D. M. Haldane, "Nobel Lecture: Topological quantum matter", Rev. Mod. Phys. **89**, 040502 (2017).

[77] I. Affleck, T. Kennedy, E. H. Lieb, and H. Tasaki, "Rigorous results on valence-bond ground states in antiferromagnets", Phys. Rev. Lett. **59**, 799 (1987).

[78] L. Savary and L. Balents, "Quantum spin liquids: a review", Rep. Prog. Phys. **80**, 016502 (2017).

[79] C. L. Kane and E. J. Mele, "Quantum Spin Hall Effect in Graphene", Phys. Rev. Lett. **95**, 226801 (2005).

[80] C. L. Kane and E. J. Mele, "Z_2 Topological Order and the Quantum Spin Hall Effect", Phys. Rev. Lett. **95**, 146802 (2005).

[81] B. A. Bernevig and S.-C. Zhang, "Quantum Spin Hall Effect", Phys. Rev. Lett. **96**, 106802 (2006).

[82] X.-L. Qi and S.-C. Zhang, "Topological insulators and superconductors", Rev. Mod. Phys. **83**, 1057 (2011).

[83] A. Kitaev and J. Preskill, "Topological Entanglement Entropy", Phys. Rev. Lett. **96**, 110404 (2006).

[84] M. Levin and X.-G. Wen, "Detecting Topological Order in a Ground State Wave Function", Phys. Rev. Lett. **96**, 110405 (2006).

[85] A. M. Turner, F. Pollmann, and E. Berg, "Topological phases of one-dimensional fermions: An entanglement point of view", Phys. Rev. B **83**, 075102 (2011).

[86] F. Pollmann, E. Berg, A. M. Turner, and M. Oshikawa, "Symmetry protection of topological phases in one-dimensional quantum spin systems", Phys. Rev. B **85**, 075125 (2012).

[87] X. Chen, Z.-C. Gu, and X.-G. Wen, "Local unitary transformation, long-range quantum entanglement, wave function renormalization, and topological order", Phys. Rev. B **82**, 155138 (2010).

[88] X. Chen, Z.-C. Gu, Z.-X. Liu, and X.-G. Wen, "Symmetry-Protected Topological Orders in Interacting Bosonic Systems", Science **338**, 1604 (2012).

[89] X. Chen, Z.-C. Gu, Z.-X. Liu, and X.-G. Wen, "Symmetry protected topological orders and the group cohomology of their symmetry group", Phys. Rev. B **87**, 155114 (2013).

[90] X.-G. Wen, "Colloquium: Zoo of quantum-topological phases of matter", Rev. Mod. Phys. **89**, 041004 (2017).

[91] E. Witten, "Quantum field theory and the Jones polynomial", Commun. Math. Phys. **121**, 351 (1989).

[92] X.-G. Wen, "A theory of 2+1D bosonic topological orders", Natl. Sci. Rev. **3**, 68 (2016).

[93] A. B. Zamolodchikov, "'Irreversibility' of the flux of the renormalization group in a 2D field theory", JETP Lett. **43**, 730 (1986).

[94] A. M. Polyakov, "Conformal Symmetry of Critical Fluctuations", JETP Lett. **12**, 381 (1970).

[95] M. O. Goerbig, "Quantum Hall Effects", arXiv:0909.1998 (2009).

[96] F. D. M. Haldane, "'Luttinger liquid theory' of one-dimensional quantum fluids. I. Properties of the Luttinger model and their extension to the general 1D interacting spinless Fermi gas", J. Phys. C: Solid State Phys. **14**, 2585 (1981).

[97] A. Luther and I. Peschel, "Calculation of critical exponents in two dimensions from quantum field theory in one dimension", Phys. Rev. B **12**, 3908 (1975).

[98] X.-G. Wen, Y.-S. Wu, and Y. Hatsugai, "Chiral operator product algebra and edge excitations of a fractional quantum Hall droplet", Nucl. Phys. B **422**, 476 (1994).

[99] J. Dubail, N. Read, and E. H. Rezayi, "Edge-state inner products and real-space entanglement spectrum of trial quantum Hall states", Phys. Rev. B **86**, 245310 (2012).

[100] G. 't Hooft, "Dimensional Reduction in Quantum Gravity", arXiv:gr-qc/9310026 (1993).

[101] L. Susskind, "The world as a hologram", J. Math. Phys. **36**, 6377 (1995).

[102] J. I. Cirac and G. Sierra, "Infinite matrix product states, conformal field theory, and the Haldane-Shastry model", Phys. Rev. B **81**, 104431 (2010).

[103] A. E. B. Nielsen, J. I. Cirac, and G. Sierra, "Quantum spin Hamiltonians for the $SU(2)_k$ WZW model", J. Stat. Mech. **2011**, P11014 (2011).

[104] R. Thomale, S. Rachel, P. Schmitteckert, and M. Greiter, "Family of spin-S chain representations of $SU(2)_k$ Wess-Zumino-Witten models", Phys. Rev. B **85**, 195149 (2012).

[105] H.-H. Tu, "Projected BCS states and spin Hamiltonians for the $SO(n)_1$ Wess-Zumino-Witten model", Phys. Rev. B **87**, 041103 (2013).

[106] H.-H. Tu, A. E. B. Nielsen, and G. Sierra, "Quantum spin models for the $SU(n)_1$ Wess-Zumino-Witten model", Nucl. Phys. B **886**, 328 (2014).

[107] R. Bondesan and T. Quella, "Infinite matrix product states for long-range $SU(N)$ spin models", Nucl. Phys. B **886**, 483 (2014).

[108] H.-H. Tu and G. Sierra, "Infinite matrix product states, boundary conformal field theory, and the open Haldane-Shastry model", Phys. Rev. B **92**, 041119 (2015).

[109] A. E. B. Nielsen, J. I. Cirac, and G. Sierra, "Laughlin Spin-Liquid States on Lattices Obtained from Conformal Field Theory", Phys. Rev. Lett. **108**, 257206 (2012).

[110] H.-H. Tu, A. E. B. Nielsen, J. I. Cirac, and G. Sierra, "Lattice Laughlin states of bosons and fermions at filling fractions $1/q$", New J. Phys. **16**, 033025 (2014).

[111] I. Glasser, J. I. Cirac, G. Sierra, and A. E. B. Nielsen, "Lattice effects on Laughlin wave functions and parent Hamiltonians", Phys. Rev. B **94**, 245104 (2016).

[112] A. Hackenbroich and H.-H. Tu, "Parent Hamiltonians for lattice Halperin states from free-boson conformal field theories", Nucl. Phys. B **916**, 1 (2017).

[113] I. Glasser, J. I. Cirac, G. Sierra, and A. E. B. Nielsen, "Exact parent Hamiltonians of bosonic and fermionic Moore-Read states on lattices and local models", New J. Phys. **17**, 082001 (2015).

[114] D. F. Schroeter, E. Kapit, R. Thomale, and M. Greiter, "Spin Hamiltonian for which the Chiral Spin Liquid is the Exact Ground State", Phys. Rev. Lett. **99**, 097202 (2007).

[115] R. Thomale, E. Kapit, D. F. Schroeter, and M. Greiter, "Parent Hamiltonian for the chiral spin liquid", Phys. Rev. B **80**, 104406 (2009).

[116] E. Kapit and E. Mueller, "Exact Parent Hamiltonian for the Quantum Hall States in a Lattice", Phys. Rev. Lett. **105**, 215303 (2010).

[117] M. Greiter, D. F. Schroeter, and R. Thomale, "Parent Hamiltonian for the non-Abelian chiral spin liquid", Phys. Rev. B **89**, 165125 (2014).

[118] A. E. B. Nielsen, G. Sierra, and J. I. Cirac, "Local models of fractional quantum Hall states in lattices and physical implementation", Nat. Commun. **4**, 2864 (2013).

[119] A. E. B. Nielsen, G. Sierra, and J. I. Cirac, "Optical-lattice implementation scheme of a bosonic topological model with fermionic atoms", Phys. Rev. A **90**, 013606 (2014).

[120] J. M. Caillol, D. Levesque, J. J. Weis, and J. P. Hansen, "A Monte Carlo study of the classical two-dimensional one-component plasma", J. Stat. Phys. **28**, 325 (1982).

[121] F. D. M. Haldane, "Exact Jastrow-Gutzwiller resonating-valence-bond ground state of the spin-1/2 antiferromagnetic Heisenberg chain with $1/r^2$ exchange", Phys. Rev. Lett. **60**, 635 (1988).

[122] B. S. Shastry, "Exact solution of an $S = 1/2$ Heisenberg antiferromagnetic chain with long-ranged interactions", Phys. Rev. Lett. **60**, 639 (1988).

[123] F. Calogero, "Ground State of a One-Dimensional N-Body System", J. Math. Phys. **10**, 2197 (1969).

[124] F. Calogero, "Solution of the One-Dimensional N-Body Problems with Quadratic and/or Inversely Quadratic Pair Potentials", J. Math. Phys. **12**, 419 (1971).

[125] B. Sutherland, "Quantum Many-Body Problem in One Dimension: Ground State", J. Math. Phys. **12**, 246 (1971).

[126] B. Sutherland, "Exact Results for a Quantum Many-Body Problem in One Dimension", Phys. Rev. A **4**, 2019 (1971).

[127] F. D. M. Haldane, Z. N. C. Ha, J. C. Talstra, D. Bernard, and V. Pasquier, "Yangian symmetry of integrable quantum chains with long-range interactions and a new description of states in conformal field theory", Phys. Rev. Lett. **69**, 2021 (1992).

[128] J. C. Talstra, "Integrability and Applications of the Exactly-Solvable Haldane-Shastry One-Dimensional Quantum Spin Chain", arXiv:cond-mat/9509178, PhD thesis (Princeton University, 1995).

[129] X.-G. Wen, Y.-S. Wu, and Y. Hatsugai, "Chiral operator product algebra and edge excitations of a fractional quantum Hall droplet", Nucl. Phys. B **422**, 476 (1994).

[130] C. Weedbrook, S. Pirandola, R. García-Patrón, N. J. Cerf, T. C. Ralph, J. H. Shapiro, and S. Lloyd, "Gaussian quantum information", Rev. Mod. Phys. **84**, 621 (2012).

[131] A. A. Belavin, A. M. Polyakov, and A. B. Zamolodchikov, "Infinite conformal symmetry in two-dimensional quantum field theory", Nucl. Phys. B **241**, 333 (1984).

[132] S. Coleman, "Quantum sine-Gordon equation as the massive Thirring model", Phys. Rev. D **11**, 2088 (1975).

[133] J. von Delft and H. Schoeller, "Bosonization for beginners – refermionization for experts", Ann. Phys. (Leipzig) **7**, 225 (1998).

[134] E. Lieb, T. Schultz, and D. Mattis, "Two soluble models of an antiferromagnetic chain", Ann. Phys. **16**, 407 (1961).

[135] D. C. Mattis and E. H. Lieb, "Exact Solution of a Many-Fermion System and Its Associated Boson Field", J. Math. Phys. **6**, 304 (1965).

[136] S. Lukyanov, "Correlation amplitude for the XXZ spin chain in the disordered regime", Phys. Rev. B **59**, 11163 (1999).

[137] J. Voit, "One-dimensional Fermi liquids", Rep. Prog. Phys. **58**, 977 (1995).

[138] I. Affleck and A. W. W. Ludwig, "Exact critical theory of the two-impurity Kondo model", Phys. Rev. Lett. **68**, 1046 (1992).

[139] I. Affleck, "Edge magnetic field in the **xxz** spin-$\frac{1}{2}$ chain", J. Phys. A: Math. Gen. **31**, 2761 (1998).

[140] N. Read and G. Moore, "Fractional Quantum Hall Effect and Nonabelian Statistics", Prog. Theor. Phys. Supp. **107**, 157 (1992).

[141] N. Read, "Non-Abelian adiabatic statistics and Hall viscosity in quantum Hall states and $p_x + ip_y$ paired superfluids", Phys. Rev. B **79**, 045308 (2009).

[142] B. I. Halperin, "Theory of the quantized Hall conductance", Helv. Phys. Acta **56**, 75 (1983).

[143] J. Wildeboer, S. Manna, and A. E. B. Nielsen, "Anyonic excitations of hardcore anyons", arXiv:1711.00845 (2017).

[144] F. D. M. Haldane, "'Spinon gas' description of the $S = 1/2$ Heisenberg chain with inverse-square exchange: Exact spectrum and thermodynamics", Phys. Rev. Lett. **66**, 1529 (1991).

[145] B. D. Simons and B. L. Altshuler, "Exact ground state of an open $s = 1/2$ long-range Heisenberg antiferromagnetic spin chain", Phys. Rev. B **50**, 1102 (1994).

[146] D. Bernard, V. Pasquier, and D. Serban, "Exact Solution of Long-Range Interacting Spin Chains with Boundaries", Europhys. Lett. **30**, 301 (1995).

[147] B. Herwerth, G. Sierra, H.-H. Tu, and A. E. B. Nielsen, "Excited states in spin chains from conformal blocks", Phys. Rev. B **91**, 235121 (2015).

[148] B. Herwerth, G. Sierra, H.-H. Tu, J. I. Cirac, and A. E. B. Nielsen, "Edge states for the Kalmeyer-Laughlin wave function", Phys. Rev. B **92**, 245111 (2015).

[149] J. Wess and B. Zumino, "Consequences of anomalous Ward identities", Phys. Lett. B **37**, 95 (1971).

[150] E. Witten, "Non-abelian bosonization in two dimensions", Comm. Math. Phys. **92**, 455 (1984).

[151] V. G. Knizhnik and A. B. Zamolodchikov, "Current algebra and Wess-Zumino model in two dimensions", Nucl. Phys. B **247**, 83 (1984).

[152] D. Gepner and E. Witten, "String theory on group manifolds", Nucl. Phys. B **278**, 493 (1986).

[153] P. Bouwknegt, A. W. W. Ludwig, and K. Schoutens, "Spinon bases, Yangian symmetry and fermionic representations of Virasoro characters in conformal field theory", Phys. Lett. B **338**, 448 (1994).

[154] B. S. Shastry, "Taking the square root of the discrete $1/r^2$ model", Phys. Rev. Lett. **69**, 164 (1992).

[155] H.-H. Tu, private communication, 2015.

[156] A. E. B. Nielsen and G. Sierra, "Bosonic fractional quantum Hall states on the torus from conformal field theory", J. Stat. Mech. **2014**, P04007 (2014).

[157] A. J. M. Spencer, "A note on the decomposition of tensors into traceless symmetric tensors", Int. J. Eng. Sci. **8**, 475 (1970).

[158] K. Schoutens, "Yangian symmetry in conformal field theory", Phys. Lett. B **331**, 335 (1994).

[159] H. Li and F. D. M. Haldane, "Entanglement Spectrum as a Generalization of Entanglement Entropy: Identification of Topological Order in Non-Abelian Fractional Quantum Hall Effect States", Phys. Rev. Lett. **101**, 010504 (2008).

[160] A. M. Läuchli, "Operator content of real-space entanglement spectra at conformal critical points", arXiv:1303.0741 (2013).

[161] A. Sterdyniak, A. Chandran, N. Regnault, B. A. Bernevig, and P. Bonderson, "Real-space entanglement spectrum of quantum Hall states", Phys. Rev. B **85**, 125308 (2012).

[162] J. Dubail, N. Read, and E. H. Rezayi, "Real-space entanglement spectrum of quantum Hall systems", Phys. Rev. B **85**, 115321 (2012).

[163] I. D. Rodríguez, S. H. Simon, and J. K. Slingerland, "Evaluation of Ranks of Real Space and Particle Entanglement Spectra for Large Systems", Phys. Rev. Lett. **108**, 256806 (2012).

[164] B. Herwerth, G. Sierra, J. I. Cirac, and A. E. B. Nielsen, "Effective description of correlations for states obtained from conformal field theory", Phys. Rev. B **96**, 115139 (2017).

[165] J.-M. Stéphan and F. Pollmann, "Full counting statistics in the Haldane-Shastry chain", Phys. Rev. B **95**, 035119 (2017).

[166] D. C. Cabra and P. Pujol, "Field-theoretical methods in quantum magnetism", in *Quantum Magnetism*, edited by U. Schollwöck, J. Richter, D. J. J. Farnell, and R. F. Bishop (Springer, Berlin, 2004), pp. 253–305.

[167] J. Villain, "Theory of one- and two-dimensional magnets with an easy magnetization plane. II. The planar, classical, two-dimensional magnet", J. Phys. France **36**, 581 (1975).

[168] G. Vidal, J. I. Latorre, E. Rico, and A. Kitaev, "Entanglement in Quantum Critical Phenomena", Phys. Rev. Lett. **90**, 227902 (2003).

[169] P. Calabrese and J. Cardy, "Entanglement entropy and quantum field theory", J. Stat. Mech. **2004**, P06002 (2004).

[170] B. Herwerth, G. Sierra, J. I. Cirac, and A. E. B. Nielsen, "Bosonic Gaussian states from conformal field theory", arXiv:1807.01943 (2018).

[171] M. S. Bartlett, "An Inverse Matrix Adjustment Arising in Discriminant Analysis", Ann. Math. Statist. **22**, 107 (1951).

[172] C. Holzhey, F. Larsen, and F. Wilczek, "Geometric and renormalized entropy in conformal field theory", Nucl. Phys. B **424**, 443 (1994).

[173] P. Calabrese and J. Cardy, "Entanglement entropy and conformal field theory", J. Phys. A: Math. Theor. **42**, 504005 (2009).

[174] P. Calabrese, M. Campostrini, F. Essler, and B. Nienhuis, "Parity Effects in the Scaling of Block Entanglement in Gapless Spin Chains", Phys. Rev. Lett. **104**, 095701 (2010).

[175] R. Thomale, D. P. Arovas, and B. A. Bernevig, "Nonlocal Order in Gapless Systems: Entanglement Spectrum in Spin Chains", Phys. Rev. Lett. **105**, 116805 (2010).

[176] R. Lundgren, J. Blair, M. Greiter, A. Läuchli, G. A. Fiete, and R. Thomale, "Momentum-Space Entanglement Spectrum of Bosons and Fermions with Interactions", Phys. Rev. Lett. **113**, 256404 (2014).

[177] S. Montes, J. Rodríguez-Laguna, and G. Sierra, "BCS wave function, matrix product states, and the Ising conformal field theory", Phys. Rev. B **96**, 195152 (2017).

[178] N. Bray-Ali, L. Ding, and S. Haas, "Topological order in paired states of fermions in two dimensions with breaking of parity and time-reversal symmetries", Phys. Rev. B **80**, 180504 (2009).

[179] R. Lundgren, Y. Fuji, S. Furukawa, and M. Oshikawa, "Entanglement spectra between coupled Tomonaga-Luttinger liquids: Applications to ladder systems and topological phases", Phys. Rev. B **88**, 245137 (2013).

[180] R. Fern, R. Bondesan, and S. H. Simon, "Structure of edge-state inner products in the fractional quantum Hall effect", Phys. Rev. B **97**, 155108 (2018).

[181] S. Manna and A. E. B. Nielsen, "Chain and ladder models with two-body interactions and analytical ground states", Phys. Rev. B **97**, 195143 (2018).

[182] D. Poilblanc, "Investigation of the chiral antiferromagnetic Heisenberg model using projected entangled pair states", Phys. Rev. B **96**, 121118 (2017).

[183] I. Glasser, N. Pancotti, M. August, I. D. Rodriguez, and J. I. Cirac, "Neural-Network Quantum States, String-Bond States, and Chiral Topological States", Phys. Rev. X **8**, 011006 (2018).

[184] E. Jones, T. Oliphant, P. Peterson, et al., *SciPy: Open source scientific tools for Python*, https://www.scipy.org/, [Online; accessed 2018-05-18], 2001–.

[185] E. Anderson, Z. Bai, C. Bischof, L. S. Blackford, J. Demmel, J. Dongarra, J. Du Croz, A. Greenbaum, S. Hammarling, A. McKenney, and D. Sorensen, *LAPACK Users' Guide* (SIAM, Philadelphia, 1999).

[186] A. M. Läuchli, "Numerical Simulations of Frustrated Systems", in *Introduction to Frustrated Magnetism*, Vol. 164, edited by C. Lacroix, P. Mendels, and F. Mila, Springer Series in Solid-State Sciences (Springer, Heidelberg, 2011), pp. 481–511.

[187] R. B. Lehoucq, D. C. Sorensen, and C. Yang, *ARPACK Users' Guide: Solution of Large-Scale Eigenvalue Problems with Implicitly Restarted Arnoldi Methods* (SIAM, Philadelphia, 1998).

[188] C. Lanczos, "An Iteration Method for the Solution of the Eigenvalue Problem of Linear Differential and Integral Operators", J. Res. Natl. Bur. Stand. **45**, 255 (1950).

[189] A. Wietek and A. M. Läuchli, "Sublattice Coding Algorithm and Distributed Memory Parallelization for Large-Scale Exact Diagonalizations of Quantum Many-Body Systems", arXiv:1804.05028 (2018).

[190] N. Metropolis and S. Ulam, "The Monte Carlo Method", J. Am. Stat. Assoc. **44**, 335 (1949).

[191] N. Metropolis, A. W. Rosenbluth, M. N. Rosenbluth, A. H. Teller, and E. Teller, "Equation of State Calculations by Fast Computing Machines", J. Chem. Phys. **21**, 1087 (1953).

[192] D. C. Handscomb, "The Monte Carlo method in quantum statistical mechanics", Math. Proc. Cambridge **58**, 594 (1962).

[193] W. K. Hastings, "Monte Carlo sampling methods using Markov chains and their applications", Biometrika **57**, 97 (1970).

[194] C. P. Robert and G. Casella, *Monte Carlo Statistical Methods* (Springer, New York, 2004).

[195] C. P. Robert, "The Metropolis-Hastings algorithm", arXiv:1504.01896 (2015).

[196] B. A. Bernevig, D. Giuliano, and R. B. Laughlin, "Coordinate representation of the two-spinon wave function and spinon interaction in the Haldane-Shastry model", Phys. Rev. B **64**, 024425 (2001).

[197] G. B. Arfken and H. J. Weber, *Mathematical Methods for Physicists*, International paper edition (Academic Press, San Diego, 2001).

[198] Arvind, B. Dutta, N. Mukunda, and R. Simon, "The real symplectic groups in quantum mechanics and optics", Pramana - J. Phys. **45**, 471 (1995).

[199] N. Schuch, J. I. Cirac, and M. M. Wolf, "Quantum States on Harmonic Lattices", Commun. Math. Phys. **267**, 65 (2006).

[200] B. L. Schumaker, "Quantum mechanical pure states with gaussian wave functions", Phys. Rep. **135**, 317 (1986).

[201] M. M. Wolf, G. Giedke, O. Krüger, R. F. Werner, and J. I. Cirac, "Gaussian entanglement of formation", Phys. Rev. A **69**, 052320 (2004).

[202] M. de Gosson, *Symplectic Geometry and Quantum Mechanics*, Operator Theory: Advances and Applications (Birkhäuser, Basel, 2006).

[203] N. Laflorencie, "Quantum entanglement in condensed matter systems", Phys. Rep. **646**, 1 (2016).

[204] I. Peschel and V. Eisler, "Reduced density matrices and entanglement entropy in free lattice models", J. Phys. A: Math. Theor. **42**, 504003 (2009).

[205] C. Navarrete-Benlloch, *An Introduction to the Formalism of Quantum Information with Continuous Variables* (Morgan & Claypool Publishers, San Rafael, 2015).

[206] J. Williamson, "On the Algebraic Problem Concerning the Normal Forms of Linear Dynamical Systems", Am. J. Math. **58**, 141 (1936).

[207] A. S. Holevo, M. Sohma, and O. Hirota, "Capacity of quantum Gaussian channels", Phys. Rev. A **59**, 1820 (1999).

[208] G. Adesso, A. Serafini, and F. Illuminati, "Extremal entanglement and mixedness in continuous variable systems", Phys. Rev. A **70**, 022318 (2004).

[209] S. Pirandola, A. Serafini, and S. Lloyd, "Correlation matrices of two-mode bosonic systems", Phys. Rev. A **79**, 052327 (2009).